

https://dspace.org/

Heat flow and heat reproduction studies in the Namaqua mobile belt and Kaapvaal craton

Jones, Michael Quentin Wilshire

2015-04-21
http://hdl.handle.net/10539/17473

Downloaded from a DSpace repository. https://dspace.org/

HEAT FLOW AND HEAT PRODUCTION STUDIES IN THE NAMAQUA MOBILE BELT AND KAAPVAAL CRATON

Michael Quentin Wilshire Jones

A Thesis Submitted to the Faculty of Science
University of the Witwatersrand, Johannesburg
for the Degree of Doctor of Philosophy

October, 1981
Johannesburg

that this thesis has not been submitted for a higher degree elsewhere. Part of the research was undertaken while employed in the Department of Geology and Mineralogy, [illegible] University.

Abstract

Terrestrial heat flow[illegible] new determinations in [illegible] South Africa. Temperatures [illegible] to [illegible] depth [illegible] and a deep and [illegible] [illegible] [illegible]

...3 ... [illegible] ..., and the lack of independent geophysical evidence ... a high mantle heat flow, suggest that the heat flow anomaly is due to enhanced upper crustal radioactivity and is correlated to complex ... the surface heat flow. Data from established heat flow provinces show that such radiogenic enrichment is not unique.

The borehole from the Slave/Bear Province yielded a heat flow and heat production of 58 mWm^{-2} and 2.1 μWm^{-3}. These values are similar to the Yellowknife Province suggesting that these regions have similar thermal parameters.

The Kisseynew Domain penetrates an Archean volcanic pile and basal sediment before entering granitic basement. The mean heat flow is 47 ± 2 mWm^{-2}; the well cores are fairly low heat flow/heat production correlation. A similar heat flow is obtained by subtracting the radiogenic contributions of Proterozoic strata from older previous investigations; the mean for the basin is 50 ± 3 mWm^{-2}, slightly lower than the worldwide mean for equivalent age provinces. The average heat production of granitic basement near Kisseynew is 2.3 ± 0.3 μWm^{-3}, almost identical to values obtained previously elsewhere in the craton. Reasonable limits for the exogenic contribution of the sedimentary strata are estimated to be 14 and 22 mWm^{-2}. The mantle heat flow is ... of parameterized equilibrium oceanic mantle heat flow and the thickness of the Kisseynew lithosphere is estimated at ... Archean equilibrium oceanic lithosphere.

The ... of the Kisseynew relative to other Archaean terranes ... that the Kisseynew lithosphere is buoyant. This buoyancy is associated with ... and kimberlitic magmatism which

reflect the introduction of volatiles into the lithosphere, a lowering of the mantle solidus and the formation of hydrous and/or carbonate minerals. This effect offsets the excess mass of the cold, thick Kaapvaal lithosphere.

A relationship between regions of great tectonic age, low heat flow and widespread occurrence of diamondiferous kimberlite is established and investigated in terms of the thermal structure of the lithosphere as deduced from present-day heat flow.

ACKNOWLEDGEMENTS

This investigation was carried out at the Bernard Price Institute for Geophysical Research, University of the Witwatersrand and the Department of Geology and Mineralogy, Oxford University. Research funds were received from the CSIR. Personal support was derived from bursaries awarded by the CSIR, the University of the Witwatersrand and the Human Sciences Trust for study while at the University of the Witwatersrand and from a Rhodes Scholarship awarded by Rhodes University for study while at Oxford University.

I would like to express my gratitude to my supervisor, Prof. L O Nicolaysen and Dr J S Hattingh, for their friendship, guidance and inspiration. I would also like to thank Dr W. Kent and Mrs S M Briggs for their invaluable practical assistance and Profs. D A Hodgson, Prof. H L Cornelius, Dr P Willcox, Dr M G Cox, Mr C R Scott, Mrs E J Barton, Dr J M Barton and Prof. R J Siegfried for many helpful discussions. Many thanks to Sue for typing this thesis.

I am grateful to the following mining companies for permission to use their properties and for supplying drill core samples and to their geological staff for their co-operation and logistic support: Rhodesian Anglo American Ltd, Anglo American Prospecting Company (Zambia) Ltd, Messina (Transvaal) Development Company Ltd, Billiton Exploration (SA) Pty Ltd, Rio Tinto Exploration (Pty) Ltd, South African Iron and Steel Industrial Corporation Ltd, Palabora Copper Company Ltd, Johannesburg Consolidated Investment Company Ltd and Anglo-Vaal Consolidated Investment Company Ltd.

This thesis is dedicated to Sandy, Genevieve, Erica and Anne.

CONTENTS

CHAPTER | PAGE

1 GENERAL TEXT 1

1.1 Plan of the thesis 1

1.2 Conduction of heat in solids 2

1.3 Oceanic heat flow 4

1.4 Continental heat flow 8

1.5 Heat flow in South Africa 18

2 TECTONIC AND GEOCHRONOLOGICAL FRAMEWORK OF SOUTHERN AFRICA 20

2.1 Introduction 20

2.2 Kaapvaal Craton 22

2.3 Limpopo Mobile Belt 25

2.4 Kheis Province 28

2.5 Witwatersrand Province 31

2.6 Namaqua-Natal Province (Namaqua Mobile Belt) 32

2.7 Pan-African Orogenic Belts 41

2.8 Cape Fold Belt 41

2.9 Summary 42

3 TEMPERATURE MEASUREMENTS IN BOREHOLES 43

3.1 Introduction 43

3.2 Logging and procedures 43

3.3 Topographic corrections 48

3.4 Perturbations of the temperature gradient 52

4 THERMAL CONDUCTIVITY MEASUREMENTS 55

4.1 Introduction 55

4.2 Measurements at NPT 55

4.2.1 The divided-bar apparatus 55

4.2.2 Temperature measurements

4.2.3 Principle of the divided-bar 61

4.2.4 Calibration of the divided-bar 66

4.2.5 Measurements on rock samples 69

4.3 Measurements at Oxford University 78

5 HEAT PRODUCTION MEASUREMENTS 82

6 HEAT FLOW AND HEAT PRODUCTION DATA 87

6.1 Introduction 87

6.2 Calculation of heat flow 90

6.3 Springbok-Okiep-Namaqua localities 95

6.4 Aggeneys AG 160 107

6.5 Puts-berg PDG 32 111

6.6 Adjoining Geologist G-2 118

6.7 Kenyon Patch KP 31 119

6.8 Areachap AC 1) 125

6.9 Boks Puts BC 12 128

6.10 Jacomyns Pan PC2-37 and PC2-30 130

6.11 Vogelstruis Suit V 41 135

6.12 Black Face Mountain BF 1 140

6.13 Naib NB 77 141

6.14 Klerksdorp district 145

6.15 Summary 158

7 EFFECTS OF SURFACE TEMPERATURE VARIATIONS ON SUBSURFACE TEMPERATURES 161

7.1 Introduction 161

7.2 Theoretical considerations 162

7.3 Near-surface systematic variations in temperature gradient 167

7.3.1 Data inversion 167

7.3.2 Causes of surface temperature variations 175

7.2.3 Corrections to the heat flow 181

7.3 Quaternary climatic variations 182

7.4 Summary 189

8 THE HEAT FLOW PATTERN IN SOUTH AFRICA AND THE THERMAL STRUCTURE OF THE LITHOSPHERE 191

8.1 Regional heat flow pattern 191

8.2 Heat flow and heat production in the Namaqua Mobile Belt 194

8.2.1 The mobile belt as a whole 199

8.2.2 Heat flow and heat production in the Springbok Sizarist 201

8.3 The Namaqualand heat flow 'anomaly' 204

8.4 Heat flow and heat production in the Richtersveld Province 209

8.5 Heat flow and heat production in the Kaapvaal Craton 209

8.6 Equilibrium thermal structure of the Kaapvaal lithosphere 220

9 ORIGIN AND EVOLUTION OF THE KAAPVAAL LITHOSPHERE 226

10 IMPLICATIONS FOR THE GENESIS OF DIAMONDS 235

11 CONCLUSIONS 241

APPENDIX

I OCEANIC HEAT FLOW 246

II COMPUTER PROGRAMMES 257

III ANALYTICAL TECHNIQUES FOR THE DETERMINATION OF U, Th AND K 269

IV HEAT FLOW AND HEAT PRODUCTION DATA 277

V A. DETAILED CIRCUIT DIAGRAM OF SIEMENS BRIDGE 300

B. HEATER CONTROL CIRCUIT 301

REFERENCES 302

LIST OF FIGURES

FIGURE		page
1.1	Mean surface heat flow and standard deviation in continental age provinces	10
1.2	Heat flow-heat production relationships in the eastern USA, Sierra Nevada and Basin and Range Province	16
1.3	Three models for the vertical distribution of heat sources in the continental crust	14
1.4	Reduced heat flow-mean surface heat flow relationship for seventeen heat flow provinces	17
2.1	Distribution of the major tectonic provinces in southern Africa	21
2.2	Distribution of granite-greenstone basement on the Kaapvaal Craton. (Localities of heat flow stations)	24
2.3	Generalized geology of the northwest Cape Province showing the distribution of the major tectonic provinces. (Localities of heat flow stations)	28
2.4	Generalized geology of the Springbok-O'okiep-Nababeep mining district. (Localities of heat flow stations)	39
2.5	Semi-schematic north-south section through the Ratelpoort synform and Springbok antiform	40
3.1	Field temperature measuring equipment	44
3.2	Thermistor probe	45
3.3	Siemens bridge	47
3.4	Surface temperature (T$_s$) as a function of surface height (H) in South Africa	50
4.1	Divided-bar apparatus	56
4.2	Flow diagram of heater control circuit	58
4.3	Calibration curves for thermistors 2, 3 and 4 relative to thermistor 1	62
4.4	Histogram of the conductivity of 'Lexan' calibrated against quartz (λ_s) at 27°C	70
4.5	Histogram of the conductivity of fused silica determined relative to 'Lexan' at 27°C	70

4.6 Plot of $(T_4-T_3)/[(T_1-T_2)+(T_4-T_3)]$ versus D_6 for sample AO 148 241.9 [illegible]

[illegible] versus D_6 plots [illegible]

5.1 Histograms of the conductivity at 'Lexan' calibrated against quartz (λ_q) at 293 and 90 [illegible]

5.2 Geothermal flux data (W/m²) - Borehole data [illegible]

5.3 Histograms of heat production data for stations in the Alligator district [illegible]

5.4 Geothermal flux (W/m²) - Borehole data [illegible]

5.5 Heat flux (W/m²) - Borehole data [illegible]

5.6 Geothermal flux (W/m²) - Borehole data [illegible]

5.7 Geothermal heat (W/m²) - Borehole data [illegible]

5.8 Histograms of heat production data for (a) A.P., (b) Tennant Creek, (c) AO 148, 'Stuart' and (d) TCD-7 [illegible]

6.1 Isotherms (°C) - Borehole data [illegible]

6.2 Vertical section of the geology intersected by TCD 12 [illegible]

6.10 Temperature distribution in the presence of a two-dimensional [illegible] and vertical thermal conductivity anomaly [illegible]

6.11 Calculated Geotherms - Borehole data [illegible]

6.12 Bonython Range NT 76 - Borehole data [illegible]

6.13 Arrowsmith NT 17 - Borehole data [illegible]

6.15 Soke Puta NT 12 - Borehole data [illegible]

6.16 Jervois Pan TCD-37 - Borehole data [illegible]

6.17 Undulating Hills TCD-10 - Borehole data [illegible]

6.18 Black Tree Mountain NT 1 - Borehole data [illegible]

6.19 Hale NT 17 - Borehole data [illegible]

6.20 Rhenosterhoek DRD 19 - Borehole data [illegible]

6.21 Rhenosterhoek DRD 5 - Borehole data [illegible]

6.22 Bethel DRD 17 - Borehole data [illegible]

6.23 Schoemansfontein BSF 1. Borehole data 151

6.24 Braksteruit BBS 1 Borehole data 153

Manemsvlei BMV 4. Borehole data 154

Borehole data 156

Temperature 164

the 'box' 166

step 10 years ago (ii) 170

Disturbance temperature and temperature gradient sinusoidal varying surface temperature 172

Disturbance temperature gradient due to a sinusoidal variation of the surface temperature amplitude A = °C period T = 600 years and phase 174

Surface temperature averaged over five year periods at meteorological stations in South Africa 179

Surface temperature averaged over ten year periods at meteorological stations in Europe and four in the USA 180

Disturbance to the temperature gradient due to climatic models and summarized in Table 6.3 186

Heat flow stations in South Africa giving heat flow mWm⁻² 194

West heat flow profile across South Africa 195

Heat flow heat production data for the Namaqua Mobile Belt 200

the heat production 202

the Klerksdorp 210

the distribution of radiogenic Kaapvaal 218

Temperature profiles for models of the Kaapvaal lithosphere compared with that of an equilibrium ocean 222

Diagrammatic west cross section of the lithosphere below South Africa for the KI and KII models 224

9.1 Time dependence of surface heat flow due to a thermal perturbation in the upper mantle at three different depths

9.2 KI and KII model geotherms in relation to the peridotite-CO_2-H_2O solidus

10.1 The distribution of major occurrences of diamondiferous kimberlites in South Africa

10.2 Kaapvaal model geotherms and a tentative geotherm for the Namaqua Mobile Belt in relation to the diamond-graphite equilibrium boundary

LIST OF TABLES

TABLE		page
1.1	Nomenclature of thermal parameters	4
3.1	A comparison of topographic corrections obtained from various grid sizes and spacings (Borehole FM 143)	51
4.1	Percentage difference of temperature drops across three subjacent secondary standards for five experiments	61
4.2	Statistics of linear relationships between $(T_0-T_1)/[(T_1-T_2)+(T_2-T_3)]$ and H_0 and thermal conductivities for nineteen rock samples	74
4.3	Effect of water saturation on thermal conductivity	76
4.4	A comparison of thermal conductivity measurements made at BPI and UU	77
4.5	Statistics of secondary standard calibration	79
5.1	Heat production rates per unit mass of U, Th and K	81
5.2	Th/U ratios for basement samples from boreholes in the Namaqua Mobile Belt and Kaapvaal Craton	85
6.1	Locality, elevations, inclinations and depth of boreholes surveyed	88
6.2	Heat production data for VHG 32	118
6.3	Simplified lithological log of KB 36	123
6.4	Heat production data for KB 36	125
6.5	Thermal conductivity data for V 41	138
6.6	Heat production data for V 41	140
6.7	Heat production data for KB 77	146
6.8	Heat production data for the Klerksdorp district	159
6.9	Summary of measurements of gradient, thermal conductivity, heat flow and heat production	160
7.1	Borehole parameters used to estimate surface temperature as a function of time for the 200 m deep feature	169
7.2	Heat flows corrected for recent (<100 year) increase in surface temperature	182

7.1	Surface temperature models used to calculate climatic perturbations shown in Figure 7.8	184
8.1	Heat flow in South Africa - locality, heat flow (q_o) and heat production (A_o)	192
8.2	Average heat flows and heat productions	197
8.3	Thermal parameters for selected Precambrian heat flow provinces and models of the Namaqua and Kaapvaal crust	206
8.4	Corrections to the surface heat flow for the radiogenic contribution of Proterozoic platform strata on the Kaapvaal Craton	213
8.5	Mean near-surface heat production in the Kaapvaal Craton	214

1 INTRODUCTION

1.1 Plan of the thesis

Heat flow measurements made in South Africa by Bullard (1939) were among the first reliable values reported from continental regions. Measurements were made at sporadic intervals since then but the coverage is sparse and South Africa has received little attention compared with other developed countries. In particular, no combined heat flow-heat production determinations have been made. To understand heat flow variations in South Africa, new measurements have been made in areas which have not been studied.

Clearly, and this South African heat flow patterns can only be understood in the light of recent developments of plate tectonic theory. Results of research in oceanic and continental heat flow will be discussed within the framework of plate tectonics in this chapter in order to provide a background for interpreting South African data. A brief introduction to the theory of heat conduction in solids is followed by a discussion of relevant aspects of oceanic heat flow observations. The discussion of continental heat flow centres on experimental observations relating (1) heat flow and age and (2) heat flow and heat production; these relationships constitute important links between heat flow studies and surface geology.

Chapter 2 introduces the major geological provinces of which southern Africa is comprised, paying particular attention to their chronological setting and tectonic character. This information is later integrated with the heat flow data.

The next three chapters deal with the experimental techniques used to determine heat flow and heat production: measurements of temperature gradient, measurements of thermal conductivity and U, Th and K analyses. Special problems encountered in taking these determinations are also discussed in detail. Chapter 6 summarizes methods of calculating heat flow and presents new heat flow and heat production data from twenty localities in South Africa.

These results are discussed in detail in the following four chapters. Chapter 7 presents a discussion of the effects of surface temperature variations, particularly those induced by past climatic variations, on subsurface temperatures and their bearing on South African heat flow. The heat flow pattern in South Africa and the thermal structure of the crust and upper mantle below the Namaqua Mobile Belt and Kaapvaal Craton are discussed in Chapter 8. Chapters 9 and 10 discuss implications of this study for uplift of the Kaapvaal crust and the genesis of diamondiferous kimberlites.

1.2 Conduction of heat in solids

Heat from the earth's interior reaches the surface primarily by conduction through its outer layers and it is pertinent to introduce some theoretical aspects of heat conduction in solids. The differential equation of heat conduction in an isotropic solid moving at velocity $\bar{u}$ is

$$\rho c \frac{\partial T}{\partial t} = \nabla(k\nabla T) - \rho c(\bar{u}.\nabla T) + A \qquad (1.1)$$

where T denotes the temperature distribution within the solid, $T(x,y,z,t)$, ρ density, c specific heat, k thermal conductivity and

A internal heat generation. Table 1.1 lists these and other important thermal parameters with their S.I. units of measure. The above expression holds for thermal properties which are temperature invariant and depend only on position, i.e., $\rho = \rho(x,y,z)$.

In general, problems involving stationary boiles ($\frac{\partial T}{\partial t} = 0$) and heat transfer in the vertical (z) direction ($\frac{\partial T}{\partial x} = \frac{\partial T}{\partial y} = 0$) will be considered. Equation (1.1 reduces to

$$\rho c \frac{\partial T}{\partial t} = \frac{\partial}{\partial z}\left(K \frac{\partial T}{\partial z}\right) + A \qquad (1.2)$$

While solutions to this equation can be complex (depending on initial and boundary conditions) some simple cases have particular relevance to this study.

In the steady state ($\frac{\partial T}{\partial t} = 0$) and for zero heat generation ($A = 0$) we have

$$\frac{d}{dz}\left(K \frac{dT}{dz}\right) = 0 \qquad (1.3)$$

which, upon integration, yields

$$K \frac{dT}{dz} = q \qquad (1.4)$$

where the constant q is the flow of heat per unit area per unit time. The surface heat flow q_0 is therefore determined as the product of the temperature gradient $\frac{dT}{dz}$ and the thermal conductivity K at the earth's surface:

$$q_0 = K \left(\frac{dT}{dz}\right)_{z=0} \qquad (1.5)$$

Table 1.1 Nomenclature of thermal parameters

Symbol	Quantity	Units*
T	temperature	K (°C)
	temperature gradient	Km^{-1} ($°Cm^{-1}$)
k	thermal conductivity	$Wm^{-1}K^{-1}$
	thermal diffusivity	m^2s^{-1}
R	thermal resistance	m^2KW^{-1}
q	heat flux	Wm^{-2} (mWm^{-2})
A	heat generation	Wm^{-3} (μWm^{-3})
	density	kgm^{-3}
c	specific heat (constant pressure)	$Jkg^{-1}K^{-1}$
	volume coefficient of thermal expansion	K^{-1} ($°C^{-1}$)

* For convenience, units shown in brackets will also be used when referring to terrestrial measurements.

If q_0 is known the temperature as a function of depth is

$$T(z) = T_0 + q_0 \int_0^z \frac{dz}{k} \qquad (1.6)$$

where T_0 is the surface temperature.

If heat is produced, equation 1.2 becomes

$$\frac{\partial}{\partial z}(K\frac{\partial T}{\partial z}) = -A(z) \qquad (1.7)$$

and the temperature is given by

$$T(z) = T_0 + \gamma_0 \int_0^z \frac{dz}{K} - \int_0^z \frac{1}{K} \int_0^z A(z)\,dz\,dz \qquad (1.8)$$

The most important source of heat within the earth is generated by the radioactive decay of ^{238}U, ^{235}U, ^{232}Th and ^{40}K. The concentration of these isotopes is relatively high in the continental crust and therefore the last term in equation 1.8 can have an important effect on the temperature distribution.

A third case of interest is the cooling of a semi-infinite region with no heat generation. The differential equation becomes

$$\rho c \frac{\partial T}{\partial t} = \frac{\partial}{\partial z}\left(K \frac{\partial T}{\partial z}\right) \qquad (1.9)$$

If the initial temperature is T_0 (for $z > 0$) and the surface $z = 0$ is kept at a constant temperature, T_s, the solution is

$$T(z,t) = T_s + (T_0 - T_s)\,\mathrm{erf}\left(\frac{z}{2\sqrt{\kappa t}}\right) \qquad (1.10)$$

(cf. Carslaw and Jaeger, 1959, pp. 98-62) where $\kappa = K/\rho c$ is the thermal diffusivity. The temperature gradient is

$$\frac{\partial T}{\partial z} = \frac{(T_0 - T_s)}{\sqrt{\pi \kappa t}} \exp\left(-\frac{z^2}{4\kappa t}\right) \qquad (1.11)$$

and the heat flow at $z = 0$ is

$$q_0(t) = \frac{K(T_0 - T_s)}{\sqrt{\pi \kappa t}} = (T_0 - T_s)\left(\frac{\rho c K}{\pi t}\right)^{\frac{1}{2}} \qquad (1.12)$$

Equations 1.1-1.12 provide a basis for the analysis and interpretation of heat flow observations. Recent developments in heat flow research are outlined in the following pages.

1.3 Oceanic Heat Flow

Certain salient aspects of oceanic heat flow and associated research are discussed in this section as they provide some important clues for the interpretation of continental heat flow patterns and will be used in later chapters. A more detailed discussion of oceanic heat flow is given in Appendix I.

The most fundamental outcome of oceanic heat flow research is the finding that heat flow decreases with the age of the ocean floor (e.g. see Sclater and Francheteau, 1970; McKenzie and Sclater, 1971; Hayman et al, 1972). Sclater et al (1971) showed that the pattern is the same for all major oceans: sea heat flow is high and variable near mid-ocean ridge crests and decreases to relatively constant values of less than 1 $HFU = 10^{-6}$ cal cm^{-2} s^{-1} in old ocean basins. This pattern is consistent with the plate tectonic model whereby oceanic lithosphere, created at the ridge crests, cools and contracts as it spreads laterally. While the heat flow predicted by thermal models for the evolution of oceanic lithosphere agrees well with observations in old ocean floor, it is considerably higher than the heat flow measured in young ocean floor (Turcotte and Oxburgh, 1967; McKenzie, 1967). This discrepancy, and the variability of heat flow in young ocean floor, has been demonstrated to be due to hydrothermally driven convective heat transport through fractured basaltic crust which is in direct contact with sea water (Lister, 1972; Williams et al, 1974; Sclater et al, 1974; Anderson and Hobart, 1976; Anderson et al, 1977; Davis and Lister, 1977). Using this information, Sclater et al (1976) showed that averaged heat flows from stations in well-sedimented crust in the Pacific Ocean are in good agreement with thermal models, which predict a square root of age ($\sqrt{t}$)

dependence in ocean floor younger than 120 m.y. The scatter in the data is, however, still considerable and masks the variation in older ocean floor.

Bathymetric data provide an independent and more accurate constraint on thermal models of the oceanic lithosphere (Sclater et al, 1971; Davis and Lister, 1974). The average depth to the floor of the Pacific Ocean increases from approximately 2500 m near ridge crests to more than 6000 m in ocean basins (Parsons and Sclater, 1977). This trend follows an inverse $\sqrt{t}$ dependence to an age of ~70 m.y. and thereafter approaches a constant value of approximately 6400 m asymptotically.

Parsons and Sclater (1977) developed methods of inverting these bathymetric and heat flow data to give physical properties of oceanic lithosphere. Best fits to the data were calculated and compared with expressions for the dependence of ocean floor depth and heat flow on age; these expressions were obtained from a simple thermal model based on that proposed by McKenzie (1967). They used values $1,00 \times 10^3$ kgm^{-3} for the density of sea water, $3,31 \times 10^3$ kgm^{-3} for the density, $1,17 \times 10^3$ kg^{-1}g^{-1} for the specific heat and $3,14$ Wm^{-1}g^{-1} for the thermal conductivity of mantle material to derive the following parameters of oceanic lithosphere at equilibrium:

plate thickness: $L = 125$ km

bottom boundary temperature: $T_1 = 1350^{\circ}$C

coefficient of thermal expansion: $\alpha = 3,2 \times 10^{-5}$ °C^{-1}

Their best estimate for the asymptotic (equilibrium) oceanic mantle heat flow is:

$$q_m = K\frac{T_L}{r} = 33{,}3 \text{ mWm}^{-2} \qquad (1.13)$$

and that for the surface heat flow, assuming [illegible] lithosphere radiogenic input of 4,2 μWm^{-3}, is 71,1 mWm^{-2}. These estimates of equilibrium values will be used for reference purposes in later discussions of the thermal structure of the lithosphere below South Africa.

1.4 Continental heat flow

In contrast to the oceans, the continental lithosphere has evolved during a much longer period of time (>4000 m.y.) by a wide variety of geological processes. The principal factors which control the variation of surface heat flow (and their mathematical representatives in equation 1.1) are:

(1) conductive cooling after thermal events ($\rho c\frac{\partial T}{\partial t}$)

(2) distribution of radiogenic heat sources in the crust ($A(x,y,z)$)

(3) time dependent diminution of these sources ($A(x,y,z,t)$)

(4) thermal effects of uplift and erosion ($\bar{u}.\nabla T$).

In general it is not possible to describe continental heat flow variations in terms of simple solutions to equation 1.1.

The surface heat flow field is perturbed by a number of superficial factors which include contrasts in vegetation, cultural activities and underground flow of water (Roy et al., 1972). Such problems are usually avoided by making measurements in deep boreholes (>200 m). Although water flows can normally be detected without difficulty (see Chapter 3), Lewis and Beck (1977) demonstrated that slow, steady state

circulation of large volumes of water has reduced the heat flow at many

[illegible] temperature gradients. Single heat flow determinations should

be [illegible]. Topographic irregularities have an important

[illegible] on surface heat flow in regions of high relief, but

[illegible] based on the analyses of Jaeger (1957) and Bullard

[illegible]. Birch (1950) derived methods to correct for

[illegible] of the topography due to uplift and erosion. Three-

[illegible] conductivity anomalies may cause [illegible] of heat

flows and refraction, (1970) and a careful examination of the local

geology is necessary to avoid making erroneous estimates of heat flow.

The [illegible], and perhaps most important environmental factor,

[illegible] climatic changes. Past surface temperature

[illegible] significant effects on subsurface temperatures

[illegible] a key reference. A considerable amount

[illegible] (1968; Lachenbruch et al., 1971; Beck, 1977; England,

[illegible] this process and it will be discussed in

[illegible]

[illegible] reconstructions a number of important patterns have

[illegible] studies. Vacquier and Uyeda (1967) demonstrated

[illegible] heat flow decreases systematically with the age

[illegible] tectonothermal event which affected the continental

[illegible] heat flow increases by approximately 40 mWm^{-2} in

[illegible] and Bell and Jessop (1971) claim that there is no

[illegible] heritage during the Precambrian. This suggests

[illegible] approaching an equilibrium value. Similar

[illegible] were reached by Sclater and Francheteau (1970) Sclater

[illegible] Pitman and Talwani (1981). Figure 1.1 shows the

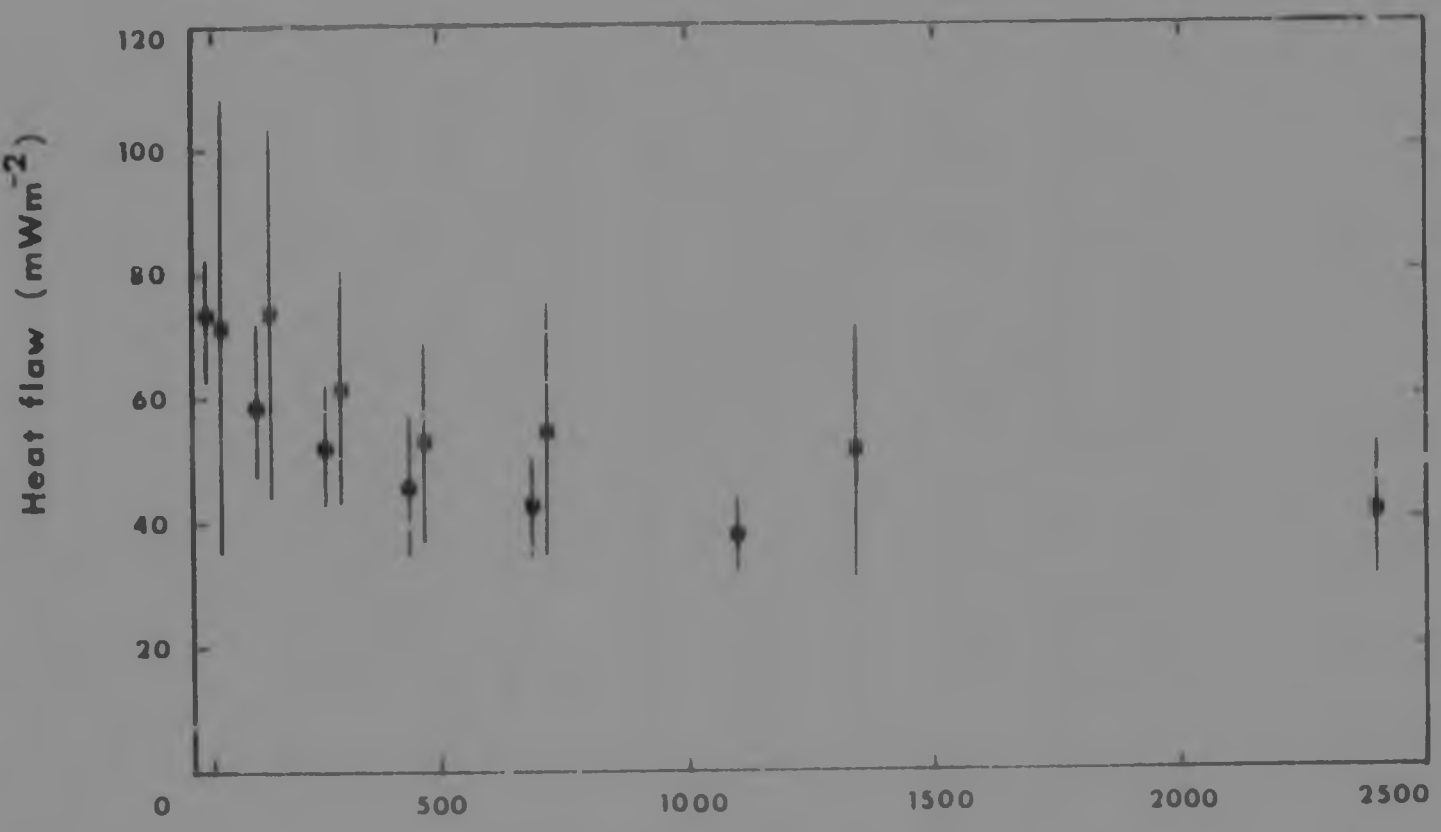

FIGURE 1.1 Mean surface heat flow and standard deviation in continental age provinces after Polyak and Smirnov (1968) - dots, and Vitorello and Pollack (1980) - squares. Data points are offset by -15 m.y. and +15 m.y. respectively from the mean age.

data summarized by Polyak and Smirnov (1968) and Vitorello and Pollack (1980) [illegible] is partly a result of climatic perturbations that have [illegible] recent heat flow measurements.

The overall decline of heat flow with age has been discussed by Jessop and Lewis (1978), Vitorello and Pollack (1980) and England and Richardson (1980) and a number of physical models have been provided. In terms of these models the variability in the data is large. Much of the scatter may be attributed to uncertainties in tectonic age and near surface perturbations. A fundamental problem is the variability of tectonothermal processes. While young orogenic belts are generally characterized by high heat flow this is not always the case. Heat flow in the Sierra Nevada is abnormally low (Roy et al, 1968a) and this has been attributed to subduction of cold oceanic lithosphere below the North American continent during late Mesozoic-early Cenozoic times (Roy et al, 1972). Similar belts of abnormal heat flow have been observed in zones of active crustal convergence in the western Pacific (Watanabe et al, 1977). It will be shown below that a particularly important cause of variation in heat flow is the variation of crustal radiogenic heat production.

The continental surface heat flow-age (q_o-t) relationship bears only a superficial resemblance to the oceanic distribution (Appendix 1, Figures I-1 and I-4). In continents, equilibrium is attained after 500-1000 m.y. and the time constant for the age dependence of heat flow is roughly five times greater than that of oceanic heat flow. Although conductive cooling may be the dominant thermal process in early post-orogenic times, England and Richardson (1980) showed that for lithosphere of the

order of 100-200 km thick excessive temperature perturbations are required to match the q_o-t distribution. One or more other time-dependent process is necessary.

Heat production from the radioactive decay of the isotopes ^{238}U, ^{235}U, ^{232}Th and ^{40}K concentrated in continental crust constitutes an important component of the surface heat flow. It was not possible to make really quantitive estimates of its magnitude until Birch *et al* (1968) and Lachenbruch (1968) recognized a simple linear relationship between surface heat flow (q_o) and near-surface heat production (A_o) in plutonic rocks in the U.S.A.:

$$q_o = q_r + bA_o \qquad (1.14)$$

Subsequently, Roy *et al* (1968a) demonstrated that three geologically distinct regions (eastern U.S.A., Basin and Range Province* and Sierra Nevada) are characterized by significantly different linear relationships (Figure 1.2) and thus introduced the concept of 'heat flow provinces'. Each province is defined by different values of the constants q_r and b which are generally referred to as 'reduced heat flow' and 'depth parameter' respectively. Similar results have been obtained in igneous, metamorphic and even slightly metamorphosed sedimentary terranes. To date there are seventeen recognized heat flow provinces (Vitorello and Pollack, 1980).

Equation 1.14 may be modelled in terms of the vertical distribution of radiogenic heat sources. Roy *et al* (1968a) envisaged a model

---

* Recent measurements in the Basin and Range Province have failed to substantiate a linear q_o-A_o relationship there (Lachenbruch and Sass, 1977).

consisting of a radiogenically enriched upper crust (z<b) in which the heat production is constant ($A(z) = A_0$), and a lower depleted crust (z>b) in which A is zero or negligible (Figure 1.3a); the heat flow across the surface z = b is constant ($=q_c$) and variations in q_o are caused by lateral variations in A_o.

Lachenbruch (1968, 1970) showed that while this and numerous other source distributions can satisfy equation 1.1a (Figure 1.3 shows three geologically feasible examples) only an exponential distribution of the form

$$A(z) = A_o \exp(-z/D) \qquad [1.13]$$

can satisfy differential problem. Here D describes the rate of decrease of A(z) with depth (or the degree of fractionation of U, Th and K) and q_c is the uniform heat flow from below the depth $z = z_r$. Although z_r is unknown it must be large enough such that $A(z_r)$ is negligible, or $bA/z_r \ll q_c$. If this were not the case lateral variations of the heat production at this depth would cause departures from equation 1.13.

Attempts to test these models have not proved conclusive. Geochemical evidence suggests a general upward concentration of U, Th and K in the crust (Lambert and Heier, 1967) and profiles in deep boreholes (Lachenbruch and Bunker, 1971) and vertical sections in the eastern Alps (Hawkesworth, 1974), Idaho Batholith (Swanberg, 1972) and Vredefort dome (Hart et al, 1970) favour a general decrease in A(z). While igneous and metamorphic processes tend to concentrate heat producing elements in the upper crust it is unreasonable to expect actual distributions to conform with mathematical models. The scatter

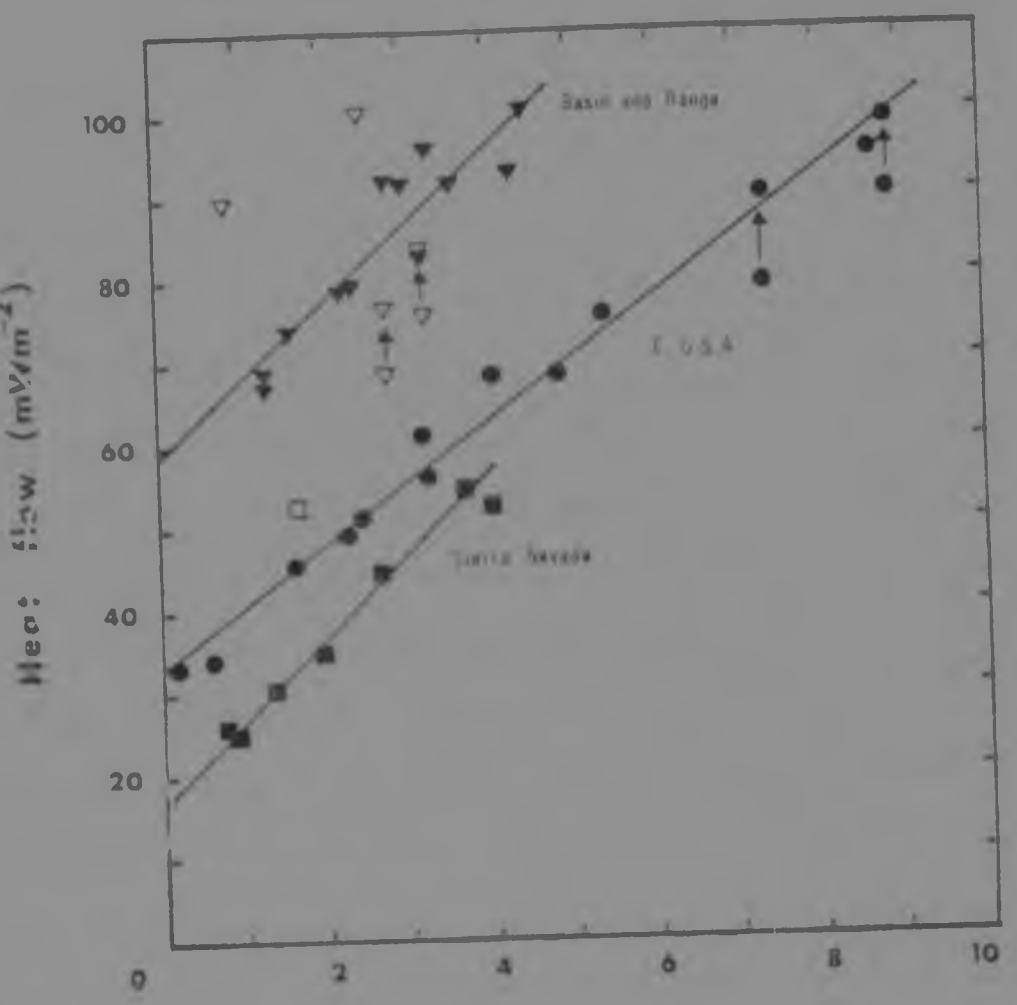

FIGURE 1.2 Heat flow - heat production relationships in the eastern USA, Sierra Nevada and Basin and Range Province (after Roy et al, 1968a).

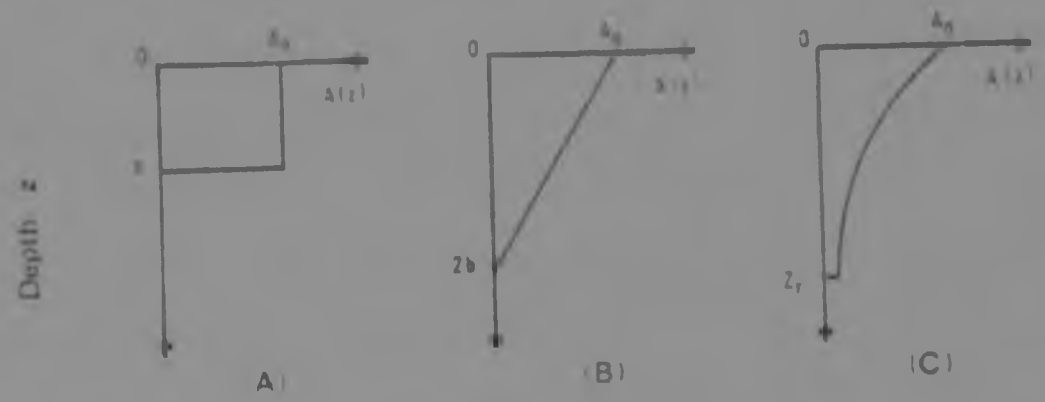

FIGURE 1.3 Three models for the vertical distribution of heat sources in the continental crust.

In q_o-A_o plots can accommodate considerable lateral and vertical variations in heat production (Allis, 1979).

Differential erosion of the crust can account for local differences in surface heat production and heat flow and therefore explain much of the scatter in the q_o-t relationship (Figure 1.1). On the average, older terranes are eroded to deeper levels than young orogenic belts and the resultant decrease in heat generated within the crust may make a significant contribution to the decrease of mean surface heat flow with age. Richardson (1975) demonstrated that an exponentially decreasing rate of erosion considerably lengthens the time dependence of surface heat flow and could, unaided, account for the entire decrease of heat flow with age.

Jessop and Lewis (1978) showed that a second important factor controlling the decrease of crustal heat production with age is the natural radioactive decay of U, Th and K. In essence, this model supposes that, on the average, comparable crustal segments received approximately equal quantities of these elements during orogeny; natural decay has resulted in smaller present-day heat productions in Archaean terranes relative to those which formed more recently. This is likely to be the overriding cause of low crustal radiogenic heat input in ancient regions which are not deeply eroded.

A feasible explanation for the decrease of heat flow with age is a combination of the diminution of the crustal radiogenic component and conductive cooling after orogenesis. Pollack and Chapman (1977a) demonstrated that the reduced heat flow is simply related to the mean surface heat flow in most established heat flow provinces:

$$q_s = 0.6q_c \qquad (1.16)$$

Although this relationship is based on a limited data collection (figure 1.4) it suggests that approximately 40% of the surface heat flow is derived from radiogenic sources in the upper crust and 60% from below. This relationship is independent of tectonic age which implies that the reduced heat flow decreases with a similar time constant to the surface heat flow.

Most models for the thermal evolution of continental lithosphere assume that the decrease of reduced heat flow is governed by conductive cooling after transient thermal events (Crough and Thompson, 1976; Pollack and Chapman, 1977a; Vitorello and Pollack, 1980). Although reduced heat flow-age data are too few to adequately constrain the models, the time constant is considerably longer than that characterizing the decay of surface heat flow. As noted previously, this requires excessive initial temperatures for lithosphere of normal thickness. Vitorello and Pollack (1980) suggested a model which requires stable (Precambrian) lithospheric thicknesses in excess of 300 km as well as a substantial radiogenic contribution from the sub-crustal lithosphere which would be necessary to ensure a reasonably low temperature at the base of the lithosphere.

A radically different approach was taken by England and Richardson (1980) who claimed that while uplift and erosion reduce the radiogenic contribution from the crust they also steepen near surface thermal gradients and therefore augment the heat flow. Thermal effects of uplift and erosion can increase the effective time constant of surface and reduced heat flow and excessive thermal perturbations or lithospheric thicknesses are not necessary. Even if these are second order effects,

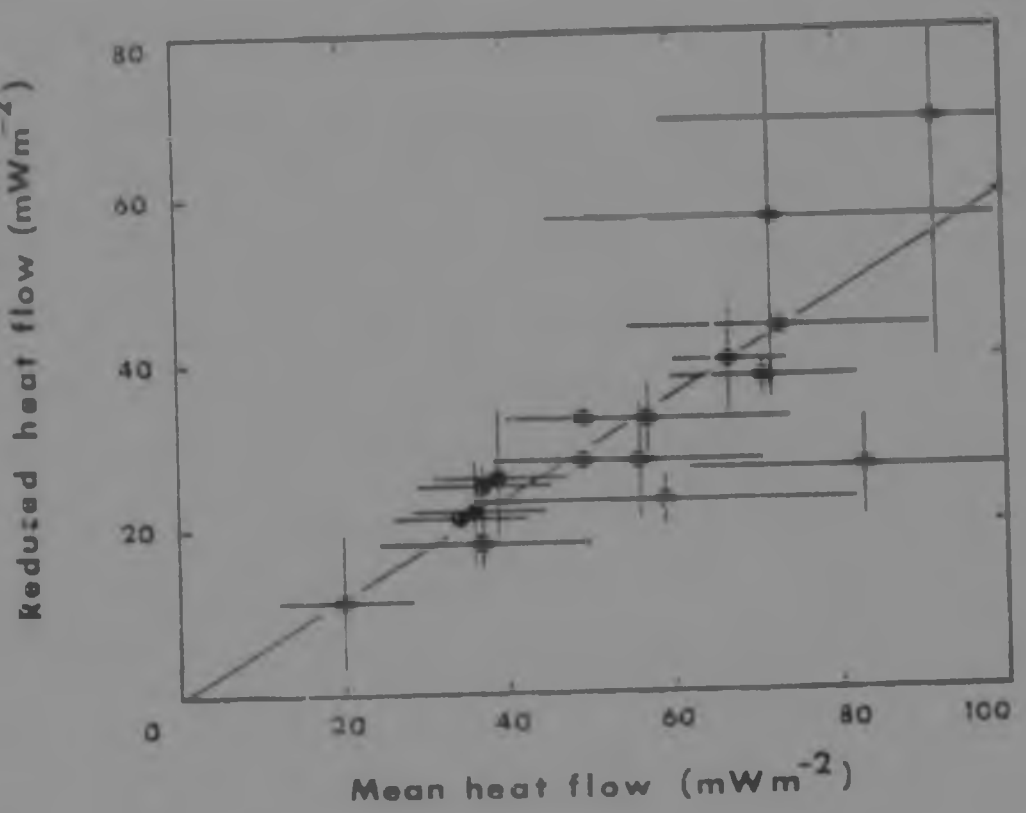

FIGURE 1.4 Reduced heat flow-mean surface heat flow relationship for seventeen heat flow provinces (after Vitorello and Pollack, 1980).

equating the reduced heat flow in young orogenic zones with the deep conductive flux may be incorrect.

1.3 Heat flow in South Africa

A discussion here of heat flow variations in South Africa would be premature. It suffices to note that most of the existing data (summarized by Cleta and van Rooyen, 1969) are from the Kaapvaal Craton, a granite greenstone terrane older than 2500 m.y., and the gneissic Namaqua-Natal Mobile Belt, older than 1000 m.y., to the south and west. The mean surface heat flow through the craton conforms with the continental q_o-A_o relationship while that through the Namaqua-Natal Mobile Belt is 25-50% higher than the mean for equivalent age provinces elsewhere. Although there are no coupled q_o-A_o data, heat production studies on basement rocks from the centre of the craton suggest that, there, the crustal radiogenic contribution is relatively high and the mantle heat flow below average (Nicolaysen et al, 1981).

Exploratory drilling projects in the craton and the Namaqua (western) section of the mobile belt have presented an opportunity to obtain a more complete coverage of heat flow data in these regions. New measurements were made with the following major objectives in mind:

(1) to study variations of surface heat flow within these tectonic domains and determine whether they can be related to variations in near-surface heat production;

(2) to determine whether the difference in mean heat flow between these regions can be attributed to mean differences in crustal radioactivity and whether the above average heat flow in the

Zimbaqua Mobile Belt is due to enhanced upper-crustal radiogenic heat input or to subcrustal thermal processes;

(3) to obtain a second estimate for the mantle heat flux below the Kaapvaal Craton in order to test the conclusions of Sinclayson et al (1987) and investigate its implications for the thermal structure of the Kaapvaal lithosphere.

2 TECTONIC AND GEOCHRONOLOGICAL FRAMEWORK OF SOUTHERN AFRICA

In the discussion of continental heat flow it was demonstrated that geologically distinct regions have distinct heat flow patterns. This chapter will introduce the major tectonic elements of which southern Africa is comprised. Some details of the geology within some of these provinces will also be discussed in order to provide a basis for understanding observed regional variations of heat flow and heat production.

General descriptions of the geology of southern Africa are given by Haughton (1969) and Truswell (1970, and reviews of the structural development of the sub-continent by Clifford (1970) and Kröner (1977a, 1977b). There has not been a comprehensive summary of the geochronological data since that of Burger and Coertze (1973) and much of the following outline is based on data accumulated by colleagues at the Bernard Price Institute for Geophysical Research during the past few years*.

The approximate extent of the major tectonic provinces that can be distinguished in southern Africa is shown in Figure 2.1. In only a few areas are the boundaries between the provinces clearly defined. In many regions they are hidden by younger sedimentary cover and even where mapping has been possible the interprovincial relationships remain obscure or are of a transitional nature. Geophysical data (such as aeromagnetic and gravity data) are available and they could assist in delineation of tectonic units, but they have been little exploited. The general features

---

* I am grateful to E S Barton, J M Barton and H L Allsopp for helpful discussions.

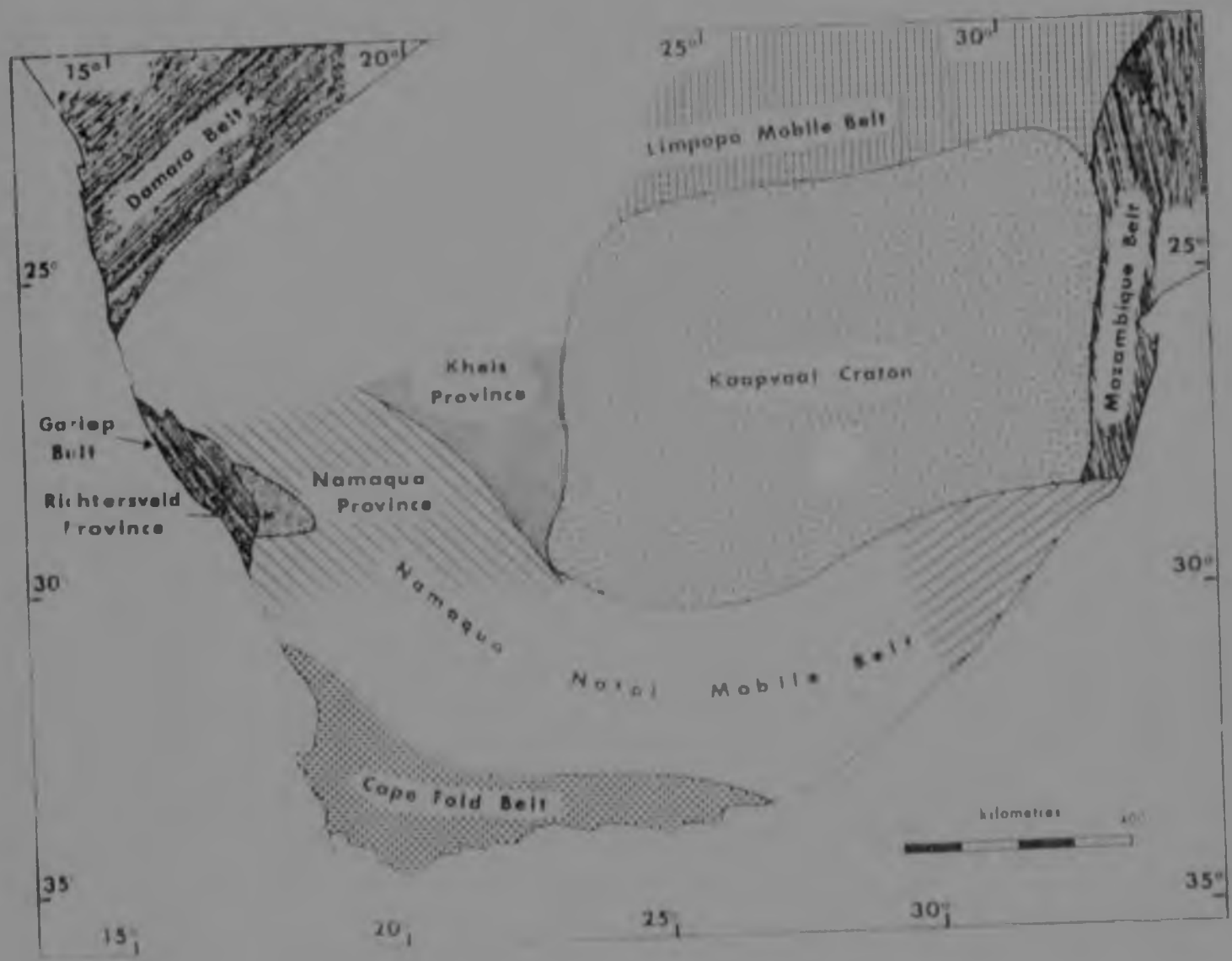

[illegible] the major basement provinces of southern Africa compiled from maps presented by Hunter (1976), Kröner and Blignault (1976), [illegible]

shown in figure 2.1 do however summarize the present understanding of the major crustal provinces of southern Africa and they provide a framework for further discussion.

These tectonic stories are characterized by distinctive assemblages of lithology, deformation, metamorphism and [illegible]. The Kaapvaal Craton, like [illegible] blocks of stable Archaean continental crust, [illegible] affected by younger [illegible] orogenic zones distinguished by [illegible] of rocks, high grade metamorphism, igneous activity and [illegible] accumulation of geosynclinal sediments. These are generally characterized by younger radiometric ages than the cratons, but [illegible] ages are preserved within the Limpopo Mobile Belt. The mobile belts formed by a variety of tectonic processes, analogous to those occurring at modern plate boundaries, and these differences are reflected in their tectonic character.

The main characteristics of the major tectonic provinces [illegible] in chronological order starting with the Kaapvaal Craton and the Limpopo Mobile Belt. The Kaapvaal Craton, [illegible] the most important bearing on [illegible] detailed attention.

2.2 Kaapvaal Craton

The Kaapvaal Craton consists of [illegible] granite-greenstone basement complex which is overlain by younger Pre-Cambrian platform strata. The distribution of the basement complex is shown in figure 2.2 [illegible] areas,

notably the Barberton Mountain Land and the Vredefort and Johannesburg domes, have been the subject of intensive study but many aspects are poorly understood. In later chapters it will be shown that the basis from the crust is reasonably constant and it is not expedient to review the many localized studies in detail. This summary, drawn largely from general accounts given by Anhaeusser et al (1969), Truswell (1970), Anhaeusser (1973), Hunter (1974a, 1974b) and Kröner (1978b), attempts to give an overview of the general geology.

The Kaapvaal basement is a complex suite of predominantly granitic rocks which were generated and deformed during a long history of discrete crust forming events between 3400 and 2600 m.y. The rock compositions vary from tonalitic and trondhjemitic to granitic; granites, migmatites and gneisses are present. Scattered remnants of volcano-sedimentary sequences are preserved within the granitic terrane. These remnants are usually strongly deformed and metamorphosed, but sometimes little altered. They are collectively referred to as greenstone belts. Geochronological data (Hart et al, 1981a; Barton, 1981) indicate that the craton developed during several cycles of tectonism. The greenstone belts and its underlying gneissic basement are among the oldest rocks present and yield radiometric ages of up to 3500 m.y. Although older ages have not been identified positively, isotopic data from the Vredefort dome suggest that the basement gneisses there may be as old as 3800 m.y. Volcanic and sedimentary rocks of the Pongola Supergroup were deposited in the extreme southeast of the craton approximately 2900 m.y. ago. Significant amounts of granitic material were formed on the craton during several tectonothermal episodes, particularly within the age ranges 3550 – 3370 m.y., 3250 – 3050 m.y., 2950 – 2750 m.y. and 2600 – 2500 m.y.

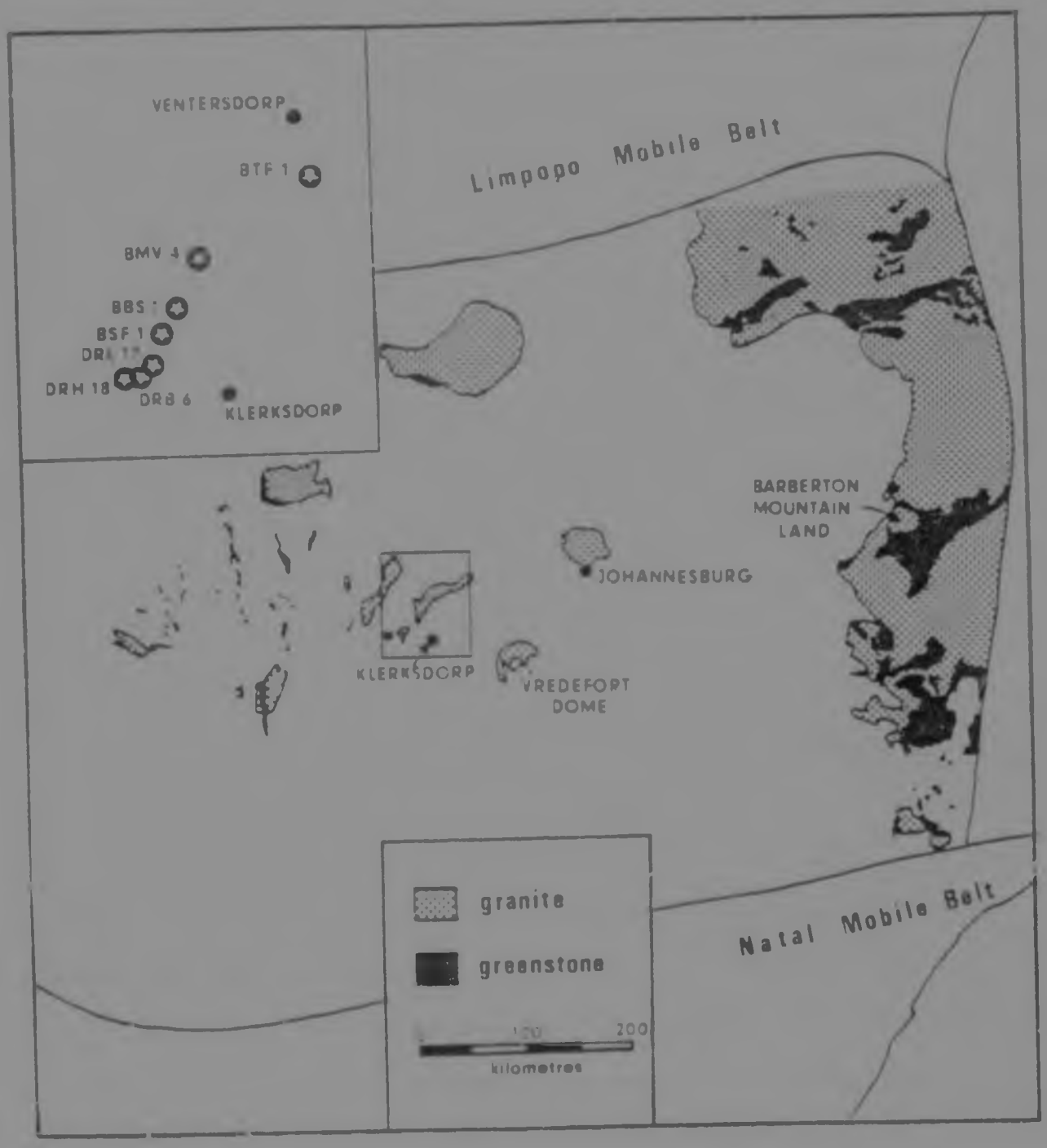

FIGURE 2.2 Distribution of granite-greenstone basement on the Kaapvaal Craton (after Truswell, 1970). Inset shows the localities of the seven new heat flow stations (stars) near Klerksdorp.

Since [illegible] m.y. ago the Kaapvaal craton has remained a relatively stable unit and gentle warping tectonics persisted for the next few hundred million years. This was initiated shortly before the final episode of plutonism ceased and led to the development of major basins and the accumulation of thick sedimentary and volcanic successions. Deposition may have begun as early as [illegible] m.y. ago in the Witwatersrand basin (south of Johannesburg) where the succession consists of the predominantly volcanic Dominion Reef Supergroup at the base, succeeded by the sedimentary Witwatersrand Supergroup and the volcanosedimentary Ventersdorp Supergroup. The available radiometric age data indicate that these units were deposited within the time interval 2900 - 2300 m.y. ago. The Ventersdorp Supergroup is overlain by volcanic and sedimentary rocks of the Transvaal Supergroup (2300 - 2100 m.y.), but the only depository of these rocks was the Transvaal basin (north of Johannesburg). Rocks of the Waterberg Supergroup (1950 - 1800 m.y. old) were deposited in a younger basin further north which overlaps onto the Limpopo Mobile Belt.

Further tectonism, but more localised events occurred on the craton between 2100 and 1950 m.y. ago. These were the intrusion of the Bushveld Igneous Complex into the succession in the Transvaal basin, the formation of the Vredefort dome, a cryptoexplosion structure, in the centre of the Witwatersrand basin, and the formation of the Johannesburg dome.

2.2 Limpopo Mobile Belt

The Limpopo Mobile Belt is a zone of polyphase metamorphism and deformation which separates the Kaapvaal Craton from the Rhodesian Craton in the north (Figures 2.1 and 2.2). It evolved during the same time interval as the Kaapvaal Craton but the mode of formation, intracontinental rifting,

and subsequent episodes of deformation have resulted in its distinctive tectonic character. The following summary is based on accounts given by Mason (1973), Barton and Key (1981) and Barton (1981).

The mobile belt consists of three zones, a fault-bounded Central Zone and Northern and Southern Marginal Zones. The Central Zone consists of a metamorphic basement gneiss complex, older than 3790 m.y., which is overlain by a supercrustal succession. The basement gneisses are the oldest identified rocks in southern Africa and probably represent part of the ancient nucleus on which the Kaapvaal and Rhodesian Cratons grew. Deposition of the supracrustal rocks was preceded by the emplacement of gabbroic dykes ~3870 m.y. ago; this age is though to mark the establishment of the mobile belt (Barton and Key, 1981). The supracrustal succession was intruded by the Messina Layered Intrusion ~3270 m.y. ago and subsequently deformed during four major events between 3270 and 3130 m.y. ago, ~3150 m.y. ago, between 2700 and 2600 m.y. ago, and ~2600 m.y. ago. Mafic dyke emplacement occurred ~2600 m.y. ago and some granitic plutonism ~2700 m.y. ago. Major tectonothermal activity ceased after the last period of deformation approximately 2600 m.y. ago.

The marginal zones consist predominantly of leucocratic gneisses but include remnants of metavolcanic and metasedimentary rocks; they represent deformed and metamorphosed equivalents of the adjacent granite-greenstone terranes. The degree of metamorphism (characteristically granulite facies within the mobile belt) and deformation decrease towards the cratons and the contact of the Southern Marginal Zone with the Kaapvaal Craton is transitional. Roughly east-west orientated shearing resulted in the pronounced structural grain of the marginal zones. Metamorphism was sufficiently intense to destroy the radiometric (Rb-Sr) record of the

early tectonic history and the oldest ages obtained so far in the Northern and Southern Marginal Zones are 2810 m.y. and 2650 m.y. Some post-tectonic granite plutons were emplaced approximately 2130 m.y. ago in the Southern Marginal Zone.

Widespread mineral ages of ~1950 m.y. reflect terminal uplift and erosion of the mobile belt. Since approximately 2000 m.y. ago the Limpopo Mobile Belt and the Kaapvaal and Rhodesian Cratons have acted as a tectonically stable continental unit.

2.4 Kheis Province

The Kheis Province is a supracrustal tectonic unit which is situated between the Kaapvaal Craton and Namaqua Province (Figures 2.1 and 2.3). It is characterized by a distinctive stratigraphy, style of deformation and metamorphic grade and by isotopic ages which are intermediate between those predominating in the Kaapvaal Craton and Namaqua Province. The following summary of the geology describes the major changes that would be encountered in a traverse from the craton, across the Kheis Province and into the Namaqua Province (see Figure 2.3). Rocks of similar antiquity and tectonic character to those in the Kheis Province occur in the Richtersveld Province in the west (Figure 2.3) and these will be discussed in Section 2.5 before dealing with the Namaqua Province as a whole (Section 2.6). Most of this account was drawn from Vajner (1974), Botha _et al_ (1976, 1977), Geringer and Botha (1977), Botha and Grobler (1979), Stowe (1981) and Barton and Burger (1981).

On the western margin of the Kaapvaal Craton, the ~3000 m.y. old basement and 2600-2200 m.y. old correlates of the Ventersdorp and Transvaal Super-

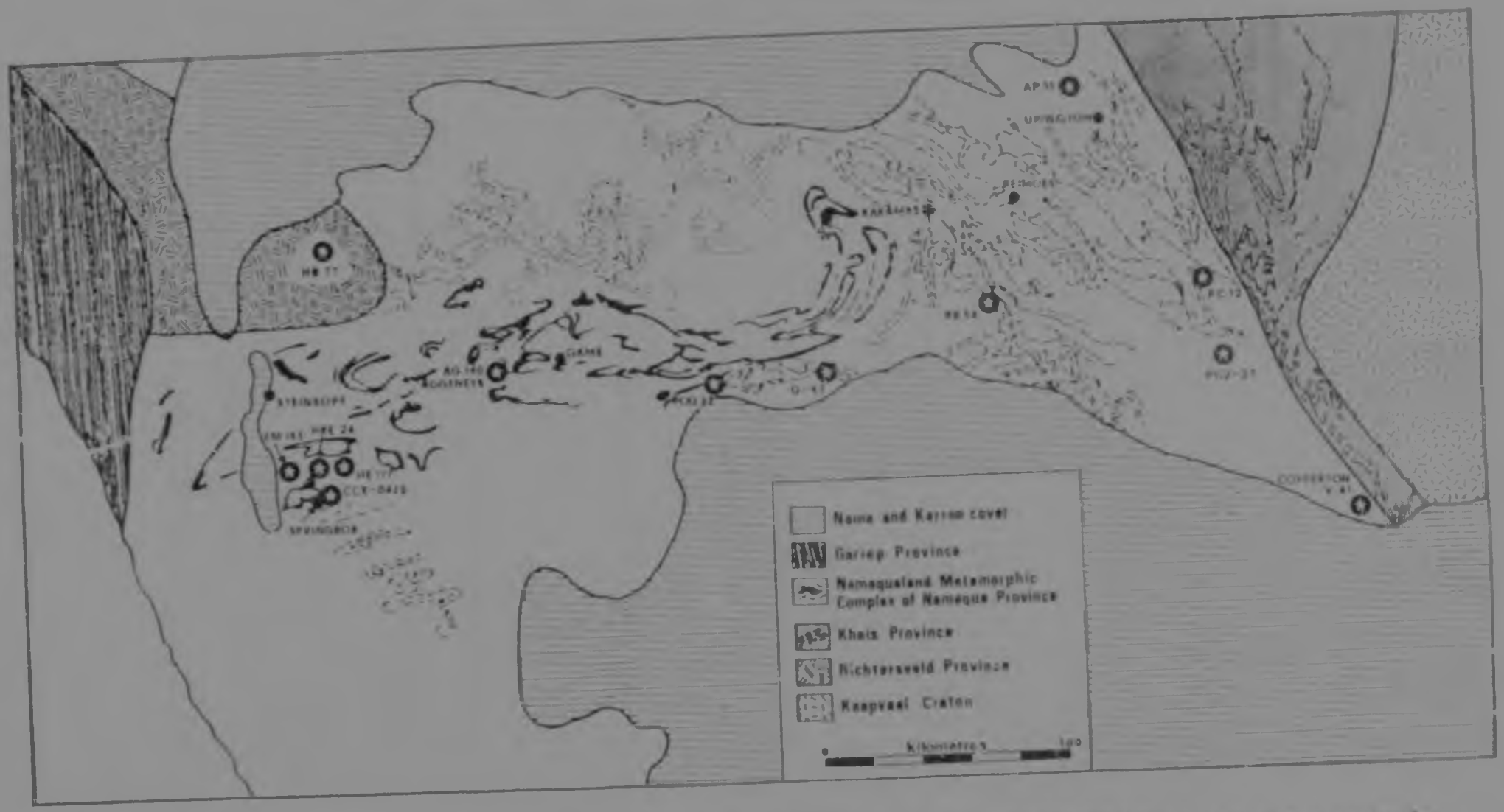

FIGURE 2.3 Generalized geology of the northwest Cape Province, showing the distribution of the major tectonic provinces (modified after Viljoen et al, 1975). Stars indicate the localities of new heat flow stations.

groups are overlain unconformably by the strata of the Matsap Group. These rocks can be traced westwards across the Kaapvaal-Kheis boundary where there is a marked change in style of deformation from open folds on the craton to diagonal northwest trending folds which are characteristic of the Kheis Province (see Figure 2.1). Radiometric age data are available from the Hartley andesite, a member of the Matsap Group: measurements by Crampton (1974) indicate an age of 2026 ± 180 m.y. while recent, more refined measurements are indicating an age of ~1850 m.y. (R A Armstrong, personal communication).

Most of the area represented as the Kheis Province in Figure 2.3 is occupied by deformed and metamorphosed volcano-sedimentary successions including the Grohiershoop, Dagbreek, Sultanaoord and Wilgenhoutsdrif Formations. These are collectively referred to as the Griqualand West sequence by Stowe (1981). Stratigraphic relationships between these formations are controversial because of intense shearing and thrusting and because of the poor exposure. However, the Wilgenhoutsdrif Formation overlies the Sultanaoord and Grohiershoop formations unconformably (Stowe, 1981) and appears to be younger.

Lithological correlations have been made between the Griqualand West sequence and the Matsap Group of the craton (eg. Vajner, 1974; Botha *et al*, 1976) and if these correlations are correct the maximum age of the Griqualand West sequence is ~2000 m.y. There are no reliable deposition ages for individual formations but a Rb-Sr errorchron, supported by U-Pb zircon data, suggests an age of ~1900-1900 m.y. for the Wilgenhoutsdrif Formation (Barton and Burger, 1981). The broad characteristics of initial $^{87}Sr/^{86}Sr$ ratio versus apparent age data from the Griqualand West sequence indicate that none of the rocks examined to date is derived from

a source which is older than 1300 m.y. (Barton and Burger, 1981). Note however that this cannot be reconciled with an age of ~1850 m.y. implied by the lithological correlation of the Griquatown West sequence with the Matsap Group.

The most important deformation event (F_1) that can be recognised in the Kheis Province resulted in isoclinal west-northwest trending folds (clearly indicated in Figure 2.1). These can be traced into the supracrustal rocks along the western margin of the Kaapvaal Craton but they become open and die out rapidly further east. Folding was accompanied by low grade regional metamorphism.

A second episode of deformation (F_2) can be recognised along the western margin of the Kheis Province. This is considered to reflect overprinting of the main Namaqua event (Stowe, 1981) which is also reflected in regional metamorphism and granitic emplacement (see Section 2.6).

In the region of the Kheis-Namaqua boundary (Figure 2.3) the pre-tectonic sequences are overlain by the Koras Group, an undeformed volcano-sedimentary succession which was deposited in graben-like basins between 1180 and 1050 m.y. (Botha et al, 1979; R S Barton, personal communication). These rocks were not affected by the main period of Namaqua deformation and 1180 m.y. represents a minimum age for this event. Post-tectonic F_2 intrusive rocks yield emplacement ages in the range 1100-1050 m.y.; some of these may be co-genetic with volcanic rocks of the Koras Group (Geringer and Botha, 1976; Barton and Burger, 1981).

Major northwest striking faults and shear zones that intersect the area are a late stage development and were partly responsible for the

juxtaposition of the high grade Namaqua Province and the lower grade Kheis Province. In Figure 2.1 the boundary between the provinces co-incides with one of these, the Brakbosch fault zone (after Viljoen et al, 1973). Shearing and faulting are partly contemporaneous with deposition of the Koras Group (Stowe, 1981), and the emplacement of late stage pegmatites and terminal uplift which are reflected in mineral ages of ~1000 m.y. (Nicolaysen and Burger, 1963).

2.3 Richtersveld Province

The Richtersveld Province, situated in the western part of Figure 2.1, is an upper crustal tectonic domain and consists of a volcano-sedimentary succession and a suite of intrusive rocks, both of early-middle Proterozoic age. The province is characterized by low grade metamorphism and an associated regional foliation. Details of the geology are given by Blignault (1974, 1977) and Reid (1977) and the geochronology by Reid (1979a, 1979b).

The predominantly calc-alkaline volcanic rocks and arenaceous sediments, previously correlated with rocks in the Kheis Province, are referred to as the Orange River Group. They are the oldest rocks recognized in the province and lavas outcropping in the east (the Haib Volcanic Subgroup) were extruded approximately 2050 m.y. ago (Reid, 1979a). The succession is extensively intruded by the co-genetic granitoids and gabbroids of the Vioolsdrif Igneous Suite, dated at approximately 1900-1750 m.y. (Reid, 1979b).

Discontinuous foliation is developed on a regional scale and may be related to east-west trending macroscopic folds in the east of the province. Low

grade metamorphism associated with this deformation characterizes the entire province. The intensity of deformation and metamorphism increases rapidly at the boundary with the Namaqua Province.

There is an apparent continuity of the regional pattern with that in the Namaqua Province. Accumulating isotopic evidence, particularly from the Steinkopf region south of the Pietersveld Province (see Figure 2.3), suggests that the main penetrative deformation and metamorphism are considerably older than the 1130-1050 m.y. old Namaqua tectogenesis and possibly as old as 1850 m.y. (Barton et al, 1981).

The western boundary of the province is marked by a zone of intense shearing and retrogression related to the development of the Pan-African Gariep orogenic belt.

2.6 Namaqua Province (Namaqua Mobile Belt)

The Namaqua Province covers a wide area including Namaqualand, Bushmanland and southern Namibia (Figure 2.3) and is underlain by granites, gneisses and deformed and metamorphosed remnants of supracrustal rocks. These are collectively referred to as the Namaqualand Metamorphic Complex. Major tectonic activity occurred between approximately 1300 and 1000 m.y. ago (Barton and Burger, 1981). This is reflected in several periods of deformation, the most important of which was accompanied by regional metamorphism and widespread granite emplacement. Events of this age had little proven effect on adjacent tectonic provinces except the western margin of the Kheis Province (Section 2.4), and, geographically, the 'Namaqua Province' and 'Namaqua Mobile Belt' (the entire area affected by 1300-1000 m.y. old orogeny) are almost identical.

...research has been carried out in two main areas, in the west ... quite recently. ... Miller et al. (1975) has ... form the basis of figure 2.5. It is ... below the numerous localized studies. ... the greater antiquity sources of ... is noted in the Nicolaysen and Burger ... (1975), Ellignault et al (1974), Ellignault ... Miller et al (1975), Botha et al ... Ettinger and Botha (1977), Stowe ...

... Province in the eastern part of ... figure 2.5 may be considered to be the marginal ... Burger, 1981). It is occupied by ... metamorphosed supracrustal rocks which comprise the Koranna- ... gneisses, schists, amphibolites, quartzites, ... granulites and ultramafic rocks are interlayered with pre-tectonic ... very gneissose, and are intruded and sometimes intensively ... syntectonic granites and post-tectonic granites and charnockitic ... the Koranna-land sequence has not been ...

... the area into several ... characterized by distinctive strati- ... grade (Stowe, 1981). As a result, ... between different rock units are ... in degree of metamorphism

and information the stratigraphic and compositional relationships of the Korannaland sequence with the Griqualand West sequence to the east, Province (Figure 2.3, Section 2.2) are also uncertain.

Four main episodes of folding have been recognised. [illegible] has been provisionally correlated with the F_1 folding in the [illegible] Province (Stowe, 1981), but has been largely obliterated by younger [illegible]. The most important folds (F_2) [illegible] are generally [illegible] recumbent and inclined in the western part of the region [illegible] become open and die out rapidly near the [illegible] boundary. Although fold characteristics differ [illegible] sectional segments, the trend is generally northwest throughout the [illegible] area except in the west where it is east-west. In Figure 2.3 a general curvilinear [illegible] manifested but the pattern is complicated by refolding of [illegible] Open, east to northeast trending F_3 folds are [illegible] F_2 folds occur in the western part of the region [illegible] folding of earlier structures has resulted in interference [illegible] of which are shown in Figure 2.3. F_4 folds [illegible] developed on very possibly genetically related to earlier [illegible] (Stowe, 1981).

Regional metamorphism was [illegible] with, or [illegible] F_2 folding (Stowe, 1981). [illegible] grade varies from mid grade, [illegible] granulite facies, in the west to greenschist facies [illegible] boundary. Major changes in metamorphic grade occur [illegible] major shear zones.

The marginal zone of the Namaqua Province is characterised by [illegible] ages in the range 1300-1000 m.y. [illegible] the complex geology

and radiometric resetting it is difficult to distinguish between specific events. The oldest ages come from metavolcanic rocks along the eastern margin of the province. Barton and Burger (1981) obtained ages close to 1300 m.y. for the Jannelspan Formation in the Upington district and Cornell (1975) obtained an age of 1317 m.y. for volcanic rocks from Copperton (see Figure 2.3). A similar age is implied by Pb isotope compositions of galenas from stratiform deposits at Copperton (Köppel, 1980). On the basis of these data and Sr and Pb evolution models Barton and Burger (1981) concluded that the supracrustal rocks were deposited between 1500 m.y. and 1300 m.y. in this region. The main Namaqua deformation (D_2) is bracketed by this age of ~1300 m.y. and the maximum age of the Koras Group, ~1180 m.y. (Section 3.6), and is also reflected in metamorphic ages of ~1270 m.y. Post-tectonic intrusive rocks yield ages of ~1130-1050 m.y.

The western part of the Namaqua Province, the area from Kakamas to Springbok (Figure 2.1), is underlain by a distinct group of deformed and metamorphosed supracrustal rocks (Willson et al, 1975) which are referred to as the Bushmanland Group. Prominent outcrops of these are indicated in black in Figure 2.3. The supracrustal rocks were intruded by similar pre-, syn- and post-tectonic rocks to those in the east. Although the existence of a basement to the supracrustal rocks has been postulated (Moore, 1977) there is no unequivocal evidence for this.

The age of the Bushmanland Group and its relationship with the Korannaland sequence are contentious. The Bushmanland Group has been correlated with the ~2000 m.y. old Orange River Group in the Richtersveld Province (Blignault, 1981); this correlation was largely based on lithological similarities and the fact that rocks of the Orange River Group can be

traced southwards and southwestwards out of the Richtersveld Province. Isotope studies have shown that ages equivalent to those of the Haib-Vioolsdrif suite (2000-1750 m.y.) have been preserved in the Steinkopf region in western Namaqualand (Barton et al, 1981). On the basis of Pb isotope compositions in galenas from stratiform ore deposits at Aggeneys,Gams and Copperton (see Figure 2.3 for localities), Köppel (1980) concluded that these deposits and their host rocks were deposited between 1500 m.y. and 1300 m.y. ago. Apparently conflicting evidence is reported by Reid (1981) who obtained model (T_{CHUR}) Sm-Nd ages of 2200-2000 m.y. for amphibolites in the Aggeneys-Gams region. The question of whether the Bushmanland Group is a comtemporary of the ~2000 m.y. old Orange River Group or the 1500-1300 m.y. old Korannaland sequence, or whether more than one generation exists, is one of the chief unsolved problems of the Namaqua Mobile Belt.

Most of the western part of the Namaqua Province had a similar and broadly contemporaneous post-depositional history as that in the east. Radiometric ages of ~1200 m.y. reflect the main period of deformation (which resulted in recumbent, isoclinal F_2 folds), regional metamorphism and syn-tectonic granite emplacement. Post-tectonic granites and charnockitic adamellites yield ages in the range 1150-1050 m.y. The early structures were deformed by open, upright F_3 folds and the net result is the generally east-west to northwest trending structures evident in Figure 2.3. Later refolding by monoclinal F_4 folds produced dome and basin structures such as those in the Okiep district. Major shear zones have east-west orientations and late brittle deformation resulted in faulting in at least three directions.

In summary, the eastern marginal zone of the Namaqua Mobile Belt was a

zone of new crust formation between 1500 and 1300 m.y. ago. Although similar ages are recorded in supracrustal rocks in the west, older (~2000 m.y. old) crust has also been preserved in the Steinkopf-Vioolsdrif region; the history of crustal evolution in this area is still enigmatic. The mobile belt is characterized by widespread radiometric ages in the range 1200-1000 m.y.; these reflect major episodes of deformation, metamorphism and magmatism, collectively referred to as the Namaqua tectogenesis. The entire province is characterized by mineral ages in the range 1000-900 m.y. and these reflect late stage pegmatite emplacement and terminal uplift and erosion.

A structurally similar group of metasediments, metavolcanic rocks, gneisses and granites outcrops in Natal (Figure 2.1). Radiometric ages of 1200-900 m.y. indicate that tectonic activity was largely synchronous with that in Namaqualand. Nicolayson and Burger (1969) suggested that these provinces may form a continuous orogenic belt, the Namaqua-Natal Mobile Belt, beneath the cover sequences of the Karroo Supergroup. This contention is supported by radiometric ages of ~1200-900 m.y. obtained for samples of basement gneiss recovered from boreholes which penetrate through the Karroo Supergroup in this region (see Burger and Coertze (1973) for data).

The geology of the Springbok-O'okiep-Nababeep district

The geology of the area surrounding Springbok (in the western part of the mobile belt, Figure 2.3) is described in more detail primarily to provide a background for understanding local heat flow variations that will be discussed in Chapter 6, but also to illustrate the complex interrelationships that exist in the Namaqualand Metamorphic Complex. This much simplified account is based on geological mapping by Benedict et al (1964).

The major geological units and the generalized structural succession are shown in Figures 2.4 and 2.5. The rocks may be divided into a suite of metamorphic supracrustal rocks and various intrusive bodies. The supracrustal rocks consist of a series of interlayered augen gneisses, granulites, metaquartzites and schists which, with pre-tectonic intrusive rocks, have been folded into open east-west trending folds (the Springbok antiform and the Ratelpoort synform). Benedict et al (1964) correlated these folds with the regional F_3 structures. They also recognised a co-axial but earlier set of isoclinal recumbent folds correlated with the regional F_2 folds. Clifford et al (1975) suggested that F_2 folding caused a tectonic duplication of the succession which consisted essentially of an augen gneiss, overlain by granulites, metaquartzites and schists.

The oldest intrusive rock is the Modderfontein gneiss which occupies the core of the Springbok antiform and which predates F_2 folding. The Concordia granite gneiss is a sheet-like body of the order of 1-2 km thick which was intruded along the structural succession. It is partly gneissic and partly unfoliated and is syn- to post-tectonic with respect to F_2 folding. The boundary between the Concordia gneiss and the underlying Nababeep gneiss is marked by a mixed zone where granitic material was injected into the Nababeep gneiss. The Rietberg granite occupies the Ratelpoort synform and is syn- to post-tectonic with respect to F_3 folding.

Rb-Sr and U-Pb isotopic measurements made by Clifford et al (1975) yielded the following pattern: the Modderfontein gneiss, gneissic components of the Concordia granite-gneiss and the supracrustal rocks yielded an age of 1187 m.y. and this was interpreted to reflect the

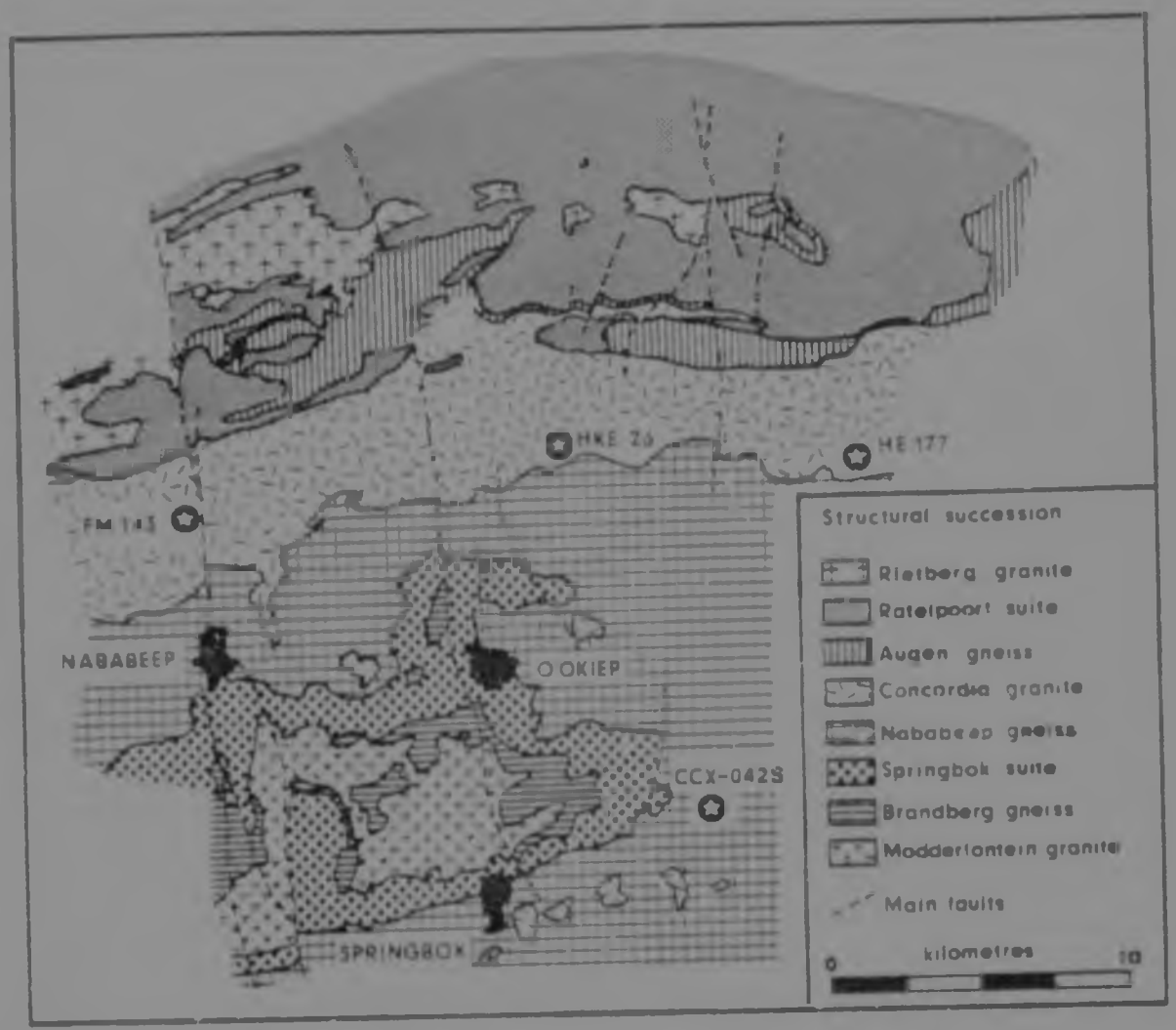

FIGURE 2.4 Generalized geology of the Springbok-O'okiep-Nababeep mining district (simplified after Benedict et al, 1964). Stars indicate the localities of new heat flow stations.

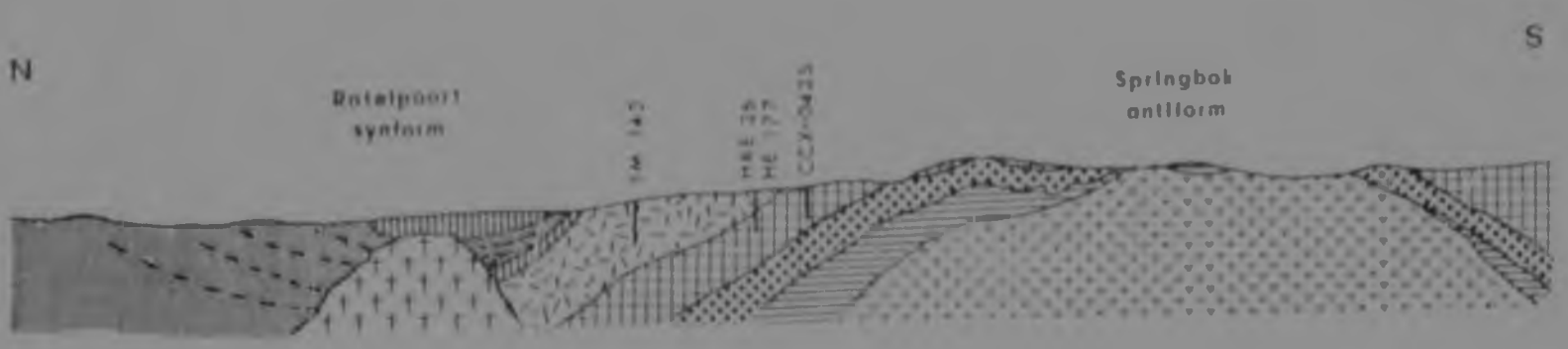

FIGURE 2.5 Semi-schematic north-south section through the Ratelpoort synform and Springbok antiform from the map of Benedict et al (1964) and based partly on the tectonic duplication model of Clifford et al (1975). The key is the same as in Figure 2.4. Borehole positions are shown schematically.

time of metamorphism. A slightly younger age (1140 m.y.) for the Kietberg granite and unfoliated Concordia granite was interpreted as an emplacement age. Later tectonic events were interpreted to reflect the intrusion of ore-bearing pegmatoid rocks and pegmatite emplacement (1000 - 850 m.y. ago).

2.7 Pan-African Orogenic Belts

The Pan-African orogenic belts are zones of tectonothermal activity characterized by radiometric ages in the range 650 - 450 m.y. In southern Africa they are represented by the Mozambique, Namaqua and Gariep Belts (Figure 2.1). Fragments of the Pan-African system are also preserved in the western Cape Province where deformed and metamorphosed sediments of the Malmesbury Group and its correlates are intruded by 600 - 500 m.y. old granitic plutons. The structural imprint of the Cape Fold Belt was later superimposed on the Malmesbury rocks.

2.8 Cape Fold Belt

The youngest orogenic episode to affect southern Africa is represented by the Cape Fold Belt (Figure 2.1). Folded sedimentary sequences of Palaeozoic and early Mesozoic age occur in two orthogonal belts, the north-south orientated Cedarberg trend in the west and the east-west Cape trend along the South coast. The earliest folds occur in the west where folding was initiated in mid-Carboniferous times, but the main phase of folding was Late Permian in age. Deformation was intense in the south, where overfolding to the north occurs, but the folds become gentle and fade out further north. Details of the geology are given by Haughton (1969) and Newton (1973).

only low grade metamorphism and volcanic insignificant igneous activity are associated with the Cape folding. However, only the northernmost foreland of the orogenic belt is represented in southern Africa and age related metamorphic and igneous rocks are preserved in extensions of the belt in South America and Antarctica (see Cox, 1979). Further large tracts of the fold belt are submerged below the waters of the Falkland Plateau and the Agulhas Bank.

2.9 Summary

The tectonic history of southern Africa may be summarised as follows (see Figure 2.1). The oldest tectonic units are the Kaapvaal Craton and the Limpopo Mobile Belt which developed in parallel between 3800 and 2500 m.y. ago; since 2500 m.y. they have been relatively stable but were the sites of accumulation of Pre-Cambrian platform strata. The Rhodes Province is underlain by low grade volcano-sedimentary successions which were deposited between 2000 m.y. and 1300 m.y. ago; the 1300-1000 m.y. old Namaqua Metamorphism had a subdued effect on the western margin of the province. The Richtersveld Province consists of a 2000 to 1750 m.y. old volcano-sedimentary succession and intrusive suite of rocks which underwent a mild deformational and metamorphic event; this is considerably older than the Namaqua metamorphism. The Namaqua Mobile Belt is a zone of predominantly 1500-1300 m.y. old crust which underwent 1300-1000 m.y. old metamorphism, deformation and plutonism; it is possibly linked with a similar terrane on the east coast to form the Namaqua-Natal Mobile Belt. Subsequent orogeneses resulted in the 650-450 m.y. old Pan African orogenic belts and finally the late Permian Cape Fold Belt. Later important episodes in the geological history of southern Africa include Jurassic Karoo volcanism, the disruption of Gondwanaland and Cretaceous kimberlite magmatism.

TEMPERATURE MEASUREMENTS IN BOREHOLES

3.1 Introduction

All measurements for the determination of heat flow were from boreholes made available by several mining companies. Temperature measurements were made in the Namaqua Mobile Belt in 1976 by the author and Dr S W Richardson of Oxford University and in the Kaapvaal Craton in 1979 by Dr Richardson. Although several dozen drilling sites were visited many boreholes were inaccessible due to caving at shallow depths and only fourteen in the Namaqua Mobile Belt and seven in the Kaapvaal Craton were deep enough and had sufficiently long depth intervals of undisturbed temperature gradient to be suitable for heat flow determination.

3.2 Apparatus and procedures

The apparatus used to measure temperatures in boreholes was constructed in the Department of Geology and Mineralogy, Oxford University, and has been discussed by Richardson and Oxburgh (1978). A thermistor probe was connected to a Wheatstone bridge network by a three-core cable. The cable was wound on a winch and lowered by means of a pulley wheel which was attached to a revolution counter (Figure 3.1).

The probe is illustrated in Figure 3.2. Four precision thermistors (Y.S.I. part number 44006) were connected as illustrated and encased at the tip of the probe. The total resistance of the probe was 2253 ohms at 25°C. The power dissipated by each thermistor depends on its resistance (i.e. temperature) but was at most 2×10^{-3} W. The



FIGURE 1. Field temperature measuring equipment. A: Wheatstone bridge. B: portable, manually operated winch. C: pulley wheel and counter.

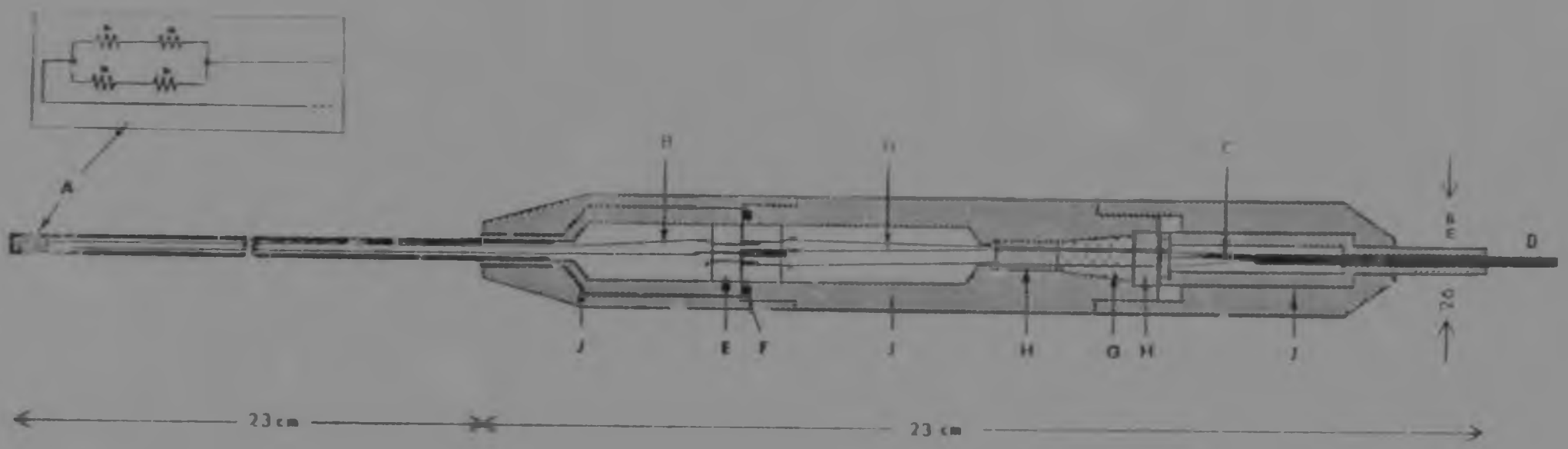

FIGURE 3.2 Thermistor probe. A: sensor — four precision thermistors (YSI No. 44006) encased at tip of stainless steel tube. Inset shows thermistor connections. B: insulated thermistor leads. C: strain washer brazed to brass disc. D: three-core cable. E: plug and socket connection. F: O-ring seal. G: rubber seal. H: bakelite. J: brass housing.

manufacturer quotes a thermistor time constant of 0,5 s/K in still air and the increase in temperature due to self-heating was therefore less than 0,002 K. The corresponding value in unstirred water should be even smaller. The time constant of the probe was approximately 15-20 seconds. In practice it was allowed to equilibrate for 1-2 minutes before readings were recorded. Rubber seals under pressure ensured that the probe was waterproof.

The probe was connected to an 800 m length of 4 mm diameter strain cable which was wound on a portable, manually operated winch. The Wheatstone bridge was connected to the cable by means of brushes and slip rings mounted on the winch reel. The bridge is illustrated schematically in Figure 3.3. (For the detailed circuit diagram see Appendix V-4.)

The probe was calibrated against a standard 400 ohm platinum-resistance thermometer in the range 0-60°C to a precision better than 0,01 K. Making allowances for the accuracy claimed by the manufacturers for the platinum-resistance thermometer, absolute temperature measurements were accurate to within 0,05 K. The resistance of the probe could be measured to a precision corresponding to 0,001 K and the uncertainty in measuring a difference in temperature (ΔT) was therefore 0,002 K (or 0,2 ΔT).

Markers were attached to the cable at 10 m intervals while the cable was under tension with the probe down a borehole. Intermediate depths were determined by interpolation using the counter attached to the pulley wheel. The estimated reproducibility of relative depth measurements was within 0,01%.

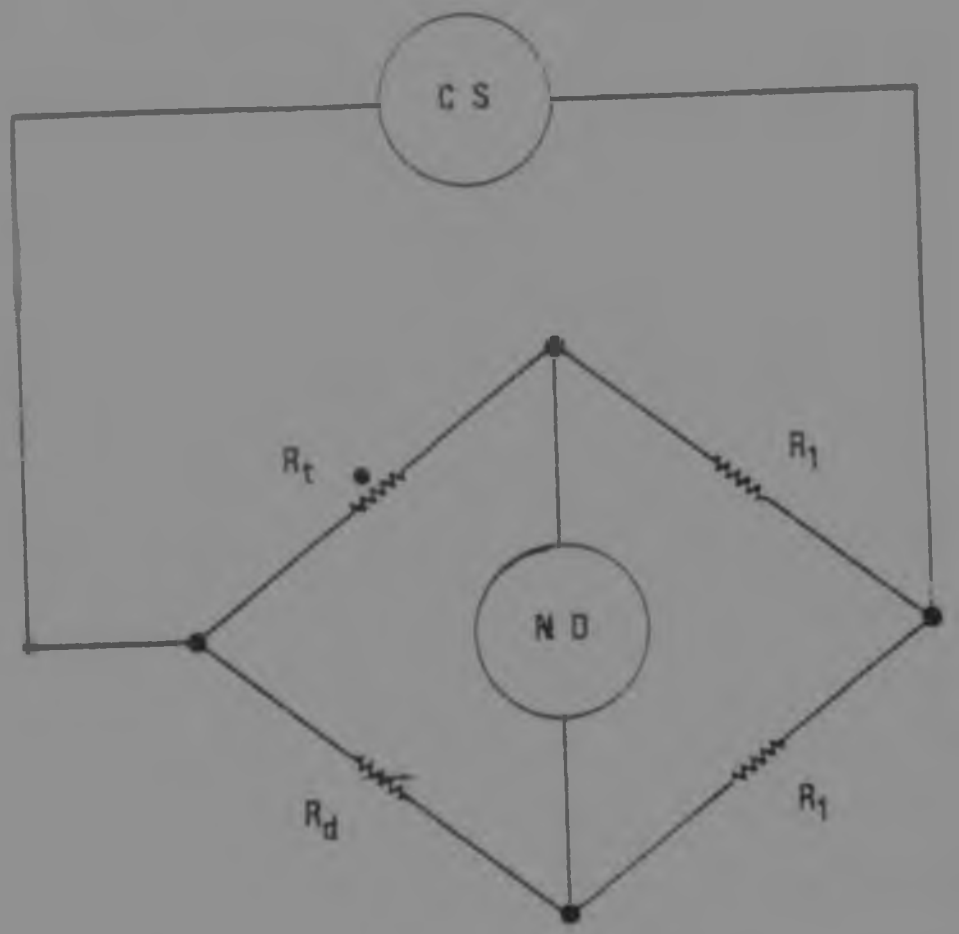

FIGURE 3.3 Wheatstone bridge. CS: current source consisting of a 1,35 v mercury cell, on-off and polarity reversing switch, potentiometer and ammeter. ND: null detector consisting of a 741 amplifier operated by two 9 v mercury cells, on-off switch and ammeter. R_d: five-decade variable resistor. R_t: thermistor sensor. R_1: 2 kΩ resistors.

The accuracy of temperature gradient measurement is approximately given by

$$(0.075 + \frac{0.2}{\Delta T})\% = (0.075 + \frac{0.2}{\delta z})\%$$

where δ is the measured gradient and Δz the depth interval of temperature measurement. For a temperature gradient of δ = 20 K/km and a depth interval of Δz = 10 m the uncertainty in the temperature gradient was approximately 1%.

Temperatures were measured, while the probe was descending, at 5, 10 or 20 metre intervals depending on the uniformity of the temperature gradient. Depths measured in inclined boreholes were adjusted to vertical depths below surface using a cubic spline interpolation between the borehole survey data (inclination or vertical depth as a function of depth along the borehole, or vertical and horizontal co-ordinates of points along the borehole). Details of the procedure are given in programme DEPTH in Appendix IIA. Resistance and depth data were reduced to give temperatures and temperature gradients as functions of depth using a polynomial fit of ln(resistance) to (1/temperature in K) which was obtained from the probe calibration. Details are given in programme BETTER in Appendix IIB.

3.3 Topographic corrections

Irregularities of heat flow caused by inequalities of surface height have a well known influence on underground temperature gradients. This effect may be considerable in areas of high relief but, fortunately,

is readily eliminated provided a sufficiently detailed knowledge of the topography is available.

To obtain a topographic correction, heights were digitized from 1:50 000 topographic maps of South Africa on a square grid with the borehole at the centre. Programme TOPO (Appendix IIC) was used to average the height of the topography over circles increasing in radius from the borehole out to 15-20 km, and calculate the disturbance to the temperature gradient as a function of depth using the method of Jeffreys (1931) and Bullard (1938). This treatment reduces the problem to that of a temperature distribution over a plane surface, the temperature in the plane being proportional to its distance from the true surface and the difference between vertical temperature gradients within the rock and at the surface. A surface temperature lapse rate for South Africa of 3,2 K/km was determined from published and unpublished borehole temperature data (Figure 3.4). Surface temperature inequalities were assumed to be in a steady state and corrections for uplift and erosion (Birch, 1950) were not incorporated.

Temperature perturbations below 150 m are small in regions of subdued topography and corrections were applied only to those boreholes surrounded by high relief. Several tests were run on borehole FM 143 to estimate the effect of varying the grid size and spacing and the results are summarized in Table 3.1. The corrections obtained from a grid of 30 x 30 km^2 with a sample spacing of 0,5 km (B) were up to 7% greater than those obtained from a grid of 20 x 20 km^2 with the same spacing (A). Column C shows that the effect of decreasing the sample interval to 0,25 km over the inner 10 x 10 km^2 was to increase the magnitude of

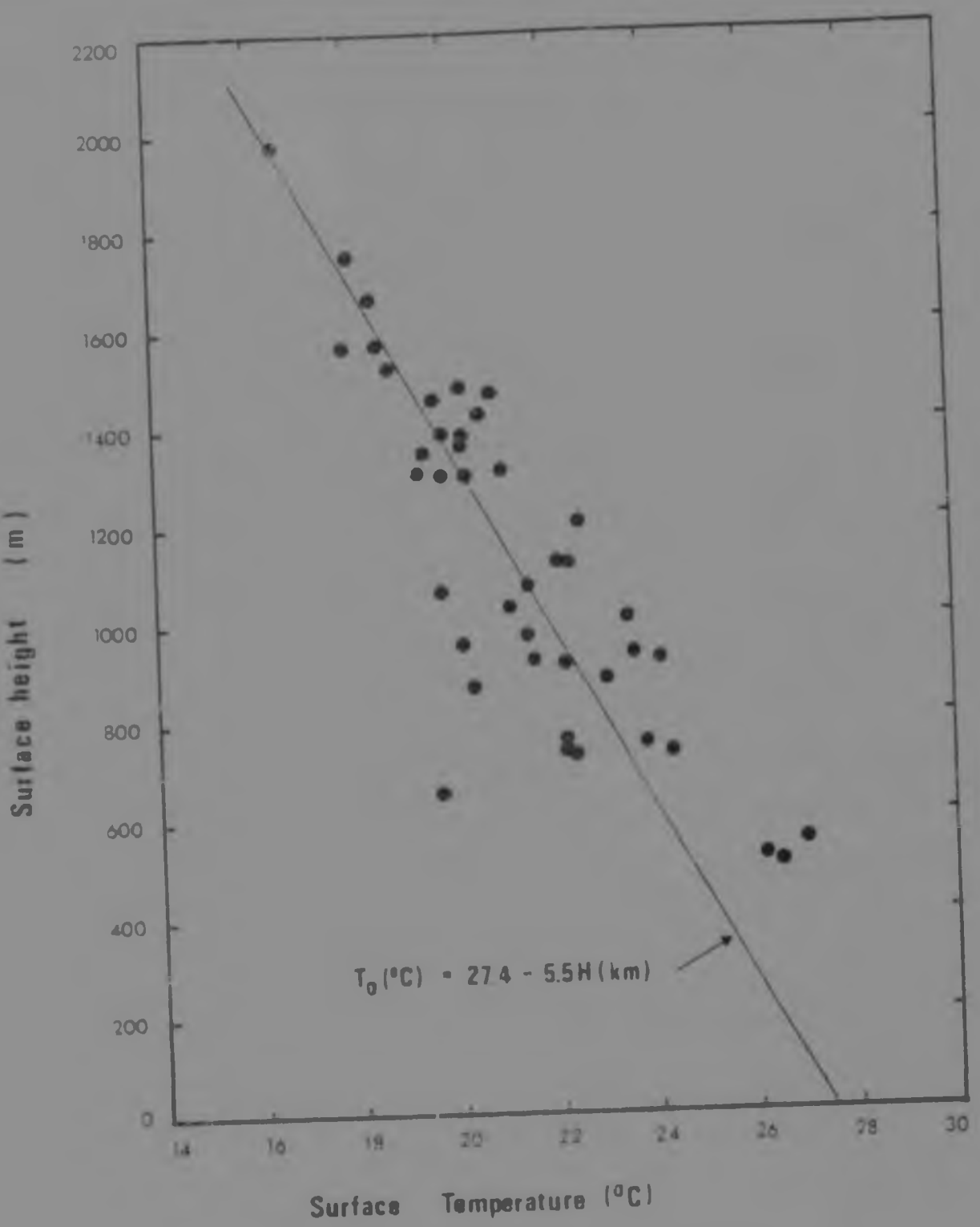

FIGURE 3.4 Surface temperature (T_0) as a function of surface height (H) in South Africa. Surface temperatures were extrapolated from borehole temperature data. Data are from Bullard (1939), Krige (1939), Carte (1954), Gough (1963) and this study (including temperature measurements in boreholes which turned out to be unsuitable for heat flow determination).

Table 5.1 A comparison of topographic corrections obtained from various grid sizes and spacings (Scirocco FM 1431)

Depth (m)	Correction to raw temperature gradient K/km			
	A	B	C	D
20	-1,210	-1,238	-0,749	-0,748
100	-1,079	-1,101	-0,825	-0,825
200	-0,855	-0,883	-0,904	-0,903
300	-0,741	-0,766	-0,873	-0,872
400	-0,661	-0,692	-0,793	-0,795
500	-0,599	-0,629	-0,710	-0,710
600	-0,549	-0,579	-0,639	-0,639
700	-0,488	-0,514	-0,556	-0,556
800	-0,431	-0,462	-0,491	-0,490

A: 30 x 30 km^2 grid (spacing = 0,5 km)

B: 30 x 60 km^2 grid (spacing = 0,5 km)

C: 10 x 10 km^2 grid (spacing = 0,25 km) superimposed on centre of 30 x 30 km^2 grid (spacing = 0,5 km)

D: 15 x 15 km^2 grid (spacing = 0,25 km) superimposed on centre of 30 x 30 km^2 grid (spacing = 0,5 km)

the correction by a further 6-15% below depths of 200 m. Increasing the dimensions of the finer spaced-grid (D) had little further effect on the correction.

The 'improved' correction obtained by using a greater frequency of readings near the borehole demonstrates the fact that much of the

correction comes from topography within a few kilometres of the borehole. It was impractical to use a spacing smaller than 0,25 km and all topographic corrections were based on grid configuration C.

3.4 Perturbations of the temperature gradient

A number of factors which perturb subsurface temperatures were listed in Chapter 1. These will be discussed in greater detail in this section in order to show how they may be recognized and to examine their effects on near-surface temperature gradients.

All the boreholes investigated were drilled for mineral exploration purposes and this introduces a possible source of bias which is unquantified in most heat flow studies. Roy et al (1968b) investigated this problem to some extent using independently drilled boreholes. They concluded that a free selection of sites would probably yield heat flow patterns similar to those observed. Most of the boreholes studied here were exploratory and not associated with mining and where mineralization was encountered it was usually stratabound. It is unlikely that there is any systematic bias in the data from this effect.

Drilling itself causes important temperature perturbations in boreholes. The net effect is a decreasing temperature gradient at depth and an increasing gradient near the surface caused by circulation of drilling fluid through the borehole. In deep boreholes such perturbations may take up to a few years to decay to negligible values (Bullard, 1947). All temperature measurements were made several months to several years after drilling and there were no obvious signs of drilling transients.

Heat transfer by the movement of ground water through fractures or through bulk porous rock is the chief cause of unreliability of temperature measurements in the upper 100-200 m of a borehole (Roy et al, 1972; Lewis and Beck, 1977). None of the areas studied was underlain by permeable rock units such as sandstone and little or no movement of water through the bulk rock can be expected. However, fractures were common in some areas and aquifers in many boreholes rendered them useless for heat flow determination. Water flows, identified by short period temperature fluctuations and peculiarities in the thermal gradient which were unrelated to petrographic variations, were encountered in some of the boreholes under study even at depths greater than 200 m. However, these were apparently minor, causing disturbances over very limited depth intervals. Relevant aspects of hydrology at each site will be discussed in Chapter 6.

Steady state refraction of heat flow caused by three-dimensional thermal conductivity anomalies is difficult to recognize unless the borehole intersects the anomalous body. Corrections are even more difficult to apply as they require a detailed knowledge of geological structures surrounding the borehole and this information is not often available. England (1976) and Jones and Osburgh (1979) have investigated a few simple structures but corrections cannot be made on a routine basis. Heat flow refraction was shown to be important in only one of the boreholes investigated and this will be discussed when the data are presented.

Finally, recent changes of surface temperature constitute a further source of subsurface temperature perturbations. Important causes

or surface temperature variation are past climatic variations, denudation or vegetation cover, recent uplift and erosion, and recent subsidence and sedimentation. It is easy to correct for this effect if a reasonable knowledge of the history of surface temperature variations is available. Pleistocene and Holocene climatic variations in particular may have marked effects on temperature gradients even at depths of a few kilometres (Birch, 1948; Beck, 1977), but heat flow determinations in deep boreholes have failed to produce convincing evidence in favour of any climatic model (Gough, 1963; Sass et al, 1971). A consensus has not been reached and a quantitative discussion of these effects and their bearing on South African data is deferred until Chapter 3.

4. THERMAL CONDUCTIVITY MEASUREMENTS

4.1 Introduction

Thermal conductivity measurements were made on core samples in two laboratories using variations of the divided-bar method described by Birch (1950). Approximately 500 samples were analysed in the Department of Geology and Mineralogy, Oxford University (OU) and another 300 at the Bernard Price Institute for Geophysical Research, University of the Witwatersrand (BPI), using an apparatus which was developed for this project.

The divided-bar at BPI was modelled on apparatus described by Roy et al. (1968b) and Richardson and Deburgh (1978). Standardization was against gem quality quartz cored perpendicular to the c-axis. Repeat measurements at BPI, and a cross-laboratory check carried out at OU, on fused silica and various rock discs showed that the apparatus was accurate and precise to within a few percent over the range of conductivities commonly encountered in rocks.

Core samples were supplied by the mining companies responsible for drilling the boreholes. With few exceptions they were coherent, impervious rocks and therefore particularly suited to measurement by the divided-bar technique.

4.2 Measurements at BPI

4.2.1 The divided-bar apparatus

The divided-bar apparatus constructed at BPI is illustrated in Figure 4.1.

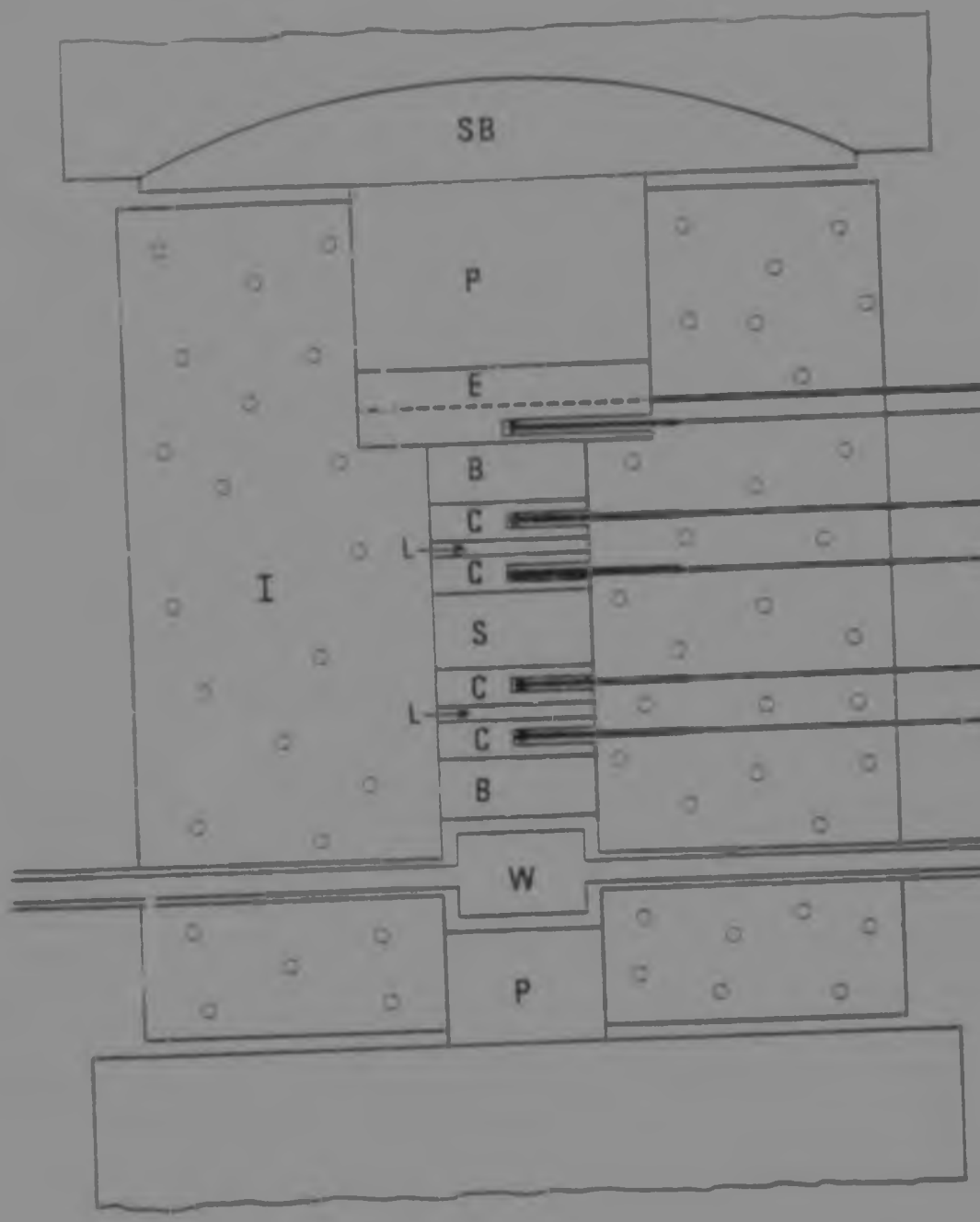

FIGURE 4.1 Divided-bar apparatus. The stack consists of interleaved discs of copper (C), secondary standard (L) and sample (S). Heat is supplied by the electric heater (E) and abstracted by the water cooler (W). Discs B are brass spacers and P 'Perspex' insulators. A load is supplied via thrust bearing (SB) and heat losses are minimized by styrofoam insulation (I). Temperatures are measured by four thermistors (T_1-T_4). T_c is the heater control thermistor.

cylindrical conductivity stack was [illegible] in diameter
[illegible] each [illegible] thick. Interleaved
[illegible] and the sample of unknown
conductivity. The secondary standards were cut from a
[illegible] low-conductivity polycarbonate plastic.
Sample thicknesses varied from [illegible] mm to 20 mm depending on the nature
of the experiment being conducted. The most single disc analyses
samples were approximately 5 mm thick.

[illegible] above and below the stack served to diffuse
[illegible] temperature variations in the water cooler (W) and electric
heater (H), and to separate the top copper disc from the heater,
thereby reducing possible edge effects due to the greater diameter
of the heater. A hydraulic press supplied a load of 300 bars via
[illegible] at the top of the stack. The stack was
protected from temperature drift of the press by 'Perspex' cylinders
(P) and lateral heat losses were minimised by insulating the stack
with expanded polystyrene (I).

The temperature of the heater was electronically controlled to ensure
a constant supply of heat to the stack. The a.c. control circuit is
illustrated schematically in Figure 4.2 and in detail in Appendix V-B.
A control thermistor (Tc in Figure 4.1), which was in close physical
contact with the heater, formed an element of a Wheatstone bridge
circuit and thus controlled the voltage supply to the heater element.
The bridge was kept in balance by virtue of the feedback between the
heater element and the thermistor. The temperature at the top of the
stack was constant to better than 0,001 K in the time it took to
record temperatures (5 to 10 minutes).

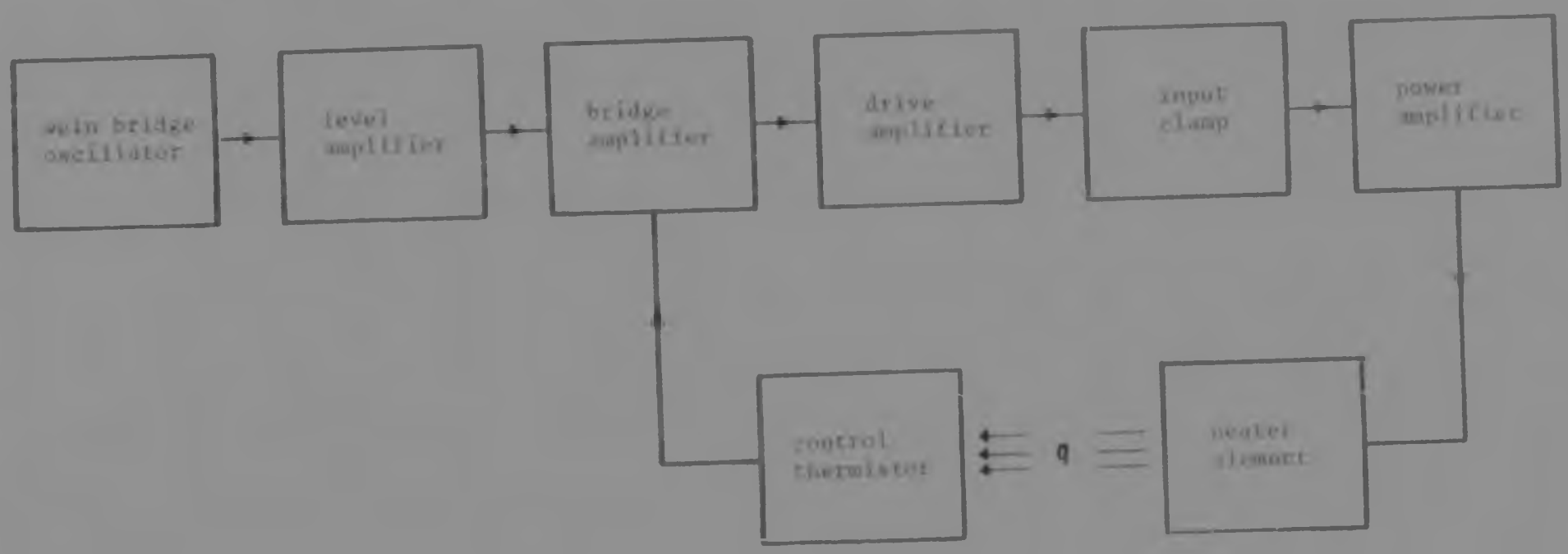

FIGURE 4.2 Flow diagram of heater control circuit

Heat was dissipated at the base by the circulation of cold tap water through the water cooler. A temperature drift in the lower end of the stack due to diurnal temperature fluctuations could not be avoided without purchasing an expensive refrigeration system. To overcome this difficult conductivity measurements were confined to times when the drift was minimal. Temperatures were recorded several times and final values were accepted when temperature variations were less than 0.005 K in five minutes.

The time taken for thermal equilibrium to be re-established after changing samples was 15-25 minutes depending on the length of exposure to room temperature and the thermal resistance of the sample. A complete conductivity measurement could be made in about thirty minutes.

By maintaining the top of the stack at 30°C an equilibrium heat flow close to 500 Wm^{-2} was established in most experiments. The resulting temperature drops across each of the secondary standards and a 15 mm thick rock sample of conductivity 3 $Wm^{-1}K^{-1}$ were approximately 2.5 K.

4.2.2 Temperature measurements

Temperatures were measured using four thermistors (YSI No 44004; 2251 ohms at 25°C) which were inserted into wells drilled radially to the centres of the copper discs (T_1-T_4, Figure 4.1) and which were connected via a four-way switch to the same Wheatstone bridge described in Section 3.7. Temperature fluctuations of 0.001 K within each copper disc could readily be detected. Initial experiments showed that uncertainties caused by variable thermal contacts between the

thermistors and the copper were as much as 10% of the temperature differences being measured. The thermistors were therefore glued into the copper discs and calibrated relative to each other. An absolute calibration was not made as only an approximate value of the sample temperature was required.

Calibrations were achieved by placing disc 2, 3 or 4 immediately below disc 1 in the stack and comparing the resistances of the thermistors over a range of temperatures by varying the voltage supplied to the heater. The value

$$\Delta Re_x = Re_x - Re_1 \qquad (4.1)$$

(where Re_1 is the (electrical) resistance of thermistor 1 and Re_x that of thermistor 2, 3 or 4) was plotted against Re_x. Smooth curves were fitted visually to the data. ΔRe_x includes:

(1) the amount by which thermistor x was offset relative to thermistor 1 (C_x)

(2) and a difference in (electrical) resistance (d_x) corresponding to an actual temperature drop between the thermistors. This was partly due to lateral heat losses and partly to the thermal resistances of the copper discs and the contacts between them.

Hence,

$$\Delta Re_x = C_x + d_x \qquad (4.2)$$

The effect of d_x was largely eliminated by interchanging the discs and generating a second set of curves

$$\Delta Re_x = C_x - d_x \qquad (4.3)$$

and adding to equation 4.2,

It was been assumed that lateral heat losses for given disc temperatures remained constant over each entire calibration run. This was achieved in part by ensuring that the experiment was performed over a small range of room temperatures (approximately 3 K). Several repeats of the above experiments yielded calibration curves (C_2, C_3 and C_4) in the temperature range 20-30°C which agreed to within 1,0 ohm. This corresponds to a temperature uncertainty of 0,01 K and the measurement of temperature differences was therefore estimated to be accurate to within 0,02 K. The average values of C_2, C_3 and C_4 are shown as functions of thermistor resistance in Figure 4.3.

Resistances were converted to temperatures by first subtracting the appropriate value of C_2 and then using a polynomial fit of ln(Re) vs 1/T (T in K) which was obtained from the thermistor calibration curve provided by the manufacturers. The procedure is almost identical to that followed in programme SETTER (Appendix IIB).

To ascertain whether the characteristics of the thermistors changed with time the calibrations were checked during and after the thermal conductivity measurements. In all cases, agreement with the curves in Figure 4.3 was within 1,0 ohm.

4.2.5 Principle of the divided-bar

The divided-bar is designed to produce a condition of linear heat flow down the stack. The thermal conductivity of an unknown can then be determined in terms of the conductivity of the secondary standard, which is in turn determined from measurements on primary

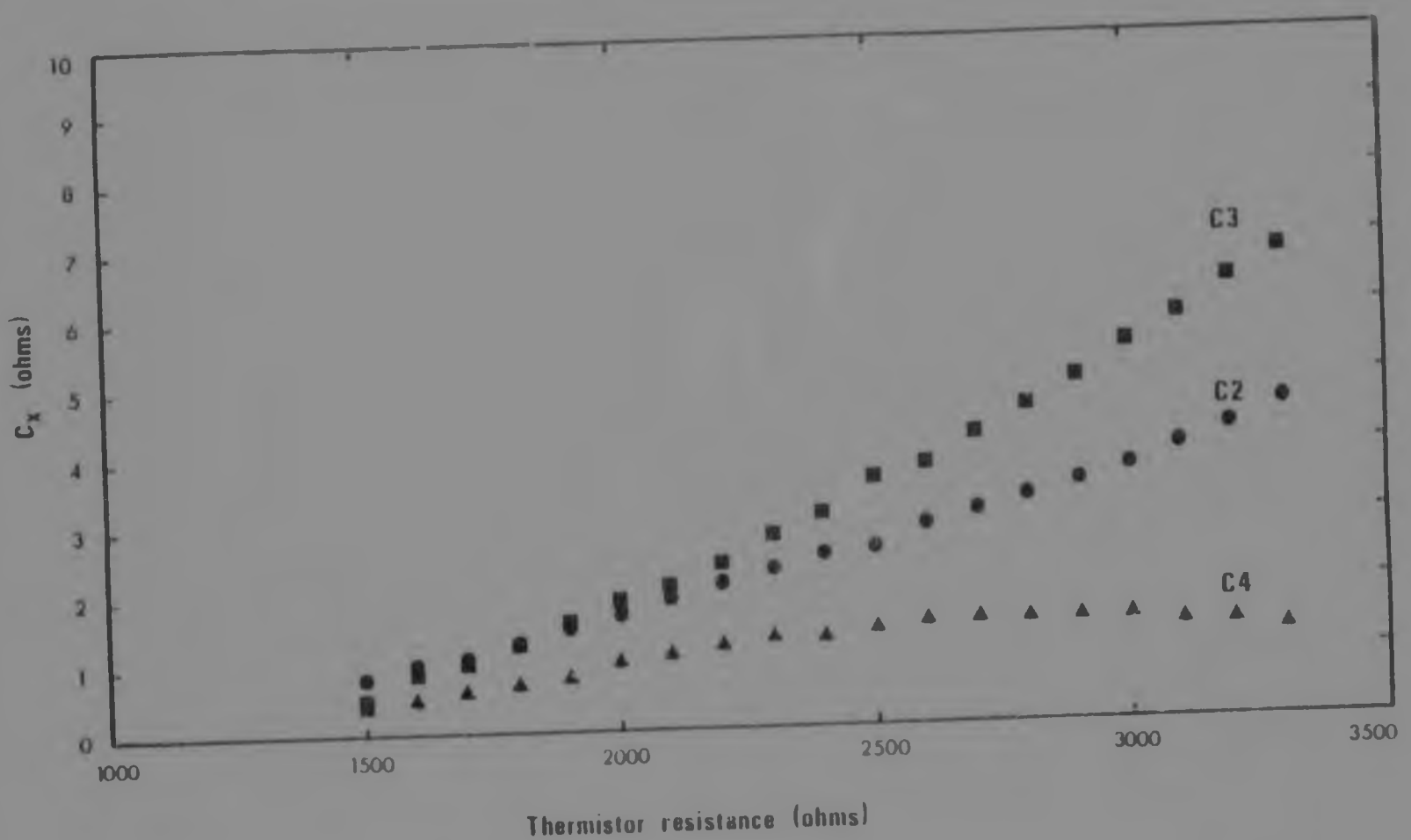

FIGURE 4.3 Calibration curves for thermistors 2, 3 and 4 relative to thermistor 1.

standards. The steady state equation of heat flow may be written:

$$q = \frac{\Delta T}{\Sigma R} \qquad (4.4)$$

where q is the heat flow, ΔT the temperature difference between surfaces perpendicular to the direction of flow, and ΣR the sum of the thermal resistances of the material between these surfaces. The thermal resistance of each unit is defined by

$$R = \frac{D}{K} \qquad (4.5)$$

where D is its thickness and K its thermal conductivity.

Applying equation 4.4 to the stack yields:

$$q = \frac{(T_3 - T_1)}{D_S/K_S + D_C/K_C + A} = \frac{(T_2 - T_3) + (T_3 - T_4)}{2D_L/K_L + 2D_C/K_C + B} \qquad (4.6)$$

Temperatures are as illustrated in Figure 4.1 and subscripts S, C and L refer to sample, copper and secondary standard. A is the combined contact resistance of both sample-copper interfaces, and B that of the four lexan-copper interfaces.

Linear heat flow in the stack is achieved only if axial heat losses are zero. In practice, it is impossible to meet this condition but heat losses can be reduced to a few percent of the total heat flow. The use of styrofoam (Figure 4.1) eliminated most of the lateral heat transfer. Jessop (1970) showed that heat losses vary as the length:diameter ratio of the stack and the use of 1 mm thick secondary standards therefore had a distinct advantage over many early variations of the divided-bar, and was particularly valuable in view of the small stack diameter. Many workers have successfully reduced heat losses to as little as 1% by using guard heaters surrounding the stack. The additional accuracy that

could be achieved by employing this technique did not justify the time and work it would require; instead, conductivities were measured at temperatures slightly above room temperature (20-25°C). Under these conditions, heat losses, measured as the percentage differences between the temperature drops across the substandards, of less than 5% were obtained.

The conductivity of the unknown was found in terms of the average heat flow measured across the two secondary standards. If heat losses were constant with height in the stack the error in measuring conductivity would be zero. Although experiments using a third substandard in place of the sample indicated that the heat loss did vary with height (Table 4.1), the resulting uncertainty in conductivity was only a fraction of the percentage heat loss.

It is necessary to either eliminate or evaluate the contact resistances represented by A and B in equation 4.6. In order to reduce contact resistances the surfaces of the copper discs were lapped with increasingly finer grades of carborundum powder to 1200 grit and polished with diamond paste*. The copper surfaces were shown to be flat to within 1-2 μm by examining the interference fringes between these surfaces and that of an optically flat glass. The secondary standards had a relief of approximately 10 μm across their surfaces but the most serious of these irregularities were removed under pressure due to the flexible nature of 'Lexan'. All surfaces were carefully cleaned and coated with silicone grease before assembling the stack.

---

* I am indebted to Mr T O Dupgan, Department of Metallurgy, University of the Witwatersrand, for undertaking this painstaking work.

Table A.1 Percentage difference of the temperature drop across three subjacent secondary standards (1, 2 and 3) for five experiments (a - e)

Position	mean loss %				
	a	b	c	d	e
1 - 2	1,06	-,31	3,49	1,06	1,07
2 - 3	0,66	-,44	2,89	0,90	0,94

and a load of 300 bars was applied to the stack.

Under these conditions thermal contact resistance R was negligible compared with the thermal resistance of the secondary standard; a self-correction for any residual in R was effectively made in the calibration (Section A.2.4). In general, it was not possible to machine surfaces of rock samples as flat as those of the copper-lexan discs and contact resistance R could not be neglected. It will be discussed in some detail in the next two sections.

Finally, it is worth noting that in most experiments the sample temperature was approximately 37°C. This is almost in the middle of the range of in situ temperatures (20-38°C). Schatz and Simmons (1972) and Richardson and Powell (1976) showed that, up to temperatures of approximately 600°C, the temperature dependence of the thermal conductivity of crystalline materials may be represented by:

$$\frac{K_T}{K_0} = \frac{A}{B + CT}$$

where K_0 is the conductivity at 0°C and T is in K. Richardson and Powell used values of a = 132, b = 70 and c = 0,17% for the constants; these values yield uncertainties of less than 1,5% in the conductivity and a correction was not applied.

4.2.4 Calibration of the divided-bar

The secondary standard was calibrated against gem quality quartz (cored perpendicular to the z-axis) and fused silica. The most widely accepted values for the thermal conductivity of quartz (k_Q), k_Q, and fused silica, k_{FS}, are given by Ratcliffe (1959) as functions of temperature (in °C):

$$k_Q = 10^3/(145,1 + 0,3783t) \quad Wm^{-1}K^{-1} \tag{4.7}$$

$$k_{FS} = (1370 + 14,7t - 0,0677t^2)10^{-4} \quad Wm^{-1}K^{-1} \tag{4.8}$$

While these are the most commonly available primary standards which span the range of conductivities found in most rocks, they have certain disadvantages. Impurities and defects in quartz reduce its thermal conductivity and it is difficult to obtain crystals which are free of visible imperfections. Only one suitable specimen was available but it was possible to compare its conductivity with those of four specimens used at CGS. Fused silica is more readily available but its thermal conductivity depends critically upon the quality of the glass. For this reason the secondary standard was calibrated against quartz and fused silica was used to check the calibration at the lower end of the conductivity scale.

A 25 mm diameter quartz disc was prepared by coring the undamaged

section of a crystal perpendicular to its optic axis. The core was set up in a lathe and the ends were ground parallel using a diamond grinding wheel. A one inch diameter disc of fused silica was obtained commercially. The surfaces of the discs were polished in the same way as those of the copper discs. The finished products were both fractionally above 12 mm long and the ends were flat to within 1-2 μm and parallel to within 10 μm.

In single disc calibrations the most crucial contact resistance is that between primary standard and copper (A in equation 4.6). The apparent effect of thermal resistance R is to reduce the conductivity of the secondary standard bar, provided this contact resistance remains constant, the error is self-correcting because the apparent conductivity is used to determine the conductivity of an unknown. The primary standard-copper contact introduces a built-in inaccuracy and it is important to estimate its magnitude. The ratio of the temperature drop across the contact to that across the quartz is

$$\frac{\Delta T_c}{\Delta T_Q} = \frac{K_Q/K_c}{D_Q/D_c}$$

where D is thickness and subscripts C and Q refer to contact and quartz respectively. The contacts had a combined thickness of about 4 μm and, ideally, were completely filled with silicone grease. The thermal conductivity quoted by the manufacturers for the silicone grease is $0.17\ Wm^{-1}K^{-1}$. The thickness and conductivity of the quartz disc were 12.1 mm and $6.92\ Wm^{-1}K^{-1}$ (at 27°C, equation 4.7). Hence

$$\frac{\Delta T_c}{\Delta T_Q} = 0.003$$

The corresponding values for fused silica should be less because of its greater thermal resistance. Δ can safely be neglected in the calibration.

With A = B = 0 and quartz substituted for rock sample in equation 4.6, it is a simple procedure to determine the conductivity of the secondary standard. The thickness of each unit of the stack was measured to within 10 um using a micrometer. Equilibrium temperatures were measured in the manner described in Section 4.2.2. The conductivity of quartz was calculated from equation 4.7 using the average of temperatures T_2 and T_3 and 398 $Wm^{-1}K^{-1}$ was used for the conductivity of copper (Clark, 1966). The conductivity of the secondary standard was calculated from equation 4.6.

Repeat measurements yielded consistent results which are summarized in the form of a histogram in Figure [illegible]. The mean and standard deviation* of fifteen measurements were

0,2157 ± 0,0026 $Wm^{-1}K^{-1}$

---

* The mean of a sample of n measurements of which x_i is the i-th value is

$$\bar{x} = \frac{1}{n}\Sigma x_i$$

The standard deviation of the sample is given by

$$\sigma_x^2 = \frac{\Sigma(x_i - \bar{x})^2}{(n-1)}$$

and the standard error of the mean by

$$\sigma_{\bar{x}}^2 = \frac{\Sigma(x_i - \bar{x})^2}{n(n-1)}$$

The use of these statistics implies a normal distribution. The sample sizes encountered in this study were seldom large enough to perform satisfactory tests for normality and where σ_x and $\sigma_{\bar{x}}$ are used a normal distribution has been assumed. The standard deviation and standard error are used somewhat arbitrarily by different authors. Although both are reported in this text, final estimates of uncertainty will be expressed in terms of the standard error in accordance with the code of practice recommended by Campion et al (1973). See Chapter 6.

A similar procedure was followed to find the conductivity of fused silica relative to the secondary standard. The results are summarized in Figure 4.3. The mean and standard deviation of eleven measurements were:

$$\sigma^{25} = \quad \pm \quad \text{Wm}^{-1}\text{K}^{-1}$$

This is [illegible] lower than the value calculated from equation 4.8 at 17°C, i.e. [illegible] Wm^{-1}K^{-1}. The most likely explanation for the discrepancy is that the [illegible] Alsiva was of inferior quality. Experiments conducted on other [illegible] (Table 4.5) showed that the conductivity of this specimen was 1-3% lower than those obtained for other, higher quality glasses. It, thus, had a mean conductivity of [illegible] lower than the value of Sabroffe's formula (Ratcliffe, 1969) and the accuracy of the calibration was therefore confirmed at the low end of the conductivity scale.

4.4.3 Preparation of rock samples

Cylinders of rock, 5 cm in diameter, were prepared from borehole cores by sawing them along their axes. The ends were machined flat and parallel using a lathe equipped with a diamond grinding wheel and finally lapped by hand using 600 grit carborundum powder. To ensure a uniform standard of flatness the samples were micrometered at the centre and in six positions on the perimeter; if the mean of these measurements differed by more than 15 μm from the [illegible] sample was rejected. This is the same tolerance adhered to by Beck (1976). Most of the completed samples were approximately [illegible] cm long.

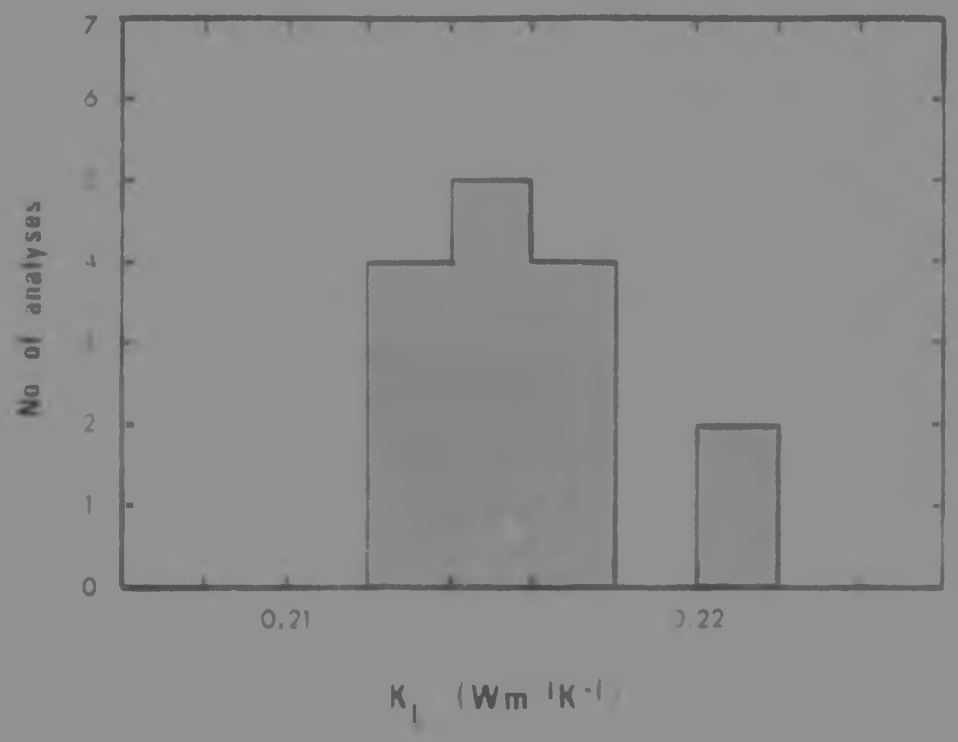

FIGURE [illegible].4 Histogram [illegible] conductivit[illegible] 'Lexa[illegible] calibrated against quartz (1[illegible]

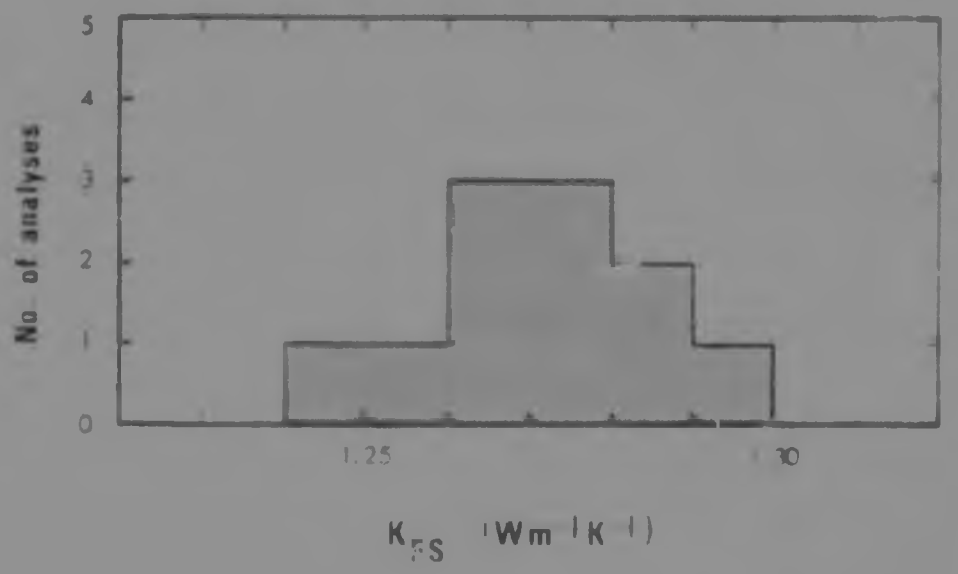

FIGURE 4. Histogram of the conductivit[illegible] fused silica determined relat[illegible] to 'Lexan' [illegible] 27°C.

In order to simulate natural conditions, rock discs were saturated with water under vacuum for one hour before being inserted in the stack. Because of the absorbent nature of rock surfaces aluminium foil discs were used instead of silicone grease at the sample-copper interfaces. With low exemptions, the samples were sufficiently coherent to withstand a load of 300 bars.

Thermal contact resistance A was estimated by making measurements on rock discs of the same conductivity but different thicknesses. With $B = 0$, equation 4.6 can be rearranged to

$$\frac{(T_2-T_3)}{(T_1-T_2)+(T_3-T_4)} = \frac{k_c r_c + A}{r_c/k_1 + 2k_c/k_2} - \frac{1/r_c}{r_c/k_1 + 2k_c/k_2} k_s \qquad (4.9)$$

The temperature ratio is a linear function of sample thickness; the intercept at zero thickness yields a measure of A and the slope a measure of the sample conductivity.

Linear relationships of this kind were generated for nineteen samples of different conductivity. In order to ensure that discs from each sample had the same conductivity, homogeneous and fine grained rocks were selected for most experiments. Inhomogeneities cause variations in conductivity from one disc to the next and thus increase the scatter in the data; this may be reduced by making stepwise measurements on a single disc of successively smaller thickness. (In this way it was possible to obtain a satisfactory result for a pegmatite, sample AG 310.3.) Minerals of high conductivity in coarse grained rocks begin to act as 'short circuits' as the disc thickness approaches the average grain size and this leads to an apparently higher thermal conductivity and incorrect values for the slope and intercept.

The temperature ratio was measured for at least three discs from each sample, varying in thickness from 5 mm to 18 mm. The intercept and slope (and their standard deviations) and the linear correlation co-efficient were determined from a least squares fit to the data. A typical result is illustrated in figure 4.8, and Table 4.2 summarises the data for all nineteen samples. A histogram of the intercept values is given in figure 4.9 and the mean and standard deviation were:

0.0073 ± 0.0097

The corresponding value for A is 3.7×10^{-5} $m^2 K s^{-1}$. This is only 1% of the thermal resistance of a 15 mm thick sample of conductivity 3 $Wm^{-1}K^{-1}$. Although the mean intercept value was not significantly different from zero at the 1-σ level it does have physical significance and a correction was applied to all measurements on single rock discs.

Much of the spread in the intercept values may be attributed to variable physical properties of rocks. For example, it is easier to machine monomineralic rocks than aggregates consisting of loosely bound phases of different hardness. This study was not sufficiently detailed to detect such features. Two relatively large negative values of the intercept were probably due to sample inhomogeneities.

The thermal conductivity and standard deviation of each sample (columns 9 and 10, Table 4.2) were calculated from the slope of equation 4.9. Errors include conductivity variations due to sample inhomogeneities and this may account for the relatively large standard deviations for samples FM 2230, A 142 and RC 176.2. The percentage error was commonly smaller than 3% (column 11). Allowing for a reproducibility

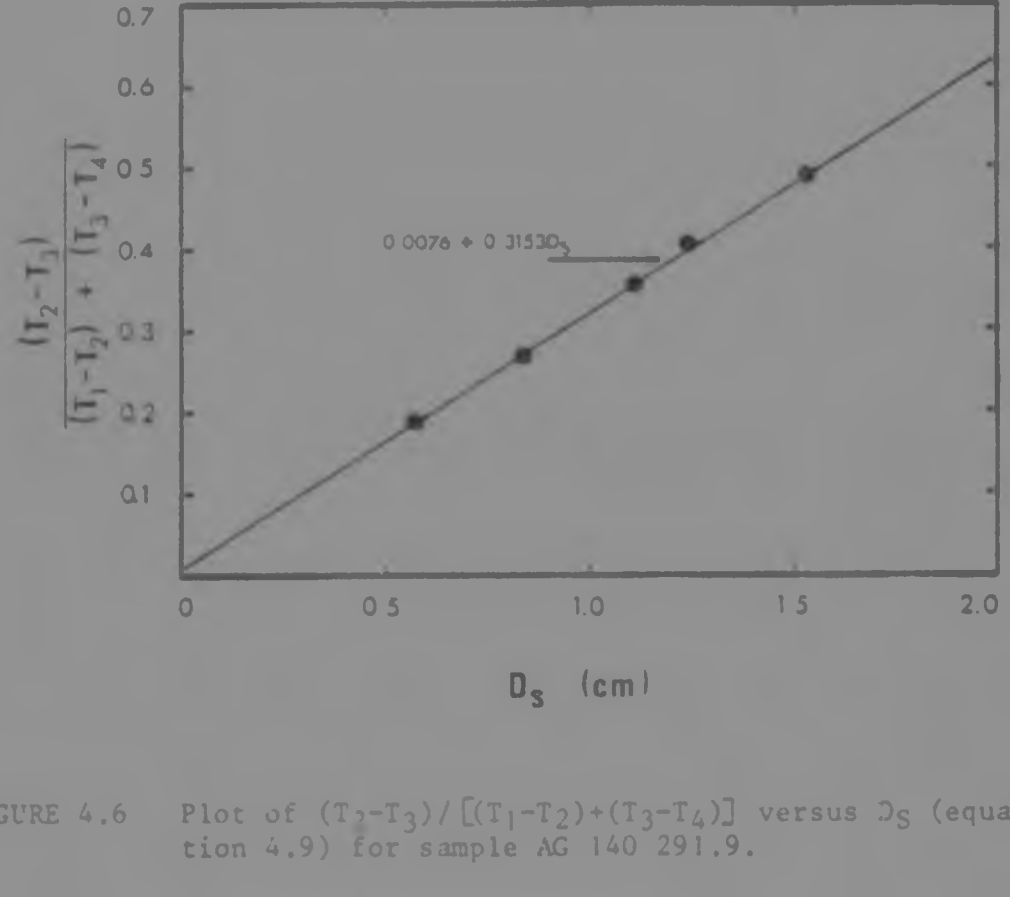

FIGURE 4.6 Plot of $(T_2-T_3)/[(T_1-T_2)+(T_3-T_4)]$ versus D_S (equation 4.9) for sample AG 140 291.9.

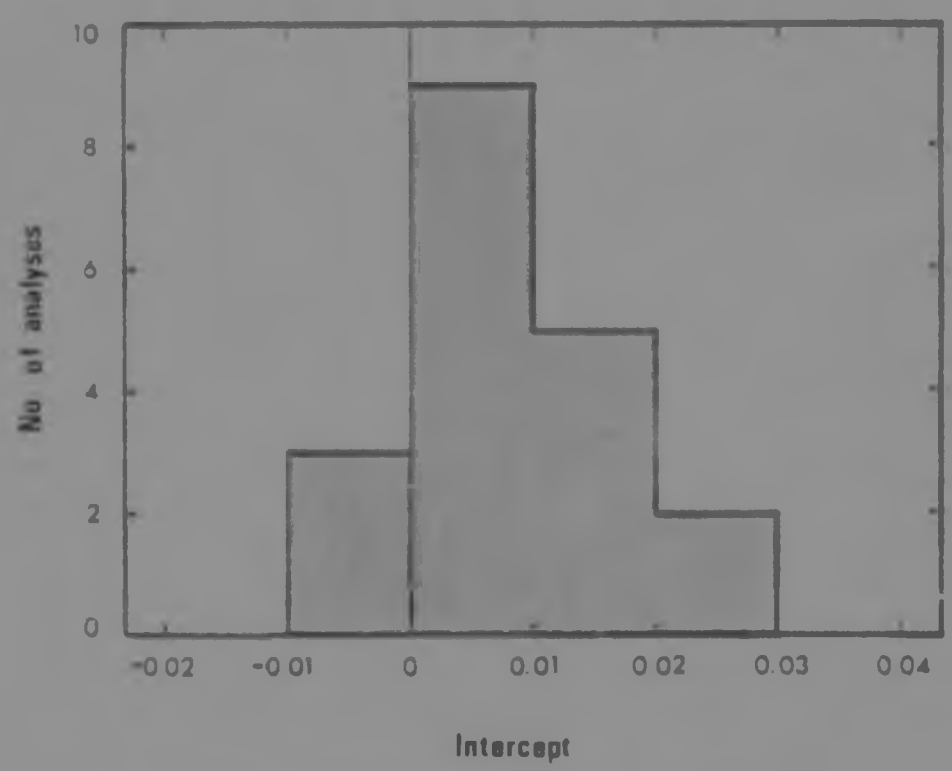

FIGURE 4.7 Histogram of intercept values of $(T_2-T_3)/[(T_1-T_2)+(T_3-T_4)]$ versus D_S plots.

Table 4.2 Statistics of linear relationships between $(T_2-T_3)/[(T_1-T_2)+(T_3-T_4)]$ and P_2 (equation 4.9) and thermal conductivities for nineteen rock samples.

Sample	Rock type	INTERCEPT		SLOPE		r^2	n	THERMAL CONDUCTIVITY		
		I	σ_I	S	σ_S			$K(Wm^{-1}K^{-1})$	$\sigma_K(Wm^{-1}K^{-1})$	σ_K%
AE 269.18	biotite gneiss	0.0003	0.0047	0.3162	0.0043	0.9999	3	3.400	0.046	1.35
" 241.9	"	0.0076	0.0089	0.3153	0.0081	0.9990	5	3.399	0.088	2.58
" 259.5	"	0.0150	0.0046	0.4772	0.0068	0.9998	4	3.283	0.068	2.07
" 107.5A	pegmatite	0.0009	0.0052	0.3340	0.0048	0.9998	3	3.367	0.070	1.76
" 329.0	biotite gneiss	0.0016	0.0040	0.3108	0.0044	0.9999	3	3.250	0.033	1.02
" 353.7	"	0.0170	0.0018	0.2806	0.0016	1.0000	4	3.488	0.021	0.60
" 389.3A	schistose gneiss	-0.0080	0.0033	0.4219	0.0028	0.9997	5	2.548	0.017	0.67
PM 1860	biotite gneiss	0.0011	0.0015	0.3188	0.0027	1.0000	3	3.380	0.024	0.86
" 2250	"	0.0277	0.0128	0.2714	0.0122	0.9990	3	3.061	0.128	3.49
" 2280	"	-0.0001	0.0121	0.3962	0.0120	0.9995	3	3.713	0.082	3.02
CCF 985	amphibolite	0.0190	0.0177	0.5773	0.0169	0.9996	3	1.862	0.055	2.95
" 1800	biotite gneiss	0.0236	0.0165	0.4501	0.0128	0.9992	4	3.388	0.068	2.03
A 142	"	0.0068	0.0179	0.3639	0.0175	0.9988	3	2.954	0.132	4.81
RC 125.8	biotite-chlorite-amphibole schist	0.0154	0.0120	0.3557	0.0113	0.9995	3	3.027	0.096	3.18
" 158.9	"	0.0180	0.0035	0.3980	0.0033	1.0000	3	2.701	0.022	0.82
" 176.2	"	0.0027	0.0337	0.3859	0.0319	0.9966	3	2.786	0.231	8.26
" 184.2	"	-0.0060	0.0122	0.4074	0.0104	0.9994	4	2.639	0.067	2.54
" 208.1	"	0.0017	0.0112	0.3678	0.0094	0.9993	4	2.922	0.075	2.57

r^2 = linear correlation co-efficient; n = number of points used in linear regression.

error of 1% in the calibration, the uncertainty in measuring the conductivity of an unknown was therefore estimated to be 4%.

All other samples were analysed using single rock discs; conductivities were calculated from equation 4.9 by substituting 0,0075 for the first term on the right hand side.

The effect of water content on thermal conductivity was investigated by measuring the conductivities of eleven samples before and after saturation with water. The results are summarized in Table 4.3. The mean of the percentage differences between 'wet' and 'dry' conductivities was 0,1 ± 2,6% and the differences exceeded 4% in only one case. This contrasts with the findings of England (1976) who showed that water saturation increased the effective conductivities of similar (gneissic) rocks from the western Alps by as much as 25%. The discrepancy can be accounted for by the higher load pressure used at RPI (300 bars as opposed to 100 bars). Walsh and Decker (1966) showed that water saturation has a similar effect to increasing the load pressure which tends to close microfissures in the rock. As a safeguard, dry samples were saturated prior to measurement.

A check on the results was provided by comparing values obtained at RPI and UU for rock discs prepared from the same drill cores. Table 4.4 shows that not all conductivities compare favourably and in some cases differences exceeded 10%. However, these could be traced to samp le inhomogeneities and there is no systematic bias in the data. Much better agreement was obtained for the conductivities of the primary standards (see Section 4.3).

Table 4.3 Effect of water saturation on thermal conductivity

Sample	Rock type	Conductivity ($Wm^{-1}K^{-1}$)		% Difference Saturated-Dry
		Saturated	Dry	
AG 248.5	biotite gneiss	3,28	3,21	2,1
AG 269.1 A	"	3,40	3,41	- 0,3
AG 269.1 B	"	3,59	3,73	- 3,9
AG 291.9	"	3,41	3,51	- 2,9
AG 299.5	"	3,29	3,30	- 0,3
AG 310.3 B	pegmatite	2,62	2,57	1,9
AG 320.0	biotite gneiss	3,25	3,34	- 2,8
AG 353.1	"	3,49	3,44	1,4
AG 389.3 A	schistose gneiss	2,55	2,57	- 0,8
AG 389.3 B	"	2,43	2,31	4,9
AG 652.8	quartzite	6,97	6,85	1,7

Table 4.4 A comparison of thermal conductivity measurements made at BPI and OU.(Duplicate values are from measurements on different rock discs)

Sample	Rock type	Conductivity ($Wm^{-1}K^{-1}$)	
		BPI	OU
AG 235.6	pegmatite	2,79	3,25
AG 244.3	"	3,87	3,42
AG 248.5	biotite gneiss	3,28	3,46
AG 251.3	"	1,62	1,73
AG 269.1	"	3,40; 3,59	3,63
AG 284.8	"	2,55	2,64
AG 291.9	"	3,41; 3,33	3,22
AG 310.3	pegmatite	3,97; 2,62	3,61
AG 320.0	biotite gneiss	3,25; 3,42	3,29
AG 348.1	"	3,58	3,54
AG 353.1	"	3,49	3,52
AG 358.3	biotite fels	2,06	1,66; 1,71
AG 367.4	amphibolite	3,04	3,24
AG 371.4	schistose gneiss	3,37	3,35
AG 396.4	"	3,46	3,19
AG 412.2	"	2,75	2,48
AG 627.8	quartzite	6,81	6,08; 6,36
AG 637.4	"	6,54	6,64
AG 644.5	"	5,87	4,94; 5,11
AG 652.8	"	6,97	6,84
AG 656.4	"	6,89	5,43
FM 1595	biotite gneiss	3,44	3,01
FM 2455	"	3,62	3,31

4.3 Measurements at Oxford University

A detailed account of measurements made at OU is unnecessary as the divided-bar and the procedures followed there were almost identical to those described in Section 4.2. The important difference in the apparatus is its design for use on 1.5 inch diameter samples which could therefore be considerably thicker (usually 1 in.) without increasing the heat loss. No correction for the contact resistance of the sample was applied as repeat measurements on uniform samples of different thickness proved to be independent of sample thickness (Richardson and Oxburgh, 1978) even though a smaller load (100 bars) was applied to the stack. The sample temperature was close to 30°C in most experiments. Richardson and Oxburgh (1978) estimated the uncertainty in measuring the conductivity of an unknown to be ±1.

Experimental work at OU involved routine conductivity measurements and a number of cross-laboratory checks using various standards. For the latter purpose it was necessary to adjust the apparatus to accommodate 36 mm diameter discs.

The conductivity of the RPI quartz standard was checked against four 1.5 in. diameter quartz standards by comparing the results of calibration measurements on discs cut from the same sheet of 'Lexan'. The results of replicate measurements are summarized in Table 4.5 (a) and Figure 4.8a. Individual averages for the conductivity of the secondary standard were in excellent agreement. The overall mean and standard deviation were:

$$0.2690 \pm 0.0039 \ \mathrm{Wm^{-1}K^{-1}}$$

Table 4.3 Statistics of secondary standard calibration.

(a) Conductivity of 'Lexan' calibrated against quartz ($\perp$c).

(b) Conductivity of fused silica relative to secondary standard.

Measurements at 0C made at 30°C and 100 bars.

(a)

Quartz standard	$\bar{K}_L$ ($Wm^{-1}K^{-1}$)	$^{\sigma}K_L$ ($Wm^{-1}K^{-1}$)	$^{\sigma}\bar{K}_L$ ($Wm^{-1}K^{-1}$)	n
Q1	6,2097	0,0030	0,0009	13
Q2	6,2094	0,0036	0,0008	13
Q3	6,2094	0,0040	0,0016	12
Q4	6,2086	0,0042	0,0013	12
Q-RRI	6,2083	0,0048	0,0017	8
Mean	6,2091	0,0039	0,0006	58

(b)

Fused silica	$\bar{F}_{FS}$ ($Wm^{-1}K^{-1}$)	$^{\sigma}K_{FS}$ ($Wm^{-1}K^{-1}$)	$^{\sigma}\bar{K}_{FS}$ ($Wm^{-1}K^{-1}$)	n
A_2	1,341	0,062	0,036	3
B_1	1,353	0,023	0,012	4
B_2	1,344	0,006	0,002	4
FS - BPI[1]	1,243	0,038	0,017	5
FS - BPI[2]	1,271	0,014	0,003	11

$\bar{K}$ = mean conductivity; $^{\sigma}K$ = standard deviation; $^{\sigma}\bar{K}$ = standard error; n = number of measurements.

1 - measurements made at 0W.

2 - measurements made at BPI (27° and 300 bars).

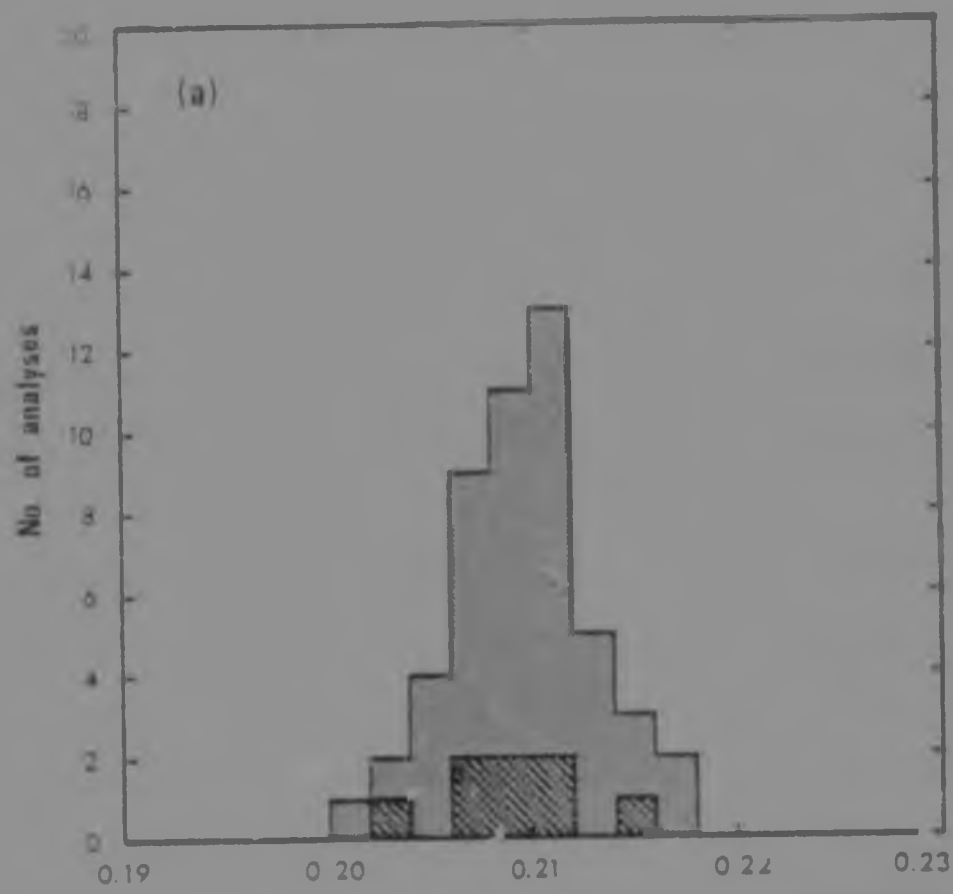

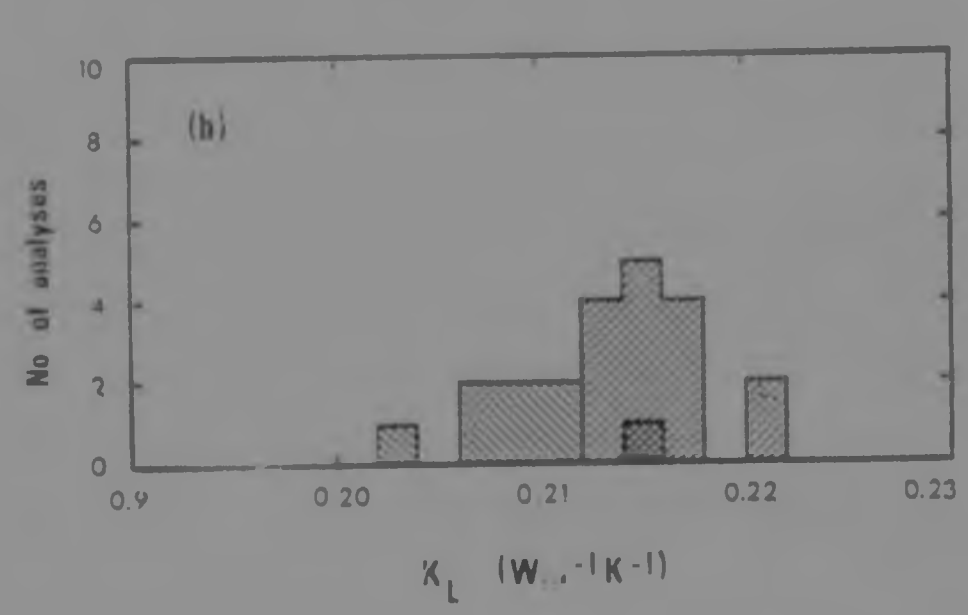

FIGURE 4.8 Histograms of the conductivity of 'Lexan' calibrated against quartz ($\perp c$) at BPI and OU. (a) Comparison of results obtained for four 1,5 in. diameter standards and the BPI standard. All measurements at OU. (b) Comparison of results obtained at OU and BPI using the BPI standard.

HEAT PRODUCTION MEASUREMENTS

Although all naturally radioactive [illegible] ^{238}U, ^{235}U, ^{232}Th and ^{40}K are in sufficient abundance and have sufficient decay energies to contribute significantly to the observed heating of rocks. The kinetic energies of particles emitted in the decay processes are converted into heat when they collide with crystal lattices in the immediate vicinity of the decaying nuclei. Table 3.1 lists constants calculated by Birch (1954) and Rybach (1971) which give the amount of [illegible] generated per unit mass of U, Th or K per unit time. Rybach's revised values are significantly lower than the values given by Birch and they will be adopted here. The data may be cast in the form of an equation which gives the heat production, A, in terms of the actual concentrations of radioactive elements:

$$A = 10,952 c_U + 0,2638 c_{Th} + 3,481 M_K \rho \quad pWm^{-3} \qquad (1)$$

where c_U and c_{Th} are the concentrations of U and Th in weight p.p.m., M_K the concentration of K in weight percent and ρ the density of the rock in kgm^{-3}.

There are obvious sampling problems in regions such as the Kaapvaal Craton, where most of the basement is covered by platform strata, and the Namaqua Mobile Belt, where the exposure is poor. Samples are necessarily limited to drill cores from the boreholes which were used for heat flow determination or from nearby boreholes. It was therefore not possible to obtain a detailed representation of the radioelement distribution within the rocks surrounding each heat flow site.

Table 5.1 Heat production rates per unit mass of U, Th and K (after Rybach, 1976)

Isotope/element	Heat production constants ($mWkg^{-1}$)	
	Birch (1954)	Rybach (1976)
^{238}U	0,094	0,0917
^{235}U	0,57	0,575
U (natural)	0,098	0,0952
^{232}Th	0,027	0,0256
K (natural)	$3,6 \times 10^{-6}$	$3,47 \times 10^{-6}$

however, there is considerable justification for restricting heat production measurements to borehole cores. U-Th-Pb isotopic studies in Precambrian granite basement in Wyoming have shown that surface samples and shallow drill cores underwent extensive U loss (up to 89%) when the granites were exposed to near surface conditions in the Cenozoic (Kosholt et al, 1973; Stuckless and Nkomo, 1978). U depletion appears to have been a regional feature. Although Th was remobilised, it appears to have been redistributed locally and there is no evidence for regional depletion. Stuckless and Nkomo (1978) showed that samples from as deep as 150 m have lost U, but this is not always the case and many samples have gained considerable amounts of U. This suggests that bulk-rock U depletion may only be important close to the surface.

Although most of the above near-surface samples had Th/U ratios in excess of the average for granitic rocks (cf. Clark et al, 1966) such

high ratios are not indicative of recent U loss. Gray and Oversby (1972) and Gray (1977) showed that central Australian granulites underwent regional U depletion during 1250 m.y. old granulite facies metamorphism. Th, on the other hand, appears to have been redistributed only locally. Most Th/U ratios are between 3 and 15 with some as high as 150. In summary, limiting heat production measurements to deep borehole cores is only a precautionary measure, and the effects of recent remobilization of U and Th can only be assessed by undertaking detailed U-Th-Pb isotopic studies.

Table 5.2 shows that samples from most of the boreholes in the Namaqua Mobile Belt have extremely variable Th/U ratios. The overall range is 0.2 to 55,1 indicating both loss and gain of U (and possibly Th). The average values for most boreholes are between 4 and 5. Basement samples from the Klerksdorp district (Kaapvaal Craton) are from closely spaced boreholes; they have a range of Th/U of 1,8-8,0 and a mean value of 3,9. The high U contents and low Th/U ratios in many samples, and the fact that the average Th/U ratio for most localities is not very different from the average of 4 given by Clark et al (1966) for most crustal rocks, suggest that U was not lost regionally, either during metamorphism or in recent times.

Samples of basement rock were collected at roughly equally spaced depth intervals but due care was taken to ensure that major rock types were selected in rough proportion to their abundance. A description of individual samples may be found in Appendix IV. Boreholes in the Klerksdorp district pass through a relatively thin sequence of volcanic rocks before penetrating basement. These were not sampled systematically but one composite sample was analysed to give an estimate of the heat production of these cover rocks.

Table 5.2 Th/U ratios for basement samples from boreholes in the Namaqua Mobile Belt and Kaapvaal Craton (Klerksdorp boreholes)

Borehole/locality	Th/U (range)	Th/U (mean)
FM 143	0,8 - 55,5	4,7*
HKE 26	1,0 - 29,0	4,6*
HE 177	0,8 - 14,9	7,1
CCX-0425	3,2 - 27,6	12,5
AG 140	2,3 - 15,0	4,9
A 9	2,1 - 9,1	4,1
POG 32	2.8 - 6,6	4,6
RB 56	3,8 - 7,3	5,2
AP 11	0,9 - 21,0	7,5
KC 12	3,5 - 12,6	6,6
PC2-27	0,2 - 14,3	4,6
V 41	2,3 - 9,0	4,8
HB 77	4,0 - 5,4	4,8
Klerksdorp	1,8 - 8,0	3,9

* The singularly high values of 55,5 and 29,0 for these boreholes were excluded when calculating the means.

The samples were cleaned and obviously weathered portions were discarded before they were crushed, powdered and homogenized. Several analytical techniques were used to determine U, Th and K concentrations. The choice of technique was largely dictated by their availability at the times the analyses were done. Delayed neutron activation analysis (DNAA) was used for U analysis, neutron activation analysis (NAA) for U and Th, X-ray fluorescence spectrometry (XRF) for Th and K and gamma-ray spectrometry (GRS) for U, Th and K. Appendix III summarizes the operating conditions and results of tests on the precision and

accuracy of each method. The results of each analysis, and the analytical method employed, are given in tables in Appendix IV.

Rock densities are required for the determination of heat production (see equation 3.4). Densities were measured in two ways:

(1) by weighing samples suspended in air and in water;

(2) by measuring the mass and volume (using a micrometer) of rock discs prepared for thermal conductivity measurements.

The densities of several non-porous rocks were measured using both techniques. No difference was detectable and the second method was used for most rock whenever possible as it was far quicker. The uncertainty in density measurement was estimated to be within 0.01×10^{3} kgm^{-3}.

The overall uncertainty in measuring heat production depends on the analytical techniques employed and the U, Th and K concentrations involved. Most of this uncertainty resides in measuring U and Th contents and, as a rough guideline, it is estimated to be within 20-25% for rocks containing 1 p.p.m. U and 4 p.p.m. Th, 10-15% for rocks containing 5 p.p.m. U and 20 p.p.m. Th and better for higher concentrations. These uncertainties are considerably less than the natural variation of heat production on the scale of a few metres in most of the boreholes investigated here.

6 HEAT FLOW AND HEAT PRODUCTION DATA

6.1 Introduction

This chapter summarizes heat flow and heat production data collected from each new station. To maintain continuity the data are presented in pictorial form in the text; and individual measurements of temperature, thermal conductivity and heat production are given in tables in Appendix IV. The relevant tables are indicated immediately below each borehole heading. In order to reduce repetition the latitude, longitude, collar elevation, inclination (at the collar and maximum depth), and the total depth surveyed (along the borehole and vertically) are listed in Table 6.1. Localities are shown in Figures 2.2 to 2.4. The boreholes are described in order from west to east (Sections 6.3 to 6.14) with the exception of two that are situated in the Richtersveld Province (Sections 6.12 and 6.13). For the sake of convenience boreholes surrounding Springbok and Kierkasdorp are grouped together in Sections 6.3 and 6.14 respectively.

Unless otherwise stated only temperatures measured below the water table were recorded. Known occurrences of water flows are documented under the relevant subheadings. These were identified from variable borehole temperatures and temperature gradients (see Section 7.4), evidence of open fractures and recent weathering in borehole cores, and from the geologists' logs when they were available.

Topographic corrections were applied to those boreholes surrounded by relatively high relief and are reported where appropriate. In most cases, corrections were small below depths of 100m. The remaining

Table 6.1 Locality, elevation, inclination and depth of boreholes surveyed

Borehole name and serial no.		Latitude	Longitude	Collar elevation (m)	Inclination (degrees): Collar	bottom	Depth surveyed (m): along hole	vertical
Nababeep Flat Mine	FM 143	29° 31,9'S	17° 41,6'E	757,5	90,0	86,0	800,0	799,3
Hoogkraal East	HKE 26	29° 32,0'S	17° 54,5'E	922,2	74,3	68,4	494,9	467,0
Homeep East	HE 177	29° 32,2'S	18° 00,6'E	1058,6	77,4	64,2	501,6	471,6
Carolusberg West	CCX-042S	29° 38,4'S	17° 58,0'E	973,8	80,6	73,7	600,0	588,6
Aggeneys	AG 140	29° 13,2'S	18° 44,7'E	883,2	90,0	90,0	752,6	752,6
Puts-berg	POG 32	29° 20,5'S	19° 38,5'E	1030,4	85,0	72,7	520,0	512,3
Adjoining Geelvloer	G-42	29° 19,5'S	20° 07,1'E	915	90,0	90,0	137,4	137,4
Rozynen Bosch	RB 56	29° 03,7'S	20° 47,4'E	741,8	90,0	65,5	469,4	452,3
Areachap	AP 11	28° 17,1'S	21° 02,5'E	920	84,3	46,5	504,4	465,4
Boks Puts	KC 12	29° 01,1'S	21° 39,2'E	1008,0	76,0	66,9	224,6	214,3
Jacomyns Pan	PC2-27	29° 19,6'S	21° 47,2'E	1045	74,0	31,3	631,7	495,5
"	PC2-30	"	"	"	90,0	90,0	161,6	161,6
Vogelstruis Bult	V 41	29° 57,7'S	22° 18,0'E	1072,5	81,0	36,2	825,2	730,5
Black Face Mountain	BF 1	28° 42,6'S	17° 18,1'E	690	90,0	90,0	311,8	311,8
Haib	HB 77	28° 41,7'S	17° 53,0'E	501,2	90,0	90,0	540,0	540,0
Rhenosterhoek	DRH 18	26° 50,3'S	26° 27,0'E	1470	85,9	75,0	520,7	510,4
Rhenosterberghoek	DRB 6	26° 49,8'S	26° 27,6'E	1425	90,0	90,0	400,0	400,0
Rietkuil	DRK 17	26° 48,6'S	26° 29,6'E	1385	90,0	90,0	265,0	265,0
Schoemansfontein	SSF 1	26° 44,9'S	26° 32,3'E	1380	90,0	76,9	757,7	750,2
Brakspruit	BBS 1	26° 42,0'S	26° 33,7'E	1345	90,0	90,0	301,2	301,2
Muhemavlei	EMV 4	26° 36,3'S	26° 37,4'E	1360	93,0	84,3	596,5	595,2
Tweelingfontein	BTF 1	26° 27,1'S	26° 51,7'E	1480	90,0	86,4	464,6	464,2

boreholes are situated in regions of extremely low relief and corrections were not computed except for borehole BC 12; the topography surrounding BC 12 is typical of these sites and there the correction was less than 0,2% of the temperature gradient even above 100 m.

Three-dimensional thermal conductivity anomalies do not present a major problem at most of the new heat flow stations. The boreholes in the Klerksdorp district pass through a section of uniform lavas before penetrating granitic basement. Those in the Namaqua Mobile Belt penetrate either uniform rock types (chiefly gneisses) or metamorphic successions which, on the average, do not contrast markedly with the surrounding rocks. In only one case, PHG 32, has heat flow refraction been shown to have an important disturbing influence: this will be discussed in detail in Section 6.3.

For most boreholes, thermal conductivity samples were collected for relatively long depth intervals which displayed uniform temperature gradients. Unsystematic variations in temperature gradient which are not related to petrological changes may be caused by water flows or refraction of heat on a small scale. Where rapid variations in gradient are related to petrological variations it is difficult to obtain reliable estimates of the mean conductivity of different rock types without analysing unrealistically large numbers of samples. In both cases it is prudent to avoid sections of non-uniform thermal gradient.

Drill core samples were too small in diameter to be re-cored in the vertical direction and thermal conductivities were therefore measured

parallel to the original core axes. This raises the question of bias in data obtained from inclined boreholes penetrating conductively anisotropic rocks. Such effects are likely to be significant in only three boreholes (NB 12, WC2-87 and V 44) where the inclination decreases to less than 60° (Table 6.1). However, in all three cases, small scale variations in rock fabric orientation mask any effect that anisotropy in thermal conductivity might have and there are no systematic trends in conductivity or heat flow with depth (see Sections 6.8, 6.10 and 6.11).

Before presenting the data it is pertinent to digress to show how heat flow is calculated from temperature gradient and thermal conductivity data.

6.2 Calculation of heat flow

In principle, the calculation of heat flow as the product of the vertical temperature gradient and thermal conductivity is a simple procedure. However, although it is possible to obtain semi-continuous temperature profiles, only a small fraction of the core is sampled for thermal conductivity measurement and considerable problems arise when performing the calculation. Several computational procedures which vary in detail are in use but no single practice is universally applicable since each heat flow determination is affected by a number of different complicating factors.

In general, the problem may be approached by computing a heat flow ($\bar{q}_j$) for each unit of 'iso-conductive' rock intersected by the borehole. If values of $\bar{q}_j$ from different units agree they may be combined to

give an overall mean heat flow ($\bar{q}$) for the borehole. As discussed in this text, iso-conductive units consist predominantly of one petrological type (eg. biotite gneiss) whose thermal conductivity differs from that of a subjacent unit (eg. metaquartzite). Iso-conductive units are best indicated by uniform temperature gradients. The thickness of each unit will be designated by Δz_i; this is of the order of 100-200 m in most of the boreholes described here. Small scale (0.1 m) variations in composition and mineral orientation of the rocks comprising each unit lead to variations in conductivity. In principle, iso-conductive units can therefore be divided into sub-units of slightly different conductivity; their thicknesses will be designated by Δd_i. The depth interval between adjacent temperature measurements is Δl_j.

The simplest way of calculating $\bar{q}_j$ is to determine a heat flow (q_i) for each depth interval between adjacent temperature measurements which is represented by a thermal conductivity (K_i)

$$q_i = K_i G_i \tag{6.1}$$

where G_i is the temperature gradient for the i-th depth interval, Δd_i. The mean and standard error are

$$\bar{q}_j = \frac{1}{n} \sum q_i \tag{6.2}$$

$$\sigma_{\bar{q}_j} = \sqrt{\frac{\sum (q_i - \bar{q}_j)^2}{n(n-1)}} \tag{6.3}$$

The method is only appropriate if the thermal conductivity for each Δd_i is well represented. Most heat flow determinations involve measuring temperatures at intervals of approximately 10 m and K_i must usually be

estimated from one or two measurements. A further problem arises out of the fact that adjacent values of q_j are not independent and are influenced by lateral as well as vertical conductivity variations. For these reasons values of q_j were calculated only for purposes of illustration.

A more reliable value for $\bar{q}_j$ may be obtained from a computed mean conductivity ($\bar{K}_j$) and thermal gradient ($\bar{\Gamma}_j$) for each iso-conductive unit:

$$\bar{q}_j = \bar{K}_j \bar{\Gamma}_j \qquad (6.4)$$

The standard error in $\bar{q}_j$ is calculated from the standard error of the conductivity ($\sigma_{\bar{K}_j}$) and the temperature gradient ($\sigma_{\bar{\Gamma}_j}$)*:

$$\sigma_{\bar{q}_j}^2 = (\bar{K}_j \sigma_{\bar{\Gamma}_j})^2 + (\bar{\Gamma}_j \sigma_{\bar{K}_j})^2 \qquad (6.5)$$

Bullard (1939) showed that the appropriate value for $\bar{K}_j$ is the harmonic mean rather than the arithmetic mean. The justification for this lies in the fact that the thermal resistance of each unit ($\Delta z_j/\bar{K}_j$) equals the sum of the thermal resistances of its constituent 'sub-units' ($\Delta z/K_k$):

$$\frac{\Delta z_j}{\bar{K}_j} = \sum \frac{\Delta z}{K_k} \qquad (6.6)$$

Re-arranging yields

$$\bar{K}_j = \frac{\Delta z_j}{\sum \frac{\Delta z}{K_k}} \qquad (6.7)$$

When borehole core is sampled for thermal conductivity measurements

---

* See Campion et al (1973)

(6.5)

gradients, $\bar{F}_j$,

. Furthermore, if

$\bar{F}_j$.

as it has the advantage of using all the temperature [illegible] avoiding the interaction between successive measurements [illegible] gradients. Where temperature gradients vary systematically with depth, [illegible] error in $\bar{q}$ will be exaggerated. The causes of [illegible] discussed in later subsections and [illegible] Chapter [illegible].

Bullard (1939) devised a method [illegible] borehole to yield an overall mean heat flow ($\bar{q}$). A conductivity [illegible] is assigned to each depth interval between temperature readings [illegible] on the basis of the petrological log, and the mean [illegible] determined from a plot of temperature against [illegible] resistances:

$$T_i = T_o + \bar{q}\Sigma\frac{\Delta d_1}{K_1}$$

where T_o is the extrapolated surface temperature. The uncertainty in $\bar{q}$ is calculated from the standard error of the thermal conductivities.

Bullard's method is very successful when detailed geological logs of boreholes are available and when the thermal conductivity of each encountered rock type is well known. Such complete information was not available for any of the boreholes discussed in this chapter. Conductivity measurements were made only for long depth intervals characterized by uniform temperature gradients, and where more than one such interval was present in a borehole they were usually separated by sections of erratic gradient for which there were no conductivity data. In such cases, the best estimate for the mean is the weighted mean:

$$\frac{\Sigma w_j \bar{q}_j}{\Sigma w_j}$$

where the weight w_j is inversely proportional to the square of the standard error of $\bar{q}_j$. The standard error of $\bar{q}$ is given by

$$\sigma_{\bar{q}}^2 = \frac{1}{\sum(1/\sigma_{\bar{q}_j})^2} \qquad (6,1)$$

These procedures are not applicable to boreholes in which units of different conductivity vary on a scale smaller than the interval of temperature measurements. Here, the thermal resistance of each depth interval, δd_j, should be estimated by assigning conductivities to each rock type and determining their thicknesses from the petrological log (eg. Gough, 1961). The best estimate for $\bar{q}$ may then be obtained from the integrated thermal resistance plot of Bullard (1939).

6,3 Springbok - O'okiep - Nababeep localities

Nababeep Flat Mine	FM 143
Hoogkraal East	HKE 26
Homeep East	HE 177
Carolusberg West	CCX-0428

Temperature surveys were carried out in four boreholes in the Springbok - O'okiep - Nababeep mining district. The names of the boreholes are given above and their localities are shown in Figure 2,4 (Chapter 2).

Two previous heat flow determinations were made in the district by Carte and van Rooyen (1969). One was from the FM 143 borehole and the second from a borehole 3 km south of CCX-0428. The values reported by Carte and van Rooyen were:

FM 143 [illegible]

ZLH265 [illegible]

The new data yield a more detailed pattern of the local variation of heat flow and also provide a useful check on the reproducibility of heat flow measurements.

The local geology was discussed in Chapter 2. The FM 143, HKE 26 and HE 177 boreholes are all located within the subcrustrop of the Concordia granite gneiss while CCX-0428 was drilled further south into the Nababeep gneiss. Petrological logs of the boreholes were not available but the structural data (Benedict et al, 1964, Plate 1) indicate that FM 143 and CCX-0428 remain within their respective gneiss units to the deepest levels surveyed. HKE 26 and HE 177 are both situated about 500 m north of the lower contact of the Concordia granite gneiss (Figure 2.3, p. 40) where granitic injections into the underlying Nababeep gneiss have produced a prominent 'mixed zone'. Here, the dip of the units is at most 30° to the north and both boreholes evidently penetrate at least the mixed zone. However, the local dips vary considerably and the area is intersected by numerous small faults; it is therefore not possible to estimate the depths to the boundaries between these rock types accurately.

The Nababeep gneiss is predominantly composed of biotite-bearing augen gneiss whereas the Concordia granite gneiss is a more quartzo-feldspathic rock with minor amounts of garnet and biotite. These general differences are reflected in core samples collected from FM 143 and CCX-0428 but specimens from HKE 26 and HE 177 are variable and include both rock types.

The characteristically flat surface of Namaqualand is interrupted in the vicinity of Springbok by hills of relatively high relief. All reported temperatures and temperature gradients have therefore been corrected for topography. The corrections were small, up to 5% and sometimes 10% of the average gradient, for all the boreholes except UCK-0429 where corrections were between 15% and 30% in the upper 200 m.

Sababoep Flat Mine FM 141

(Table IV-1)

Temperatures were measured to a depth of 750,5 m in FM 141 and profiles of the temperature and temperature gradient are shown in Figure 6.1a. Slightly unstable temperatures at 220 m suggested some flow of water at this depth. The temperature gradients above 360 m are not uniform and samples for thermal conductivity measurement were collected from the depth range 180-800 m at intervals of approximately 10 m. The conductivities are plotted against depth in Figure 6.1b. The gneisses have a uniform conductivity and there are no systematic variations with depth. The harmonic mean conductivity and standard error are:

$$\bar{k} = 3,14 \pm 0,08 \text{ Wm}^{-1}\text{K}^{-1} \quad \text{(41 values)}$$

The heat flows calculated for 20 m intervals (q_i) are shown in Figure 6.1c. There is a small decrease in heat flow and temperature gradient (about 8%) at 660 m. The reason for this is not obvious. There were no waterflows at this depth and no indications of three-dimensional refraction of heat. The decrease may be related to palaeoclimatic surface temperature variations which will be discussed in the next chapter. However, this difference is approximately the

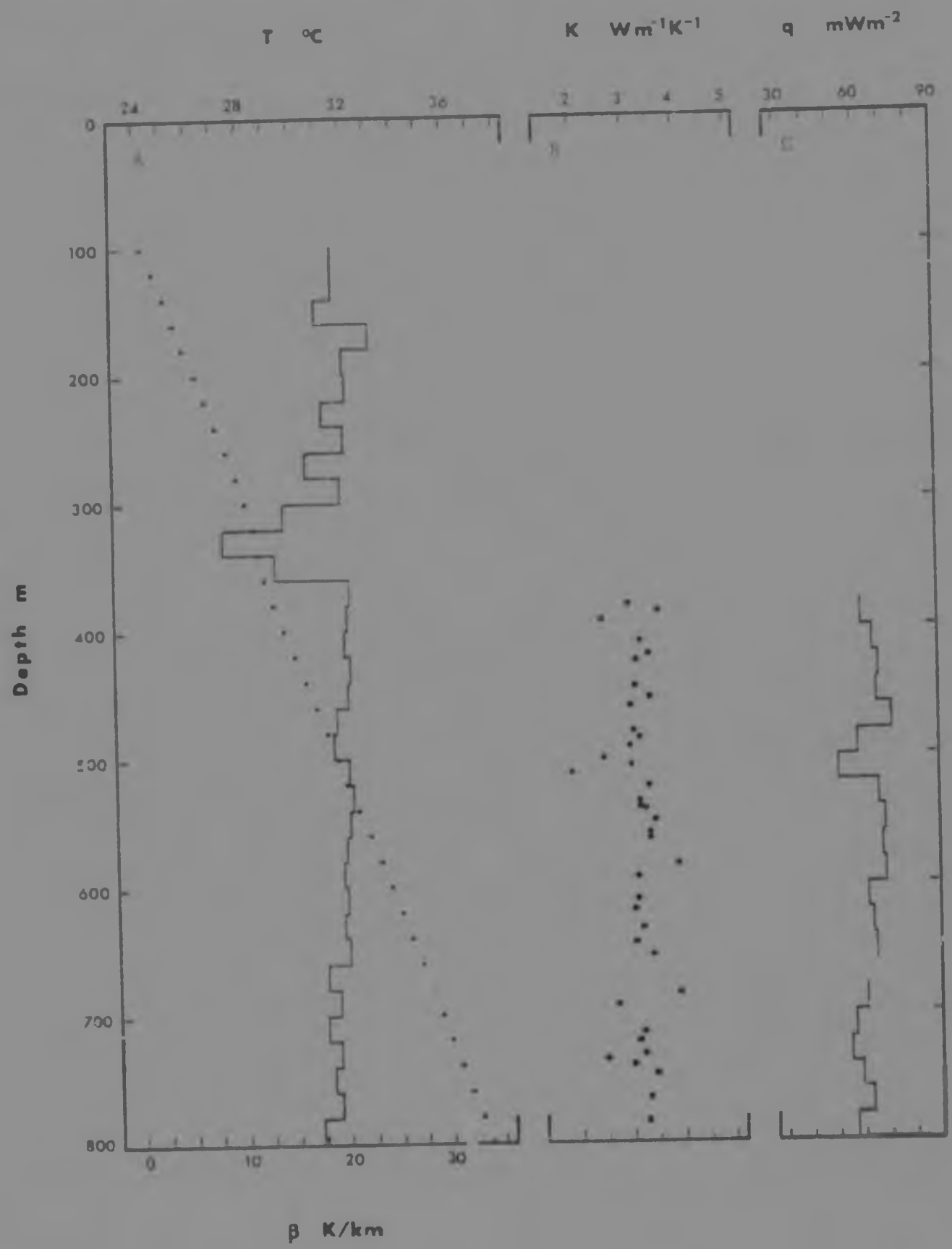

FIGURE 6.1 Nababeep Flat Mine FM 143. Borehole data showing (a) temperature (dots, top scale) and temperature gradien (steps, bo t m scale), (b) thermal onductivity and (c) heat flow as unction of depth.

same size as the standard deviation of the heat flow, and mean conductivities above and below 600 m are almost identical (3,13 ± 0,39 $Wm^{-1}K^{-1}$ and 3,16 ± 0,11 $Wm^{-1}K^{-1}$ respectively). There is no obvious reason to treat the data separately.

The least squares straight line through the temperature data between 350,0 m and 798,3 m is:

$$T(^{\circ}C) = (21,90 \pm 0,95) + (19,50 \pm 2,08)z(km)$$

and the mean heat flow and standard error computed from equations 6.4 and 6.5 are

$$\bar{q} = 61,2 \pm 1,6\ mWm^{-2}$$

This value is only 1,5% higher than that reported by Carte and van Rooyen (1969). If a topographic correction were applied to their data the discrepancy would increase to only 4%. The heat flows are therefore in excellent agreement.

Twenty-two heat production measurements were made on samples of drill core from FH 143 and the data are shown in the form of a histogram in Figure 6.2a. The obvious features of the distribution are the very high heat productions and the wide spread in the data. A precursory glance at the data for BKE 26 and BH 1?? (Figures 6.2b and 6.2c) suggests that high heat production is a characteristic of the Concordia granite gneiss and possibly of the immediately adjacent country rocks. There is no obvious correlation of heat production with depth and the mean and standard error are:

$$\bar{A} = 7,96 \pm 0,97\ \mu Wm^{-3}$$

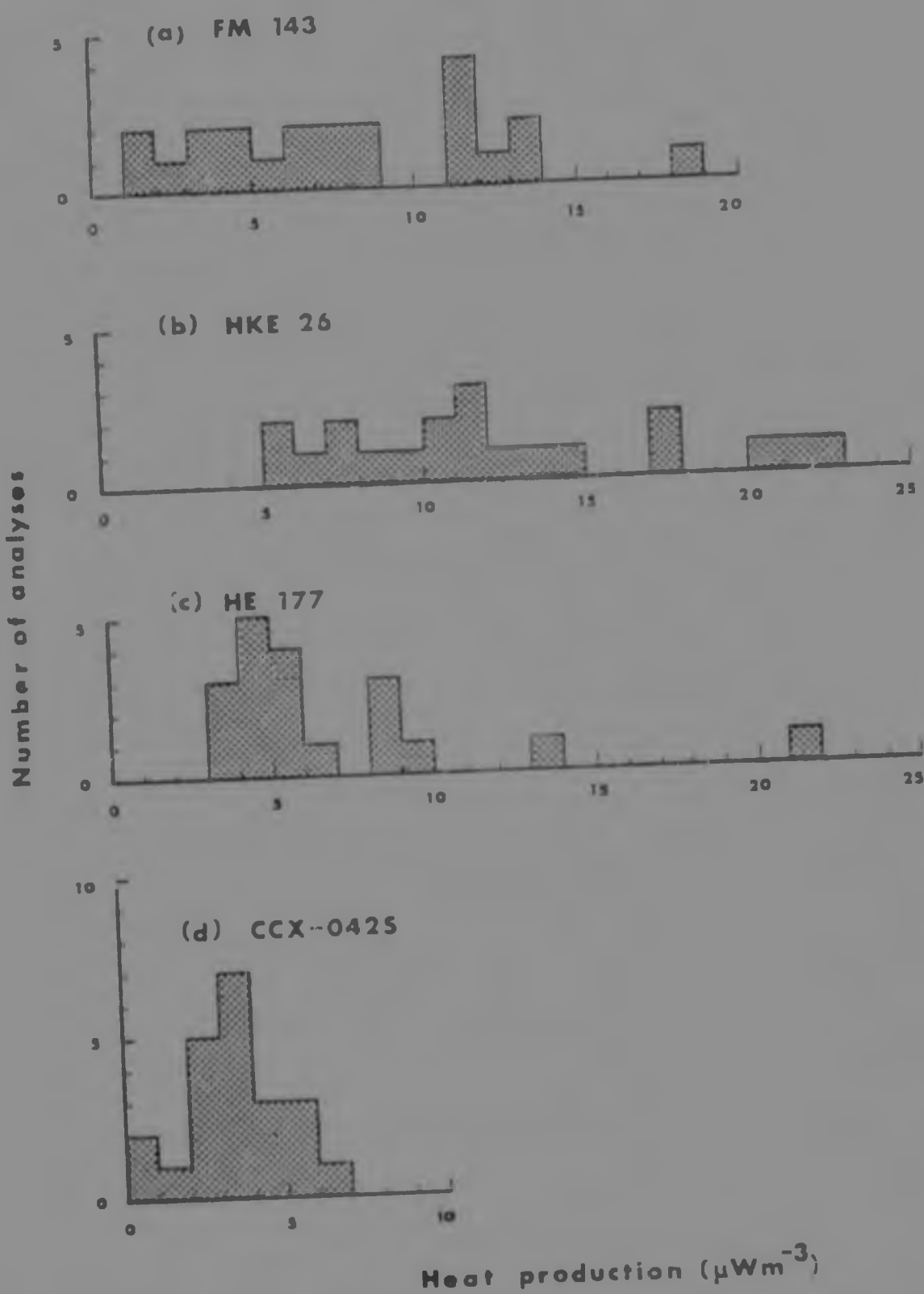

FIGURE 6.2 Histograms of heat production data for stations in the Springbok district.

Hoogkraal East HKE 26

(Table IV-2)

Temperatures in HKE 26 were measured to a vertical depth of 487,0 m. Figure 6.3 shows profiles of temperature and temperature gradient, the results of thirty-two conductivity measurements and heat flows for individual 10 m intervals.

There is a systematic increase in the temperature gradient between 40 m and 160 m. Below 160 m the gradient is uniform and close to 20 K/km. No water flows were detected in this borehole and variations in gradient cannot be attributed to near-surface water circulation. Temperature measurements were made four months after drilling ceased and, in this respect, HKE 26 is the 'youngest' borehole surveyed. This period is long enough for all large disturbances due to drilling to have subsided (Bullard, 1947) and there is no evidence for drilling transients near the bottom of the borehole. The harmonic mean conductivities above and below 160 m are $3,94 \pm 0,12$ and $3,78 \pm 0,10$ $Wm^{-1}K^{-1}$ and this difference is too small to account for the difference in the average gradient. Furthermore, the increase in gradient is not matched by a systematic trend in the thermal conductivity. An increasing temperature gradient to depths of approximately 200 m is a feature that has been observed in many of the boreholes under study and it is consistent with a recent increase in the surface temperature (eg. a climatic warming). It will be discussed in detail in Chapter 7.

The harmonic mean conductivity and standard error are:

$$\bar{K} = 3,82 \pm 0,09 \ Wm^{-1}K^{-1} \qquad (32 \text{ values})$$

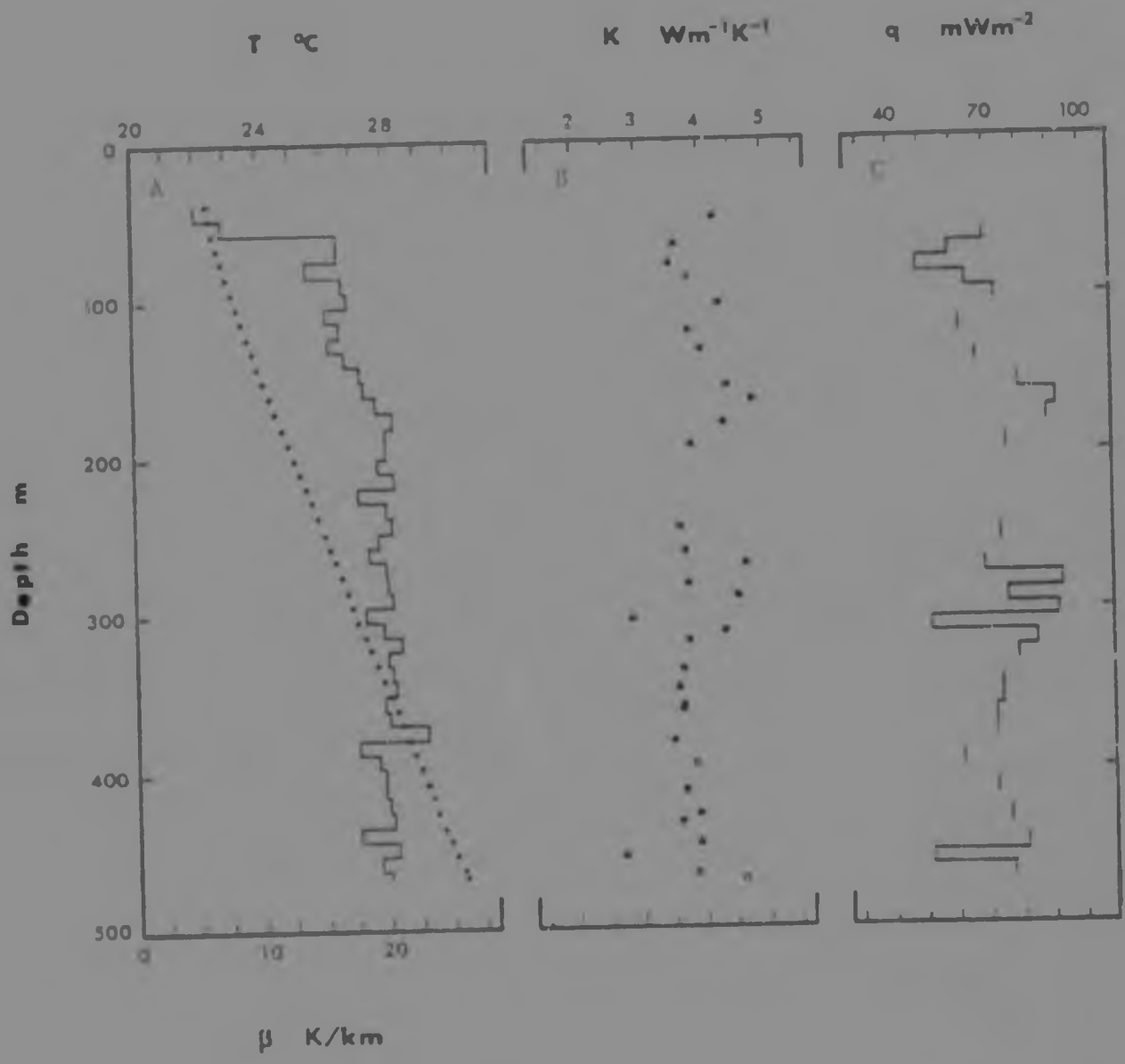

FIGURE 6.3 Hoogkraal East HKE 16. Borehole data.

and a least squares straight line fit to the temperature data between 57,6 m and 467,0 m yields:

$$T(^{o}C) = (21,25 \pm 0,03) + (19,26 \pm 0,09)z(km)$$

The mean heat flow and standard error are:

$$\bar{q} = 73,6 \pm 1,8\ mWm^{-2}$$

Slightly higher values for the temperature gradient and heat flow are obtained if temperatures above 160 m are neglected:

$$T(^{o}C) = (21,06 \pm 0,01) + (19,81 \pm 0,04)z(km)$$

$$\bar{q} = 75,7 \pm 1,8\ mWm^{-2}$$

However, this presumes that the observed variation in temperature gradient is caused by past variations in surface temperature. Such effects will be discussed in Chapter 7 and no attempt will be made to correct for them in this chapter.

As in the case of FM 143, heat production data show no correlation with depth or rock type. The data are extremely variable and the mean value is even higher than that for FM 143 (Figure 6.2b). The mean heat production and standard error are:

$$\bar{A} = 12,30 \pm 1,14\ \mu Wm^{-3} \quad (20\ values)$$

Homeep East HE 177

(Table IV-3)

HE 177 was surveyed to a vertical depth of 473,0 m. The variations of temperature gradient, thermal conductivity and heat flow with depth

are illustrated in Figure 6.2.

The temperature gradient and heat flow both show a systematic increase with depth. The trends are not as marked as those in BKB 26 but they extend to a greater depth. There is no indication of a systematic variation in the thermal conductivity data and the curvature of the temperature profile is probably caused by a similar process to that operating in BKB 26.

The straight line through the temperature data (97,6-471,6 m), harmonic mean conductivity and heat flow are:

$$T(^{\circ}C) = (19,88 \pm 0,04) + (18,2 \pm 0,1)z(km)$$

$$\bar{k} = 3,49 \pm 0,09\ Wm^{-1}K^{-1} \quad (27\ values)$$

$$\bar{q} = 63,6 \pm 1,7\ mWm^{-2}$$

The heat production data (Figure 6.2c) are less variable than those of the preceding boreholes and only two samples have abnormally high values. Nineteen measurements yield a mean and standard error of:

$$\bar{A} = 0,90 \pm 0,99\ \mu Wm^{-3}$$

Carolusberg West CCX-0425

(Table IV-4)

Temperature gradients in the first 200 m of CCX-0425 (Figure 6.3) are very erratic and this section of the borehole has not been used for the determination of heat flow. The water table was encountered at 210 m and this may account for very low and negative gradients

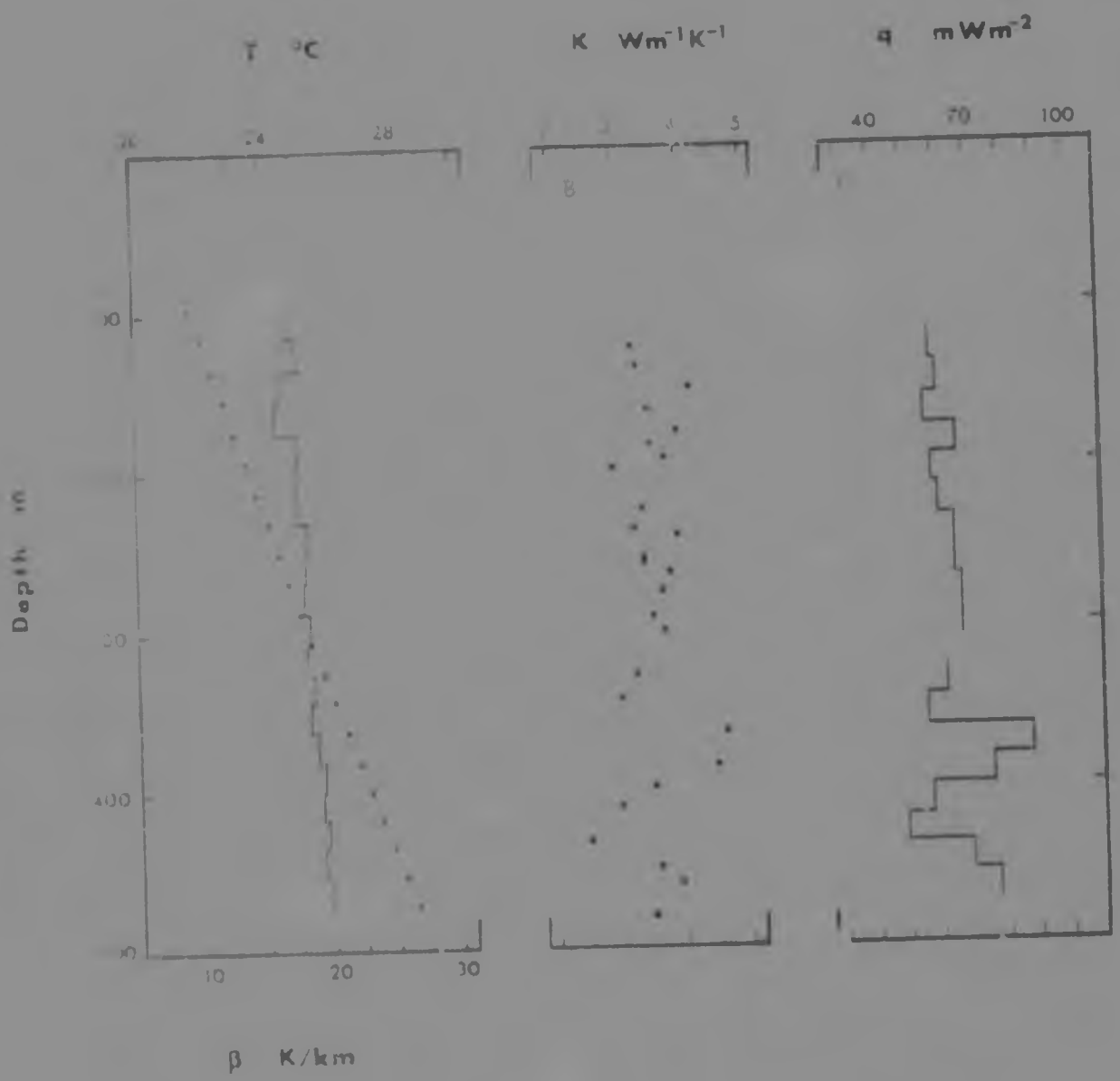
T °C
K Wm⁻¹K⁻¹
q mWm⁻²
40
70
100
Depth m
400
10
20
30
β K/km

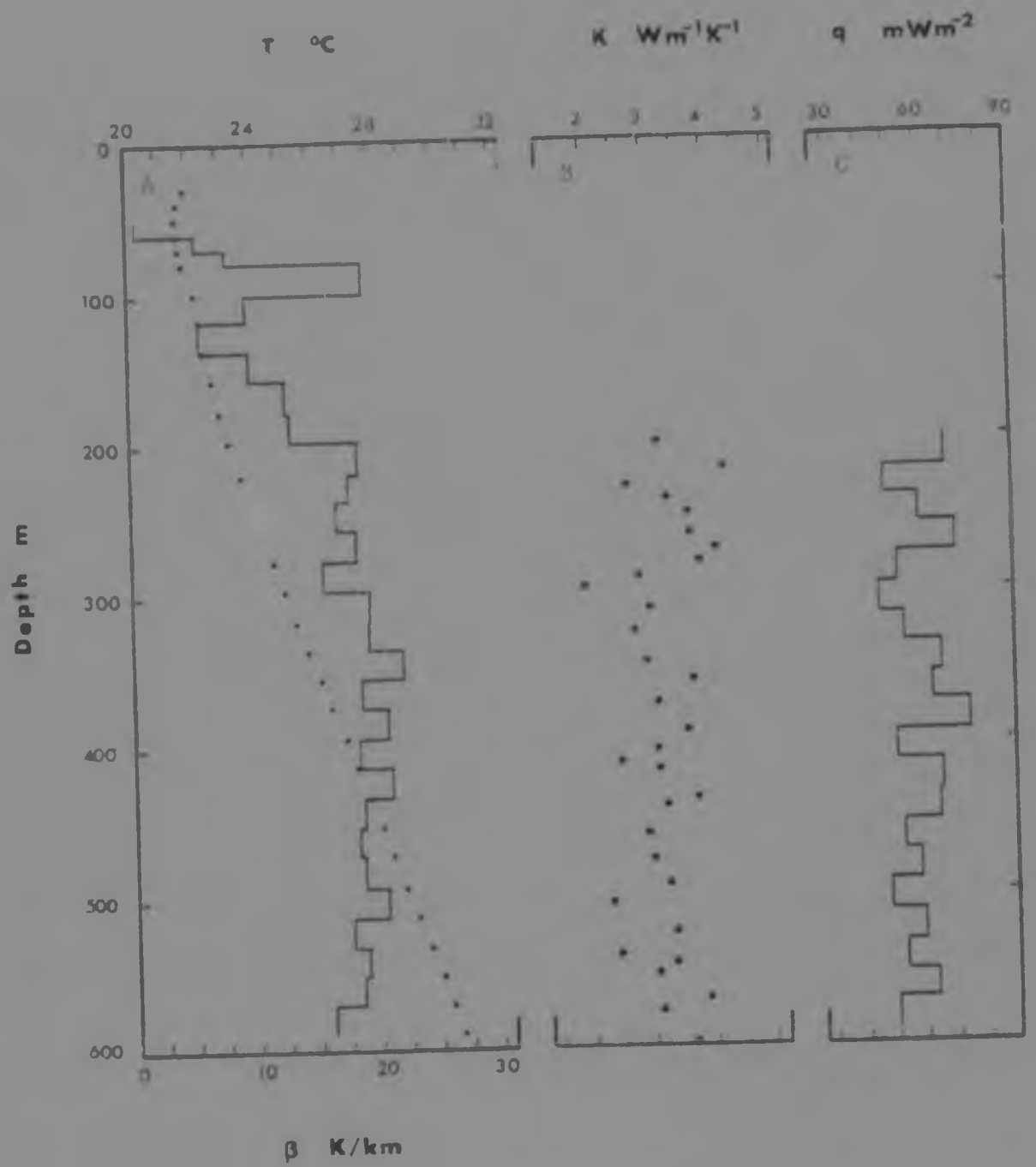

FIGURE 6.5 Carolusberg West CCX-042S. Borehole data.

above this depth. No obvious water flows were observed. The thermal conductivity and heat flow data are also shown in Figure 6.3.

There are no systematic trends in the data below 200 m and the least squares straight line through the temperature data between 197,7 m and 588,6 m, harmonic mean conductivity and heat flow are:

$$T(^{\circ}C) = (19,39 \pm 0,14) + (19,13 \pm 0,09)z(km)$$

$$\bar{K} = 3,11 \pm 0,10 \text{ Wm}^{-1}\text{K}^{-1} \quad (32 \text{ values})$$

$$\bar{q} = 59,5 \pm 1,9 \text{ mWm}^{-2}$$

The heat flow is in close agreement with the value obtained 3 km further south by Carre and van Rooyen (1968), 59,0 mWm^{-2}.

The mean heat production and standard error of twenty-two measurements on core samples are:

$$\bar{A} = 3,64 \pm 0,34 \text{ nWm}^{-3}$$

The range of heat production is small (Figure 6.2d) and the data suggest that the Nababeep Gneiss is considerably less 'enriched' than the Concordia granite gneiss.

6.4 Aggeneys AG 140

(Table IV-5)

AG 140 was drilled on the farm Zuurwater, 60 km west-southwest of Pofadder, and temperatures were measured to a depth of 752,6 m. The prospect has since been developed into the Black Mountain Mine. The site is surrounded by the Aggeneys to Berge and Kwartberg ranges of

hills and a small negative topographic correction was applied. The corrected temperatures and temperature gradients are shown in Figure 6.6.

The borehole passes through a succession of gneisses, schists and metaquartzites. From below the soil cover to a depth of 337 m the rock is mainly biotitic pink and grey gneiss interrupted by several thin pegmatite bands. From 337 m to 386 m there is a mixture of gneisses and schists with some bands of amphibolite and pegmatite. Between 386 m and 570 m schists and schistose gneisses predominate, and from 570 m to 730 m there is a section of impure metaquartzite. At 730 m the borehole passes into more schists.

No obvious water flows were detected and the rapid variation of thermal gradient at greater depths in the borehole is evidently related to rapid variations of rock type. Samples for thermal conductivity measurement were collected from two sections of uniform gradient, 200-440 m and 600-670 m. Thermal conductivities and heat flows are shown in Figure 6.6.

For the interval between 200 m and 440 m, the straight line through the temperature data, harmonic mean conductivity and heat flow are:

$$T(^{\circ}C) = (22,94 \pm 0,03) + [18,62 \pm 0,09]z(km)$$

$$\bar{k} = 2,94 \pm 0,14 \text{ Wm}^{-1}\text{K}^{-1} \quad (19 \text{ values})$$

$$\bar{q} = 54,7 \pm 2,6 \text{ mWm}^{-2}$$

A rather less precise value for the heat flow was obtained from the section between 600 m and 670 m. Here:

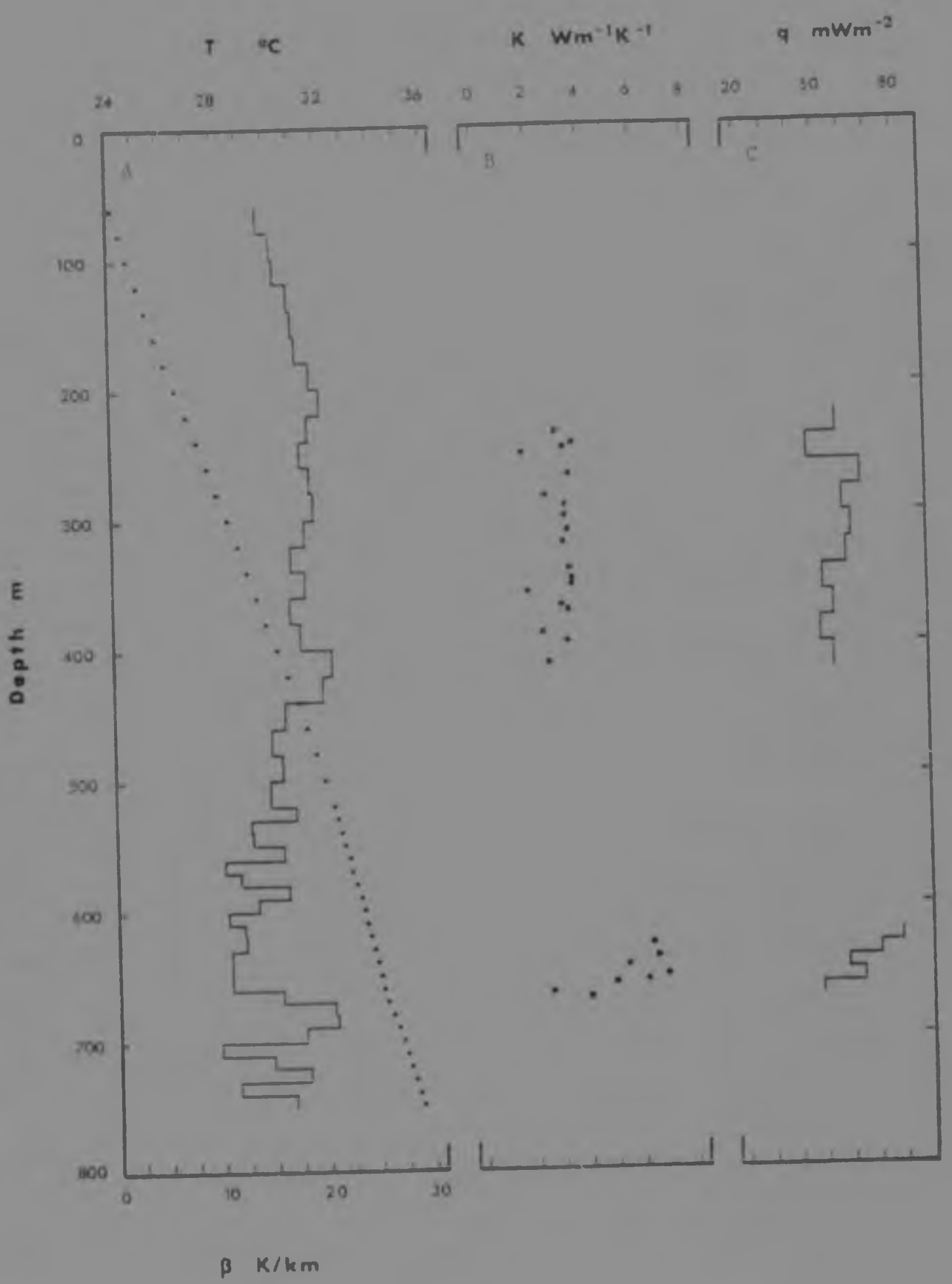

FIGURE 6.6 Aggeneys AG 140. Borehole data.

$$T(^{\circ}C) = (20,40 \pm 0,13) + (13,69 \pm 0,21)z(km)$$

$$\bar{R} = 4,89 \pm 0,56\ Wm^{-1}s^{-1} \qquad (8\ values)$$

$$\bar{q} = 57,1 \pm 6,6\ mWm^{-2}$$

The close agreement between these values indicates that no heat is gained or lost in the intervening depths and the overall mean heat flow and standard error calculated from equations 6.10 and 6.11 are:

$$\bar{q} = 55,0 \pm 2,5\ mWm^{-2}$$

Temperature gradients above 280 m in AG 140 show a similar trend to that defined by HKT 26. Although there are no thermal conductivity data for this section of the borehole the relatively uniform petrography of the gneiss above 387 m suggests that the whole unit is iso-conductive and that the variation of near-surface gradients is caused by a similar effect to that in HKT 26.

Complete heat production measurements were made on seventeen core samples. There are too few data to make reliable correlations between heat production and rock type. The average values for nine gneisses and four schistose gneisses are:

gneiss	$1,27 \pm 0,21\ \mu Wm^{-3}$
schistose gneiss	$2,35 \pm 0,19\ \mu Wm^{-3}$

Single analyses on four other rock types yielded

pegmatite	$1,82\ \mu Wm^{-3}$
biotite fels	$3,03\ \mu Wm^{-3}$
amphibolite	$1,32\ \mu Wm^{-3}$
quartzite	$1,81\ \mu Wm^{-3}$

A histogram of the data (Figure 6.7a) shows that the range of heat production is fairly limited and a mean and standard error for all seventeen samples have been calculated:

$$\bar{A} = 2,75 \pm 0,20 \ \mu Wm^{-3}$$

6.5 Puts-berg POG 32

(Table IV-6)

POG 32 is situated on the farm Puts-berg, 35 km southeast of Pofadder. The topography is very subdued and a correction was not applied. Temperatures were measured to a vertical depth of 512 m and are shown in Figure 6.8. There is a small but steady increase in temperature gradient to a depth of about 20[illegible] m.

The borehole passes through a nearly vertical succession of gneiss and metaquartzite and the structural relationships are illustrated in Figure 6.9. For the purpose of heat flow determination the borehole has been divided into two units:

(1) 0-345 m: heterogeneous biotite gneiss. The rock is schistose and friable in places, particularly close to the surface. There is a thin metaquartzite layer at 325 m.

(2) 345-512 m: metaquartzite containing variable amounts of biotite and other impurities. This unit includes bands of gneiss at 445 m and schist at 490 m.

Thermal conductivity measurements were made on representative samples from the two major rock units and the data are shown in Figure 6.8. The conductivities are very variable due to the heterogeneous nature

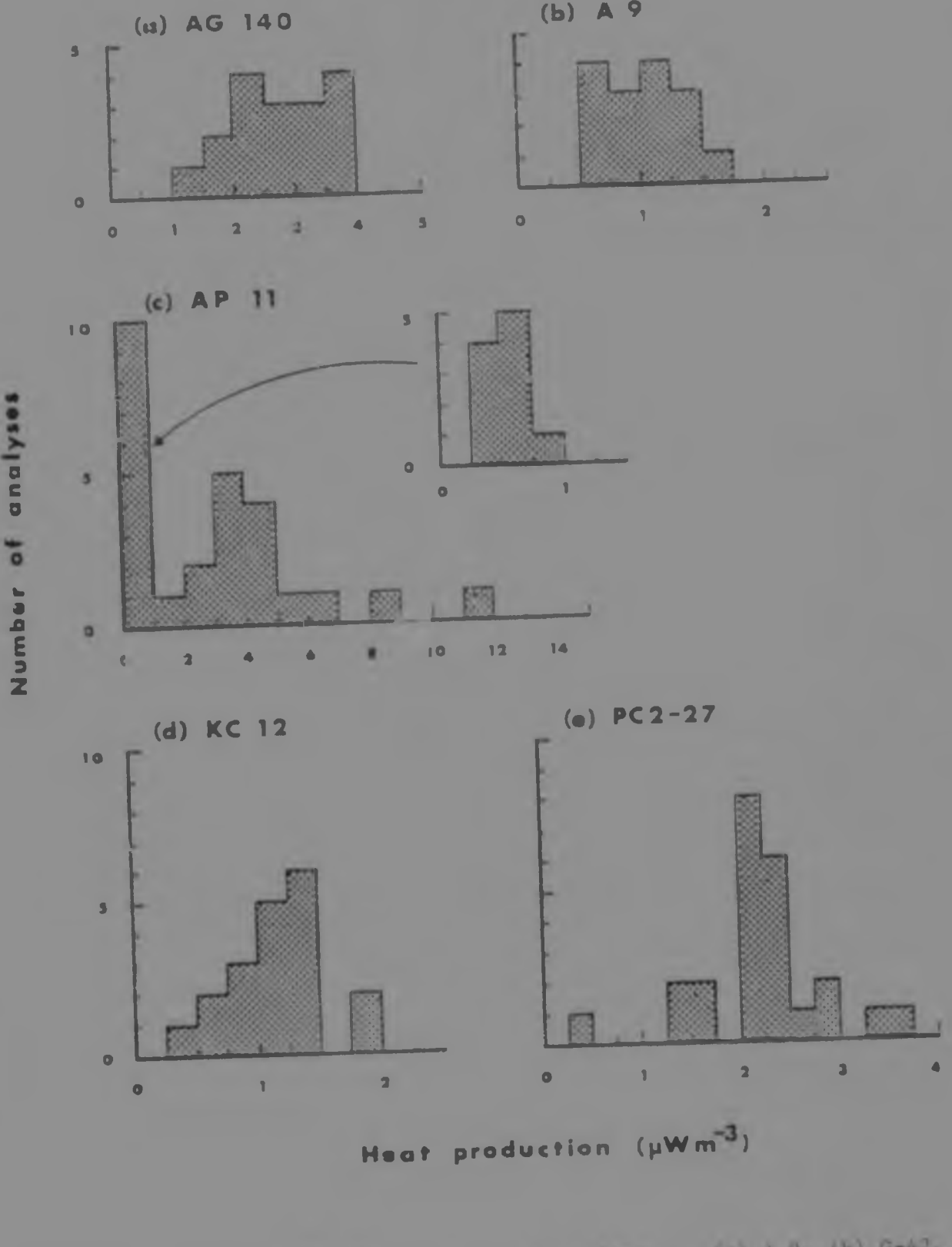

FIGURE 6.7 Histograms of heat production data for (a) A 9, (b) G-42, (c) AP 11, (d) KC 12 and (e) PC2-27.

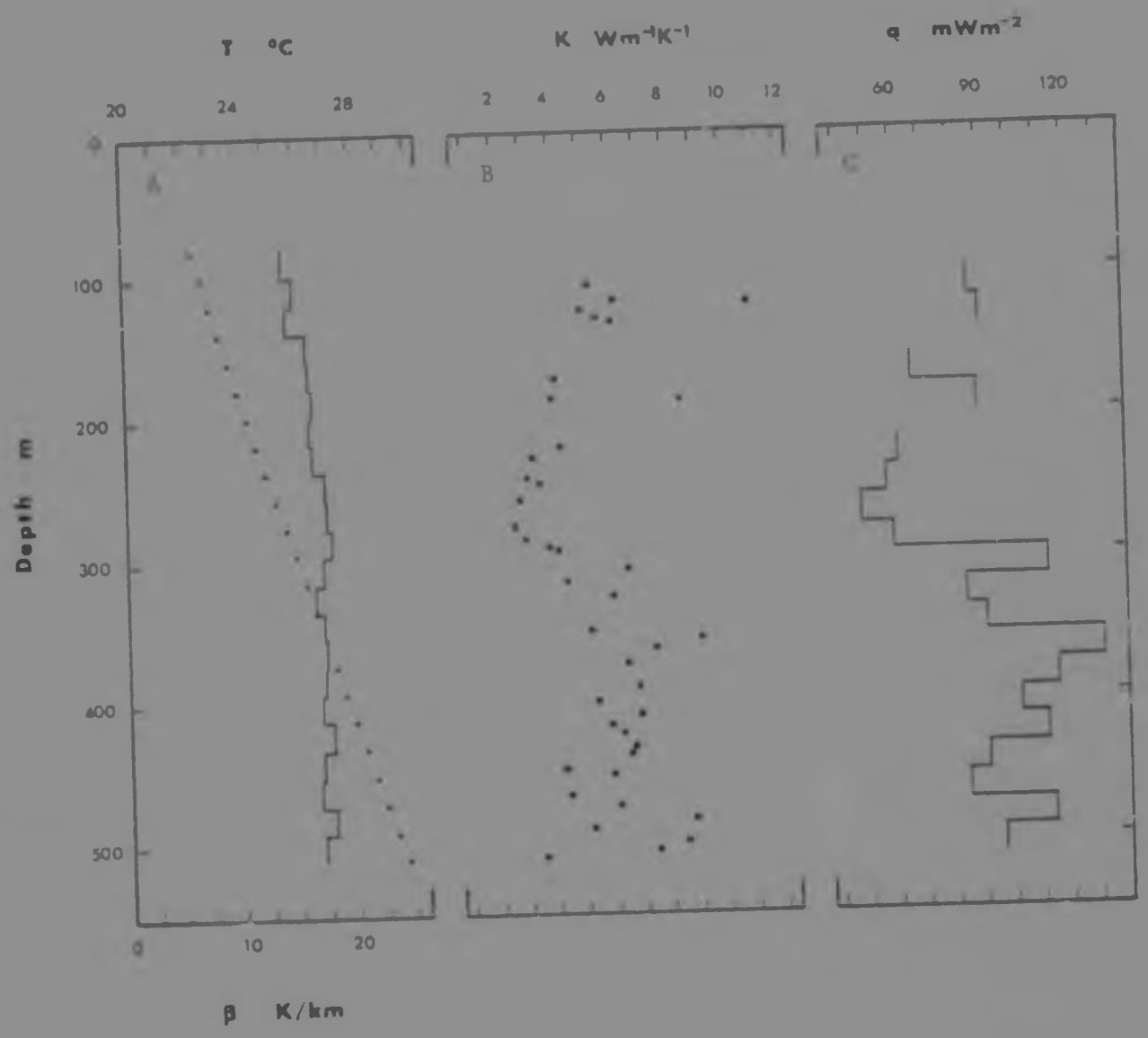

FIGURE 6.8 Puts-berg POG 32. Borehole data.

of both rock types and in some cases they are unusually high. Thin sections were made from the two most anomalous samples from each unit (sample numbers 122.5, 191.2, 362.1 and 509.7). Both gneiss* and metaquartzite samples contained large quantities of finely recrystallized quartz, and, although it was not possible to determine the orientation of all quartz grains, their c-axes were presumably well aligned parallel to the cores' axes. (The conductivity of quartz parallel to the c-axis is $\sim$12 $Wm^{-1}K^{-1}$ (Clark, 1966).

The temperature data, harmonic mean conductivity and heat flow for each unit are summarized below:

(1) 80-345 m:

$T(^{o}C) = (21,02 \pm 0,04) + (16,57 \pm 0,15)z(km)$

$\bar{K} = 4,31 \pm 0,46\ Wm^{-1}K^{-1}$ (21 values)

$\bar{q} = 71,4 \pm 7,6\ mWm^{-2}$

(2) 345-512 m:

$T(^{o}C) = (20,81 \pm 0,02) + (17,31 \pm 0,04)z(km)$

$\bar{K} = 6,00 \pm 0,34\ Wm^{-1}K^{-1}$ (20 values)

$\bar{q} = 103,9 \pm 5,9\ mWm^{-2}$

Although the uncertainties in the heat flows are large they are clearly not large enough to accommodate the discrepancy between the means. No water flows were recorded, but it is possible that the gneisses are sufficiently permeable to permit slow, steady state movement of water through the rock. The metaquartzite appears to be virtually impermeable and the heat flow measured in this unit is nearly twice the average for the Namaqualand belt. The downward movement of a considerable volume of water would be necessary to reduce

* The term "gneiss" has been used somewhat indiscriminately; certain samples called gneisses have high modal quartz.

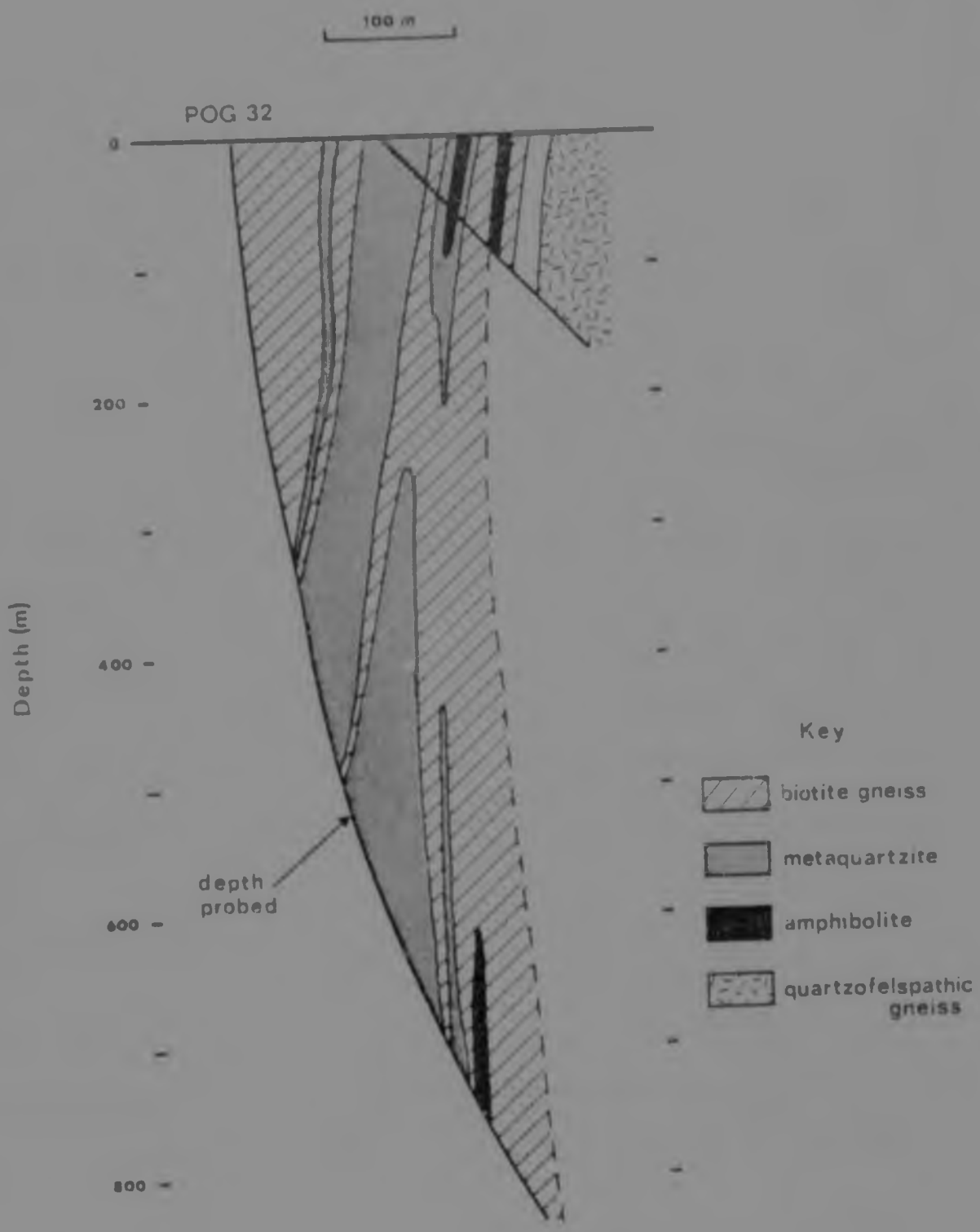

FIGURE 6.9 Vertical section of the geology intersected by POG 32 (simplified from section provided by Phelps Dodge of Africa Ltd).

the heat flow in the gneissic unit by 30 mWm^{-2} and as Puts-berg situated in a region of very low rainfall this explanation is unsatisfactory.

The metaquartzite unit is relatively narrow and almost vertical (Figure 6.9) and the similarity of the temperature gradients in both rock units, in spite of the conductivity contrast, suggests that the isotherms are not appreciably deflected by the metaquartzites. In order to test this possibility, the two-dimensional temperature field in the presence of the simple conductivity anomaly shown in Figure 6.10 was investigated. A finite difference technique was used to determine temperatures at grid points in this section*. The boundary conditions were zero surface temperature, zero heat flux across the vertical boundaries of the model (x = 500 m) and a constant heat flux of 70 mWm^{-2} into the base (z = 1000 m). The temperature distribution is summarized in the form of isotherms.

The important result of the analysis is that the conductivity anomaly is too narrow to perturb the temperature field appreciably and that temperature gradients measured in the metaquartzite pertain to the surrounding gneiss. For this reason measurements from the metaquartzite unit have been discarded and the heat flow is taken to be 71,4 mWm^{-2}.

The results of heat production measurements made on four aggregrate samples are summarized in Table 6.2. The metaquartzite has a significantly lower heat production than the gneiss. The gneisses are volumetrically more representative of the rocks surrounding the borehole

---

* I am grateful to Dr P C England of the Department of Geodesy and Geophysics, Cambridge University, for performing the computation.

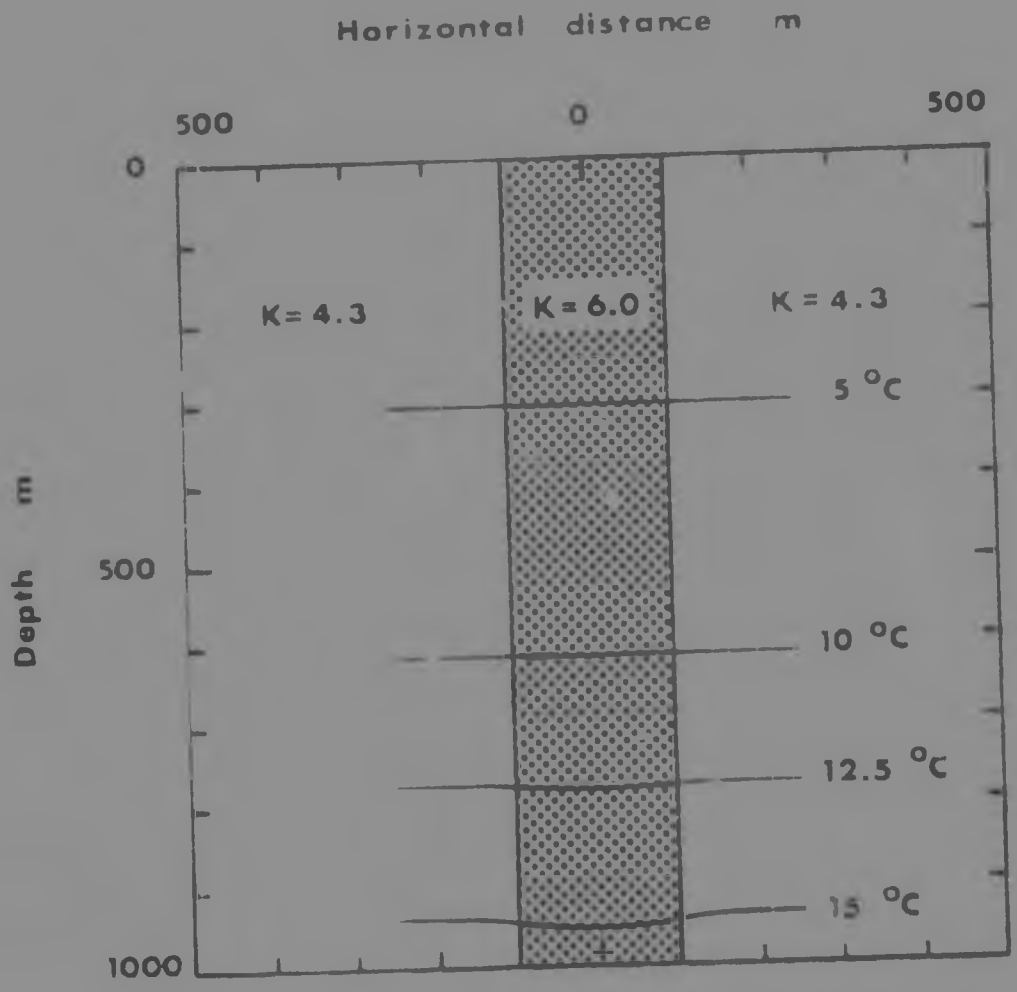

FIGURE emperature distribution (shown as isotherms) n the presence of a two-dimensional, 1000 m .ide and vertical thermal conductivity nomaly. Conductivities in $Wm^{-1}K^{-1}$. See .ext for discussion.

Table 6.2 Heat production data for POG 32

Sample	Depth range (m)	Description	Heat production μWm^{-3}
POG 1	100 - 200	Friable biotite gneiss	3,04
POG 2	180 - 280	Biotite gneiss	2,52
POG 3	330 - 440	Impure metaquartzite	1,24
POG 4	450 - 520	Metaquartzite	1,30

and the heat production for POG 32 is taken to be the average of values for samples POG 1 and POG 2:

$$\bar{A} = 2,78\ \mu Wm^{-3}$$

6.6 Adjoining Geelvloer G-42

(Table IV-7)

G-42 is a vertical air-drill hole located on the farm Adjoining Geelvloer, 70 km east-southeast of Pofadder. Temperatures were measured at 5 m intervals to the bottom at 137,4 m, and are shown in Figure 6.11a. G-42 is the shallowest borehole in which temperature measurements were made. A topographic correction was not made as there is virtually no relief in the vicinity of the borehole.

Samples for thermal conductivity and heat production analysis were collected from the lower, uniform section (98-187 m) of a nearby blocked borehole (A9) which is approximately 200 m north of G-42 on the down-dip side of the succession. Depths in A9 and G-42 were correlated

using a geological section through both boreholes. It was not possible to estimate equivalent depths of individual samples accurately, but the equivalent depth range in Deep was 28-143 m. The rocks are predominantly fine grained schistose biotite gneisses with few coarser, less homogeneous varieties.

The thermal conductivity data are summarized in the form of a histogram in Figure 6.11b and the harmonic mean and standard error are

$$\bar{K} = 3,40 \pm 0,12 \text{ Wm}^{-1}\text{K}^{-1} \quad (38 \text{ values})$$

The temperature gradient decreases between 30 m and 45 m and this section was not used in the heat flow calculation. No water flows were encountered and the low temperature gradients at 110 m are probably caused by variations in the thermal conductivity. The straight line through the temperature data between 45 m and 137,4 m is:

$$T(^{\circ}C) = (22,26 \pm 0,02) + (17,58 \pm 0,11)z(km)$$

The heat flow and standard error are:

$$\bar{q} = 59,8 \pm 2,2 \text{ mWm}^{-2}$$

There is very little spread in the heat production data (Figure 6.7c) and the mean and standard error of fifteen measurements are:

$$\bar{A} = 1,02 \pm 0,08 \text{ }\mu\text{Wm}^{-3}$$

6.7 Rozynen Bosch Nr. 56

(Table IV-8)

Rozynen Bosch is situated approximately 45 km northwest of Kenhardt.

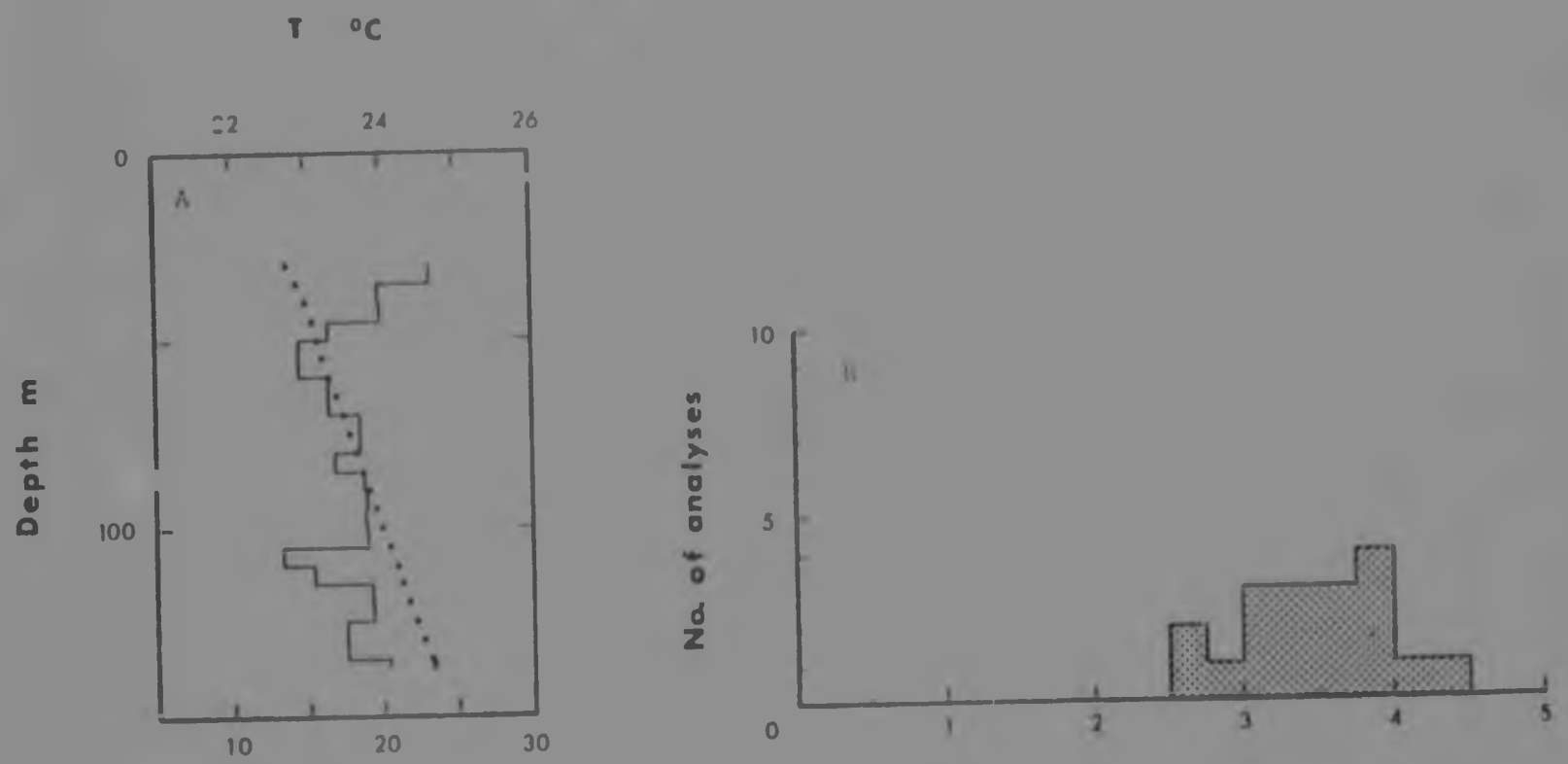

FIGURE 6.11 Adjoining Geelvloer G-42. (a) Temperature and temperature gradient as functions of depth in G-42. (b) Histogram of thermal conductivity data from A 9.

emperatures were measured to the bottom of the borehole at a vertical depth of 457,3 m. A topographic correction was not applied and the observed temperatures and temperature gradients are shown in Figure 6.12.

The temperature gradients are variable over most of the borehole. Fortunately, a summary of the petrological log was made available and from this and a brief examination of the core it was possible to show that rapid changes in rock type (and thermal conductivity) were responsible for most of the variation in temperature gradient. The borehole passes through a succession of variably biotitic gneisses with subordinate amphibolites, associated calc-silicate rocks and pegmatites, and terminates in a unit of gneiss locally referred to as 'basement' gneiss. A simplified lithological log is presented in Table 6.3 and a comparison of this with Figure 6.11a shows that high temperature gradients are correlated with rocks of low thermal conductivity, notably amphibolite.

Thermal conductivity measurements were made on representative samples collected from the three longest sections of uniform rock type and thermal gradient. The conductivity data and heat flows for 10 m intervals are illustrated in Figure 6.12. The harmonic mean conductivity, straight line through the temperature data and mean heat flow for each unit are given below:

(i) 139,3-188,2 m:

$\bar{k}$ = 3,11 ± 0,09 $Wm^{-1}K^{-1}$ (10 values)

$t(^{\circ}C)$ = (24,53 ± 0,05) + (22,09 ± 0,29)z(km)

$\bar{q}$ = 68,6 ± 2,2 mWm^{-2}

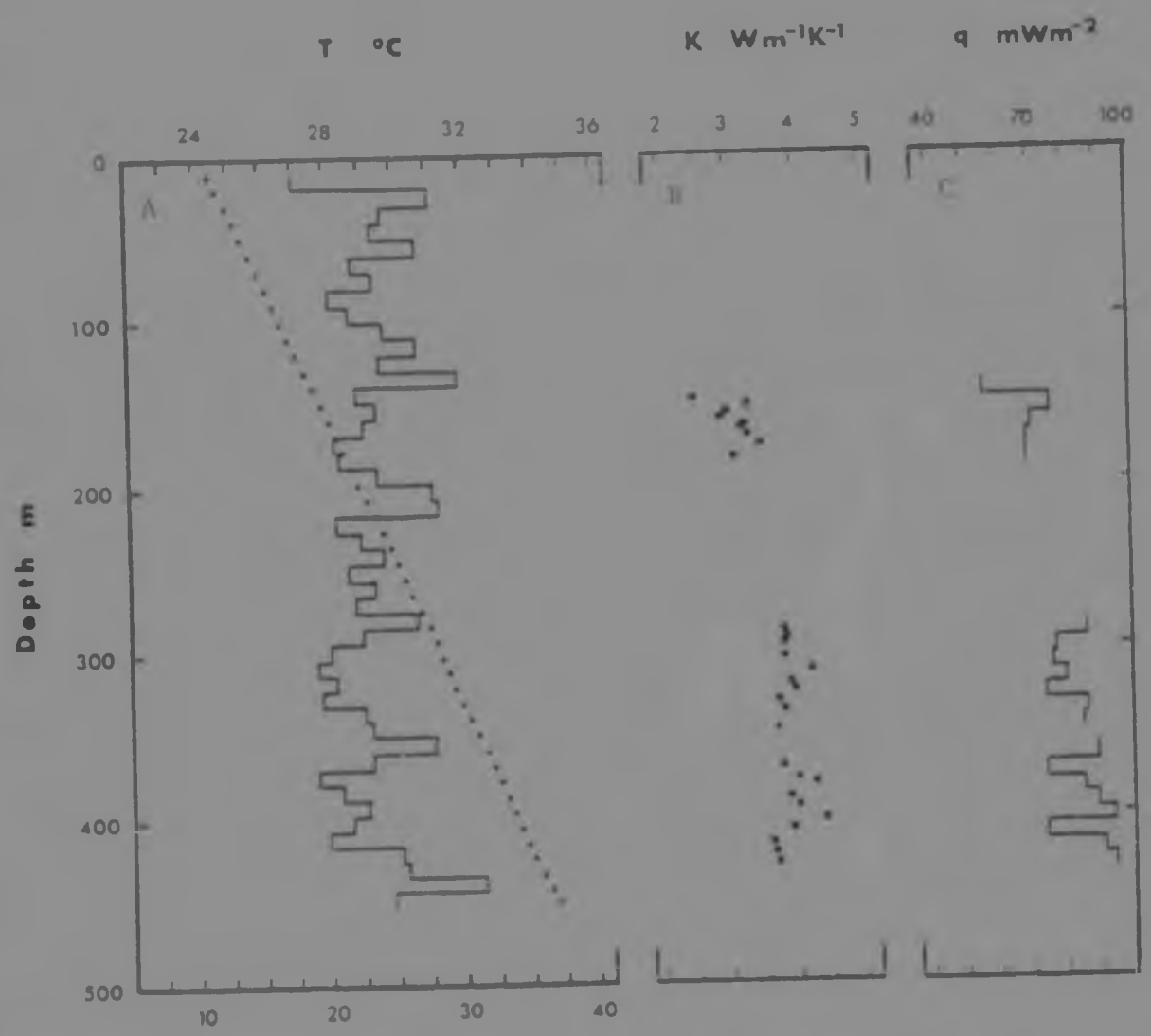

FIGURE 6.12 Rozynen Bosch RB 56. Borehole data.

Table 5.5 Simplified lithological log of RB 56 (after log compiled by Phelps Dodge of Africa Ltd). Depths are vertical. Brackets indicate units sampled for thermal conductivity.

Depth (m)	Rock Type
0 - 113	Variably biotitic gneiss with bands of amphibolite and dark calc-silicate rocks
113 - 138	Biotite rich gneiss
(138 - 172	Biotite gneiss
(172 - 184	Pegmatite
184 - 216	A mixture: predominantly amphibolite and associated calc-silicate rocks with bands of pegmatite and biotite gneiss
216 - 260	Biotite gneiss with numerous pegmatite bands and one minor amphibolite band
260 - 288	Amphibolite and calc-silicate rocks
(288 - 350	Garnet gneiss and biotite gneiss
350 - 355	Amphibolite and calc-silicate rocks
(355 - 366	Pegmatite
(366 - 430	Biotite gneiss
430 - 443	Amphibolite and calc-silicate rocks
443 - 447	Biotite rich gneiss
447 - 452	'Basement' gneiss

(2) 284,4-350,5 m:

$\bar{K} = 3{,}85 \pm 0{,}05\ Wm^{-1}K^{-1}$ (10 values)

$T(^{\circ}C) = (25{,}11 \pm 0{,}08) + (20{,}69 \pm 0{,}24)z(km)$

$\bar{q} = 79{,}6 \pm 1{,}4\ mWm^{-2}$

(3) 359,9–534,0 m

$\bar{K}$ = 3,89 ± 0,04 $Wm^{-1}K^{-1}$ (10 values)

T(°C) = (24,76 ± 0,13) + (81,92 ± 0,29)z(km)

$\bar{q}$ = 85,3 ± 2,3 mWm^{-2}

The heat flow obtained from the first unit is significantly lower than the heat flows from units (2) and (3) which differ by only 7%. This implies that heat is lost in the intervening depth (188–284 m). There is no reason to suspect that heat is conducted away laterally. Although no water flows were evident while measuring the temperatures, an examination of the borehole core showed that the calc-silicate rocks at 270 m (vertically) contain open fractures and zones of oxidation. This suggests that convective heat transfer occurs at this depth and only the lower two units were used to calculate the overall mean heat flow and standard error for this borehole:

$\bar{q}$ = 81,1 ± 1,2 mWm^{-2}

Heat production measurements were made on five aggregate samples of gneiss, one from each of the units discussed above and two from the 'basement' gneiss. The data are summarized in Table 6.4. The two 'basement' samples, KR 4 and KR 5, have heat productions which are respectively lower and higher than values obtained from the gneisses of units (1), (2) and (3) and there is no good reason to separate the data. The overall mean heat production and standard error are:

$\bar{A}$ = 1,78 ± 0,26 μWm^{-3}

Table 6.4 Heat production data for KE 56

Sample	Depth range (m)	Description	Heat production (μWm^{-3})
KB 1	148 - 170	Biotite gneiss	2,62
KB 2	288 - 324	Biotite gneiss and garnet gneiss	3,82
KB 3	369 - 427	Biotite gneiss	3,51
KB 4	447 - 450	'Basement' gneiss	2,35
KB 5	450 - 453	'Basement' gneiss	6,61

6.8 Areachap AP 11

(Table IV-9)

AP 11 is situated near the disused Areachap mine approximately 22 km northwest of Upington and was drilled during a phase of renewed exploration interest. Temperatures were surveyed to the bottom at a vertical depth of 463,4 m.

The borehole penetrates a steeply dipping and rapidly alternating gneissic succession. The major rock types are biotite gneiss and amphibolite, but other varieties, including quartzo-feldspathic gneiss, augen gneiss and biotite amphibole gneiss are abundant. Samples for thermal conductivity and heat production measurements were collected on a semi-random basis and all important rock types are well represented.

The relief is very subdued and a topographic correction was not applied. The temperatures and temperature gradients, thermal conductivity data

and heat flow are plotted against depth in Figure 6.13.

There is considerable small scale variation in thermal conductivity due to the rapid change in rock type and fabric orientation. Gradation between different rock types makes it impossible to distinguish well-defined lithological subdivisions and calculation of heat flow by the integrated thermal resistance method is therefore inappropriate. The uniform temperature gradient below 180 m indicates that, as a whole, the succession acts as an 'isn-conductive unit'.

The borehole inclination decreases to 46,5° at the base (Table 6.1) and this raises the possibility that the conductivities, which were measured parallel to the cores' axes, are in error in the lower part of the borehole. However, individual conductivity measurements and averages calculated for successive 30 m intervals (Figure 6.13b) do not vary systematically with depth. The harmonic mean conductivity and standard error of all measurements are:

$$\bar{K} = 2,62 \pm 0,08 \ Wm^{-1}K^{-1} \qquad (36 \text{ values})$$

The marked increase in temperature gradient to a depth of 180 m is similar to that observed in many of the above boreholes and these effects almost certainly have a common cause. The sharp increase in gradient at the bottom of the borehole arises out of difficulties in measuring the final depth accurately and the bottom temperature was not used to calculate the average thermal gradient. The least squares straight line through the temperature data from 89,4 m to 462,3 m and the mean heat flow and standard error are:

$$T(°C) = (21,63 \pm 0,02) + (19,85 \pm 0,06)z(km)$$

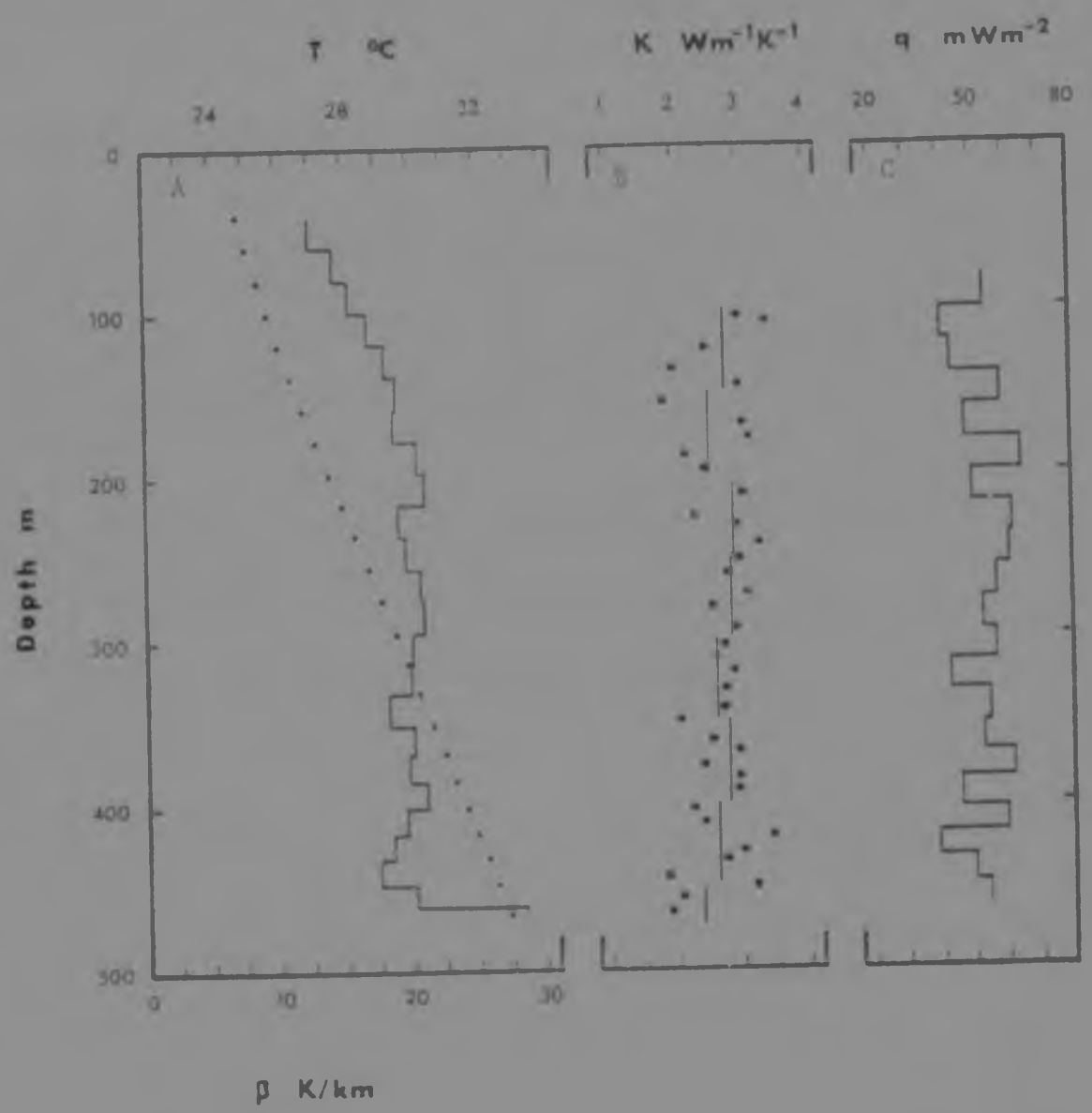

FIGURE 6.13 Areachap AP 11. Borehole data.

The heat production data for twenty-six samples are summarized in Figure 6.7c. The amphibolites have a very much smaller heat production than the gneisses; the mean values and standard errors being:

gneiss	$4,21 \pm 1,26\ \mu Wm^{-3}$	(17 values)
amphibolite	$0,59 \pm 0,07\ \mu Wm^{-3}$	(9 values)

The numbers of heat production samples of each rock type were selected roughly in proportion to their relative abundance and the heat production of the succession as a whole is given by the mean for all samples:

$$\bar{A} = 2,96 \pm 0,53\ \mu Wm^{-3}$$

6.9 Boks Puts KC 12

(Table IV-10)

Boks Puts is situated 55 km northwest of Kenhardt and temperatures in KC 12 were surveyed to a vertical depth of 214,3 m. The relief near the borehole is low, and although a topographic correction was computed, it was found to be negligible (less than 0,2% of the average temperature gradient). The temperature-depth data plotted in Figure 6.14 show that the temperature gradient increases between 60 m and 120 m but is remarkably constant below 120 m. The temperature at the bottom of the hole has been discarded for the reason expressed in the previous section and the temperature data from 115,8 m to 210,0 m yield the straight line:

$$T(^{o}C) = (23,02 \pm 0,02) + (13,46 \pm 0,07)z(km)$$

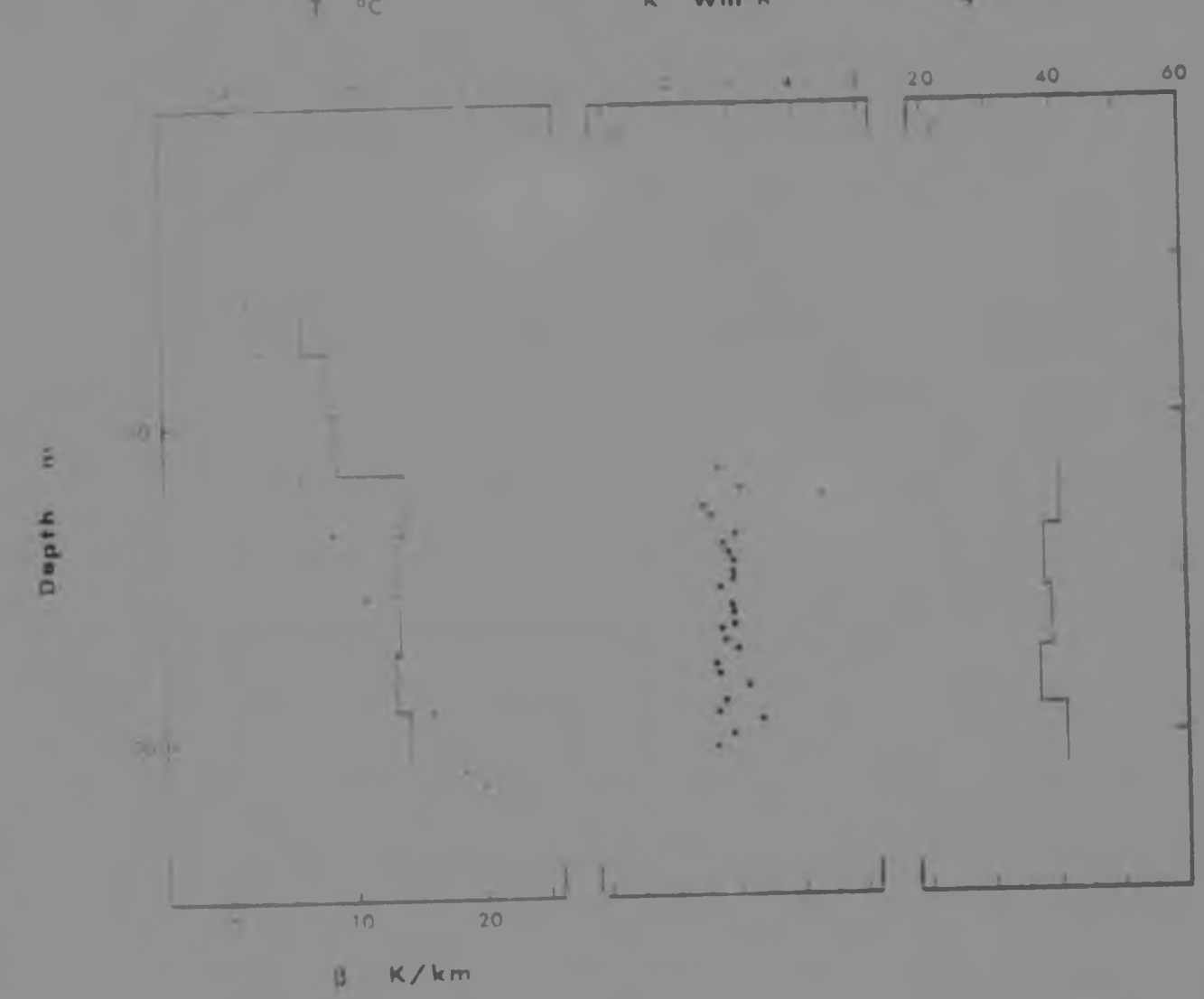

renole data.

The rock below [illegible] is very uniform, consisting of very coarse biotite-chlorite-amphibole schist with [illegible] quartz veins and migmatous bands. The thermal conductivity data are real [illegible] very little variation (Figure 6.14). The harmonic mean conductivity and the mean heat flow are

$$\bar{K} = [illegible]\ W\,m^{-1}\,K^{-1}$$

$$\bar{q} = [illegible]\ mW\,m^{-2}$$

Heat production measurements were made on [illegible] samples. There is little spread in the data (Figure 6.15) and the mean and standard error are:

$$\bar{A} = [illegible]\ \mu W\,m^{-3}$$

6.10 Jacomyns Pan PC2-27 and PC2-30

(Table IV-1)

Several boreholes were drilled on the Jacomyns Pan which is located 64 km east of Kambardt. Most of these were inaccessible due to caving at shallow depths and temperatures were measured in only two of them. The deeper borehole, PC2-27, was inclined and open to a vertical depth of 495.3 m; the second, PC2-30, drilled 315 m northwest of PC2-27, was vertical but blocked at 161.0 m.

The boreholes intersect a steeply dipping succession of uniform gneisses. The predominant rock type is biotite gneiss which contains variable amounts of garnet. There are smaller amounts of leucocratic [illegible] amphibole gneiss and some thin pegmatite veins.

The drill cores were lying in sleeves close to the boreholes and only samples whose depths could be identified from the drillers' markings were collected. Cores from PC2-30 span the depths surveyed in that borehole, but those from PC2-27 are limited to the depth range 270-445 m. However, it was possible to correlate depths between the two boreholes reasonably accurately using the structural dip of the gneisses: samples from 60-170 m in PC2-30 have an equivalent depth range of 200-270 m in PC2-27. The inclination of PC2-27 approaches 31° near the base but, as in the case of borehole AP 11, the conductivity data (Figure 6.15) do not vary systematically with depth.

The conductivity data for both boreholes are plotted against depth in Figures 6.15 and 6.16. The harmonic means and standard errors are:

PC2-27 3,48 ± 0,11 $Wm^{-1}K^{-1}$ (32 values)

PC2-30 3,78 ± 0,26 $Wm^{-1}K^{-1}$ values)

An analysis of variance test (see Campion et al, 1973) showed that the means do not differ significantly and all thirty values have been used to calculate a mean conductivity for the PC2-27 borehole:

$$\bar{K} = 3,55 \pm 0,11 \ Wm^{-1}K^{-1}$$

A systematic increase in temperature gradient above 200 m is present in both boreholes (Figures 6.15 and 6.16). There is also a marked increase in gradient near the bottom of PC2-27. There were no water flows at this depth and the reason for the increase is not known; it may be due to a change of rock type or refraction of heat flow.

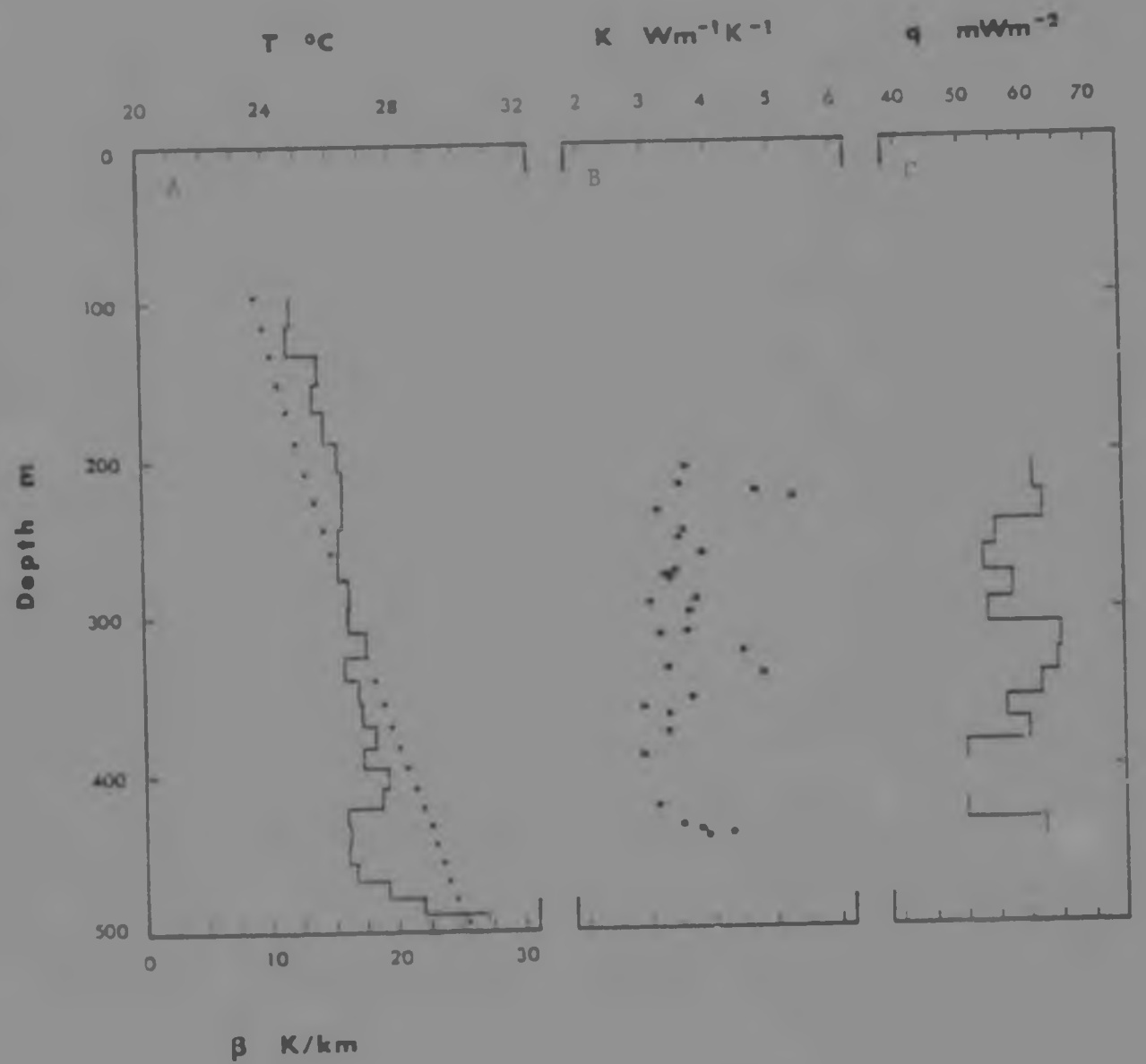

FIGURE 6.15 Jacomyns Pan PC2-27. Borehole data.

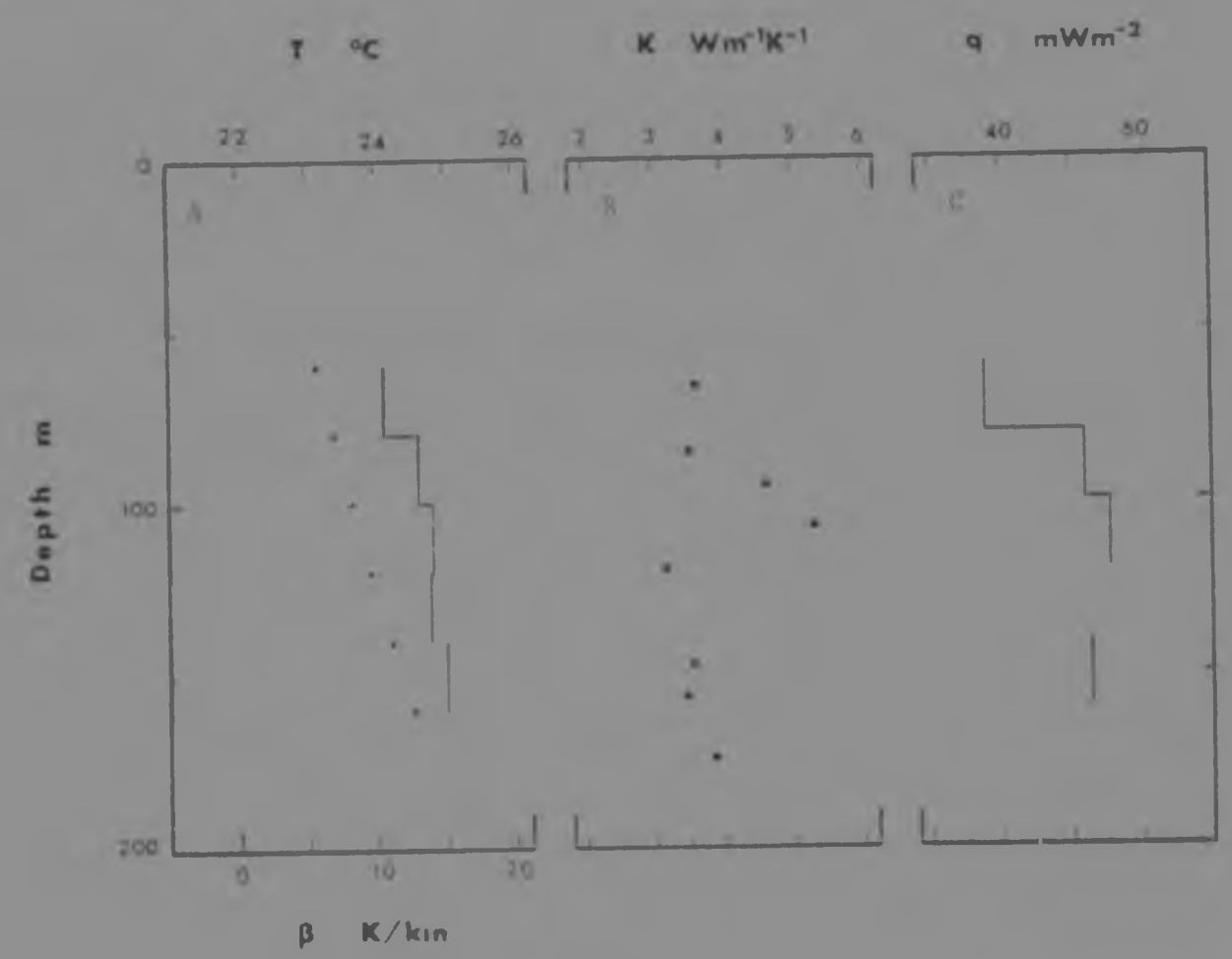

FIGURE 6.16 Jacomyns Pan PC2-30. Borehole data.

The straight line through the temperature data between 188,9 m and 445,4 m in PC2-27 is:

$$T(^{o}C) = (21,62 \pm 0,05) + (16,82 \pm 0,12)z(km)$$

and the mean heat flow is:

$$\bar{q} = 59,7 \pm 1,9 \text{ mWm}^{-2}$$

PC2-30 is too shallow to yield as precise an estimate of the heat flow, but it provides a useful check on the above result. The data between 60 m and 160 m yield:

$$T(^{o}C) = (22,24 \pm 0,03) + (14,00 \pm 0,20)z(km)$$

$$\bar{q} = 52,9 \pm 3,7 \text{ mWm}^{-2}$$

The heat flows are in reasonable agreement considering that measurements in PC2-30 were confined to the zone of systematically increasing temperature gradients (0-200 m), where the average temperature gradient and heat flow should be smaller than those observed at greater depths.

Heat production measurements were made on twelve samples from PC2-27, eight from PC2-30 and five from a third borehole, PC2-31, situated 100 m northeast of PC2-27. The means and standard errors for each borehole are given below:

PC2-27	$2,24 \pm 0,09$ μWm^{-3}
PC2-30	$2,03 \pm 0,33$ μWm^{-3}
PC2-31	$2,44 \pm 0,33$ μWm^{-3}

There are clearly no significant differences between the means and the overall mean and standard error have been calculated using all the data:

$$\bar{A} = 2,21 \pm 0,13\ \mu Wm^{-3}$$

The data are summarized in the form of a histogram in Figure 6.7e.

6.11 Vogelstruis Bult V 41

(Table IV-12)

V 41 is located near the Prieska Copper Mine on the farm Vogelstruis Bult, 64 km southwest of Prieska. The borehole passes through a steeply dipping heterogeneous succession of schists, gneisses and amphibolites. From the surface to 424 m the predominant rock types are quartz-biotite schist and quartz-feldspar gneiss. There are small amounts of amphibolite below 400 m and this section of the borehole is intersected by a few minor diabase dykes. From 424 m to 726 m amphibolites and amphibole gneisses predominate over quartz-biotite schists and quartzo-feldspathic rocks. There is a metaquartzite layer between 665 m and 670 m. At 706 m the borehole enters a mixed zone of schist, gneiss and amphibolite.

Temperatures were surveyed to a vertical depth of 730,5 m. A topographic correction was not applied and temperatures and temperature gradients are shown in Figure 6.17. Fluctuating temperatures at a depth of 180 m indicated the presence of a water flow and this is reflected in the variable temperature gradients at about this depth.

The drill core was lying in semi-order next to the borehole. There were insufficient cores with depth markings to provide a representative suite for the borehole and several groups of marked and unmarked samples were collected from various depth intervals. Each group (denoted A-H) was

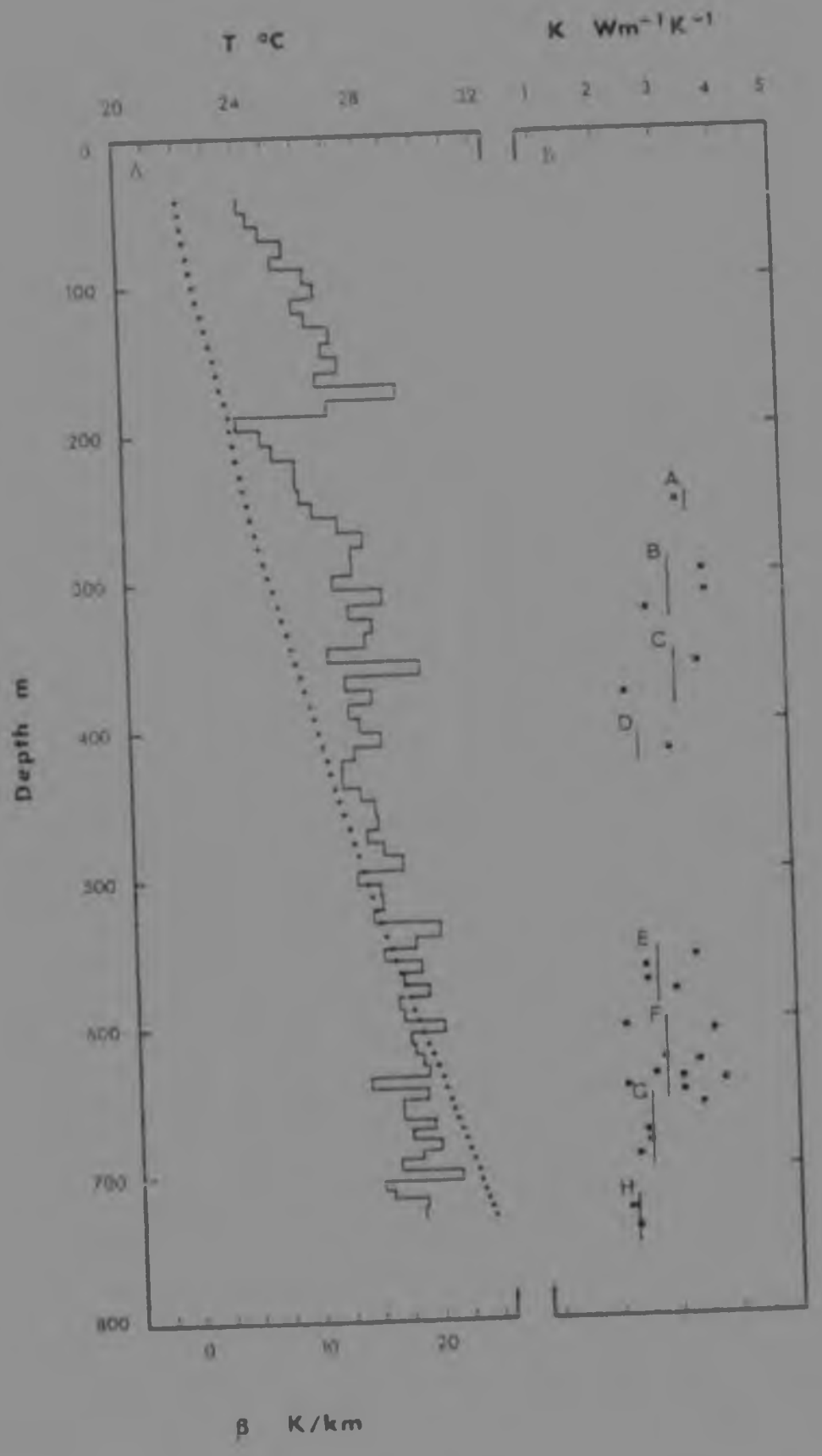

FIGURE 6.17 Vogelstruis Bult V 41. Borehole data.

characterized by a few samples whose depths were marked and contained several other representative samples which were selected with the aid of the petrological log of the borehole. The approximate depth range and harmonic mean conductivity of each group are listed in Table 6.3. The data for samples of known depth and the mean conductivity of each group are shown in Figure 6.17.

Groups A, B and C fall within the upper lithological unit (0-424 m). An analysis of variance test showed that their mean conductivities are not significantly different and an overall harmonic mean conductivity was calculated and combined with the temperature data between 247,4 m and 402,2 m. The data are summarized below:

$\bar{\gamma}$ = 3,20 ± 0,12 $Wm^{-1}K^{-1}$ (18 values)

$T(^{o}C)$ = (20,48 ± 0,04) + (14,40 ± 0,10)z(km)

$\bar{q}$ = 46,1 ± 1,9 mWm^{-2}

Group D straddles the boundary at 424 m. The mean conductivity differs from that of Groups A, B and C and has been applied to the temperature data from 402,2 m to 459,7 m:

$T(^{o}C)$ = (20,8 ± 0,1) + (13,63 ± 0,2)z(km)

$\bar{q}$ = 34,3 ± 2,1 mWm^{-2}

An analysis of variance test on groups E-F shows that E, F and G are homogeneous while the mean conductivity of group H is different at the 95% level of significance. The inclination of the borehole varies between 60° and 36° below 500 m but this has not resulted in a significant trend in the conductivity data (cf. groups E, F and G).

Table 6.5 Thermal conductivity data for V 41

Group	Approximate depth range (m)	$\bar{K}$ ($Wm^{-1}K^{-1}$)	$\sigma_{\bar{K}}$ ($Wm^{-1}K^{-1}$)	n
A	240-260	3,39	0,21	6
B	290-330	3,08	0,21	6
C	350-390	3,15	0,24	6
D	410-430	2,52	0,14	5
E	550-590	2,72	0,15	10
F	600-660	2,82	0,18	11
G	650-700	2,54	0,15	8
H	710-730	2,28	0,08	7

The data from groups E, F and G were combined and the harmonic mean conductivity applied to temperatures in the range 530,5-703,2 m. The data are summarized below:

$$\bar{K} = 2,71 \pm 0,10\ Wm^{-1}K^{-1} \quad (29\ values)$$

$$T(^{o}C) = (18,66 \pm 0,03) + (17,99 \pm 0,05)z(km)$$

$$\bar{q} = 48,7 \pm 1,8\ mWm^{-2}$$

The mean conductivity of group H was applied to the depth range 703,2-730,5 m and:

$$T(^{o}C) = (19,16 \pm 0,37) + (17,29 \pm 0,51)z(km)$$

$$\bar{q} = 39,4 \pm 1,8\ mWm^{-2}$$

The above estimates for the heat flow differ significantly. There is no systematic variation with depth and the differences cannot be

attributed to convective heat transfer (as there were no water flows below 180 m) or heat flow refraction. Heat flows from the depth intervals 402,2-449,1 m and 703,2-730,5 m are less reliable as they were calculated using few conductivity measurements (five and seven respectively), which may not adequately represent the rocks within these depth intervals. Group D lies on richer side of a boundary at 434 m which separates units consisting predominantly of schist and gneiss above and amphibolite below. Such a change in rock type is not reflected in the temperature gradient at this depth (Figure 6.17) and this indicates that the relative proportions of different rock types above and below 434 m are not sufficiently different to affect the overall conductivity of the rock: most of the samples from group D are amphibolites and the mean conductivity may be biased on the low side. Group H samples fall above and below the deepest temperature measurement and the average temperature gradient applied to their mean conductivity may be inappropriate.

For these reasons, these two estimates for the heat flow were discarded and the overall mean heat flow for the borehole was calculated by combining the data from the depth intervals 247,2-402,2 m and 530,5-703,2 m:

$$\bar{q} = 47,5 \pm 1,1 \text{ mWm}^{-2}$$

The heat production data for five aggregate samples are summarized in Table 6.6. Values for the amphibolite and amphibole gneisses (V4 and V5) are considerably lower than those for the more quartzo-feldspathic rocks (V1-V3). However, sample numbers were selected in rough proportion to the rock type encountered in the borehole and the overall heat production of the succession is best represented by the

Table IV-1 Heat production data for V 61

Sample	Description	Heat production (μWm^{-3})
V 1	Quartz-biotite schist from groups A, B and C	1,54
V 2	Quartz-poor biotite schist from groups A-E	0,71
V 3	Quartz-biotite schist from groups F, G and H	1,35
V 4	Amphibolite and amphibole schist from groups D, E and F	0,15
V 5	Amphibolite and amphibole-biotite schist from groups G and H	0,17

arithmetic mean of all five analyses:

$$\bar{A} = 0,79 \pm 0,27\ \mu Wm^{-3}$$

6.12 Black Face Mountain BF 1

(Table IV-11)

This and the following borehole were situated in the Richtersveld Province. BF 1 is situated near Black Face Mountain approximately 34 km northwest of Vioolsdrift. The borehole was drilled vertically through a succession of tuffs and agglomerates to a depth of 316,3 m. Unfortunately, it was not possible to recover drill core samples for thermal conductivity measurement and a second field trip to the Richtersveld to collect outcrop samples was not feasible. However, it is useful to make a rough estimate of the heat flow.

...emper... ...shown in Figure 6.18
...thou... ...drift, it was not
...nsider... ...the absence
... any ... ...erate ... yielded little
...norma... ...of ... pyroclas...
...aterial ... ...from Koodepoort borehole No. ...,
...ksdo... ... ... $W m^{-1} K^{-1}$ (Mossop and Gatner,
... ..., Thisheu district, range
... $W m^{-1} K^{-1}$ ... and ... Rooyen, 1969). Unpublished
... (Oxi... ...ea ... ...dicani... ash from the Borrowdale
... ... within the range 2,0 - 2,6 $W m^{-1} K^{-1}$

...gg... ... ...dominant ... K-type below 100 m and a rough guess
... the ... ... is 3-4 $W m^{-1} K^{-1}$. The average
...mpera... ... ... 13,5 K/km and the heat flow is
...imated ... ... mWm^{-2}. This is somewhat
... ...lowing borehole.

... ...ABLE ...AB ...

...

... border of Namibia/South West Africa and
... ...-northeast of Vioolsdrift. The borehole is
... ... depth of 341,8 m.

... ... porphyry. A basic
... ... and 319 m and zones showing varying
...gree... ... ... in the intervals 192-214 m, 250-294 m
... ... Representative core samples

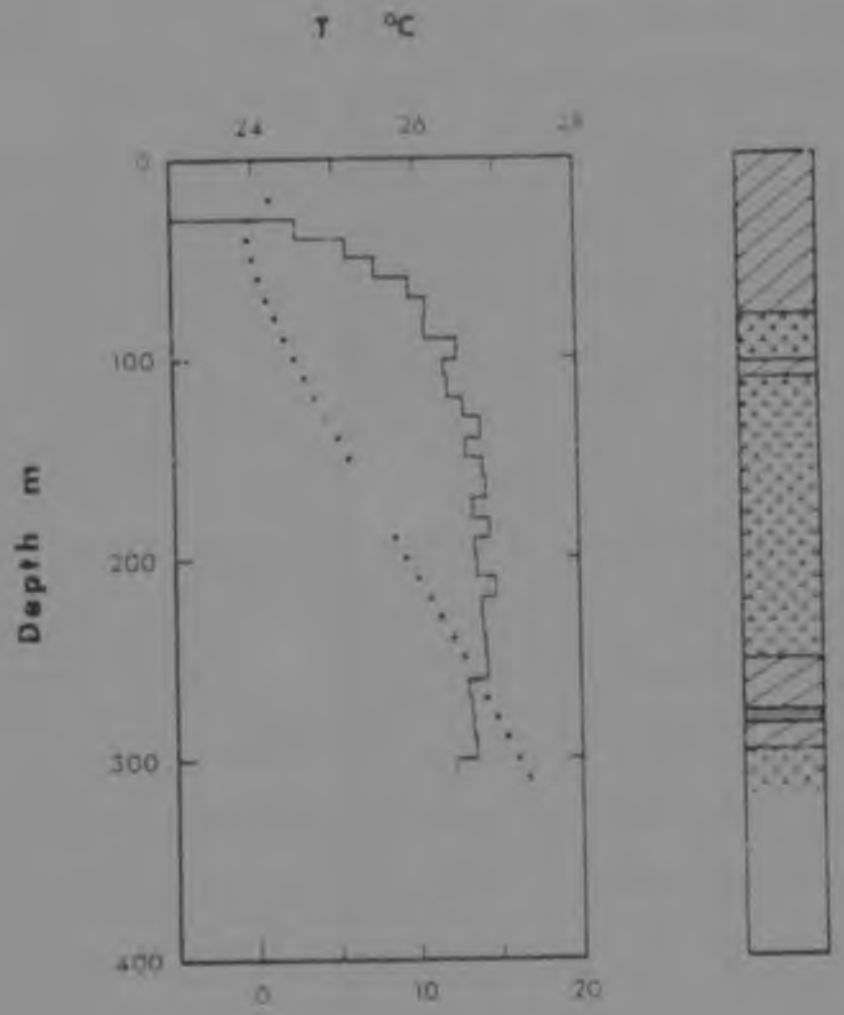

FIGURE 6.18 Black Face Mountain BF 1. Borehole data. Temperature and temperature gradient as functions of depth and the petrological log (diagonal line tuffaceous volcanic rock, triangle agglomerate, dots - sheared quart pornhyry).

were collected at 10-20 m intervals from below 100 m. All cores had been split longitudinally and halves were ground flat and glued together before recoring them for conductivity measurements. As the joins were parallel to the cores' axes they contributed negligible errors to the thermal conductivities. The conductivities shown in Figure 6.19 are very uniform and the harmonic mean is:

$$\bar{k} = 3,43 \pm 0,07 \text{ Wm}^{-1}\text{K}^{-1} \quad (23 \text{ values})$$

The terrain surrounding the borehole is extremely rugged and considerable care had to be exercised when digitizing the topography. However, the effect of the averaged topography proved to be small at all depths of interest. The topographically corrected temperatures and temperature gradients are shown in Figure 6.19. Slightly unstable temperatures between 340 m and 380 m suggested possible water movement at these depths but there is no indication of this in the temperature gradient. There is a systematic increase in temperature gradient and it extends to a greater depth (600 m) than similar trends in other boreholes. The conductivities are slightly greater above 300 m than those below, but the difference is not sufficient to alter the pattern greatly and the heat flow (Figure 6.19c) increases to a depth of at least 300 m. Possible reasons for this are discussed in Chapter 7.

The least squares straight line through the temperature data from 100 m to 560 m and the heat flow are:

$$T(^{\circ}C) = (26,34 \pm 0,11) + (17,22 \pm 0,31)z(\text{km})$$

$$\bar{q} = 59,1 \pm 1,6 \text{ mWm}^{-2}$$

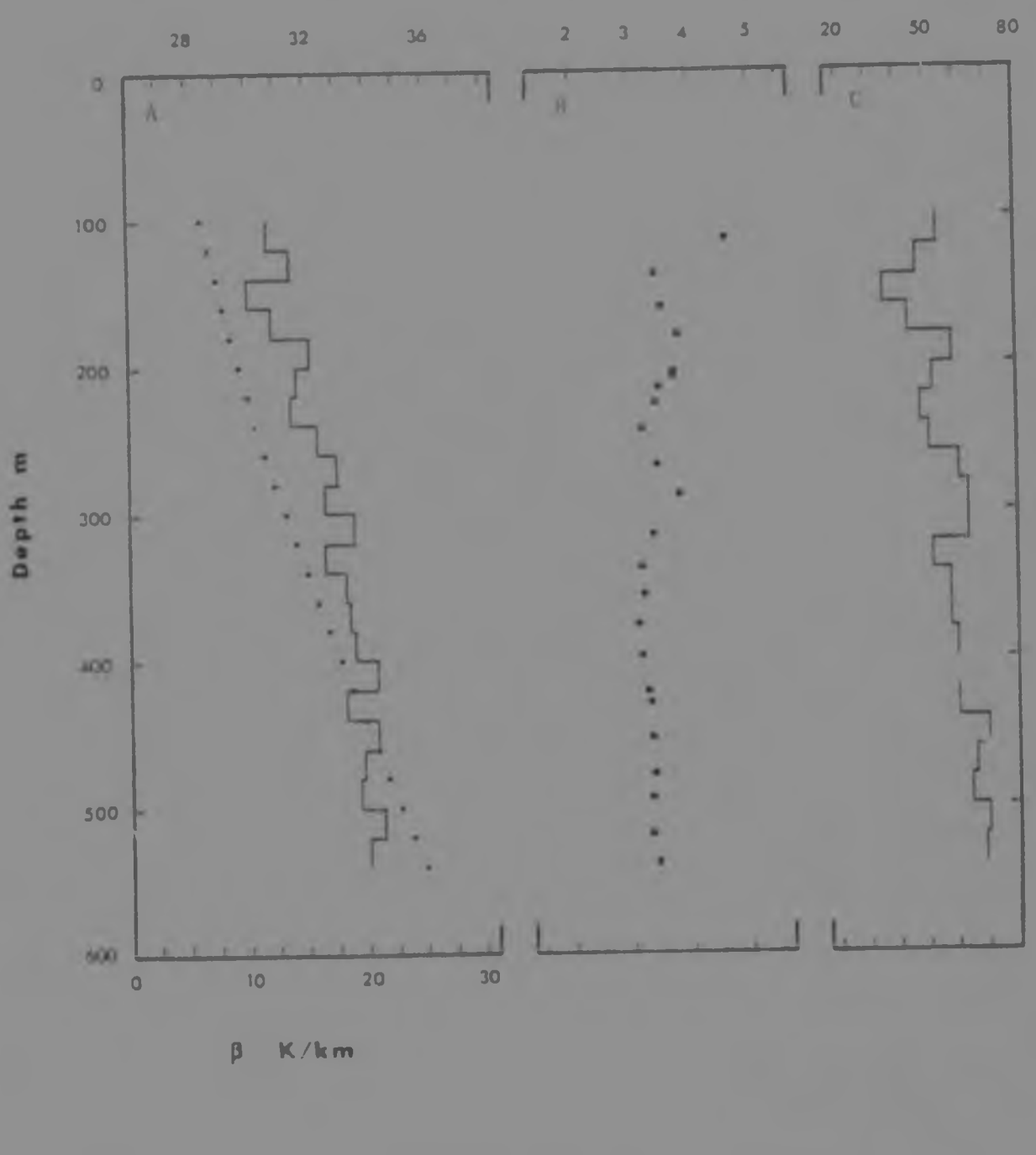

FIGURE 6.19 Haib HB 77. Borehole data.

The results of heat production measurements made on four aggregate samples are summarized in Table 6.7. The altered rocks (sample HB 4) have a lower heat production than the fresh quartz-feldspar porphyries and the alue for this sample has been discarded. The mean and standard error for the quartz-feldspar porphyry are:

$$\bar{A} = 2,05 \pm 0,07 \ \mu Wm^{-3}$$

6.14 Klerksdorp District

Rhenosterhoek	DRH 18
Rhenosterberghoek	DRB 6
Rietkuil	DRL 17
Schoemansfontein	BSF 1
Brakspruit	BBS 1
Mahemsvlei	BMV 4
Tweelingfontein	BTF 1

Heat flow measurements on the Kaapvaal Craton were made in seven boreholes all of which are situated in the Klerksdorp district. The borehole serial numbers and the farms on which they were drilled are listed above and their distribution is shown in Figure 2.2.

The boreholes are all close to the vertical and all pass through considerable thicknesses of Dominion Reef lava before penetrating the granite basement of the Kaapvaal Craton. Thin horizons of clastic sediments mark the unconformity between the basement gneiss and the Dominion Reef Supergroup. The lavas are predominantly felsitic and may be porphyritic or amygdaloidal. There is little variation from one borehole to the next.

Table 6.7 Heat production data for HB 77

Sample	Depth range (m)	Description	Heat production (μWm^{-3})
HB 1	114-226	Quartz-feldspar porphyry	2,12
HB 2	244-398	Quartz-feldspar porphyry	2,10
HB 3	422-494	Quartz-feldspar porphyry	1,92
HB 4	——	Altered rocks (from all three zones)	1,52

Temperatures were surveyed at 10 m intervals and the data are summarized in Figures 6.20-6.26. Although there is little relief in the area topographic corrections were computed for the first five boreholes. The corrections were small (less than 0,5% of the average temperature gradients) and the temperature data have not been adjusted. The boreholes were all free of water flows with the exception of DRB 6 where severe water losses in the upper 120 m were recorded during drilling.

Increasing temperature gradients in the upper 200 m of all boreholes except BBS 1 are consistent with similar observations made in boreholes in the Namaqua Mobile Belt. It is surprising that these trends persist in DRB 6 in spite of the water flows encountered in the upper 120 m; it is possible that the aquifers were sealed during drilling. A secondary feature which was not observed in the Namaqua Mobile Belt is a decreasing temperature gradient to a depth of about 60 m in most of the Klerksdorp boreholes. This will be discussed in detail in Chapter 7.

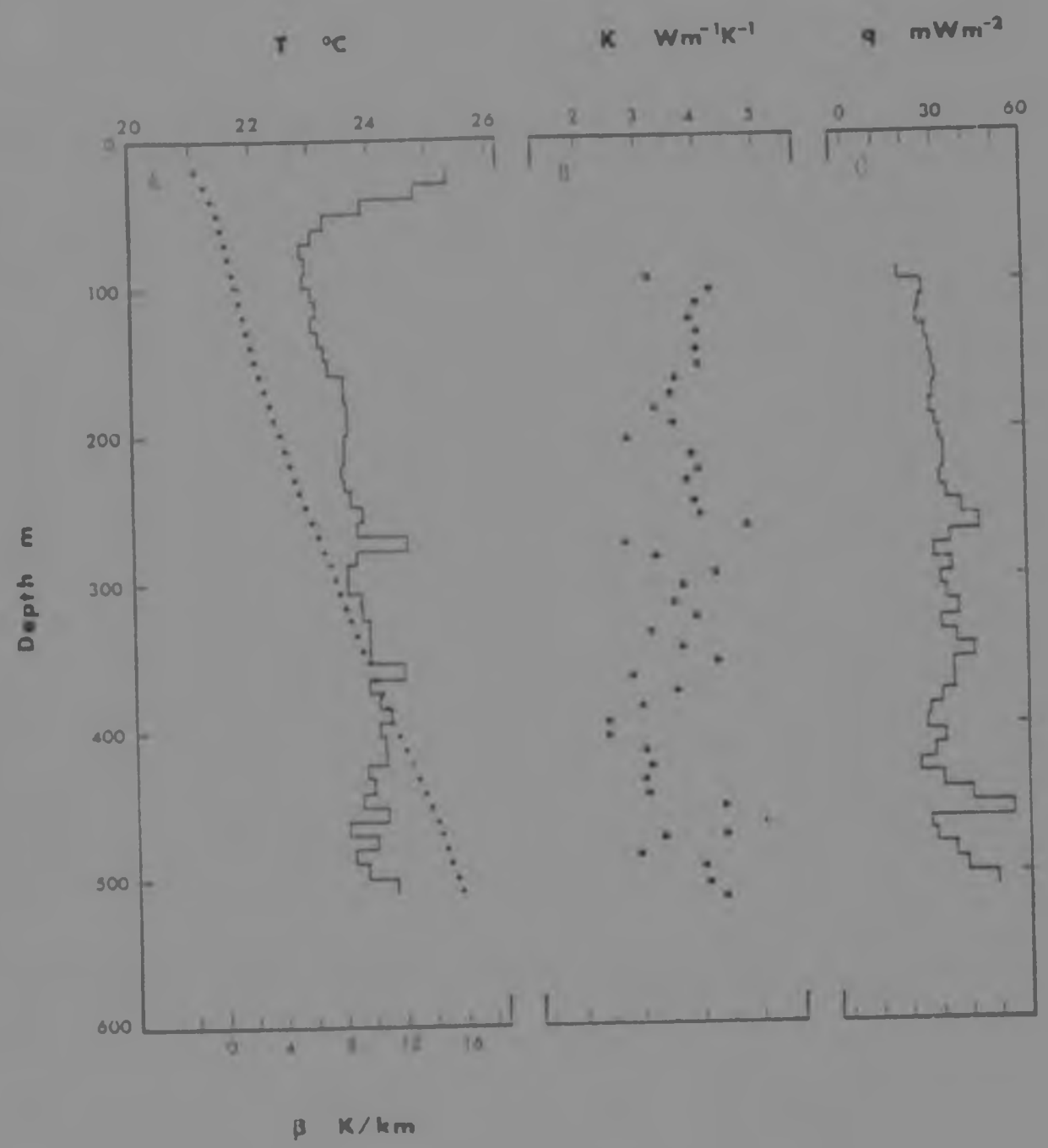

FIGURE 6.20 Rhenosterhoek DRH 18. Borehole data.

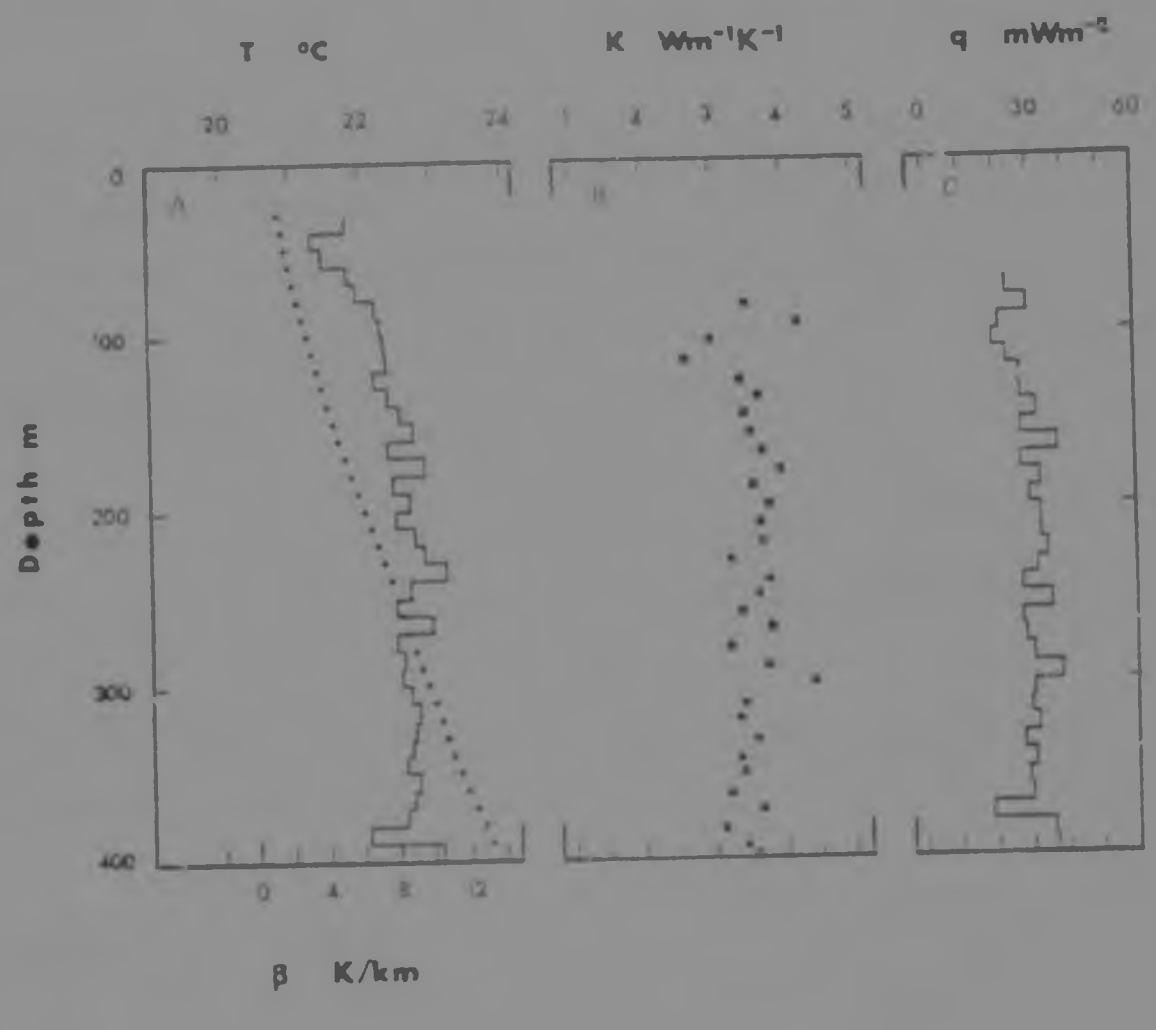

FIGURE 6.2! Rhenosterberghoek DRB 6. Borehole data.

Few of the boreholes penetrate far into the basement gneisses and only the Dominion Reef lavas were sampled systematically for thermal conductivity measurement. Samples were collected at approximately 10 m intervals and the conductivity data are summarized in Figures 6.20-6.26. Although the conductivities vary considerably on the scale of a few metres the large scale uniformity of the lavas is demonstrated by the similarity of the mean conductivities for different boreholes (see below). The lowest four points in Figure 6.24 are data for the gneisses penetrated in the lowest 40 m of BRS 1.

The least squares straight line through the temperature data, harmonic mean conductivity and mean heat flow for each borehole are summarized in semi-tabular form below. All reported depths are measured vertically from the surface. The relevant figures are indicated below each borehole heading.

Rhenosterhoek DRH 18

(Table IV-17, Figure 6.20)

DRH 18 penetrated the basement at a depth of 959 m but was blocked at 510,4 m. Conductivity samples were collected for the depth interval 49,7-510,4 m and the derived quantities are:

$$T(^{o}C) = (30,67 \pm 0,03) + (18,21 \pm 0,10)z(km)$$

$$\bar{K} = 3,51 \pm 0,10 \text{ Wm}^{-1}\text{K}^{-1} \quad (41 \text{ values})$$

$$\bar{q} = 62,4 \pm 0,9 \text{ mWm}^{-2}$$

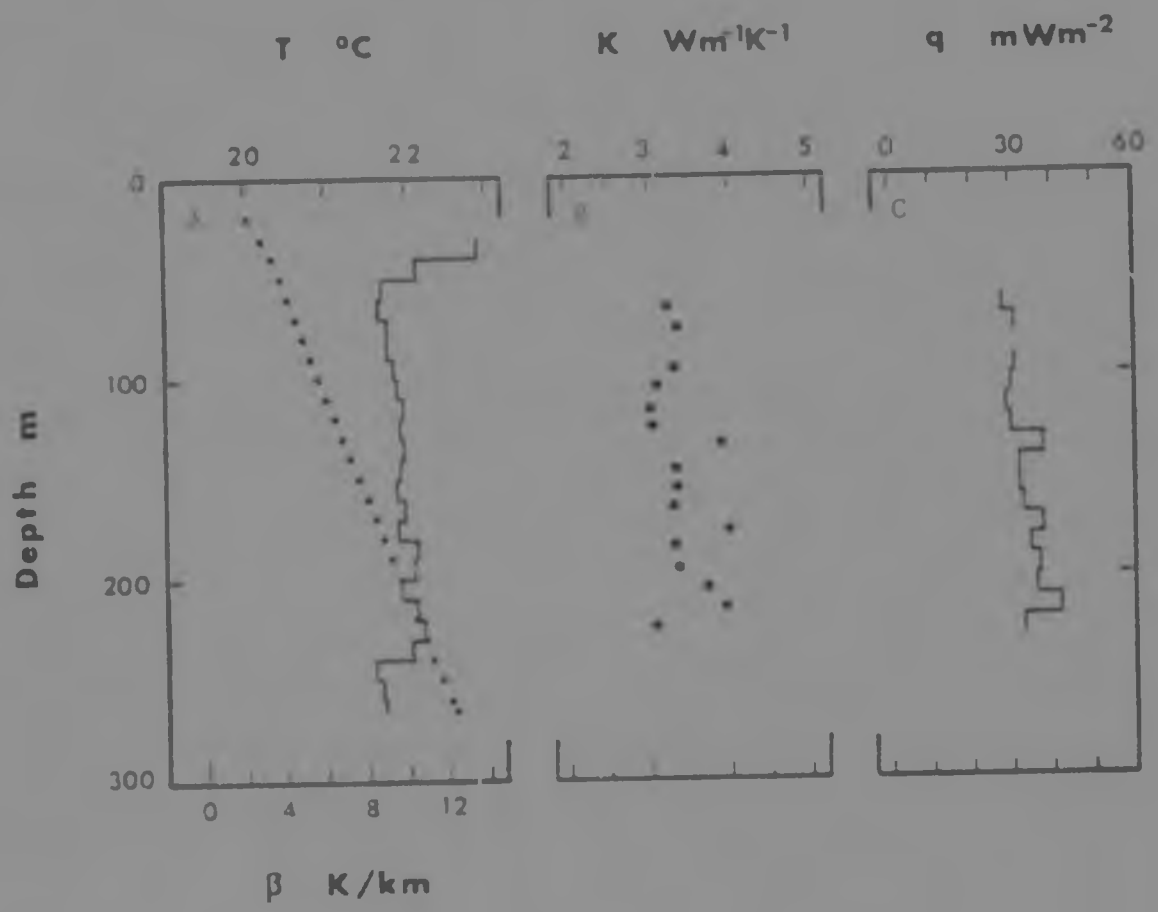

FIGURE 6.22 Rietkuil DRL 17. Borehole data.

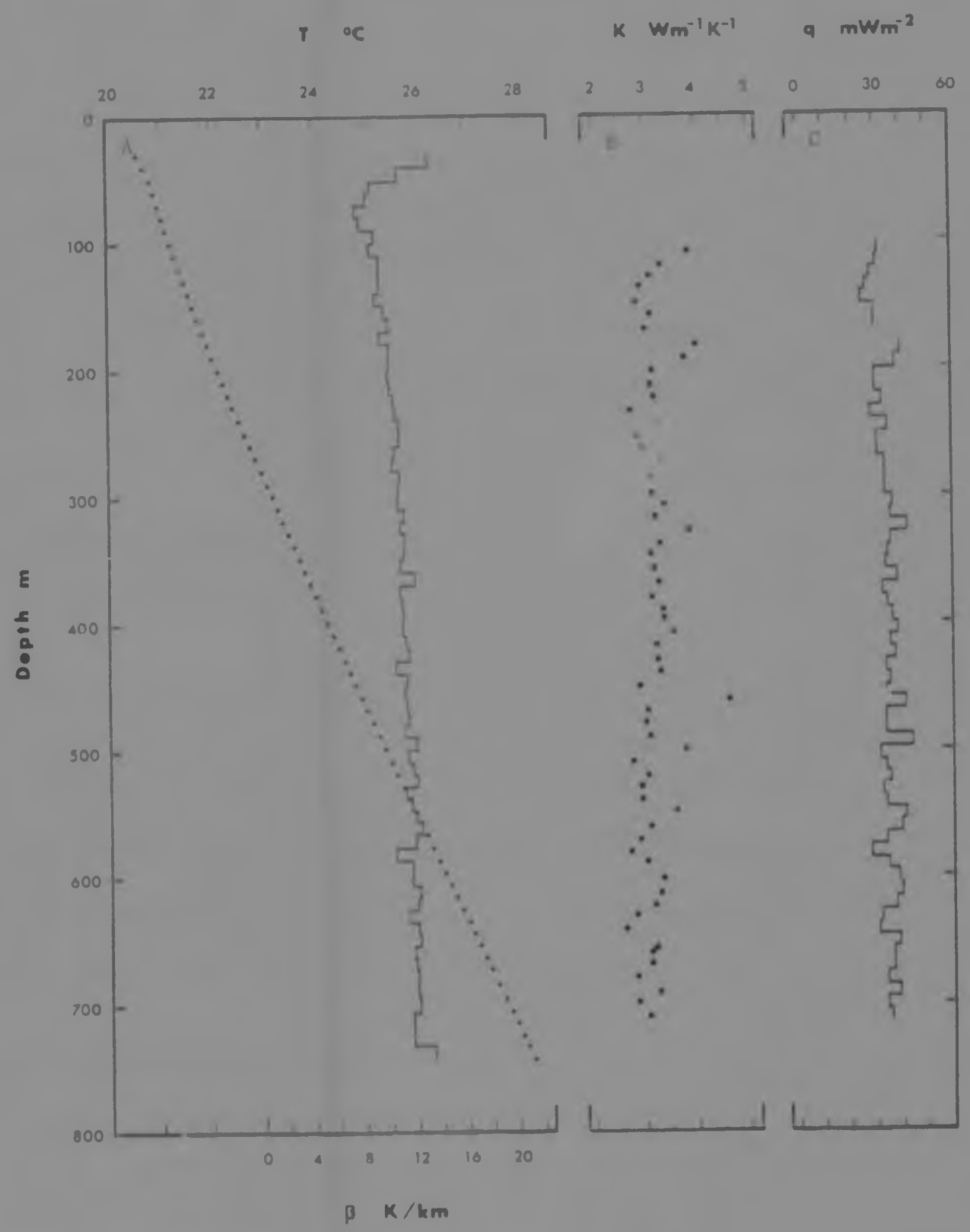

FIGURE 6.23 Schoemansfontein BSF 1. Borehole data.

Rhenosterhoekpoort ORE 9

(Table IV-16, Figure 6.21)

The basement was intersected at a depth of 1270 m but the borehole was blocked at 400 m. Measurements of temperature and thermal conductivity for the interval 60,0-400,0 m yield:

$$T(^{\circ}C) = (20,55 \pm 0,01) + (8,61 \pm 0,04)z(km)$$
$$\bar{\lambda} = 3,50 \pm 0,08 \text{ Wm}^{-1}\text{K}^{-1} \quad (12 \text{ values})$$
$$\bar{q} = 80,1 \pm 0,5 \text{ mWm}^{-2}$$

Rietkuil ORE 17

(Table IV-17, Figure 6.22)

The borehole passes through 244 m of lava and 28 m of sediment before penetrating the basement gneiss at 272 m. Temperatures were surveyed to a depth of 365 m but conductivity measurements were confined to the lavas. The data between 60,0 m and 230,0 m yield:

$$T(^{\circ}C) = (16,95 \pm 0,01) + (9,76 \pm 0,05)z(km)$$
$$\bar{\lambda} = 3,37 \pm 0,09 \text{ Wm}^{-1}\text{K}^{-1} \quad (16 \text{ values})$$
$$\bar{q} = 32,9 \pm 0,8 \text{ mWm}^{-2}$$

Schoemansfontein BSF 1

(Table IV-18, Figure 6.23)

Temperatures were surveyed to a depth of 730,2 m and thermal conductivity measurements were made on samples of lava from the depth range 100-710 m. Below this depth the borehole penetrates sediments and basement gneisses. The conductivity and temperature data between 100,0 m and 713,5 m

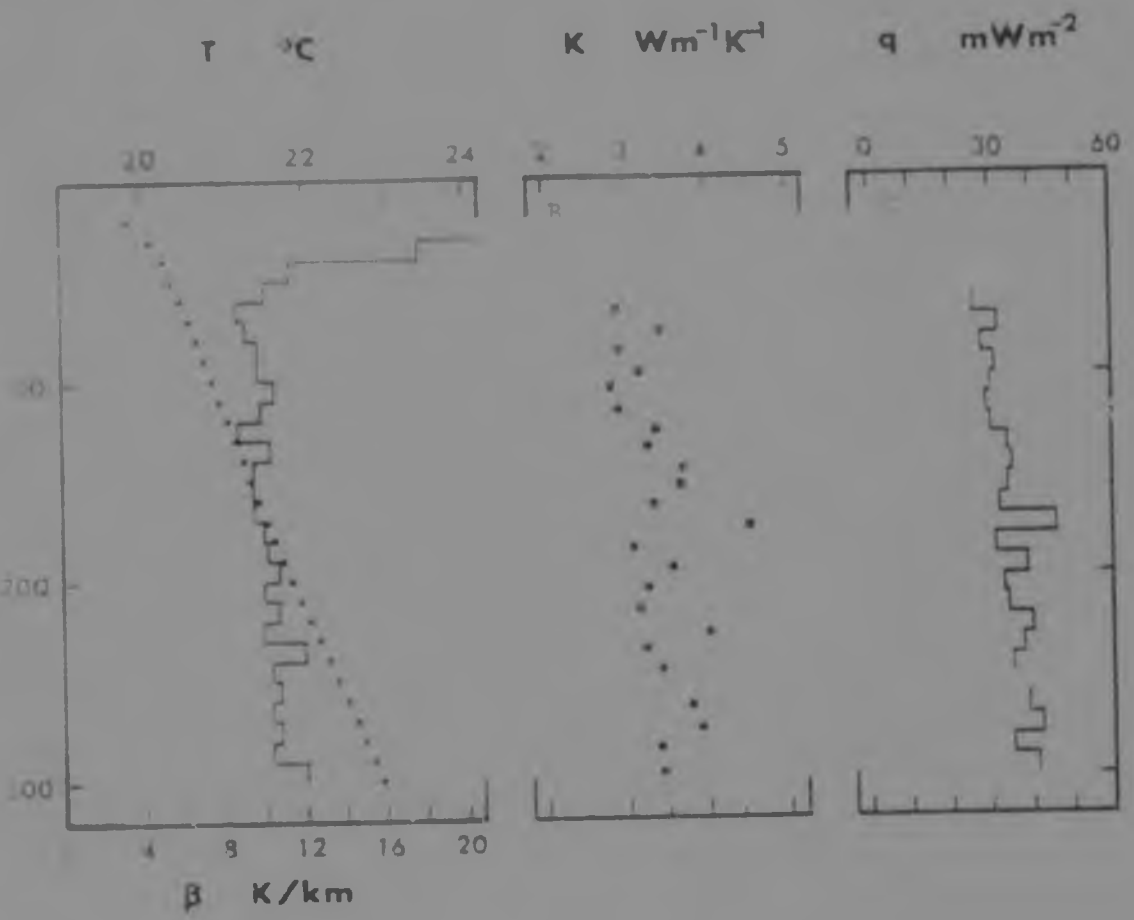
T °C
K Wm⁻¹K⁻¹
q mWm⁻²
Depth m
20
22
24
3
4
5
0
30
60
100
200
4
8
12
16
20
β K/km

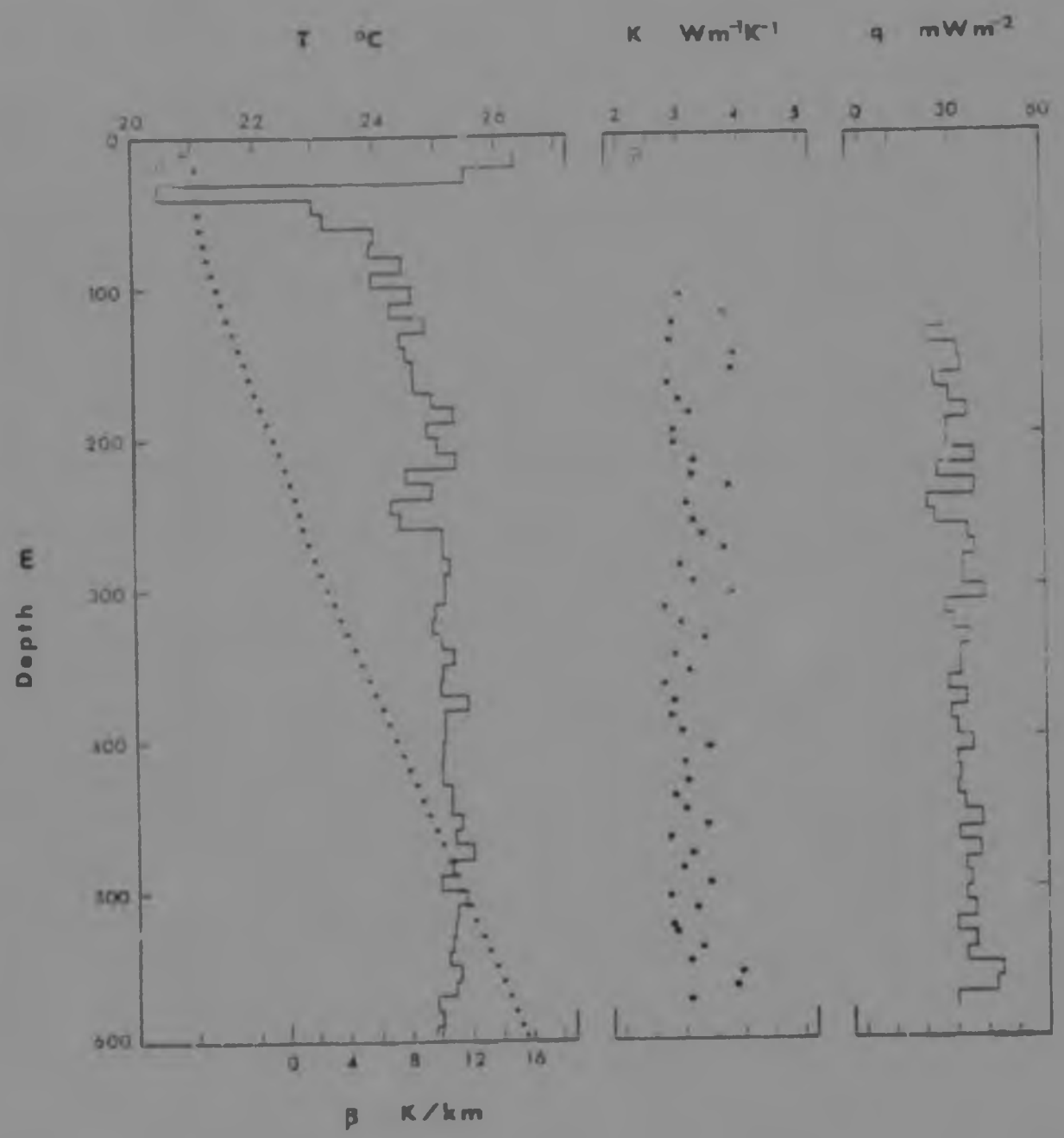

FIGURE 6.25 Mahemsvlei BMV 4. Bo-ehole data.

yields

$$T(^{\circ}C) = (\quad\quad \pm \quad\quad)z(km) + (\quad\quad \pm \quad\quad)$$
$$\bar{K} = \quad\quad \pm \quad\quad \text{Wm}^{-1}\text{K}^{-1} \qquad (\quad\quad \text{values})$$
$$\bar{q} = 33,0 \pm 0,3 \text{ mWm}^{-2}$$

Braksprull BBS 1

(Table IV-19, Figure p.24)

BBS 1 was open to the bottom at 401,2 m. The lowest 60 m of the borehole are in basement gneiss and thermal conductivity measurements were made on four samples of gneiss and nineteen samples of lava.

The lavas from 60,0 m to 250,0 m yield the following results:

$$T(^{\circ}C) = (19,87 \pm 0,07) + (10,01 \pm 0,06)z(km)$$
$$\bar{K} = 3,29 \pm 0,10 \text{ Wm}^{-1}\text{K}^{-1} \qquad (19 \text{ values})$$
$$\bar{q} = 33,0 \pm 1,7 \text{ mWm}^{-2}$$

and the gneiss unit from 260,0 m to 400,0 m gives:

$$T(^{\circ}C) = (19,71 \pm 0,08) + (10,78 \pm 0,19)z(km)$$
$$\bar{K} = 3,66 \pm 0,14 \text{ Wm}^{-1}\text{K}^{-1} \qquad (4 \text{ values})$$
$$\bar{q} = 38,8 \pm 1,7 \text{ mWm}^{-2}$$

The difference of more than 6mW between the heat flows is probably caused by inadequate sampling of the gneisses. The latter result has therefore been discarded and the heat flow for BBS 1 has been taken to be 33,0 mWm^{-2}.

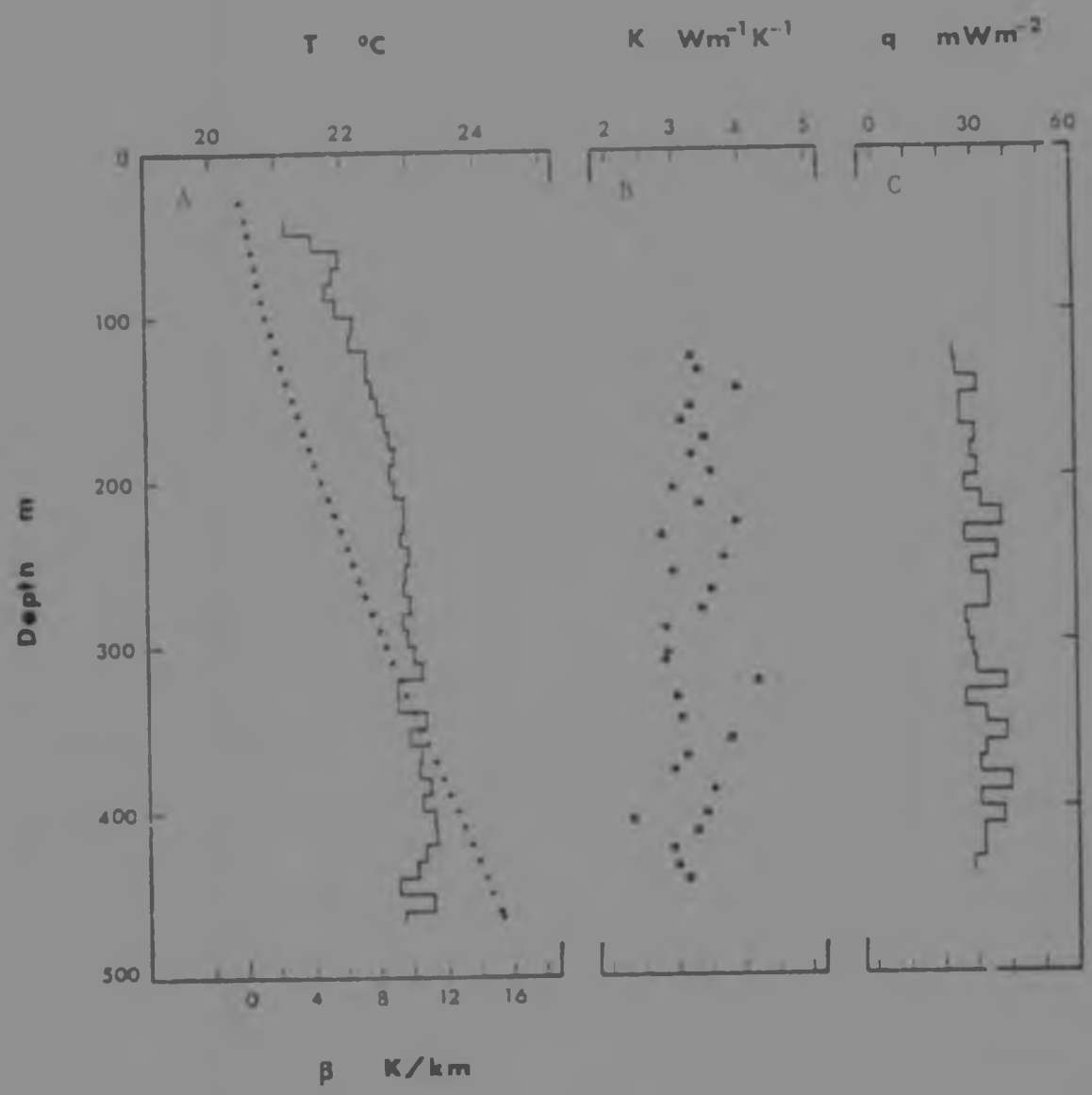

FIGURE 6.26 Tweelingfontein BTF 1. Borehole data.

Mahemsvlei BMV 4

(Table IV-20, Figure 6.25)

Temperatures were measured to the bottom of BMV 4 at 596,5 m. The borehole just penetrates the basement gneiss and the heat flow was calculated from measurements in the lava unit from 100,0 m to 578,9 m:

$$T(^{o}C) = (20,22 \pm 0,03) + (10,20 \pm 0,06)z(km)$$

$$\bar{K} = 3,14 \pm 0,05\ Wm^{-1}K^{-1} \quad (49\ values)$$

$$\bar{q} = 32,0 \pm 0,5\ mWm^{-2}$$

Tweelingfontein BTF 1

(Table IV-21, Figure 6.26)

BTF 1 was open to the bottom at 464,6 m. The basement gneiss was intersected at a depth of 460,5 m and the temperature and conductivity data from the lava between 120,0 m and 449,6 m give:

$$T(^{o}C) = (19,72 \pm 0,03) + (9,75 \pm 0,07)z(km)$$

$$\bar{K} = 3,21 \pm 0,08\ Wm^{-1}K^{-1} \quad (32\ values)$$

$$\bar{q} = 31,3 \pm 0,7\ mWm^{-2}$$

There is very little variation in the heat flow over the distance spanned by the boreholes (60 km) and an overall mean heat flow may be calculated for the Kierksdorp district by combining means for all seven boreholes. The values were weighted as in equation 6.9 and the overall mean and standard error are:

$$\bar{q} = 32,3 \pm 0,3\ mWm^{-2}$$

Table 6.8 summarizes heat production measurements made on nineteen samples of basement gneiss and one of Dominion Reef lava (Sample BBS 1). The heat production of BBS 1 is small and the lava succession contributes a neglitible amount to the surface heat flow. The average heat production of the gneisses differ considerably between boreholes (column 4, Table 6.8). The overall mean heat production for the Klerksdorp district is:

$$\bar{A} = 2,27 \pm 0,19\ \mu Wm^{-3}$$

6.15 Summary

The heat flow and heat production data for the above boreholes are summarized in Table 6.9. Topographic corrections were applied where indicated. No account has been taken of the curvature in the temperature profiles observed in the upper few hundred meters in many of the boreholes; this will be discussed in the following chapter. Two boreholes, PC2-30 and BF 1, were excluded from the list for the following reasons: PC2-30 yields a far less reliable value for the heat flow than PC2-27 which is located only 200 m away; and the heat flow estimated for BF 1 is no more than a crude guess as there were no conductivity data for the borehole.

Table 5.8 Heat production data for the Klerksdorp district

Sample*	Depth (m)	A (μWm^{-3})	$\bar{A}$ (μWm^{-3})
DRH 1	963	1,62	1,88
DRH 2	963	1,78	
DRH 3	967	2,25	
DRB 1	1278	2,15	2,14
DRB 2	1279	1,97	
DRB 3	1280	2,29	
DRL 1	282	1,34	1,14
DRL 2	283	1,14	
DRL 3	288	1,53	
BSF 1	770	3,21	3,40
BSF 2	773	3,69	
BSF 3	775	3,29	
BBS 1	100 - 250	0,16	2,49
BBS 2	264 and 274	3,89	
BBS 3	285 and 297	1,38	
BMV 1	597	1,74	1,49
BMV 1	600	1,23	
BIF 1	469	3,18	2,96
BIF 2	470	3,32	
BIF 3	472	2,48	

* All samples are quartzo-feldspathic basement gneiss except BBS 1 which is an aggregate of Dominion Reef lava.

Table 6.9 Summary of measurements of gradient, conductivity, heat flow and heat production

Borehole	Depth range (m)	$\bar{\beta} \pm \sigma_{\bar{\beta}}$ (K/km)	$\bar{K} \pm \sigma_{\bar{K}}$ (n) ($Wm^{-1}K^{-1}$)	$\bar{q} \pm \sigma_{\bar{q}}$ (mWm^{-2})	$\bar{A} \quad \sigma_{\bar{A}}$ (μWm^{-3})
FM 1 3	360,0 - 799,3	19,50* 0,08	3,14 0,08 41	61,2 1,6	7,96 0,97
HKE 26	57,6 - 467,0	19,26* 0,09	3,82 0,09 32	73,6 1,8	12,30 1,14
HE 177	[illegible] - 491,0	18,22* 0,11	3,49 0,09 27	63,6 1,7	6,90 0,99
CCX-042S	197,[illegible] - 588,6	19,13* 0,09	3,11 0,10 32	59,5 1,9	3,64 0,34
AE 140	200,0 - 440,0	18,62* 0,09	2,94 0,14 19	54,7 2,6	
	600,0 - 670,0	11,69* 0,21	4,89 0,56 8	57,2 6,6	
				55,0 2,5	2,75 0,20
POG 32	80,0 - 336,7	16,57 0,15	4,31 0,46 21	71,4 7,6	2,78 -
G-42	45,0 - 137,4	17,58 0,11	3,40 0,12 18	59,8 2,2	1,02 0,08
RB 56	284,4 - 350,5	20,69 0,24	3,85 0,05 10	79,6 1,4	
	359,9 - 434,0	21,92 0,29	3,89 0,09 10	85,3 2,3	
				81,1 1,2	3,78 0,76
AP 11	99,4 - 462,3	19,85 0,06	2,62 0,08 39	52,0 1,6	2,96 0,53
KC 12	115,8 - 210,0	13,46 0,07	2,89 0,07 26	38,9 1,0	1,14 0,10
PC2-27	186,9 - 445,4	16,82 0,12	3,55 0,11 30	59,7 1,9	2,21 0,13
V 41	247,4 - 402,2	14,40 0,10	3,20 0,12 18	46,1 1,9	
	530,5 - 703,2	17,99 0,05	2,71 0,10 29	48,7 1,8	
				47,5 1,3	0,79 0,27
HB 77	100,0 - 540,0	17,22* 0,31	3,43 0,07 23	59,1 1,6	2,05 0,07
DRM 18	89,7 - 510,4	9,21 0,10	3,51 0,10 44	32,3 0,9	1,88 -
DRB 6	80,0 - 400,0	8,61 0,04	3,50 0,06 32	30,1 0,5	2,14 -
DRL 17	60,0 - 230,0	9,76 0,05	3,37 0,09 16	32,9 0,8	1,34 -
BSF 1	100,0 - 713,5	11,06 0,05	3,16 0,05 60	35,0 0,5	3,40 -
BBS 1	60,0 - 250,0	10,03 0,06	3,29 0,10 19	33,0 1,0	2,49 -
BMV 4	100,0 - 378,9	10,20 0,06	3,14 0,05 49	32,0 0,5	1,49 -
BTF 1	120,0 - 449,6	9,75 0,07	3,[illegible] 0,08 32	31,3 0,7	2,96 -

* indicates topographic correction was applied

7 EFFECTS OF SURFACE TEMPERATURE VARIATIONS ON SUBSURFACE TEMPERATURES

7.1 Introduction

Two features of the temperature gradient in the study areas stand out above variations that may be attributed to local effects. The more marked feature which is found in most of the boreholes is a steadily increasing temperature gradient to a depth of approximately 200 m. This trend is nowhere matched by complementary trends in the thermal conductivity and must reflect a recent increase in the surface temperature. In three boreholes (BR 77, HE 177 and BSP 1) the gradient continues to rise to depths of at least 400 m, but below 200 m the rate of increase is small. This may be an enhancement caused by local effects superimposed on those operating in other boreholes; or, similar perturbations at these depths in the other boreholes may be obscured by variations in the thermal conductivity. The trends are not present in all boreholes and factors such as water movement and non-vertical heat transfer may conceal the pattern locally. Only boreholes with well-defined trends will be discussed in this chapter.

The second feature is apparent in the boreholes near Klerksdorp where a sharp decrease in the temperature gradient from the surface to approximately 60 m is superimposed on the deeper feature. This trend suggests an even more recent decrease in the surface temperature in this area.

It will be shown below that these perturbations are caused by changes in the surface temperature within the past 150 years and that older events affect temperatures to considerably greater depths. None of the boreholes

studied here is deep enough to show clear evidence of surface temperature variations which occurred before 1000 years b.p. However, Bullard (1939) measured heat flow in several deep boreholes (up to 3022 m) in the Witwatersrand and, in most cases, observed a systematic increase in the temperature gradient with depth. Similar observations were made in boreholes up to 2000 m deep by Carte (1954) in the Witwatersrand and Gough (1963) in the southern Karroo and both authors concluded that the heat flow increases with depth. Although these data are consistent with a recent (post-Pleistocene) climatic warming, the trends are not well defined in any of the boreholes and, in some cases, may have other causes. These will be discussed in Section 7.4.

This chapter has two main aims:

(1) to identify the cause of the observed systematic variations in the temperature gradient at shallow depths and estimate corrections to the heat flow;

(2) to discuss the effects that secular variations of the surface temperature during the Pleistocene and Holocene might have on heat flow in South Africa and determine whether the application of a climatic correction is justified.

7.2 Theoretical considerations

Carslaw and Jaeger (1959, pp. 62-3) discuss the temperature distribution within a semi-infinite solid of uniform thermal diffusivity (κ) when the temperature at the surface ($z = 0$) varies as a function of time ($\phi(t)$). If $\phi(t)$ is measured relative to some fixed reference temperature the

disturbance to the temperature at any time (t) and depth (z) is given by:

$$\Delta V(z,t) = \frac{z}{2\sqrt{\pi\kappa}} \int_0^t \phi(\tau)\exp\left(\frac{-z^2}{4\kappa(t-\tau)}\right)(t-\tau)^{-3/2}\,d\tau \qquad (7.1)$$

where τ is an auxiliary variable and $\kappa = K/\rho c$.

Our knowledge of past temperature variations at the earth's surface is far from complete and it is rarely possible to approximate the surface temperature variation by simple mathematical forms such as linear or sinusoidal functions. For most of the applications discussed here surface temperature variations are adequately represented by dividing past time into intervals during which the temperature is taken to be constant.

The simplest case from which more complex models of the surface thermal history may be constructed is a single 'box' function (Figure 7.1). The surface temperature variation $\phi(t)$, measured relative to the present-day surface temperature, is constant at A°C for all times between $-t_2$ and $-t_1$ (the 'event'), and zero at all other times. Negative signs are used because time is measured backwards. The solution to equation 7.1 at time t = 0 (i.e. the present time) may be obtained from Carslaw and Jaeger (1959, p. 85):

$$\Delta V(z) = A\,\mathrm{erf}\left(\frac{z}{2\sqrt{\kappa t_1}}\right) - A\,\mathrm{erf}\left(\frac{z}{2\sqrt{\kappa t_2}}\right) \qquad (7.2)$$

Differentiation with respect to z yields the disturbance to the temperature gradient:

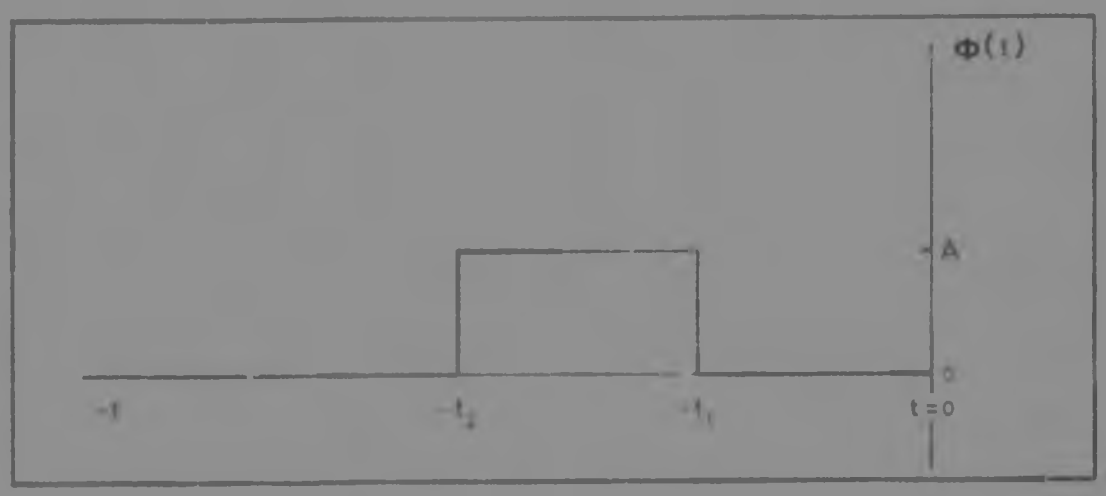

FIGURE 7.1 Simple 'box' function for surface temperature variation.

[illegible] change in the temperature gradient [illegible] parameters in equation 7.3. $\lambda(z)$ has been [illegible] Appl. 18 : 98-104)

[illegible] thermal diffusivity (κ)

[illegible] diffusivities in the range $(\kappa_1 - \kappa_2)$

[illegible] the thermal diffusivity.

[illegible] range of thermal diffusivity values within the range 10^{-6} to 10^{-5} $m^2 s^{-1}$ (see Table 7.1) assumed that, for many common rock [illegible] range of the constant is fairly limited and centred on $\kappa = 10^{-6}$ $m^2 s^{-1}$ and that thermal diffusivity is nearly proportional [illegible] conductivity. The heat conductivities of most rock units [illegible] are high and the majority fall within the [illegible] a value of $\kappa = 1.5 \times 10^{-6}$ $m^2 s^{-1}$ will be used as [illegible] in this and subsequent illustrations. This choice [illegible] the same as that used by several authors (eg. Sass et al, 1971; [illegible] Birtwell, 1978) and facilitates comparison with their results.

[illegible] surface temperature gradient are shown in Figure 7.2. It [illegible] that the most recent events have the most marked effects close [illegible] the surface while the past events are 'preserved' at greater depth . [illegible] events result in more marked disturbances. Decreasing the [illegible] from $\kappa_1 = 10^{-6}$ $m^2 s^{-1}$ to $\kappa_2 = 10^{-6}$ $m^2 s^{-1}$ causes an [illegible] in the amplitude of the disturbance and a decrease in the [illegible] of the maximum; however, the differences are small.

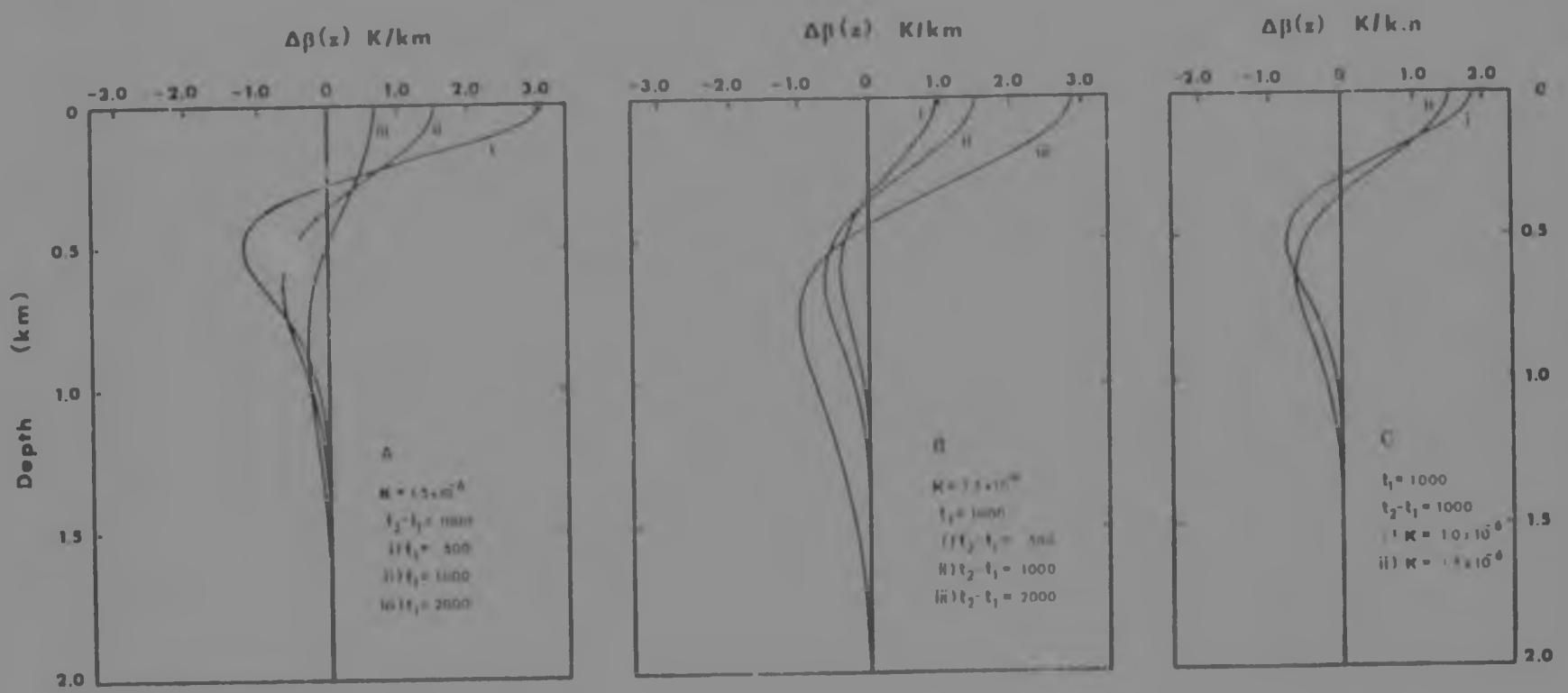

FIGURE 7.2 Disturbance to the temperature gradient, $\Delta\beta$, due to the 'box' function shown in Figure 7.1 for various values of: (a) the time elapsed since the event, t_1, (b) the duration of the event, t_2-t_1 and (c) the diffusivity, κ. Δ = 2°C in all cases. Curves ii are identical.

7.3 Near-surface systematic variations in temperature and heat flow

7.3.1 Data inversion

Systematic trends observed in most boreholes have been divided into those in which the temperature gradient increases to a depth of approximately 200 m and those in which it decreases to approximately 60 m. The shallow depths of penetration indicate that these trends are caused by very recent changes in the surface temperature. The form of the disturbance is simple in both cases and this suggests that surface temperature changes also had a simple form. A quantitive estimate of the amplitude and timing of the changes may be obtained by considering simple models for the surface temperature variation and estimating these parameters directly from observed temperature and temperature gradient profiles.

A detailed analysis of this kind was only attempted in the case of the 200 m deep feature as it is more widespread and better defined than the 60 m deep feature. Two models for the variation of surface temperature have been considered: a single step and a sinusoidal variation. Details of each model are described below.

(1) The step function. The surface temperature variation and the resulting disturbances at $\tau = 0$ are

$$\begin{aligned} \phi(t) &= 0 \qquad t < t_1 \\ \phi(t) &= A \qquad -t_1 < t < 0 \end{aligned} \tag{7.4}$$

$$N(z) = A\,\mathrm{erfc}\left(\frac{z}{2\sqrt{\kappa t_1}}\right) \tag{7.5}$$

$$\Delta V(z) = \frac{A}{\sqrt{\pi t_1}} \exp\left(\frac{-z^2}{4\kappa t_1}\right) \qquad (7.6)$$

Since $\Delta V(0) = A$, the size and sign of the step are most readily estimated from the curvatures of the temperature profiles. As discussed here, the temperature residual at any depth is the difference between the observed temperature and the temperature projected linearly from the deeper, straight section of the temperature profile. A was estimated by visually extrapolating the temperature residual to the surface. In the Klerksdorp boreholes the temperature fluctuations above 60 m were ignored for the purposes of this analysis. Nine boreholes have sufficiently well defined trends in the uppermost section to yield reasonably reliable estimates of A; all have a uniform lithology in the upper 200 m and the conductivities were assumed to be constant. Table 7.1 shows that estimates of A range from $-0,6^{\circ}C$ to $+1,2^{\circ}C$ and a value of $1,0^{\circ}C$ has been taken for the step in the surface temperature.

The time since the step occurred is most easily estimated from the variation in the temperature gradient. At a characteristic depth z_c given by:

$$z_c^2 = 4\kappa t_1 \qquad (7.7)$$

the disturbance to the gradient (equation 7.6) is equal to 1/e (or 37,8%) of its surface value, $\Delta\Gamma(0)$. The residual in the gradient at any depth is the difference between the observed gradient at that depth and the average 'constant' gradient at depths below the zone showing systematic variations. For each of the above-mentioned boreholes $\Delta\Gamma(0)$ was estimated by visually extrapolating this residual to the surface, and z_c was estimated as the depth at which the residual was 38% of its surface value. The effects shallower than 60 m in the Klerksdorp boreholes

Table 7.1 Borehole parameters used to estimate surface temperature as a function of time for the 200 m deep feature

Borehole	$\Delta V(0)$ (^{o}C)	$\Delta B(0)$ (K/km)	z_c (m)	t_1 (years)	$\lambda/4$ m	I (years)
HKE 26	+1,2	-8,0	140	93	160	622
AG 140	+0,7	-6,5	110	75	140	616
POG 32	+0,8	-5,0	160	108	190	777
AP 11	+1,0	-10,0	100	70	120	510
PC2-27	+0,9	-9,0	130	87	160	669
DRH 18	+0,7	-6,0	120	75	150	595
DRB 6	+0,6	-7,0	110	63	130	448
BMN 4	+1,0	-8,0	120	84	150	665
BTF 1	+1,1	-8,0	140	111	160	740

were again ignored. t_1 was calculated from equation 7.7 using the average conductivity of the uppermost rock unit in each borehole and assuming $\rho c = 2,3 \times 10^{6}\ Jm^{-3}K^{-1}$. Values for t_1 fall within the range 60-120 years (Table 7.1); for the sake of simplicity, 100 years will be taken to represent the time elapsed since the step occurred.

The disturbance to the temperature gradient due to a +1 °C step in the surface temperature 100 years ago is shown in Figure 7.3 using a thermal diffusivity of $1,5 \times 10^{-6}\ m^{2}s^{-1}$.

(2) The sinusoidal function. The surface temperature variation is given by:

$$\phi(t) = A\cos(\omega t - \varepsilon) \qquad (7.8)$$

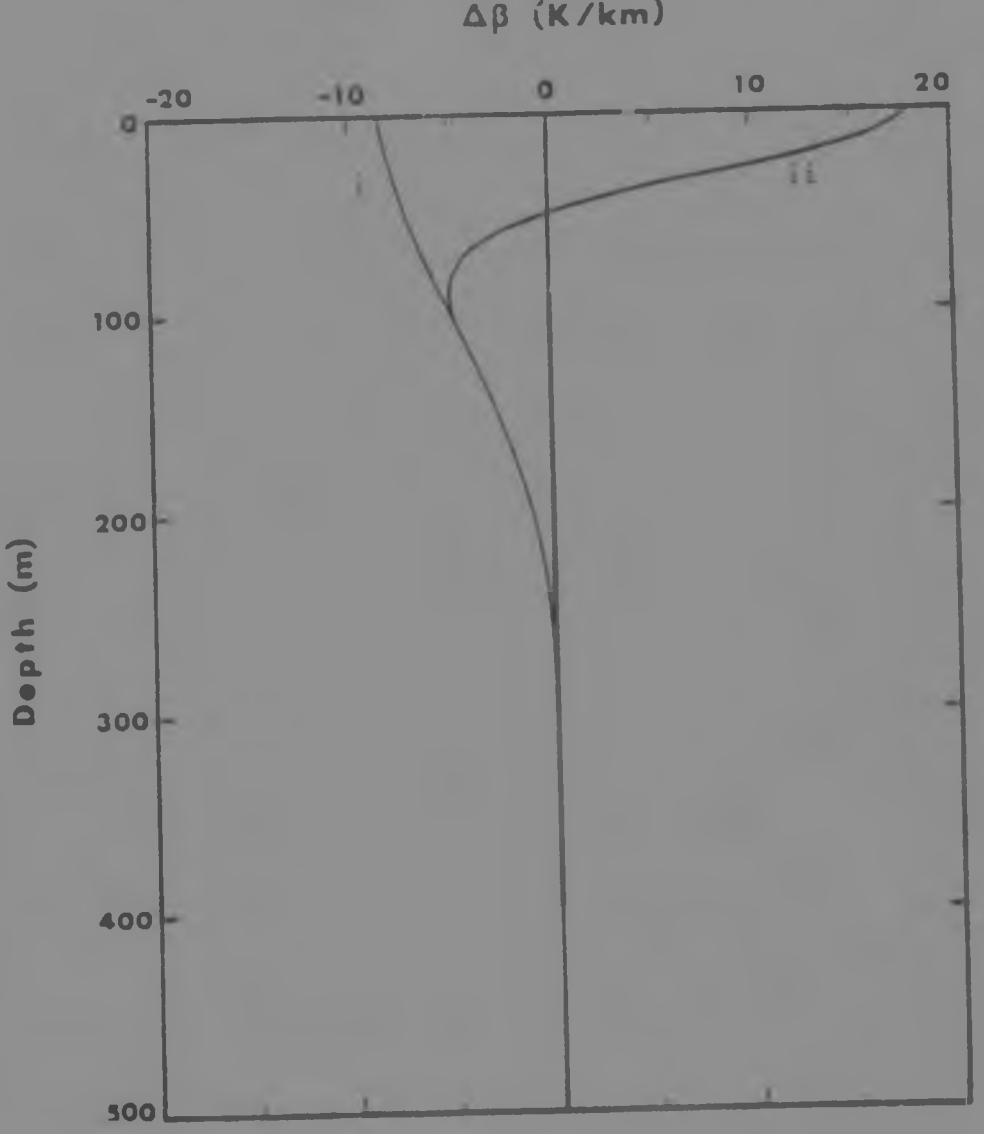

FIGURE 7.3 Disturbance to the temperature gradient due to a step of +1°C in the surface temperature 100 years ago (i) and a +1°C step 100 years ago followed by a -1°C step 10 years ago (ii). $\kappa = 1.5 \times 10^{-6}$ m^{2}s^{-1}.

where ε is the phase difference and indicates the present position on the temperature-time wave. ω is the frequency of the oscillation and:

$$\omega = \frac{2\pi}{T} \tag{7.9}$$

where T is the period. The disturbance to the temperature and temperature gradient (at t = 0) may be obtained from Carslaw and Jaeger (1959, p. 65):

$$\Delta V(z) = A \exp(-(\frac{\omega}{2\kappa})^{\frac{1}{2}} z)\cos(\varepsilon + (\frac{\omega}{2\kappa})^{\frac{1}{2}} z) \tag{7.10}$$

$$\Delta\beta(z) = -A(\frac{\omega}{2\kappa})^{\frac{1}{2}} \exp(-(\frac{\omega}{2\kappa})^{\frac{1}{2}} z)\{\sin(\varepsilon + (\frac{\omega}{2\kappa})^{\frac{1}{2}} z) + \cos(\varepsilon + (\frac{\omega}{2\kappa})^{\frac{1}{2}} z)\} \tag{7.11}$$

It is not as easy to characterize this model of the surface temperature since it is necessary to specify three parameters: phase (ε), amplitude (A) and period (T). The previous discussions and the curvatures of both temperature and gradient profiles suggest that the surface temperature is close to a maximum if the variations above 60 m near Klerksdorp are ignored. Figure 7.4 shows ΔV(z) and Δβ(z) for five different values of ε varying from $-\pi/2$ to $+\pi/2$. Only the curves characterized by ε = 0 and ε = $+\pi/4$ closely approximate the shapes of the observed variations of both temperature and temperature gradient and, as a first approximation, ε is taken to be zero.

With ε = 0, A is equal to ΔV(0) and may therefore be estimated in the same way as for the step function. Hence A = 1°C.

The wavelength of ΔV(z) is given by:

$$\lambda = (4\pi\kappa T)^{\frac{1}{2}} = 2\pi(\frac{2\kappa}{\omega})^{\frac{1}{2}} \tag{7.12}$$

and at a depth equal to λ/4 (and with ε = 0) we have:

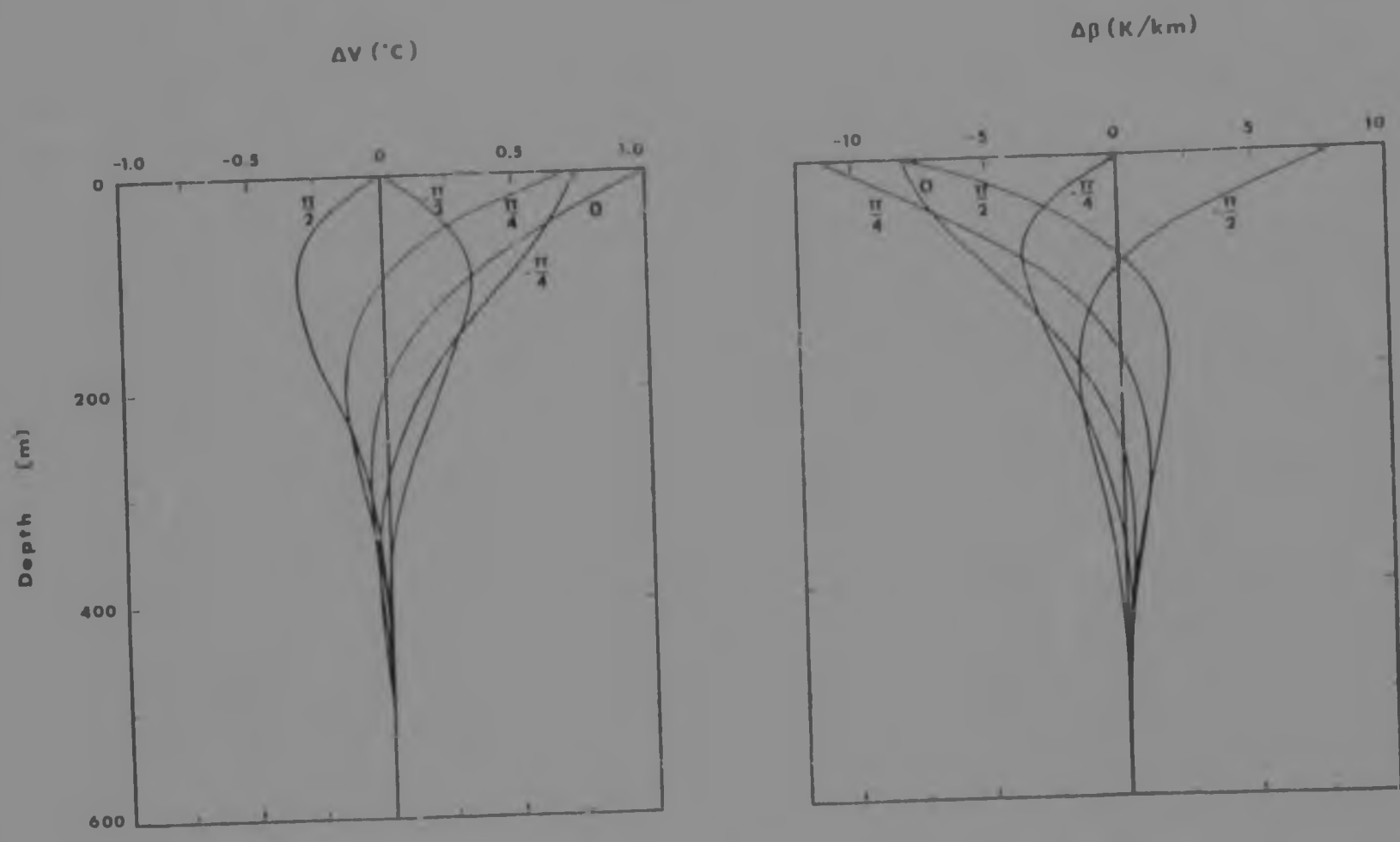

FIGURE 7.4 Disturbance to the temperature, ΔV, and temperature gradient, $\Delta\beta$, due to a sinusoidally varying surface temperature for different values of the phase, ε. $A = 1°C$, $T = 1000$ years and $\kappa = 1{,}5 \times 10^{-6}\ m^2 s^{-1}$.

$$\Delta V(\lambda/4) = 0 \qquad (7.13)$$

$$\Delta\beta(\lambda/4) = -0,208A\left(\frac{\omega}{2\kappa}\right)^{\frac{1}{2}} \qquad (7.14)$$

$\lambda/4$ may be estimated from the depth at which the temperature residual becomes negligible and the depth at which the residual in temperature gradient is 21% of its surface value. The latter method is less subjective and is used below. The period may be calculated from equation 7.12. Estimates of $\lambda/4$ for the nine boreholes are between 120 and 190 m and values for T between 450 and 750 years (Table 7.1). The central value, 600 years, was chosen as the best estimate of T.

The disturbance to the gradient due to a sinusoidal variation of the surface temperature of amplitude 1°C, period 600 years and phase zero is shown in Figure 7.5 for a diffusivity of $1,5 \times 10^{-6}$ $m^2 s^{-1}$.

The 60 m deep perturbations in the Klerksdorp boreholes were not analysed in the same detail. They clearly reflect a very recent decrease in surface temperature and this raises the possibility that they are due to seasonal variations. These borehole temperatures were measured during the winter when the enhancement of temperature gradient is close to a maximum, but Carslaw and Jaeger (1959, p. 81) showed that seasonal changes in surface temperature have observable effects to depths of only ~20 m. Figure 7.3 shows that a reasonably good approximation to the observed trends may be obtained if the step function is modified by a 1°C decrease of the surface temperature occurring 10 years ago. A similar effect may be obtained by changing the phase of the sinusoidal variation and in Figure 7.5 $\Delta\beta(z)$ is shown for $\varepsilon = -\pi/2$.

Equally good, or better, fits to the observed trends may be obtained by using slightly different values for A and t_1 (case 1) and A, T and ε

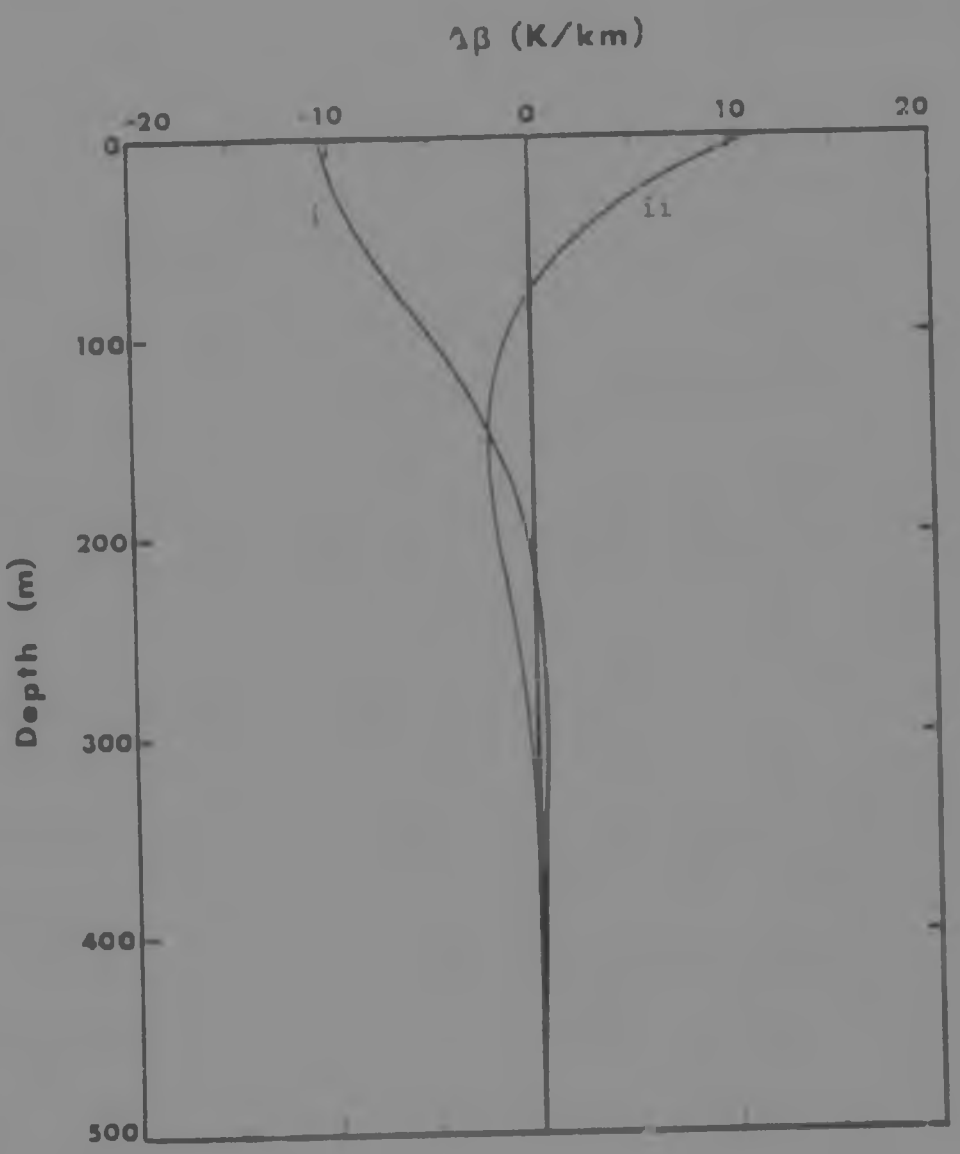

FIGURE 7.5 Disturbance to the temperature gradient due to a sinuscidal variation of the surface temperature of amplitude A = 1°C, period T = 600 years and phase $\varepsilon = 0$ (i) and $\varepsilon = -\pi/2$ (ii). $\kappa = 1{,}5 \times 10^{-6}$ m-s^{-1}.

(case 2), or using different models for $\phi(t)$ such as a linear increase of the surface temperature. However, the conclusions of this section would not be seriously affected and they may be summarized as follows:

(1) The surface temperature over much of South Africa has been elevated by about 1°C during the past century.

(2) Data from the Klerksdorp boreholes suggest that the surface temperature has started to decline during the past decade or so.

It should be possible to relate both events to historical records, and possible causes of surface temperature changes are discussed below.

7.3.2 Causes of surface temperature variations

Important causes of widespread changes in surface temperature include uplift and erosion, sedimentation, changes in vegetation and climatic variations. Each of these factors and their bearing on near-surface variations in temperature will be discussed below.

Uplift and erosion

The effect of uplift and erosion is to increase near surface temperature gradients by exposing deeper, warmer regions to surface conditions. This effect may be considerable where large quantities of material have been removed by recent, rapid erosion (Birch, 1950; England, 1978). The present cycle of erosion is in a mature stage over most of southern Africa and in most places the effect of erosion on the temperature gradient is negligible (cf. Gough, 1963). The most likely borehole to be affected is HB 77 in the Richtersveld where the deeply dissected

land surface suggests that erosion may be a significant factor. However, the observed trend in the temperature gradient is opposite in sense to that which would be caused by erosion.

Sedimentation

Sedimentation has the opposite effect to erosion on the surface temperature and result in an increasing temperature gradient with depth. Deposition of 50-100 m of sediment would be required to generate the observed perturbations; this has clearly not occurred in the study areas in the last few hundred years.

Vegetation changes

Land clearing for agricultural and pastoral purposes has a well known effect on temperature gradients and can cause systematic trends of the same sign and magnitude as the 200 m deep feature (Jaeger, 1970; Roy et al, 1972).

The climate of southern Africa is mainly arid to semi-arid and much of the Namaqua Mobile Belt has little vegetation cover while the area surrounding Klerksdorp is covered by short grassveld. It is an established fact that most of southern Africa is undergoing increasing aridity. Wilcocks (1977) reviewed factors which lead to desertification and concluded that there is no evidence for progressive climatic dessication and that farming activities, particularly overgrazing, appear to have had a much more important effect. However, desert encroachment was first observed by many nineteenth century white explorers and appears to have been a long-continued process. H J Deacon (personal communication) has

pointed out that herding and agriculture appeared in South Africa within the last 2000 years and desertification may have commenced as early as this.

Van Zinderen Bakker (1976) noted that constant changes in average temperature of as little as 1°C can alter the vegetation distribution pattern, a factor which was not considered by Wilcocks (1977). It will be shown below that southern Africa has experienced a general increase in surface temperature during the past century and increased evaporation may be an important contributing factor to the environmental deterioration.

In summary, desert encroachment has had a long history in southern Africa. The major cause of this appears to be human intervention, but recent changes in temperature may have played an important role. There is no evidence for widespread land clearing during the past century or so.

Climatic variations during the period of the meteorological record

It has been shown that observed variations in temperature gradient are due to surface events which are recent enough to be preserved in the meteorological record. Mean annual air temperatures at several meteorological stations in South Africa, Europe and the U.S.A. are summarized in this section, and these data give clear evidence for recent climatic variations which are consistent with the observed borehole trends.

Five-year averages of the air temperatures at six stations in South

Africa are shown in Figure 7.6. The Royal Observatory in Cape Town has the longest record and the most striking feature of this is a steady temperature increase amounting to nearly 1°C between the years 1900-1930. Most other stations show similar trends but none of these records is long enough to be convincing in itself. The temperatures, averaged over ten year periods, for some of the oldest stations in Europe and the U.S.A.(Figure 7.7) show a general increase in temperature starting as early as 1820 in Berlin and 1840 in Copenhagen. There is strong evidence for a recent climatic warming on a global scale.

It should be noted that urbanization may cause extraneous increases in temperatures at meteorological stations situated in large cities. However, such effects are unlikely to be significant in small cities and towns such as Queenstown, O'okiep and even Cape Town. Furthermore, Brown (1963) showed that there has been a considerable increase in sea and air temperatures in the Atlantic Ocean between 30°N and 30°S from about 1910-1920 onwards. Finally, in a review of studies on climatic fluctuations Veryard (1963, p. 5) noted that:

> 'It is now generally accepted that the most striking feature of climatic fluctuations during the period of the meteorological record has been a warming in many parts of the world since about 1850 until a decade or two ago when in some places, but not all, there appears to have been a levelling-off or a fall of temperature.'

The meteorological data therefore provide the most reasonable explanation for observed trends in temperature gradient. Variations in the amplitude and time of inception of the surface temperature increase are to be expected and can account for local differences in these trends. Decreasing temperature gradients to depths of 60 m in the Transvaal

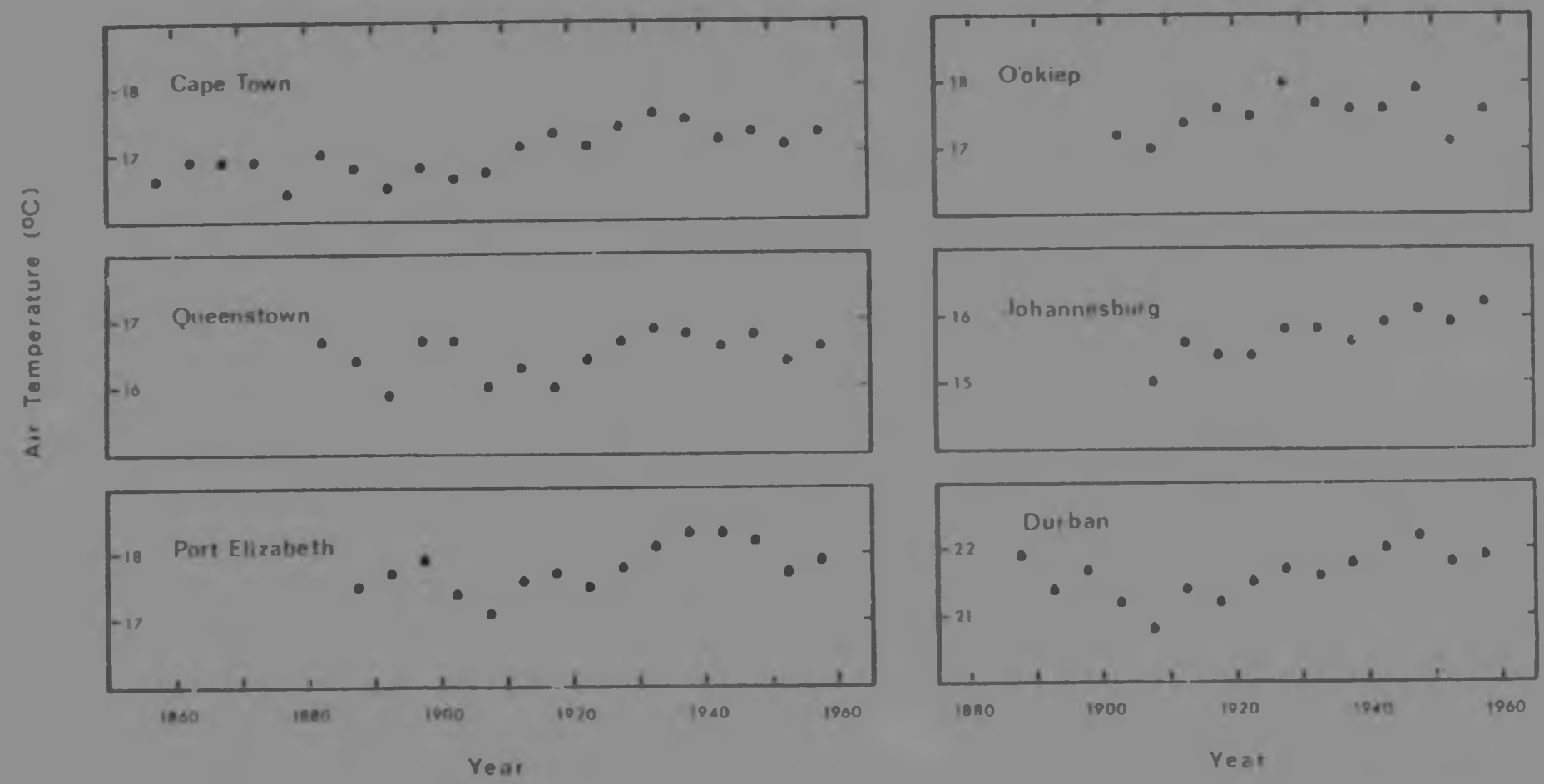

FIGURE 7.6 Surface temperature averaged over five year periods at six meteorological stations in South Africa. The data were obtained from Schulze (1965).

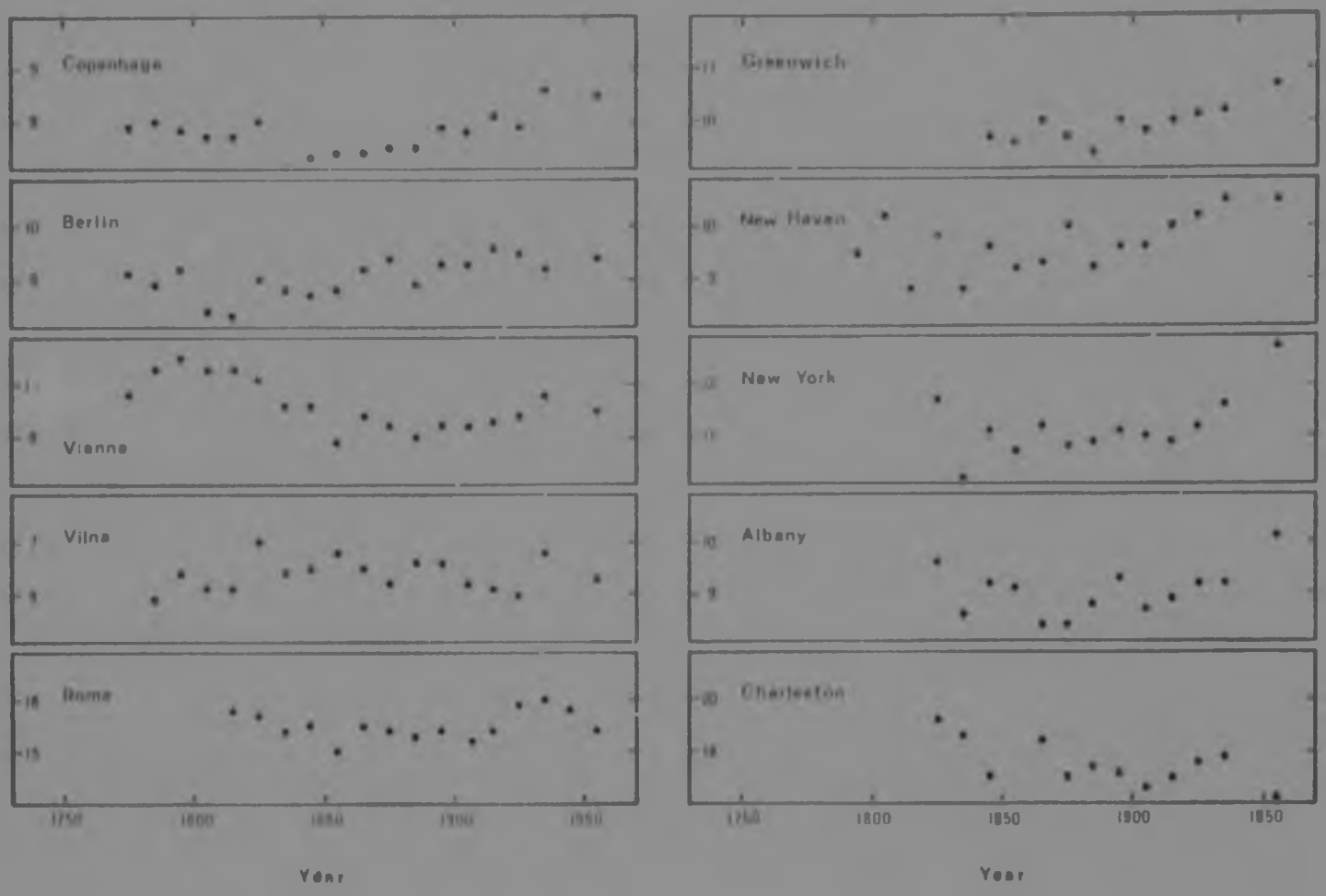

FIGURE 7.7 Surface temperature averaged over ten year periods at six meteorological stations in Europe and four in the USA. The data are from the World Weather Records, Smithsonian Miscellaneous Collection volumes 79, 90 and 105 and the US Department of Commerce volumes 1 - 3. Records for the decade 1941 to 1950 were missing except for Rome.

a d also consistent with world-wide changes in the 'weather cycle'. In Cape Town there is a negative correlation between changes in mean annual rainfall and temperature (Mormyr and Scholse, 1963) and such an interplay between rainfall, temperature and therefore vegetation may also lead to local differences in the pattern of subsurface temperature perturbations.

7.4.3 Corrections to the heat flow

It has been established beyond reasonable doubt that curvatures observed in many of the boreholes under study are due to a climatic change within the past 100 years and it is therefore appropriate to apply corrections to the heat flow.

There are no conductivity data in the upper 200 m of six boreholes (FM 143, GCX-0425, AG 140, BB 36, PC2-27 and V 4/3) and the heat flows remain uncorrected. Three relatively shallow boreholes (G-42, KC 12 and BSS 1) do not show systematic trends in the gradient and there is no justification for correcting their heat flows. Corrections were applied to the remaining boreholes. It has already been noted that recent surface temperature changes are subject to local irregularities and corrections based on a constant climatic mode' would be inappropriate. A more suitable approach is to exclude temperature data within the upper variable zone when calculating the mean temperature gradient. The 'corrected' gradients calculated in this way are listed in Table 7.2. The 'corrected' heat flow for each borehole was obtained by combining the new gradient with the mean of all the conductivity data and is compared with the uncorrected heat flow in Table 7.1. HB 77, HE 177 and BSF 1 show small increases in

Table 7.1 Heat flows corrected for recent (~ 100 year) increase in surface temperature

Borehole	Depth range (m)	Corrected gradient (K/km)	Corrected heat flow (mWm^{-2})	Uncorrected heat flow (mWm^{-2})
VRB 16	162,7 – 467,0	19,81	75,7	73,6
WE 137	213,3 – 471,2	18,73	67,4	65,8
BOK 12	138,8 – 356,7	17,15	74,3	71,4
AP 1	138,8 – 462,7	19,48	52,7	52,0
BE 77	200,0 – 340,7	18,79	54,4	39,1
DRR 181	199,1 – 510,4	9,63	33,8	34,3
DKB 6	160,0 – 400,1	8,19	30,8	30,1
BFL 17	100,0 – 330,4	9,82	32,4	32,9
BSH 1	149,8 – 710,1	11,30	35,7	35,6
BMV 4	150,0 – 578,9	10,31	33,3	32,0
BTZ 1	199,9 – 449,8	10,11	32,5	31,3

temperature gradient to depths of approximately 400 m. The reason for the variations at greater depths in these boreholes is not known and the 'corrected' gradients were calculated using the temperature data below 400 m.

In all cases, corrections to the heat flow are small. This is mainly due to the absence of conductivity data in the upper 400 m of most boreholes and the fact that opposing trends in the Klerksdorp boreholes partly cancel each other.

7.4 Quaternary climatic variations

The first comprehensive study of the effect of recent climatic history

on heat flow was made by Birch (1948) who showed that surface temperature variations during the past million years may disturb subsurface temperatures to depths of several kilometres. In a more recent investigation Beck (1977) concluded that climatic warming after the Pleistocene glaciations may depress the heat flow in high latitudes by as much as 25%. However, the heat flow measured in a 3 km deep borehole in the Canadian Shield shows no systematic variation with depth (Sass et al, 1971) in spite of the fact that the borehole lies within the area that was covered by the Laurentide ice sheet. England (1978) argued that erosion accompanying glaciation may compensate for the climatic effect of the ice age and even result in net positive perturbations to the heat flow. To date, there has been no convincing demonstration of the effect of Pleistocene and Holocene climatic variations and this casts some doubt on the validity of climatic corrections that are often applied to heat flow determinations. However, it is important to estimate how large the perturbations may be and two reconstructions of the surface thermal history of the northern continents are considered below.

Table 7.3 shows two climatic models in which past time has been divided into discrete intervals during which the surface temperature differed from the present temperature by a constant amount. Model I is that of Birch (1948, model 2B) as modified by Sass et al (1971). Model II is that proposed by Beck (1977) for latitudes 20-40° except that climatic variations during the past 900 years have been removed; the fine detail for this period in the original model has a large effect close to the surface and is unlikely to apply on a global scale.

The temperature disturbance due to a series of step changes of the

Table 7.3 Surface temperature models used to calculate climatic perturbations shown in Figure 7.8

Model I (Birch, 1948)		Model II* (Beck, 1977)	
Time (1000 years B.P.)	Surface temperature (^{o}C)	Time (1000 years B.P.)	Surface temperature (^{o}C)
∞ - 1000	+1,0	∞ - 80	0,0
1000 - 900	-3,5	80 - 45	-6,0
900 - 700	+1,0	45 - 12	-7,5
700 - 600	-3,5	12 - 9	0,0
600 - 300	+1,0	9 - 2,5	+1,0
300 - 200	-3,5	2,5 - 1,2	0,0
200 - 100	+1,0	1,2 - 0,9	+0,5
100 - 80	-3,5	0,9 - 0	0,0
80 - 60	0,0		
60 - 40	-3,5		
40 - 30	0,0		
30 - 10	-3,5		
10 - 5	+2,0		
5 - 0	0,0		

* Times have been rounded to convenient figures and temperatures to the nearest 0,5 C.

surface temperature may be deduced by expanding equation 7.2. The final expression is equivalent to that formulated by Birch (1948) and is

$$\Delta V(z) = \sum_{i=1}^{n} (A_i - A_{i+1}) \operatorname{erfc}\left(\frac{z}{2\sqrt{\kappa t_i}}\right) \qquad (7.15)$$

where A_i is the difference between the surface temperature during the time interval $t_i - t_{i+1}$ and the present surface temperature. The

disturbance to the temperature gradient is

$$\Delta T(z) = \sum_{i=1}^{n} \frac{A_i - A_{i+1}}{\sqrt{\pi \kappa_i}} \exp\left(\frac{-z^2}{4\kappa_i}\right) \qquad (7.16)$$

Disturbances to the temperature gradient due to models I and II are shown in Figure 7.8 and may be as large as -7,3 K/km above a depth of 1 km. This amounts to 10-15% of the temperature gradients measured in the Namaqua Mobile Belt and 25% of that in the Klerksdorp district. If climatic changes similar to those summarized in Table 7.3 occurred in southern Africa the heat flow may be seriously underestimated.

However, Shackleton (1980) has noted that, while the climatic history was very similar in North America, Europe and over much of the ocean surface, it appears to have been quite different in Africa. Climatic 'corrections' may be considerably different in southern Africa and it is not appropriate to apply corrections calculated on the basis of climatic models for Europe and North America. The climatic history of southern Africa must be reconstructed using local information.

Most of the information regarding climatic and environmental changes in southern Africa during the Quaternary has been reviewed by van Zinderen Bakker (1976) and Lancaster (1979). At present, there is very little quantitative evidence for the magnitude and timing of surface temperature changes, and palaeoclimatic models discussed by these authors lack detail and may require substantial revision as new data become available. Although there is no doubt that temperatures were significantly depressed during the late Pleistocene, little is known about temperature fluctuations during the Holocene. Recent

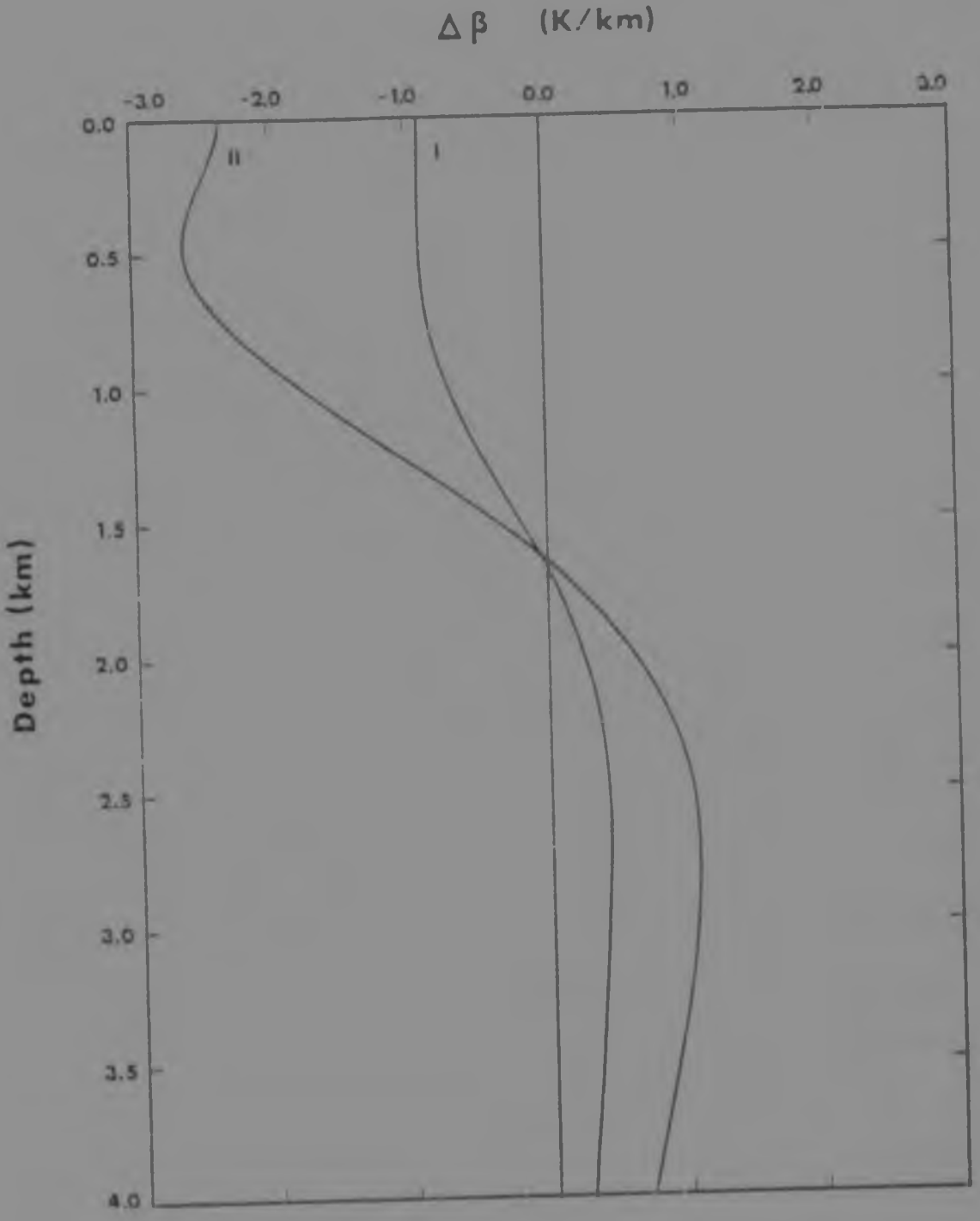

FIGURE 7.8 Disturbance to the temperature gradient due to climatic models I and II summarized in Table 7.3.

climatic changes have the most important effect on near-surface temperature gradients and a proper evaluation of palaeoclimatic effects on heat flow in South Africa must await more precise climatic reconstructions. Perhaps the best evidence for surface temperature changes will come from oxygen isotope studies; a few results are already available (Talma et al, 1974) and it is interesting to note that such studies are currently in progress in the southern Cape (H J Deacon, personal communication) and, hopefully, will commence in East and West Africa (Shackleton, 1980).

A suggestion that palaeoclimatic changes may have depressed the near-surface heat flow in South Africa comes from measurements in several deep boreholes (up to 5 km) in the Witwatersrand (Bullard, 1939; Carte, 1954) and the southern Karroo (Gough, 1963). All three investigators observed increases in the thermal gradient with depth, but the cause for this was not established unassailably.

Bullard (1939) showed that systematic trends evident in the lower part of several boreholes would practically be removed if a slightly smaller mean conductivity were applied to the lower depth range. He concluded that a constant conductivity had been assumed over too great a depth interval and that there was no evidence for a variation of heat flow with depth.

Carte (1954) calculated heat flows for several boreholes in the Klerksdorp district and northern Free State. Ten boreholes pass through Ventersdorp lava before penetrating Witwatersrand quartzite. The heat flow, calculated separately for each rock unit, was found to be consistently higher in the quartzite by 7-24%. At these localities

the dip of the strata is as much as 30° and a preliminary investigation indicates that the anomaly can be attributed to heat flow refraction caused by the conductivity contrast between the quartzite and the lava (S W Richardson, personal communication).

Gough (1963) observed systematic increases in heat flow with depth in three boreholes in the southern Karroo, and showed that the trends could be attributed to Pleistocene climatic variations. However, the data were not sufficiently precise to definitely link the trends with a specific climatic reconstruction.

There is a clear need to resolve the effect of palaeoclimatic surface temperature variations; this is particularly important for measurements on the craton as they could conceivably be depressed by as much as 25%. There are several reasons why areas such as the Namaqua Mobile Belt and Kaapvaal Craton are particularly suitable for this purpose. Pleistocene temperatures were not sufficiently lowered to result in glaciation and possible disturbances due to glacier erosion will be absent. The low rainfall reduces the risk of interference from waterflows. Topographic effects are negligible in most areas and there has been no recent uplift and erosion, or sedimentation. Finally, many localities are underlain by rock units which have a uniform thermal conductivity; this largely avoids heat flow refraction effects and facilitates comparisons between model perturbations and actual observations. Heat flow measurements in deep boreholes in these areas, accompanied by palaeoclimatic investigations, may go a long way to solving the problem.

SUMMARY

[illegible] systematic [illegible] temperature gradient measurements in boreholes. Provided [illegible] sufficiently long, undisturbed and uncomplicated it is possible to reconstruct simple models of the surface temperature as a [illegible] and estimate the rate and timing of temperature [illegible] trends. Several examples have been [illegible] a step function and a sinusoidal [illegible] the surface temperature variation. The models indicate [illegible] a rise in surface temperature of about 1°C over [illegible] during the past century. Data from the Transvaal [illegible] temperature has started to fall again during the past [illegible] Variations of the mean annual air temperature during the last [illegible] of meteorological stations in southern Africa, [illegible] correlate extremely well with the borehole data; [illegible] temperatures, starting up to 130 years ago, seem to be [illegible] climatic phenomenon. It has been necessary to apply [illegible] corrections for this effect to several heat flow determinations.

[illegible] pertinent climatic variations within the last few hundred [illegible] marked effects on near-surface temperature gradients. [illegible] of extraclimatic events, which are usually measured in [illegible] of years, may be completely obscured in the upper few [illegible] of a borehole. For this reason, the use of heat flow [illegible] in studies of models as supporting evidence for Quaternary [illegible] fluctuations (e.g. Lachenbruch, 1980) is inconclusive.

[illegible] models based on data from North America and Europe

indicate that the heat flow in these regions may be depressed by as much as 25%. It is unlikely that these models are representative of the climatic history in southern Africa and, as local climatic modelling is in an early stage of development, it is not possible to estimate perturbations to the heat flow at all reliably. For this reason, and because of the lack of clear-cut evidence for climatic perturbations in deep boreholes, corrections have not been applied to the heat flow determinations.

8 THE HEAT FLOW PATTERN IN SOUTH AFRICA AND THE THERMAL STRUCTURE OF THE LITHOSPHERE

8.1 Regional heat flow pattern

With the data reported here there are now a total of fourty-eight heat flow stations in South Africa. The locality, heat flow and heat production (where determined) of each station are listed in Table 8.1, and Figure 8.1 shows the variation of heat flow within the tectonic framework discussed in Chapter 2. Although the coverage is still sparse and the distribution of stations irregular it is possible to make some general conclusions about the regional heat flow pattern.

The observation made by Carte and van Rooyen (1969) is clearly substantiated; the lowest heat flow values are found on the Kaapvaal Craton, while in the mobile belts the heat flow is relatively high. This feature is emphasised Figure 8.2 in which heat flow is plotted against distance from the Atlantic coast along a line passing through the highest density of stations (A-B, Figure 8.1). All points within about 100 km of A-B and the mean heat flows for the Namaqua Mobile Belt and the Kaapvaal Craton are shown; there is clearly a significant difference in the heat flow between these regions.

The lowest heat flow values are found in the centre of the Kaapvaal Craton. The central cluster of sixteen stations gives a mean and standard deviation of 40 ± 7 nWm^{-2}. There is an increase of heat flow away from the centre and the remaining eight stations within the craton boundaries give an average of 54 ± 8 mWm^{-2}. However, it should be noted that the positions of these boundaries are not known accurately.

Table 8.1 Heat flow in South Africa - locality, heat flow (q_o) and heat production (A_o). Heat flows have been rounded to 1 mWm^{-2} and heat productions to 0.1 μWm^{-3}

No.	Borehole Name	Latitude	Longitude	q_o (mWm^{-2})	A_o (μWm^{-3})	Source
1	Jacobs	27° 18'S	26° 24'E	40	-	1
2	Doornhoutrivier	27° 18'S	26° 24'E	41	-	1
3	Gerhardminnaaron	26° 30'S	27° 12'E	50	-	1
4	Doornkloof	26° 18'S	27° 30'E	50	-	1
5	Reef Nigel	26° 18'S	28° 18'E	51	-	1
6	Dubbledevlei	30° 36'S	21° 30'E	64	-	1
7	HB 13	26° 48'S	26° 54'E	44	-	2
8	Roodepoort	26° 54'S	28° 36'E	38	-	2
9	Messina	22° 18'S	30° 06'E	57	-	2
10	Kastell	28° 18'S	28° 42'E	54	-	2
11	Sambokraal*	32° 42'S	21° 20'E	58	-	3
12	Koggelfontein*	32° 30'S	25° 20'E	61	-	3
13	Bothadale*	32° 48'S	22° 15'E	54	-	3
14	Kalkkop*	32° 42'S	24° 21'E	51	-	3
15	Carolusberg Wuns (2.0265)	30° 40'S	17° 59'E	39	-	4
16	Bishopswood	27° 42'S	22° 51'E	48	-	4
17	Dingle	27° 51'S	22° 57'E	52	-	4
18	Petrusville	30° 05'S	24° 30'E	69	-	4
19	Weltevrede	30° 43'S	26° 47'E	49	-	4
20	Oakham	30° 10'S	29° 16'E	54	-	4
21	Brandfort	28° 39'S	26° 32'E	58	-	4
22	Hopewell	28° 41'S	29° 33'E	69	-	4
23	Somkele	28° 21'S	32° 06'E	68	-	4
24	Leeuwpoort	26° 25'S	27° 30'E	46	-	4
25	Rustenburg	25° 38'S	27° 16'E	46	-	4
26	New Consort Mine	26° 41'S	28° 05'E	49	-	4

Table 8.1 (contd.)

No.	Borehole Name	Latitude	Longitude	q_o (mWm^{-2})	A_o (μWm^{-3})	Source
27	Umkoanesstad	24° 19'S	29° 54'E	47	-	4
28	Wiegel Shaft	23° 54'S	30° 41'E	55	-	4
29	Nababeep Flat Mine FM 143	29° 32'S	17° 42'E	61	8,0	4;5
30	Hoogkraal East HKE 26	29° 32'S	17° 54'E	76	12,3	5
31	Homeep East HE 177	29° 32'S	18° 01'E	65	6,9	5
32	Carolusberg West CCX-042S	29° 38'S	17° 58'E	60	3,6	5
33	Aggenys AG 140	29° 13'S	18° 45'E	55	2,8	5
34	Puts-berg POG 32	29° 21'S	19° 38'E	74	2,8	5
35	Adjoining Geelvloer G-42	29° 20'S	20° 07'E	60	1,0	5
36	Rozynen Bosch RB 56	29° 04'S	20° 47'E	81	3,8	5
37	Areachap AP 11	28° 17'S	21° 03'E	52	3,0	5
38	Boks Puts KC 12	29° 01'S	21° 39'E	39	1,1	5
39	Jacomyns Pan PC2-27	29° 20'S	21° 47'E	60	2,2	5
40	Vogelstruis Bult V41	29° 57'S	22° 18'E	48	0,8	5
41	Haib HB 77†	28° 42'S	17° 53'E	64	2,1	5
42	Rhenosterhoek DRH 18	26° 50'S	26° 27'E	34	1,9	5
43	Rhenosterberghoek DRB 6	26° 50'S	26° 28'E	31	2,1	5
44	Rietkuil DRL 17	26° 49'S	26° 30'E	33	1,3	5
45	Schoemansfontein BSF 1	26° 45'S	26° 32'E	36	3,4	5
46	Brakspruit BBS 1	26° 42'S	26° 34'E	33	2,5	5
47	Mahemsvlei BMV 4	26° 36'S	26° 37'E	33	1,5	5
48	Tweelingfontein BTF 1	26° 27'S	26° 52'E	33	3,0	5

¤ climatically uncorrected heat flows

† HB 77 is located just within the borders of Namibia

References: 1 = Bullard (1939), 2 = Carte (1954), 3 = Gough (1963)
4 = Carte and van Rooyen (1969), 5 = This work.

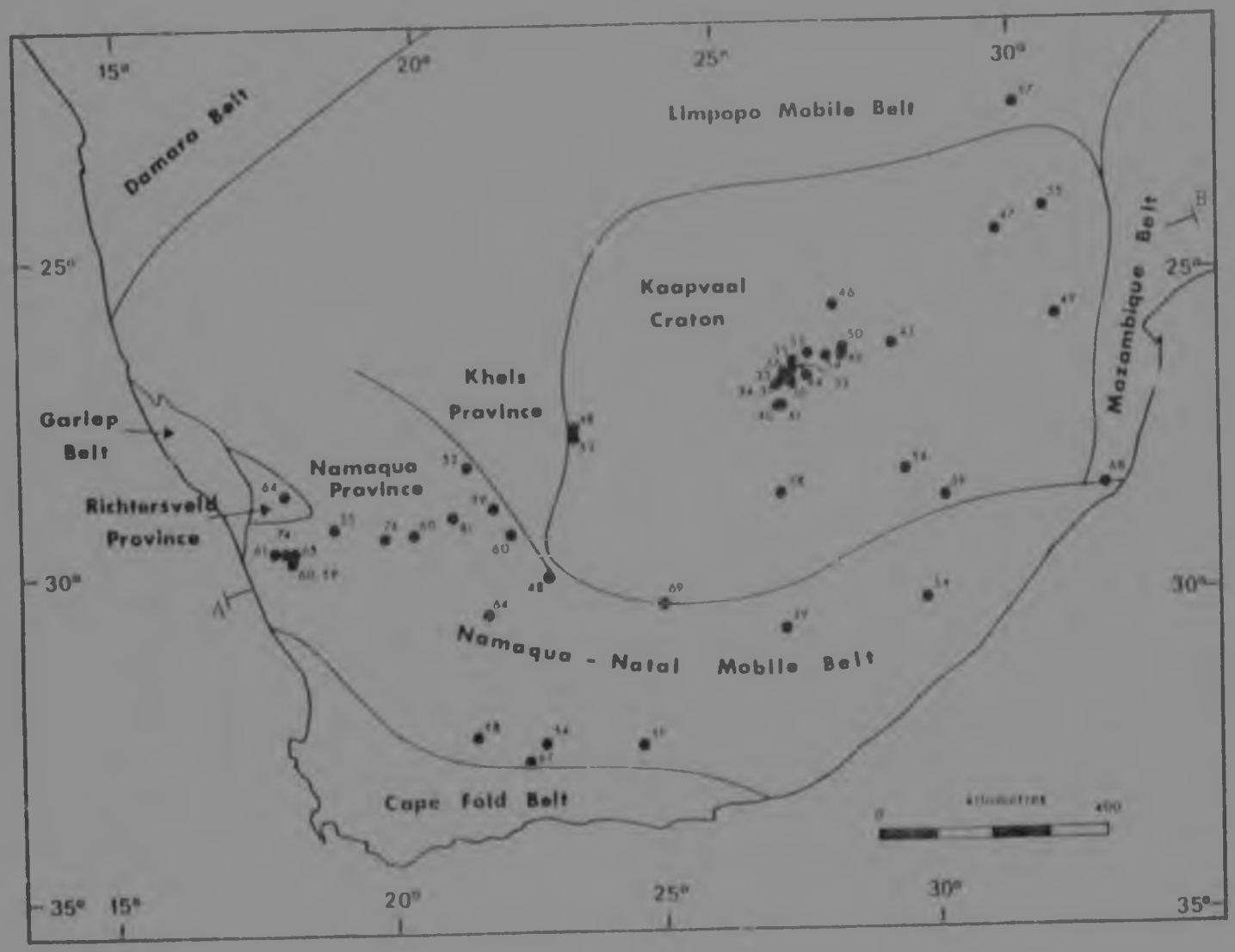

FIGURE 8.1 Heat flow stations in South Africa giving heat flow in mWm^{-2}. Tectonic boundaries are those discussed in Chapter 2. A-B is the line of the heat flow profile in Figure 8.2.

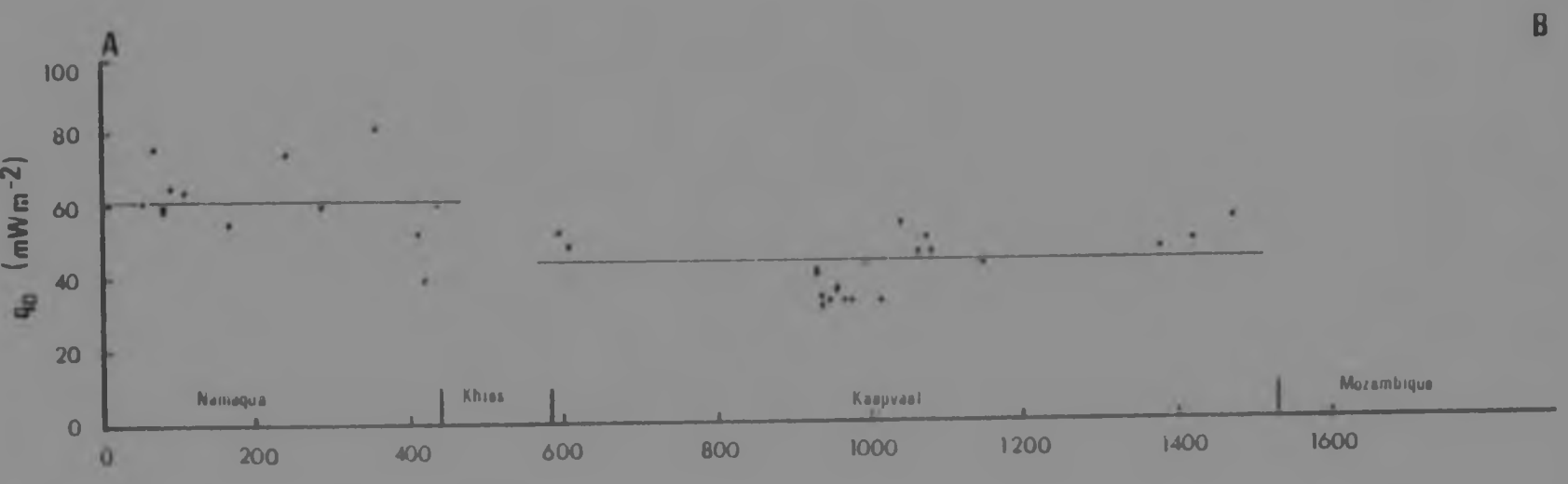

FIGURE 8.2 East-west heat flow profile across South Africa (A-B in Figure 8.1). Dots are individual values, solid lines represent means for the Namaqua Mobile Belt and Kaapvaal Craton. The approximate positions of tectonic boundaries are indicated.

The average for the craton as a whole is 44 ± 10 mWm^{-2}.

In a compilation of continental heat flow data Polyak and Smirnov (1968) showed that the mean heat flow decreases with tectonic age to roughly constant values of 35-40 mWm^{-2} in Precambrian terranes. In more recent reviews Sclater *et al* (1980) and Vitorello and Pollack (1980) use slightly higher values for the Precambrian heat flow (40-50 mWm^{-2}). This discrepancy is partly due to Pleistocene climatic corrections that are regularly applied to recent heat flow measurements. The heat flow through the Kaapvaal Craton is close to the equilibrium value of Polyak and Smirnov.

Although there are no heat flow values within the Kheis Province four stations from the Namaqua Mobile Belt are close to the Kheis-Namaqua boundary (Figures 2.3 and 8.1). Their average heat flow, 50 ± 9 mWm^{-2}, is considerably lower than the mean for the remaining ten boreholes within the Namaqua Mobile Belt, 66 ± 9 mWm^{-2} (see Table 8.2) and this may reflect a transition between different thermal regimes. Two values in particular, 48 mWm^{-2} for borehole V 41 and 39 mWm^{-2} for borehole KC 12, are suggestively close to values obtained within the Kaapvaal Craton. It will be shown below that the differences in heat flow can be equally well ascribed to variations in upper crustal radioactivity and there is no reason to separate these data. The overall mean for the Namaqua Mobile Belt is 61 ± 11 mWm^{-2} (14 values); this is 20-25 mWm^{-2} higher than the average of Polyak and Smirnov (1968). The implications of this will be discussed in Section 8.4.

The single value from the Richtersveld Province, 64 mWm^{-2}, is not very different from the Namaqua mean. It is possible that the Richtersveld

Table 8.1 Average heat flows and heat productions

Region	$\bar{q}_o \pm \sigma_q$ (mWm^{-2})	(n)	$\bar{A}_o \pm \sigma_A$ (μWm^{-3})	(n)
Richtersveld Province	64	(1)	2,1	(1)
Interior Namaqua Province	66 ± 9	(10)	*2,8 ± 1,1	(5)
Namaqua/Kheis margin	50 ± 9	(4)	1,8 ± 1,0	(4)
Namaqua Province overall	61 ± 11	(14)	*2,3 ± 1,2	(9)
Central Kaapvaal craton	36 ± 5	(16)	2,3	

σ = standard deviation; n = number of values

* : three highly radioactive values from Springbok district were excluded in calculation

Province, like the Namaqua Province, is characterized by above average heat flow but more measurements are necessary to substantiate this.

Four heat flow stations are close to the northern margin of the Cape Fold Belt (Figure 8.1; Gough, 1963). Their average (climatically uncorrected) heat flow is 56 ± 5 mWm^{-2}, not much less than the mean for the Namaqua Mobile Belt. It would appear that thermal events associated with late-Permian Cape folding were not sufficiently severe to increase the heat flow in this region above that characteristic of the mobile belt. On the other hand, the average is close to the value of 52 mWm^{-2} given by Polynk and Smirnov (1968) for regions affected by Hercynian orogenic events. The question of whether Cape folding was accompanied by significant thermal resetting or whether it was a relatively 'cold' event can only be answered when more data are available from this area.

There are no heat flow data in the Pan-African orogenic belts and only one from the Limpopo Mobile Belt and these regions will not be discussed further.

The new heat flow data have served some important purposes. Seven measurements from the centre of the craton confirm the low heat flow there; in fact, these data are all lower than the lowest previously reported value. Twelve measurements in the Namaqua Mobile Belt cover a large area between Springbok and the boundary with the Kheis Province where there were no previous values. These data confirm the generally high heat flow in the mobile belt and provide a background for future investigations of heat flow transitions across the Namaqua-Kheis and Kheis-Kaapvaal boundaries. The measurement from the Richtersveld Province raises the possibility that this area is characterized by similar thermal parameters to the Namaqua Mobile Belt in spite of their different tectonic character.

It was shown previously that in many 'heat flow provinces' there is a simple linear relationship between surface heat flow (q_o) and near-surface heat production (A_o):

$$q_o = q_r + bA_o \qquad (8.1)$$

where the constants are interpreted as the heat flux from the lower crust, or 'reduced' heat flow (q_r), and a depth parameter characterizing the vertical distribution of radioactive sources in the crust (b). In most Precambrian terranes q_r ranges between 20 and 30 mWm^{-2} and most of the variation of heat flow can be attributed to the upper crustal component, bA_o. One of the main objectives of this research was to investigate whether local and regional variations of heat flow

in South Africa are related to variations in the radioactive heat production of basement rocks.

8.2 Heat flow and heat production in the Namaqua Mobile Belt

8.2.1 The mobile belt as a whole

The q_o-A_o pairs for all twelve sites in the Namaqua Mobile Belt are plotted in Figure 8.3. The scatter in the data is disappointing and it is not possible to define a heat flow province. This is not altogether surprising and the scatter may be attributed to a number of factors. Local differences in the degree of metamorphism and deformation, a lack of knowledge about the 'basement-cover' relationship and possible recent loss of near-surface U all lead to uncertainties in the meaning of heat production values at each site.

The three highly radiogenic points (29-31, Figure 8.3) come from the same granitic intrusion in the Springbok district. This extreme enrichment in radiogenic heat producing elements is a local phenomenon which has not been observed in the rest of the Namaqua Mobile Belt and there is reason to believe that the heat productions at these sites are only representative of the upper kilometre or so of crust. These data will be discussed in further detail in the next subsection. A least squares straight line fit to the rest of the data in Figure 8.3 yields:

$$q_o(mWm^{-2}) = (42 \pm 9) + (7{,}2 \pm 3{,}3)A_o(\mu Wm^{-3})$$

with a correlation co-efficient of 0,66.

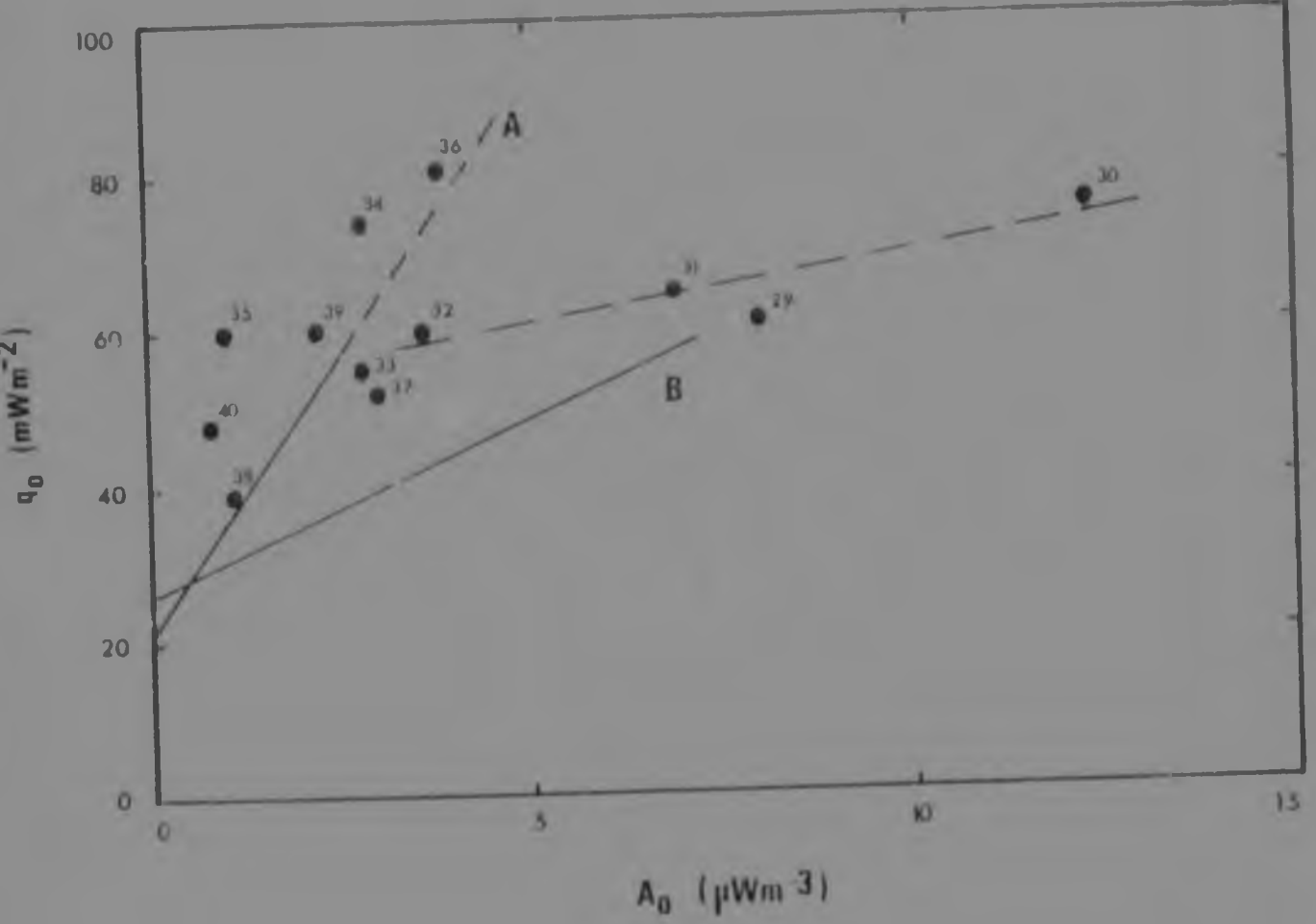

FIGURE 8.3 Heat flow-heat production data for the Namaqua Mobile Belt. Numbers are for cross-reference with Table 8.1. Lines A and B are q_0-A_0 relationships for the Superior Province (Jessop and Lewis, 1978) and the western Australian Shield (Sass and Lachenbruch, 1979). Dashed line is the least squares fit to points from the Springbok district.

(1) [illegible] exceptional [illegible] and 3c the heat production data were obtained from paragneisses and regionally metamorphosed sedimentary and volcanic rocks and much of the scatter may be due to incomplete homogenization of radiogenic heat producing elements during the Namaqua tectogenesis. It may be possible to obtain better statistics by eliminating other points from the regression analysis but there is no obvious justification for doing this and it is preferable to accept the data at face value rather than force a fit. It should be stressed that [illegible] data from the Namaqua Mobile Belt do not define a heat flow province

It was shown in Section 8.1 that the four stations near the Kheis-Namaqua boundary yield a lower mean heat flow than the remaining stations in the Namaqua Province. The average heat flows and heat productions for these subsets of the data are compared in Table 8.2 and Figure 8.5 (points I and II) and show that the low heat flow is correlated with low heat production. It is noteworthy that the two stations near the Kheis-Namaqua boundary with the lowest heat flows also have the lowest heat productions (stations 38 and 40, Figure 8.3). A difference in heat production, integrated to depths of several kilometres, is the most likely explanation for the difference in heat flow.

Heat flow and heat production in the Springbok district

Data [illegible] 9-12 in Figure 8.1 were derived from boreholes located in the Springbok-O'okiep-Nababeep mining district. There appears to be a [illegible] correlation between the surface heat flow and heat production and a least squares straight line fit to these data gives:

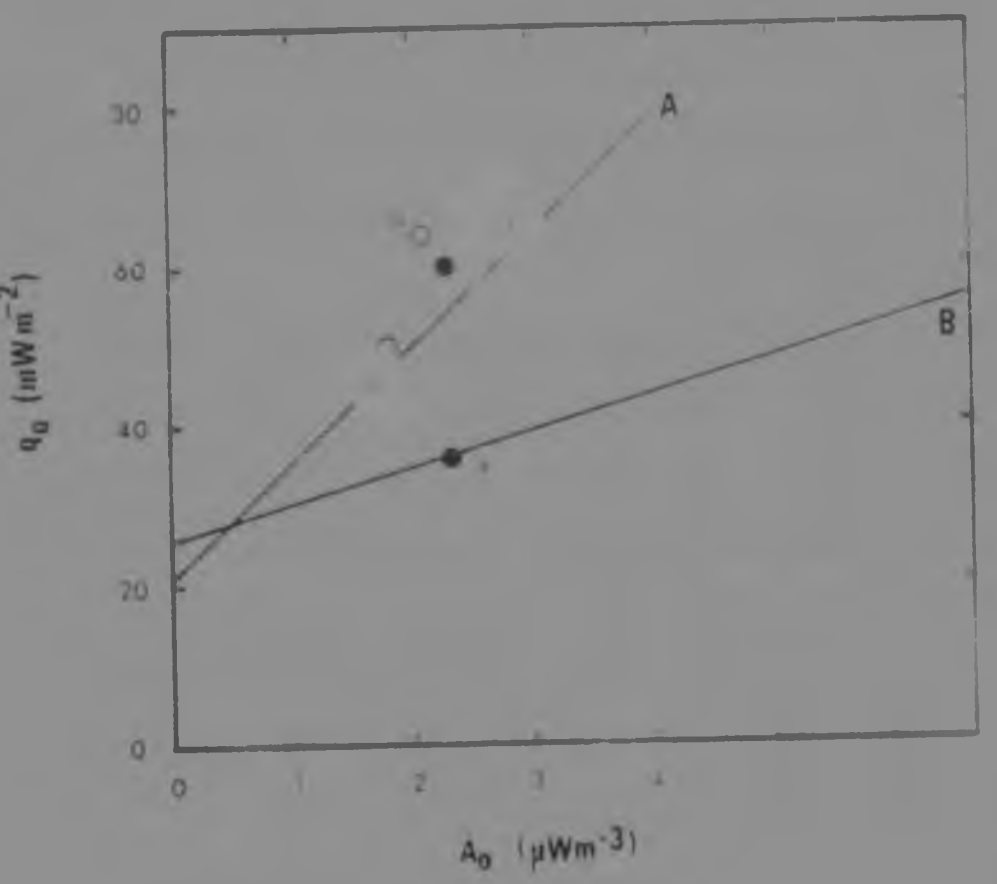

FIGURE 8.4 Mean heat flow and mean heat production for

I stations near the Kheis-Namaqua boundary
II remaining stations within the Namaqua Mobile Belt
III the Richtersveld Province
IV the Namaqua Mobile Belt as a whole
V the Kaapvaal Craton

Lines A and B are as in Figure 8.3.

$$q_o(mWm^{-2}) = (32 \pm 6) + (1,8 \pm 0,7)A_o(\mu Wm^{-3})$$

with a correlation co-efficient of 0,89 (dashed line, Figure 8.3).

The implications of this correlation are best appreciated by referring to Section 2.6 and particularly to Figures 2.4 and 2.5. The borehole with the lowest ('normal') heat production (CCX-042S) is entirely within the Nababeep gneiss, a member of the pre existing suite of rocks which was metamorphosed and isoclinally folded during the Namaqua tectogenesis. This station also has the lowest heat flow.

Points 29-31 are characterized by abnormally high heat productions and they are derived from boreholes situated within the outcrop of the Concordia granite gneiss (FM 143, HKE 26 and HE 177). Although HKE 26 and HE 177 probably penetrate the underlying 'mixed zone' (Nababeep gneiss with injections of Concordia gneiss) the anomalous concentrations of radiogenic heat producing elements are apparently associated with the Concordia gneiss. This body is a sheet-like intrusion which was emplaced during the main period of isoclinal folding and it is of the order of 1-2 km thick (Benedict et al, 1964; Clifford et al, 1975). McCarthy (1976) argued on geochemical grounds that the granite was derived from partial melting of lower crustal source rocks of intermediate composition and evolved by feldspar fractionation during crystallization and ascent. Enrichment of granitophile elements during such a process may account for the extreme concentrations of U, Th and K.

If gneissic bodies like this are derived in a pseudo one-dimensional fashion from the lower crust the overall crustal radiogenic contribution

is not altered and nor is the surface heat flow. Hence, the average heat flow for the Springbok district (66 ± 8 mWm^{-2}) is not significantly different from that of the Namaqua Mobile Belt as a whole. However, even small amounts of differential erosion of highly radiogenic bodies may produce detectable variations of the surface heat flow. This is the most likely interpretation of the rough q_o-A_o 'correlation' in this region and the similarity in magnitude of the depth parameter and the thickness of the enriched layer. In this interpretation the 'background' heat flow for the region is obtained at zero thickness of the enriched layer and is represented by measurements in the Nababeep gneiss.

These observations are not unique and similar relationships have been found in the Ukrainian Shield (Kutas, 1977) and the western Australian Shield (Jeager, 1970). Unfortunately, little use has been made of these relationships. Heat production measurements from thin, enriched layers may contribute significantly to estimates of the mean surface value in gneissic terranes such as the Namaqua Mobile Belt and therefore lead to overestimates of the bulk crustal radiogenic component of the surface heat flow. A detailed study of the extent and relative importance of bodies such as the Concordia granite gneiss is clearly called for.

8.3 The Namaqualand heat flow 'anomaly'

There are sufficient data in the Namaqua Mobile Belt to estimate the mean surface heat flow with considerable confidence. This value (61 mWm^{-2}) is considerably higher than the means for most Precambrian terranes. The increase of 20-25 mWm^{-2} above the average of Polyak and Smirnov (1968) represents a significant anomaly. The effects of uplift and erosion (England and Richardson, 1980) are clearly not an important

consideration in the Namaqua Mobile Belt, and the additional heat must be due to a greater radiogenic contribution from the crust or an enhanced mantle heat flux.

Because of the poor correlation between heat flow and heat production (Figure 8.3) it is not possible to estimate the relative importance of these components directly. The high average heat production from the nine 'representative' stations in the mobile belt (2,3 μWm^{-3}) suggests that some of the anomaly may be due to crustal sources. A more meaningful parameter is the depth integrated average heat generation, or the average upper crustal contribution, $b\bar{A}_o$. In most regions where linear q_o-A_o relationships have been defined the average heat flow ($\bar{q}_o$) is better known than the average heat production ($\bar{A}_o$) and the most reliable estimate for the value $b\bar{A}_o$ may be obtained from equation 8.1:

$$b\bar{A}_o = \bar{q}_o - q_r$$

alues for $\bar{q}_o$, q_r, b and $\bar{q}_o$-q_r from selected Precambrian heat flow provinces are listed in Table 8.3. In the remaining reported Precambrian provinces the depth parameter has been assumed or only two points have been utilized in defining the q_o-A_o relationship. Table 8.3 shows that:

(1) with the exception of the Indian Shield, all values of q_r fall between 20 and 30 mWm^{-2}; most of the variation appears to be in the upper crustal contribution,

(2) with the exception of the western Australian Shield, all the b values lie between 7 and 15 km and the average value is 11,5 ± 3,2 km.

Table 8.1 Thermal parameters for selected Precambrian heat flow provinces and models of the Namaqua and Kaapvaal crust

Province	n	$\bar{q}_o$ (mWm^{-2})	q_r (mWm^{-2})	b (km)	$\bar{q}_o - q_r$ (mWm^{-2})	References
Superior*	11	40	21	14,4	19	Jessop & Lewis (1978)
Baltic Shield	3	37	22	8,3	15	Sweobers et al (1974)
Ukrainian Shield	12	37	25	7,1	12	Rutas (1977)
Brazilian Coastal Shield	4	36	28	13,3	25	Vitorello & Pollack (1980)
Indian Shield (Proterozoic)	6	71	38	4,8	33	Rao et al (1976)
Western Australian Shield	9	49	36	4,3	13	Sass & Lachenbruch (1979)
Central Australian Shield	10	63	27	11,1	36	Sass & Lachenbruch (1979)
SOUTH AFRICAN MODELS						
Namaqua I	-	61	35	(11,5)	26	-
Namaqua II	-	61	28	(14,4)	33	-
Kaapvaal I	-	36	15	(9,3)	21	-
Kaapvaal II	-	36	26	(4,5)	10	-

n is number of points defining the q_o-A_o relationship

* values for climatically uncorrected heat flows

As a first step towards estimating the crustal and mantle contributions to the heat flow in the Namaqua Mobile Belt, a value of 11,5 km has been taken to represent parameter b. Corresponding values for the reduced heat flow and upper crustal contribution were calculated by substituting $b = 11,5$ km, $A_o = \bar{A}_o = 2,3\ \mu Wm^{-3}$ and $q_o = \bar{q}_o = 61\ mWm^{-2}$ in equation 8.1:

$$q_r \sim 35\ mWm^{-2}$$
$$b\bar{A}_o \sim 26\ mWm^{-2}$$

These values are included in Table 8.3 (model Namaqua I) for comparison with the data from established heat flow provinces. The reduced heat flow is similar to that predicted by the q_r-$\bar{q}_o$ relationship (Pollack and Chapman, 1977a):

$$q_r = 0,6\bar{q}_o \sim 37\ mWm^{-2} \qquad (8.2)$$

The above values for q_r are slightly higher than the norm for Precambrian shields (cf. Table 8.3) and this could be taken to imply that the Namaqua Mobile Belt has an above average mantle heat flow. However, there is considerable uncertainty involved in both these estimates and such a deduction should be treated with caution. The linear q_o-A_o relationship that has been observed in the Superior Province* (Jessop and Lewis, 1978) is shown in Figures 8.3 and 8.4; the Namaqua data scatter on either side of this line (Figure 8.3) and the mean q_o-A_o pairs plot close to it (Figure 8.4, points I, II and IV). If the b value for the Superior Province (14 4 km) is applied to the Namaqua data equation 8.1 yields:

---

* The values used here are for climatically uncorrected heat flows.

q_r ~ 20 mWm^{-2}

bA_o ~ 34 mWm^{-2}

These values are within the ranges observed in most Precambrian provinces (see Table 8.3; Namaqua II model).

The only heat flow measurements in southern Africa which have been made in regions roughly equivalent in age to the Namaqua Mobile Belt are from rocks of Kibaran to Katangan age (1300-500 m.y.) in Zambia (Chapman and Pollack, 1977). The average heat flow for eleven sites (66 mWm^{-2}) also constitutes an anomaly. The six sites for which there are both heat flow and heat production data yield means of 64 mWm^{-2} and 2,4 μWm^{-3} respectively; the data do not define a linear q_o-A_o trend. Chapman and Pollack attributed less than half of the Zambian heat flow anomaly to enhanced crustal radioactivity and inferred that lithospheric thinning (possibly associated with a southwesterly extension of the East African Rift System) accounts for the residual anomaly. They were able to support this contention with other geophysical information, notably seismic data, which suggests that this region is one of incipient rifting.

The Namaqua Mobile Belt is an aseismic zone and there is no independent geophysical evidence for high mantle heat flow, lithospheric thinning or incipient rifting. The most likely explanation for the heat flow anomaly is therefore enhanced crustal radioactivity which, according to the Namaqua II model (Table 8.3), may contribute 50-60% to the surface heat flow.

8.4 Heat flow and heat production in the Richtersveld Province

There is only one heat flow-heat production pair in the Richtersveld Province. The heat flow (64 mWm^{-2}) is comparable with data from the Namaqua Province and considerably higher than the mean for equivalent age provinces elsewhere. The heat production (2,1 μWm^{-3}) is close to the Namaqua mean. This pair is plotted in Figure 8.4 (point III); it is offset to higher heat flow-lower heat production compared with averaged data from the Namaqua Mobile Belt and with the line for the Superior Province. As in the Namaqua Mobile Belt, there is no indication of present tectonic instability and the high heat flow is probably due to enhanced crustal radioactivity. Further measurements are required to determine the thermal characteristics of this crustal domain.

8.5 Heat flow and heat production in the Kaapvaal Craton

Heat flow and heat production data for the seven new stations near Klerksdorp are plotted in Figure 8.5. The small range in surface heat flow precludes a q_s-A_0 correlation and the upper crustal radiogenic contribution to the surface heat flow and the deep component must be inferred by other methods or from other sources of information. At this stage it is worth emphasising some features of these results. Although the range in surface heat flow is small, there is considerable variation in the heat production. The most likely explanation for this is insufficient sampling of inhomogeneous upper crust and the average heat production has more statistical meaning. The mean heat flow (33 ± 2 mWm^{-2}) and heat production ($2,2 \pm 0,8$ μWm^{-3}) for these stations and most of the individual results fall below the line for the western

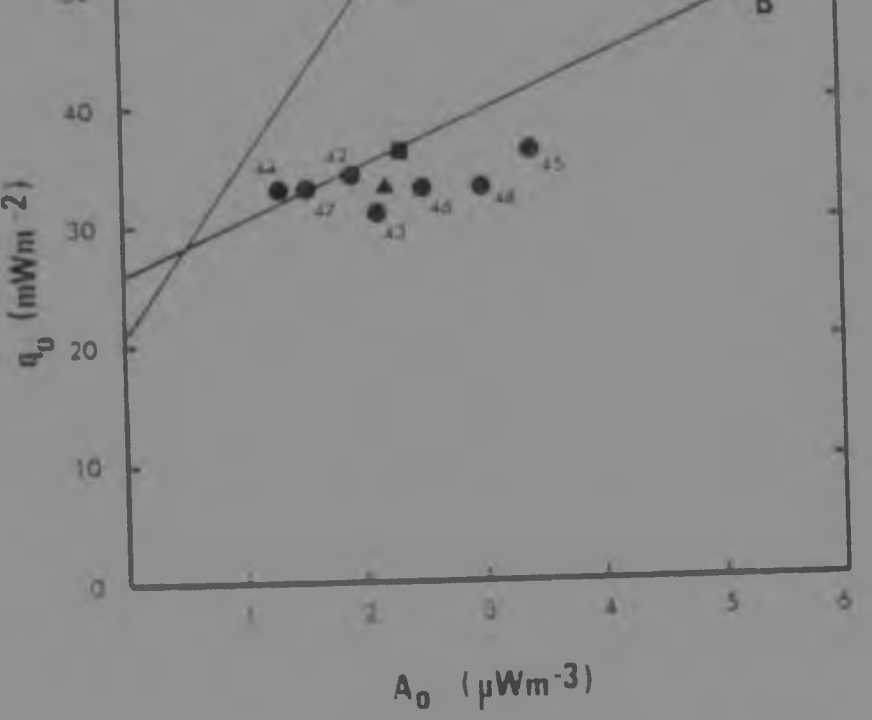

FIGURE 8.5 Heat flow-heat production data for the Klerksdorp district. Dots are individual values (numbers refer to Table 8.1), the triangle is the mean for these stations and the square is the mean for the centre of the craton. Lines A and B are as in Figure 8.3.

Australian Shield. For heat productions greater than about 1.2 μWm^{-3}, linear q_s-A_o relationships observed in other shield areas all plot above this line and this suggests that in the Kaapvaal Craton the radiogenic heat producing elements are concentrated in an unusually thin enriched layer* or that the reduced heat flow is anomalously low.

Although there are no other q_s-A_o pairs within the craton, Hart et al (1981b) and Nicolaysen et al (1981) have made detailed studies of the distribution of radiogenic heat sources in basement rocks exposed in the Vredefort dome structure which is located some 50 km southeast of the central cluster of heat flow stations. The central part of the craton is therefore well represented in terms of the amount of heat flow and heat production data. There are very few heat production data from elsewhere in the craton. Partly for these reasons, and partly because the increase of heat flow towards the margins of the craton (see Figure 8.1) probably reflects a transition between different thermal regimes, only the data from the central portion will be considered here.

The average heat flow for the central sixteen sites, 40 ± 7 mWm^{-2}, is almost identical to the average of 38 ± 6 mWm^{-2} given by Polyak and Smirnov (1968) for continental shields. Eight of the nine previously reported measurements were made in localities which are underlain by several kilometres of Proterozoic platform strata belonging to the Dominion Reef, Witwatersrand, Ventersdorp and Transvaal Supergroups. Nicolaysen et al (1981) showed that these rocks contain relatively high concentrations of radiogenic heat producing elements and that their contribution to the surface heat flow is substantial. In order to compare the heat flow with the heat production of the basement rocks it

* If this effect is related to extensive Kaapvaal erosion then the presence of 2500-2400 m.y. old relatively undisturbed layered strata shows that such erosion must have occurred before ~2500 m.y. ago.

is necessary to remove this contribution. The first six entries in Table 6.4 show the measured heat flow, the estimates of Nicolaysen et al for the thickness of the stratified rocks and their overall contribution to the surface heat flow, and the corrected heat flow at six of these stations. The average correction for these stations (7 mWm^{-2}) was applied to the other two stations that are underlain by considerable thicknesses of platform strata (Roof Ridge and Leeuwpoort, Table 6.4). The heat flow at Boshoffberg (station number 15, Table 6.1) is unaffected as this measurement was made in crystalline rocks of the Bushveld Igneous Complex. The seven new Klerksdorp boreholes pass through a relatively thin layer of Dominion Reef lava and a basal conglomerate before penetrating basement gneiss. As the lavas have a very low heat production (approximately 0,18 μWm^{-3}, see Table 5.8), and are of the order of 1 km thick, their radiogenic contribution is negligible (<0,2 mWm^{-2}) and the measured values are good estimates of the heat flow from the local basement. The average of the corrected heat flows for these eleven stations is 49 ± 5 mWm^{-2}.

As the heat production data presented in Figure 6.3 come from a small area near Klerksdorp, their high average value may reflect a local enrichment in the upper kilometre or so of granitic basement. A more representative estimate for the near surface heat production of the Kaapvaal crust may be obtained by including data from elsewhere on the craton. The only area that has been studied in detail is the Vredefort dome where Proterozoic strata form an overturned collar which encloses a core of basement gneiss. There is considerable evidence that the gneissic core is itself overturned and radial traverses are interpreted to represent a 15 km thick section of Archaean granitic crust 'turned on edge' (eg. Hart et al, 1981b; Nicolaysen et al, 1981). In this

Table 8.4 Corrections to the surface heat flow for the radiogenic contribution of Proterozoic platform strata on the Kaapvaal Craton

	Surface heat flow (mWm^{-2})	Sedimentary thickness of strata (km)	*Radiogenic contribution (mWm^{-2})	Corrected heat flow (mWm^{-2})
Vacoba		0,8		33
Doornhoek		0,4		34
Verhardminne		7,3	8	46
Doornk		6,5	7	43
		0,9	7	37
		6,5	7	29
			(7)†	36
			(7)†	39

† Jaeger, Hasselsen et al (198

* Value assumed equal to average for other six sites

The concentration of radiogenic heat producing elements in the outermost portion of the Vredefort basement is representative of the uppermost crust. The heat production calculated form averaged thorium and uranium concentrations for all data from the outermost 3 km is 2,1 μWm^{-3} (Table 8.3), only fractionally higher than the mean for the Werksdorp area, 1,9 μWm^{-3}. These results indicate that the heat production in the upper crust in the central part of the craton is quite uniform, with an average value of 2,1 μWm^{-3} (in significant figures). The surface heat production. Further confidence

Table 8.3 Mean near-surface heat production in the Kaapvaal Craton

Area	U(p.p.m.)	Th(p.p.m.)	K(%)	A_0 (μWm^{-3})
Klerksdorp (new q_0-A_0 sites)	4.1	14.1	3.1	5.1
*Vredefort (upper 3 km)	3.1	17.5	3.1	4.8
*Eastern Transvaal and Swaziland	3.1	13.1	2.1	4.1

* Data from Nicolaysen et al (1981). A_0 calculated using a density of 2.65×10^3 kgm^{-3}.

for this value is derived from data reported by Nicolaysen et al (1981) for the eastern Transvaal and Swaziland where U, Th and K contents in Archaean basement rocks yield a mean heat production of 4.1 μWm^{-3} (Table 8.3).

Data from the Vredefort dome also provide a means of estimating the upper crustal radiogenic contribution to the surface heat flow and deep component. Hart et al (1981b) showed that the average heat production of the basement rocks decreases towards the centre of the structure to a distance of approximately 3 km. The 'crust + dome' model (Fig. 8.4) represents a decrease of heat production with increasing depth. Although it was not possible to distinguish the nature of this decrease clearly, an exponential distribution provided a better fit to the data than a linear function. The characteristic depth of the best fit exponential curve was 5.3 km. Using this value (eq.) in combination with the surface heat flow (46 mWm^{-2}) and heat production (A_0 = 4.8 μWm^{-3}, Table

yields:

$$bA_o = \bar{q}_o - q_r = 21 \text{ mWm}^{-2}$$

$$q_r = 19 \text{ mWm}^{-2}$$

Although this estimate for bA_o is well within the observed range a value of 19 mWm^{-2} for q_r is considerably lower than well established values elsewhere (see Table 8.5). However, it is not an unreasonable value because 9,1 km is close to the centre of the observed range of depth parameters.

The point defined by a heat flow of 40 mWm^{-2} and a heat production of 2,3 μWm^{-3} is plotted in Figures 8.4 and 8.5; it falls very close to the line for the western Australian Shield. The average surface heat flow is low compared with most shields characterized by such high heat productions. A second estimate for the upper crustal radiogenic contribution and the deep component may therefore be obtained by assuming that the Kaapvaal Craton is characterized by a similar distribution of radioactive sources to the western Australian Shield. Using a value of 4,5 km for parameter b, equation 8.3 yields:

$$bA_o = \bar{q}_o - q_r = 10 \text{ mWm}^{-2}$$

$$q_r = 25 \text{ mWm}^{-2}$$

Because 4,5 km is the lowest reliable value for b that has been observed in Precambrian terranes, these estimates for q_r and bA_o may be regarded as a maximum and a minimum respectively.

The above estimates for bA_o and q_r are included in Table 8.5 where they are denoted as models KI and KII respectively. They bracket the

values predicted by the $q_s - \bar{q}_o$ relationship which yields:

$$q_r = 2.6\bar{q}_o = 22 \text{ mWm}^{-2}$$

$$bA_o = 0.4\bar{q}_o = 14 \text{ mWm}^{-2}$$

This adds credence to their applicability and in the remainder of this chapter they will be regarded as the probable ranges within which the true values lie.

Using these limits it is possible to estimate the likely range of mantle heat flux below the Kaapvaal Craton. A procedure used by Pollack and Chapman (1977b) will be adopted for this purpose. The heat production in the lower crust is assumed to be constant with depth and denoted by A_1 while the heat production in the upper enriched layer is assumed to decrease exponentially with depth according to:

$$A(z) = A_o \exp(-z/b) \qquad (8.3)$$

to a depth defined by

$$z_1 = b\ln(A_o/A_1) \qquad (8.4)$$

This is distinct from the depth at which the heat flow is equal to q_r

$$z_r = b[1 + \ln(A_o/A_1)] \qquad (8.5)$$

If the thickness of the continental crust is z_c the heat flux through the top of the mantle is

$$q_m = q_r - A_1 z_c + A_1 b[1 + \ln(A_o/A_1)] \qquad (8.6)$$

The following parameters were used to calculate q_m for models KI and KII:

$q_o = \bar{q}_o = 36$ mWm^{-2}

$A_o = \bar{A}_o = 2,3$ μWm^{-3}

$A_1 = 0,2$ μWm^{-3}

$b = 9,3$ km (model KI)

$= 4,5$ km (model KII)

$z_m = 35$ km

Estimates for the heat production of the lower crust generally fall within the range 0,1 - 0,5 μWm^{-3} (cf. Heier and Adams, 1965; Smithson and Decker, 1974; Pollack and Chapman, 1977b; Nicolaysen et al, 1981) and a slightly conservative estimate is used in the model calculations. The average crustal thickness is based on seismic refraction measurements made in the Transvaal by Gane et al (1956) and is compatible with most estimates for stable continental regions.

The distribution of radioactive sources for each model and the variables defined in equations 8.4 to 8.6 are shown in Figure 8.6. The mantle heat flux is 14 and 22 mWm^{-2} for models KI and KII respectively. No attempt has been made to assign errors to these values. The overall uncertainties will be determined by systematic errors in $\bar{q}_o$ and $\bar{A}_o$ and uncertainties in the assumed values of A_1 and z_m, but the overriding uncertainty is in the distribution of heat sources in the upper crust. Until this is known more accurately there is little point in attempting to evaluate other sources of error. These estimates are in relatively good agreement with those made by Nicolaysen et al (1981) who used a slightly different approach.

The mantle heat flows for models KI and KII may be compared with that below an 'equilibrium' ocean. Parsons and Sclater (1977) estimated the equilibrium background (sub-lithospheric) heat flow to be 33,5 mWm^{-2}

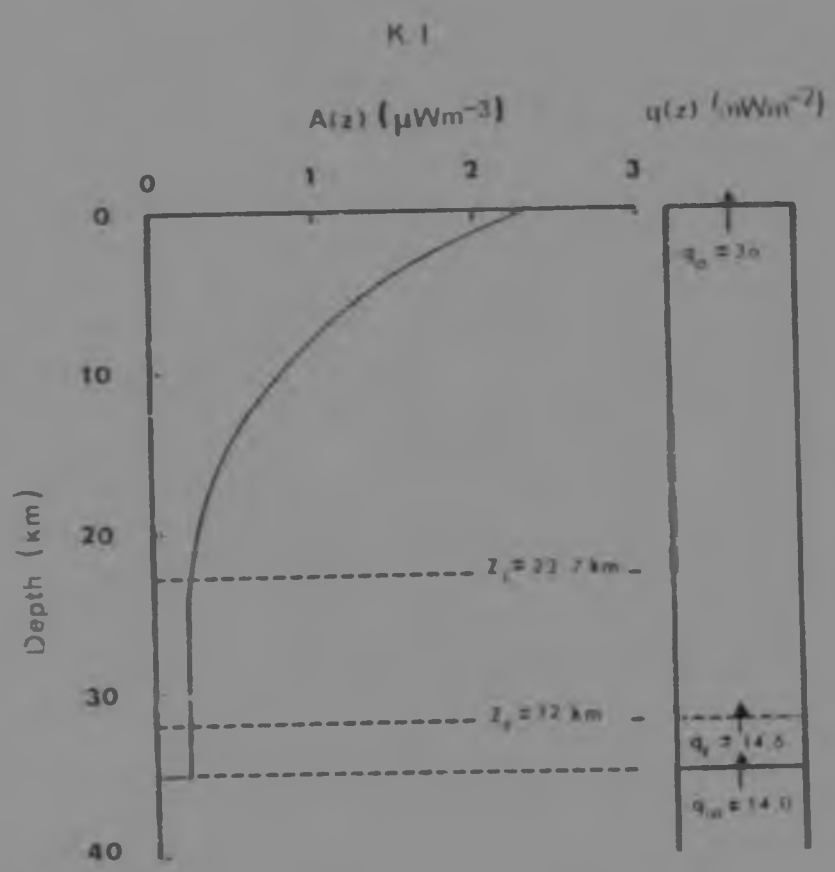

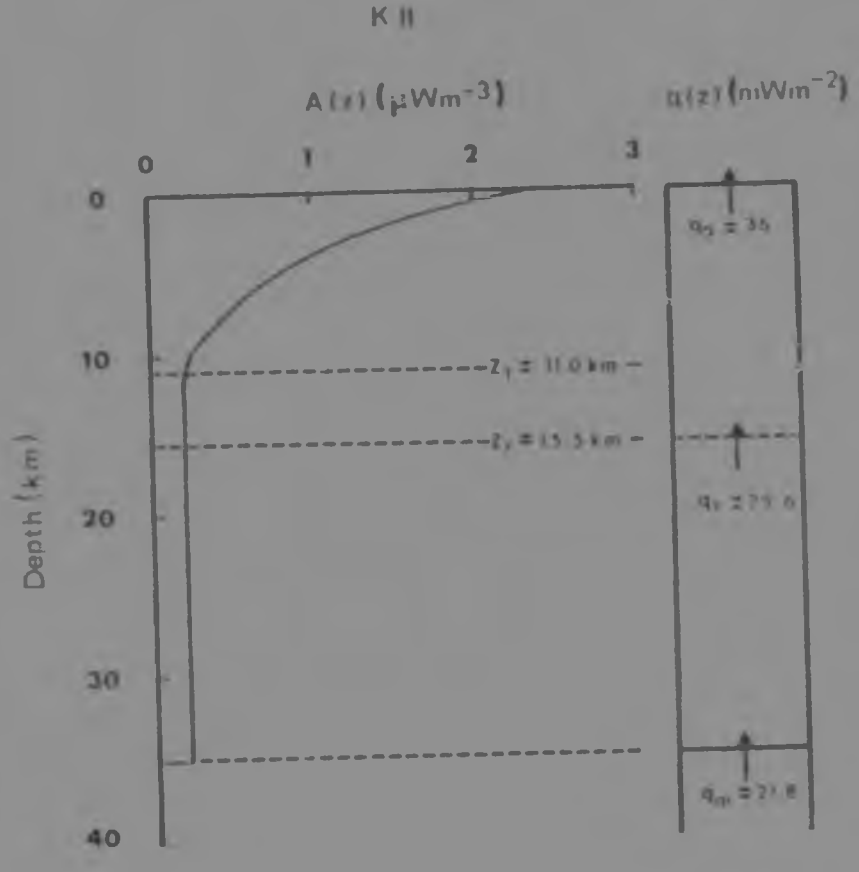

FIGURE 8.6 Models KI and KII for the distribution of radiogenic heat sources in the Kaapvaal crust. Depths z_1 and z_r and the mantle heat flow q_m were calculated from equations 8.4-8.6.

and considered the radiogenic contribution from the lithosphere to be approximately 4 mWm^{-2} and, hence, the equilibrium surface heat flow to be 37,5 mWm^{-2}. To a first approximation radiogenic heat sources are confined to the crust and the equilibrium mantle heat flow is 33,5 mWm^{-2}. This is 1,5 to 2,5 times greater than corresponding values estimat . for the Kaapvaal Craton and considerable differences in the thermal structure of the upper mantle can be expected.

Before discussing lithospheric thermal structures it is important to emphasise that certain near-surface factors could reduce the surface heat flow and lead to underestimates of the mantle heat flux below the craton.

(1) Palaeoclimatic variations. The effect of past surface temperature variations on the present surface heat flow was discussed in detail in the preceeding chapter. These events could reduce the continental heat flow by up to 25%. In the absence of detailed palaeoclimatic data for South Africa confirmed by heat flow measurements in deep boreholes, it is preferable to accept the measurements at face value rather than apply a correction whose uncertainty exceeds its own magnitude. However, the effect of surface temperature variations must be considered as a contributing factor to the low surface heat flow and should be a prime target for future investigations.

(2) Small upper crustal radiogenic component. If the radiogenic heat producing elements are strongly concentrated in the upper 1-2 km of the crust, the mantle contribution has been seriously underestimated. Such extreme differentiation is unlikely in the face of heat production data from the Vredefort profile and from the fact that the mean near-surface heat production is very similar at widespread localities. Limits for the upper crustal contribution

to the surface heat flow have been discussed in some detail and are believed to be realistic.

(3) The downward migration of meteoric water. The centre of the Kaapvaal Craton is approximately 1,5 km above sea level and if the upper section of the crust is sufficiently permeable a significant amount of heat may be transported by groundwater seeping downward through the rock. It is difficult to estimate the macroscopic permeability of the upper crust but this explanation for a low surface heat flow is unlikely because most of the boreholes were probed to depths approaching sea level and in some cases this depth was exceeded.

The alternative, a subnormal mantle heat flow, is the most likely explanation for the low surface heat flow and in the next section the equilibrium thermal structure below the craton will be compared with that below an equilibrium ocean basin.

8.6 Equilibrium thermal structure of the Kaapvaal lithosphere

Sclater and Francheteau (1970) showed that the average mantle heat flux below continental shields is approximately half its counterpart below ocean basins. Hence, they argued that if the base of the lithosphere is defined by an isotherm it is approximately twice as thick in shield areas. An equilibrium mantle heat flow may therefore be regarded as a measure of lithospheric thickness and this implies that the Kaapvaal lithosphere is 1,5 - 2,5 times as thick as the equilibrium oceanic lithosphere.

A more quantitive evaluation of the problem may be made by comparing geotherms for the Kaapvaal models with that of an equilibrium ocean. These geotherms can be calculated using the following equation:

$$T(z) = T_o + q_o\int_o^z \frac{dz}{k} - \int_o^z \frac{1}{k}\left[\int_o^z A(z)dz\right]dz \qquad (8.7)$$

In all cases the surface temperature, T_o, is taken to be zero.

The oceanic geotherm was calculated using lithospheric parameters estimated by Parsons and Sclater (1977) from observed variations in mean heat flow and depth of the ocean floor with age. They estimated the heat flow through the base of the lithosphere in the equilibrium state to be 33,5 mWm^{-2} and the surface heat flow, allowing for a radiogenic contribution of 4 mWm^{-2} from the lithosphere, to be 37,5 mWm^{-2}. Any reasonable estimate for the heat production of the upper mantle has a negligible effect on the geotherm and in the following models of the lithosphere all radiogenic heat is assumed to be derived from the crust. The oceanic crust is taken to have a thickness of 8 km, constant heat production of 0,5 μWm^{-3} and constant thermal conductivity of 2,5 $Wm^{-1}K^{-1}$. Although measurements on rock of probable upper mantle composition indicate that the thermal conductivity varies considerably with temperature to depths of a few hundred kilometres (Schatz and Simmons, 1972; Richardson and Powell, 1976) the rate of change and the absolute values are not well know. For simplicity, the same, constant value of 3,14 $Wm^{-1}K^{-1}$ assumed by Parsons and Sclater (1977) will be used. The relative positions of the geotherms and differences in lithospheric thickness calculated in this section would not be affected seriously if variable thermal properties were considered.

The oceanic geotherm (O) is shown in Figure 8.7. Parsons and Sclater (1977)

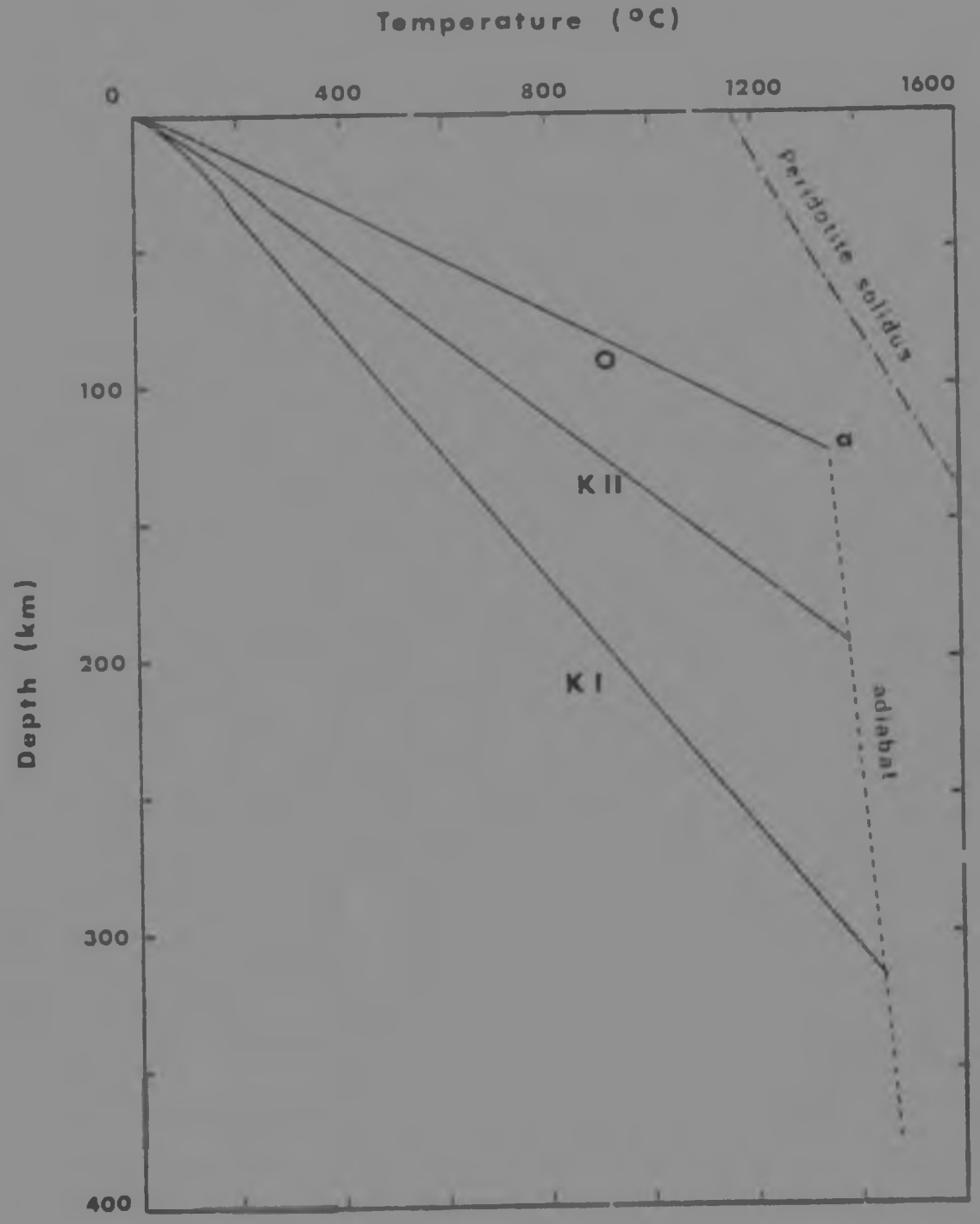

FIGURE 8.7 Temperature profiles for models of the Kaapvaal lithosphere (KI and KII) compared with that of an equilibrium ocean (O). The solidus of anhydrous peridotite is after Wyllie (1980). The 0,5 K/km adiabat 'defines' the base of the lithosphere. See text for discussion.

estimated the thickness of the lithosphere and the bottom boundary temperature to be approximately 125 km and 1350°C respectively (point a); below this depth the temperature gradient is likely to be adiabatic. A transition in rheological behaviour near the base of the lithosphere has not been considered and the sharp boundary is diagrammatic. Parsons and McKenzie (1978) offer a detailed model of the thermal structure in this region (see Appendix I).

The surface heat flow and vertical distribution of crustal heat sources for the Kaapvaal models are those shown in Figure 8.6. A reasonable estimate for the average thermal conductivity of continental crust is 3,0 $Wm^{-1}K^{-1}$. Thermal properties of the upper mantle are those specified for the oceanic model. Figure 8.7 shows the temperature profiles (KI and KII) calculated from equation 8.7.

Turcotte and Oxburgh (1969) showed that the temperature gradient below the lithosphere is likely to be adiabatic and they discussed the variation of adiabatic gradient with depth in the upper mantle in some detail. Four different methods predict adiabatic gradients of between 0,4 and 0,6 K/km for the depth interval 200-400 km. If there are no substantial horizontal temperature gradients in the asthenosphere, the base of the lithosphere can be regarded as being defined by an adiabat. In figure 8.7 an adiabatic gradient of 0,5 K/km is matched to the point defining the base of the oceanic lithosphere. The thickness of the lithosphere for each continental model may be obtained from the intersection of the adiabat with the lithospheric temperature profile. Respective values for models KI and KII are 315 km and 195 km.

Figure 8.8 shows diagrammatic E-W sections of the lithosphere below

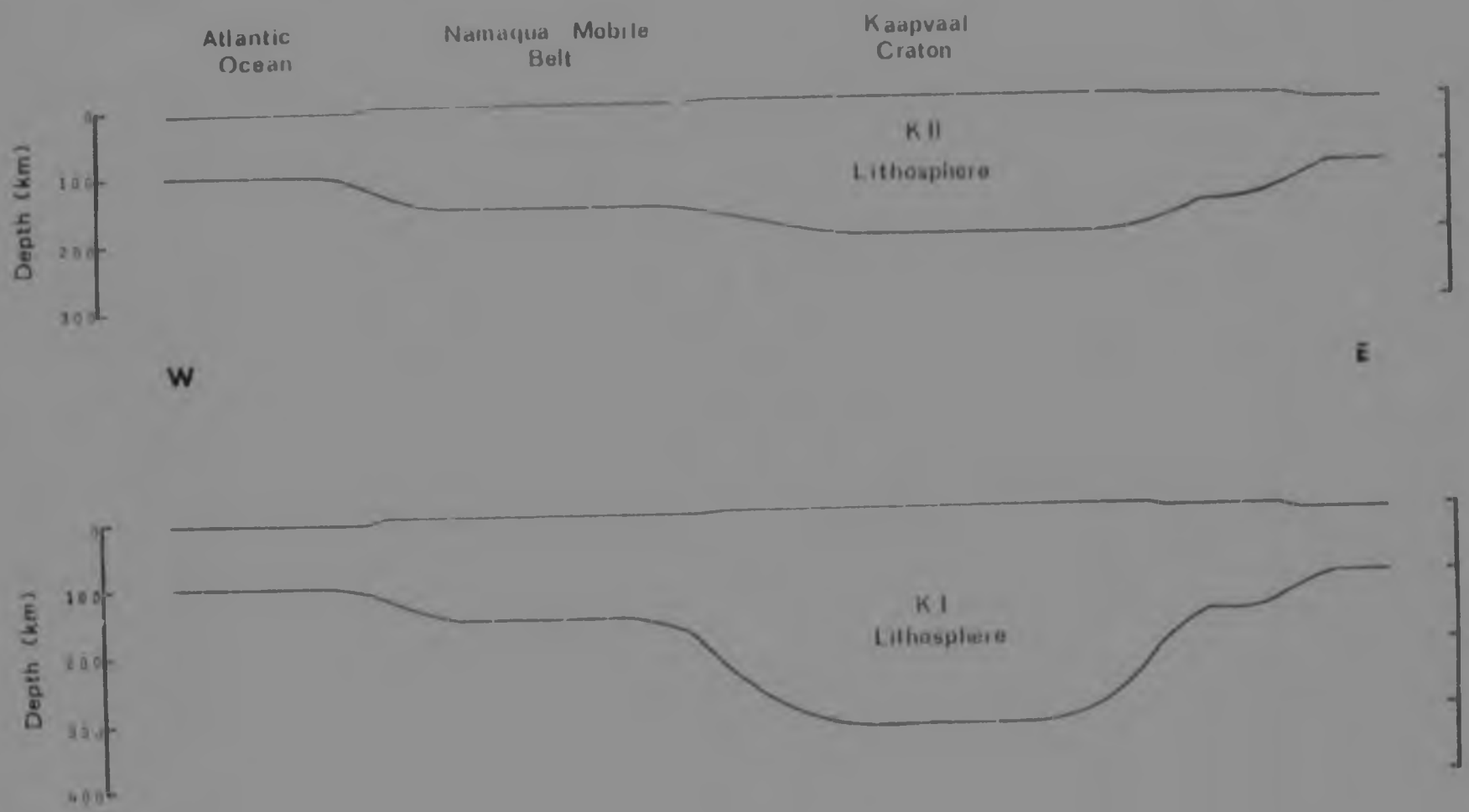

FIGURE 8.8 Diagrammatic east-west cross-section of the lithosphere below South Africa for the KI and KII models. Horizontal and vertical scales are approximately equal.

anhydrous peridotites

depress the solidus by several

the existence of a zone of

In the presence of small amounts of

the fluxing of the mantle should still be

of the interlocking network of solid grains and

should not be affected.

9 DENSITY AND BOUYANCY OF THE KAAPVAAL LITHOSPHERE

The contrast in lithospheric temperature and thickness between the Kaapvaal Craton and an equilibrium ocean has important implications the density structure of the upper mantle. The variation of densit within the mantle is primarily controlled by mineralogical composition and temperature. If the lithospheric mantle is compositionally identical in continental and oceanic regions it should be denser be ow the craton by virtue of the greater degree of thermal contraction. Such an increase in density should result in isostatic subsidence (Jordan, 1978; Turcotte, 1980) and a significant negative anomaly in the oid height (Turcotte and McAdoo, 1979).

In reality there are no geoid anomalies above South Africa (Turcotte and McAdoo, 1979, Figure 6) and the Kaapvaal Craton is approximately 1,5 km above sea level. The local lithosphere is therefore bouyant with respect to surrounding lithosphere profiles. This implies that there is a compositional difference between the continental lithosphere on the one hand and the oceanic lithosphere and the asthenosphere on the other such that the density is intrinsically lower within the continental lithosphere (cf. Jordan, 1978).

A compositional decrease in the density of the Kaapvaal lithosphere can be related to two important stages in the geological history of the craton. The first embraces the major episodes of crust formation and evolution which occurred before ~2000 m.y. ago (see Section 2.2). The second is Cretaceous kimberlite magmatism and uplift.

Although the initial phase of crust development is likely . have had an important effect on the composition of the Kaapvaal lithosphere it is difficult to estimate the effect on its density. Oxburgh and Parmentier (1977) showed that the extraction of basaltic melts from the lithosphere in the formation of oceanic crust is likely to produce a less dense, depleted lithosphere; the decrease in density is of similar magnitude to the density increase due to thermal contraction of oceanic lithosphere as it ages. Jordan (1975,1978) used a similar argument to show that basalt genesis can produce a lower density continental lithosphere and therefore permit lower temperatures below continents than below oceans. Some support for this conjecture comes from the fact that the most abundant type of upper mantle nodule erupted with South African kimberlites has a relatively depleted composition (Gurney and Harte, 1980). However, because of the variety of processes involved in the formation of continental crust and the wide compositional spectrum of material extracted from the mantle such simple models for the evolution of continental lithosphere may be inappropriate. The magnitude and sign of the overall change in density of continental lithosphere (due both to thermal contraction and crust genesis) are uncertain.

Although a solution to the problem may lie in the subsidence history of ancient cratonic regions this history is not well understood. In particular, it is not known whether Archaean and Proterozoic sedimentary basins on the Kaapvaal Craton formed as a result of thermal subsidence (Sleep, 1971; Turcotte, 1980) or dynamic processes such as lithospheric stretching (McKenzie, 1978).

Whatever the effect of crustal evolution on continental lithosphere the following important fact remains: many continental shields (eg.

the western Australian Shield and the Canadian Shield) lie close to sea level which indicates that this is the equilibrium height for continents. Although little is known about the history of the Kaapvaal Craton during the past 2000 m.y. erosional forces are likely to have ensured a near zero elevation throughout most of this time. The accumulation of extensive sedimentary sequences (notably the Karoo Supergroup) during the Palaeozoic and Mesozoic also suggests that the subcontinent was low-lying during its latter geological history. The present surface height of approximately 1,5 km on the craton therefore reflects a recent decrease in lithospheric density.

Geomorphological data indicate that major, geologically persistent uplift of southern Africa occurred in Cretaceous times (du Toit, 1954; King, 1963). Uplift was temporally and spatially associated with widespread emplacement of kimberlites, melilite basalts and nephelinite basalts (Dawson, 1970) which suggests that these events were related to the same geodynamic process. Subsequent phases of uplift indicate that the subcontinent responded to these, or related, processes over a prolonged period of time. The most important period of kimberlite emplacement in southern Africa appears to be 130-90 m.y. (H L Allsopp, personal communication).

Several different mechanisms have been proposed to account for plateau uplift (see McGetchin et al, 1980) but few can be applied to South Africa. Any mechanism that explains South African Cretaceous uplift must also explain the associated kimberlite magmatism and must be consistent with the heat flow data.

Thermal processes within the upper mantle can cause expansion of the lithosphere and uplift of the magnitude observed. Important processes include heating caused by hot spots (Crough, 1979) and frictional heating caused by shear at the base of the lithosphere (Yuen and Schubert, 1981). However, transient thermal processes cannot account for Cretaceous uplift in southern Africa. Figure 9.1 shows that thermal events in the uppermost mantle should have important effects at the surface after 100-150 m.y. and this is inconsistent with the low heat flow on the Kaapvaal Craton. Nor can such thermal transients result in <u>persistent</u> uplift.

A simple mechanism for South African uplift which fits the facts best involves the introduction of volatiles into the lithosphere and ensuing hydration and/or carbonation of mantle peridotite; this results in a permanent lowering of the density and isostatic uplift (Hess, 1954; McGetchin and Silver, 1972; Lloyd and Bailey, 1975). It can be achieved with little or no heat input and also provides a plausible mechanism for the genesis of kimberlites (Wyllie, 1980).

Figure 9.2 shows melting relationships in the system peridotite-CO_2-H_2O (after Wyllie) in relation to the Kaapvaal geotherms. The solidus for anhydrous peridotite lies well above the geotherms and melting could not occur without a substantial thermal perturbation. If CO_2 and H_2O were introduced adiabatically from below, partial melts of kimberlitic composition would be generated at the point where they cross the peridotite-CO_2-H_2O solidus (a). Above (a) excess CO_2 and H_2O would be dissolved in interstitial melts. Wyllie suggested that partially melted diapirs would rise adiabatically until they reached the temperature maximum on the peridotite-CO_2-H_2O solidus where volatiles would

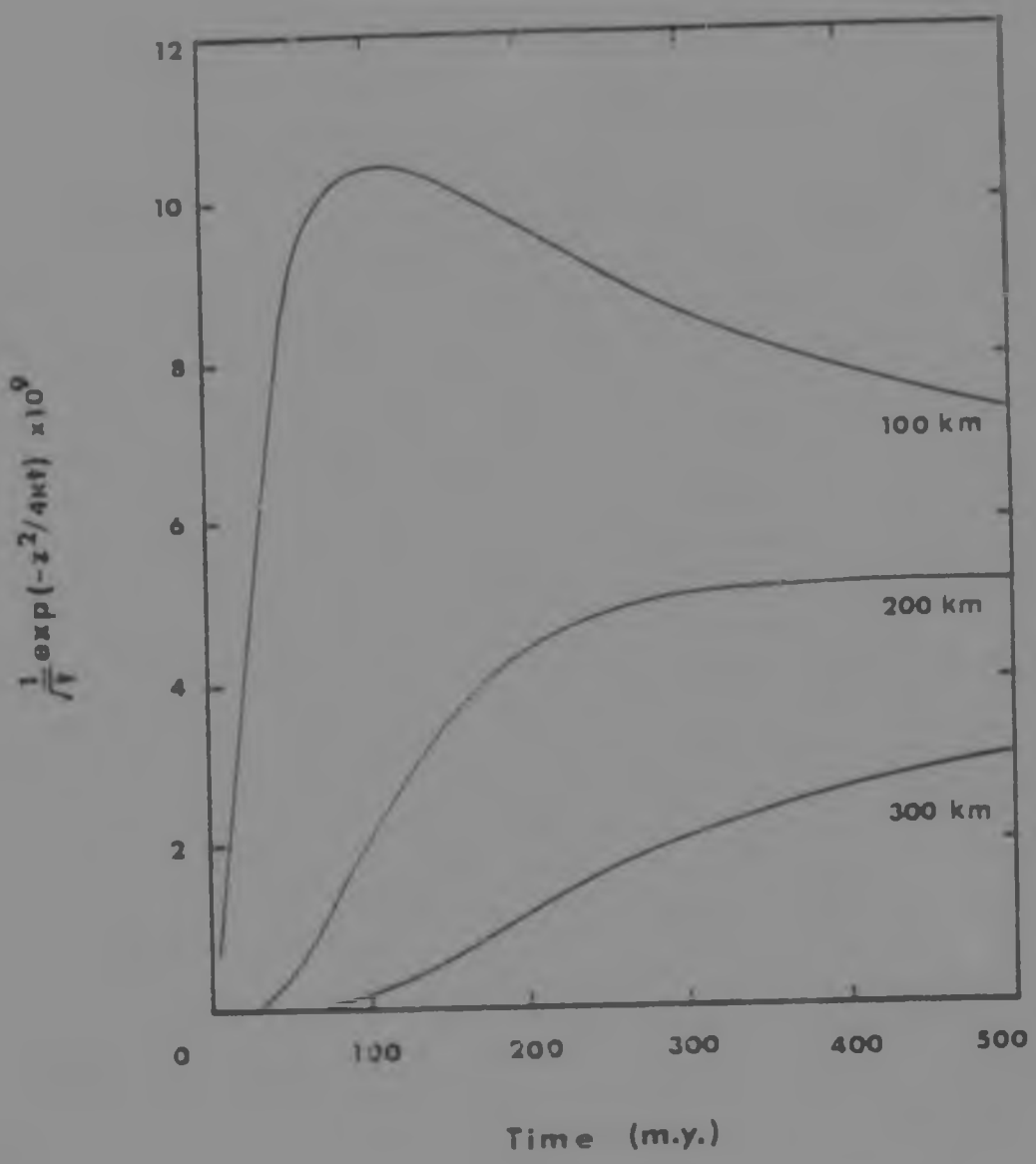

FIGURE 9.1 The time dependence of surface heat flow due to a thermal perturbation in the upper mantle at three different depths.

be released; this may result in the propagation of cracks to the surface and explosive eruption. Ascent is not necessarily adiabatic within the lithosphere and diapirs or kimberlitic melts may follow a path closer to the geotherm. Levels (b) and (c) at which the KI and K.I geotherms intersect the solidus represent the maximum depths at which volatiles can evolve or crack propagation can be initiated.

In the framework outlined by Wyllie, when release of volatiles does not result in kimberlite eruption, kimberlitic magmas will crystallize at the point where they enter the subsolidus field: CO_2 and H_2O become available to react with peridotitic mantle and produce minerals such as dolomite, phlogopite and amphibole. Similar reactions could also occur at depths below (a) where the 1350 C adiabat intersects the solidus.

It is possible to make rough estimates of the overall decrease in lithospheric density caused by such reactions and the degree of carbonation or hydration required for given amounts of uplift. Simple isostatic theory shows that the decrease in bulk lithospheric density ($\Delta\rho$) is given by

$$\frac{\Delta\rho}{\rho_o} = \frac{\Delta h}{h}$$

where ρ_o is the original density of the mantle, Δh is the amount of uplift and h is the total thickness of mantle that has undergone partial alteration. The volume content of carbonated or hydrated material within this zone is

$$x = \left(\frac{\Delta\rho}{\rho_o - \rho_x}\right)100\%$$

where ρ_x is the density of the alteration product. Values for $\Delta\rho$ and x

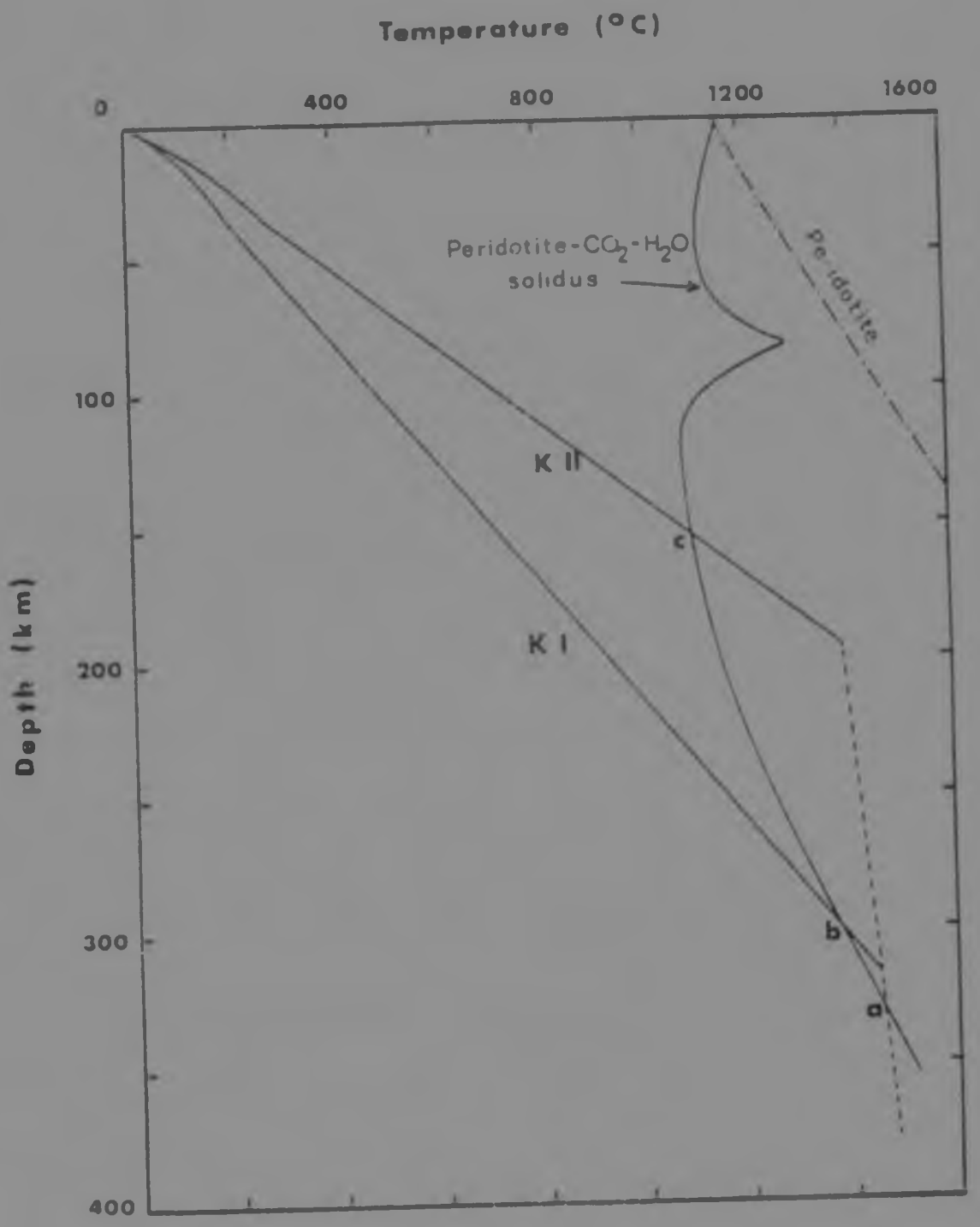

FIGURE 9.2 KI and KII model geotherms in relation to the peridotite-CO_2-H_2O solidus (after Wyllie, 1980).

have been calculated assuming $\rho_o = 3,36 \times 10^3$ kgm^{-3} and $\rho_x = 2,9 \times 10^3$ kgm^{-3}. For an uplift of $\Delta h = 1,0$ km and for h = 200 km:

$$\Delta\rho \sim 0,017 \times 10^3 \text{ kgm}^{-3}$$

$$x \sim 3,7\%$$

and for h = 300 km:

$$\Delta\rho \sim 0,011 \times 10^3 \text{ kgm}^{-3}$$

$$x \sim 2,4\%$$

Phlogopite appears to be the most abundant secondary mineral* in that section of the mantle sampled by kimberlites (100-200 km) (Gurney and Harte, 1980). Although minor amounts of phlogopite occur in many mantle inclusions the overall abundance in the mantle is not known; in order to keep the content of secondary minerals below a reasonable level it would appear that a considerable thickness of mantle (possibly more than 300 km) has been affected. In this calculation it is supposed that movements associated with isostatic adjustment occur below the lithosphere. Although glacial uplift phenomena indicate that creep can occur at shallower depths the lower viscosity of the asthenosphere permits more efficient flow and the Kaapvaal lithosphere as a whole is bouyant.

A possible consequence of the model is that influx of volatiles may be accompanied by light element metasomatism of the mantle (Lloyd and Bailey, 1975; Wyllie, 1980). Incompatible trace elements, including U and Th, may be incorporated in the lithosphere. Figure 9.1 shows

---

* In this context 'secondary' refers to minerals formed in situ rather than by incorporation of xenoliths in kimberlite melts.

that a significant increase in radiogenic heat production within the lithosphere approximately 100 m.y. ago should have an effect at the surface today. As noted previously, this is not consistent with the low cratonic heat flow. Although evidence for the introduction of incompatible elements on a small scale is indisputable (see Gurney and Harte, 1980), widespread introduction of U and Th cannot be supported.

Different suggestions have been advanced for the mechanism by which volatiles are introduced. Wyllie (1980) suggested that minor thermal perturbations could release the components C-H-O from deep-seated mantle reservoirs. Lloyd and Bailey (1975) produced evidence to show that volatile influx is enhanced in zones of tension in the lithosphere. Nicolaysen (1981) has developed a model which couples mantle degassing and crystallization state in the core; the stage of active devolatilization is coupled to core contraction and a stage of volatile storage is coupled to core expansion. Although this model is dependent on the controversial theory of Schloessin and Jacobs (1980) it nevertheless predicts upper Cretaceous kimberlite eruptivity.

Whatever the cause, the abundance of kimberlite in southern Africa indicates that large quantities of CO_2 and H_2O were available during the Cretaceous. Important consequences are that these volatiles could (1) lower the mantle solidus far enough to generate kimberlitic partial melts and (2) react with the mantle to produce less dense hydrous and/or carbonate assemblages and hence cause uplift; these could be achieved without a significant thermal perturbation.

10 IMPLICATIONS FOR THE GENESIS OF DIAMONDS

Although diamonds constitute a minor component of the kimberlite inclusion suite their economic value has promoted much research into the genesis of their host magmas and the physical and chemical nature of the upper mantle from which they are derived. Clifford (1966) noted that diamondiferous kimberlites in Africa are apparently confined to the older cratonic regions and that the younger orogenic belts are virtually barren. The discovery of numerous kimberlites in recent years confirms this observation and Figure 10.1 shows that all known major occurrences of diamondiferous kimberlite in South Africa are restricted to the Kaapvaal Craton. Gurney and Harte (1980) noted further that the economic potential of diamond occurrences generally increases towards the centre of the craton. A comparison of these observations with the heat flow data summarized in Figures 8.1 and 8.2 shows that there is a strong correlation between heat flow, tectonic age and abundance of diamondiferous kimberlite.

The implication of this is that lateral variations of the thermal structure of the lithosphere can account for the distribution of diamondiferous kimberlites. MacGregor (1975) and MacGregor and Basu (1974) have shown that temperature-pressure estimates based on studies of mineral equilibria in kimberlite xenoliths indicate that the lithosphere is cooler and thicker below the Kaapvaal Craton than its surroundings. Other authors (eg. Nixon et al, 1973; Boyd and Nixon, 1980) have suggested that only in the cratonic regions is the lithosphere thick enough for zones of diamond stability to exist. In this chapter, it will be shown that differences in the thermal structure of the lithosphere below the Namaqua Mobile Belt and the Kaapvaal Craton,

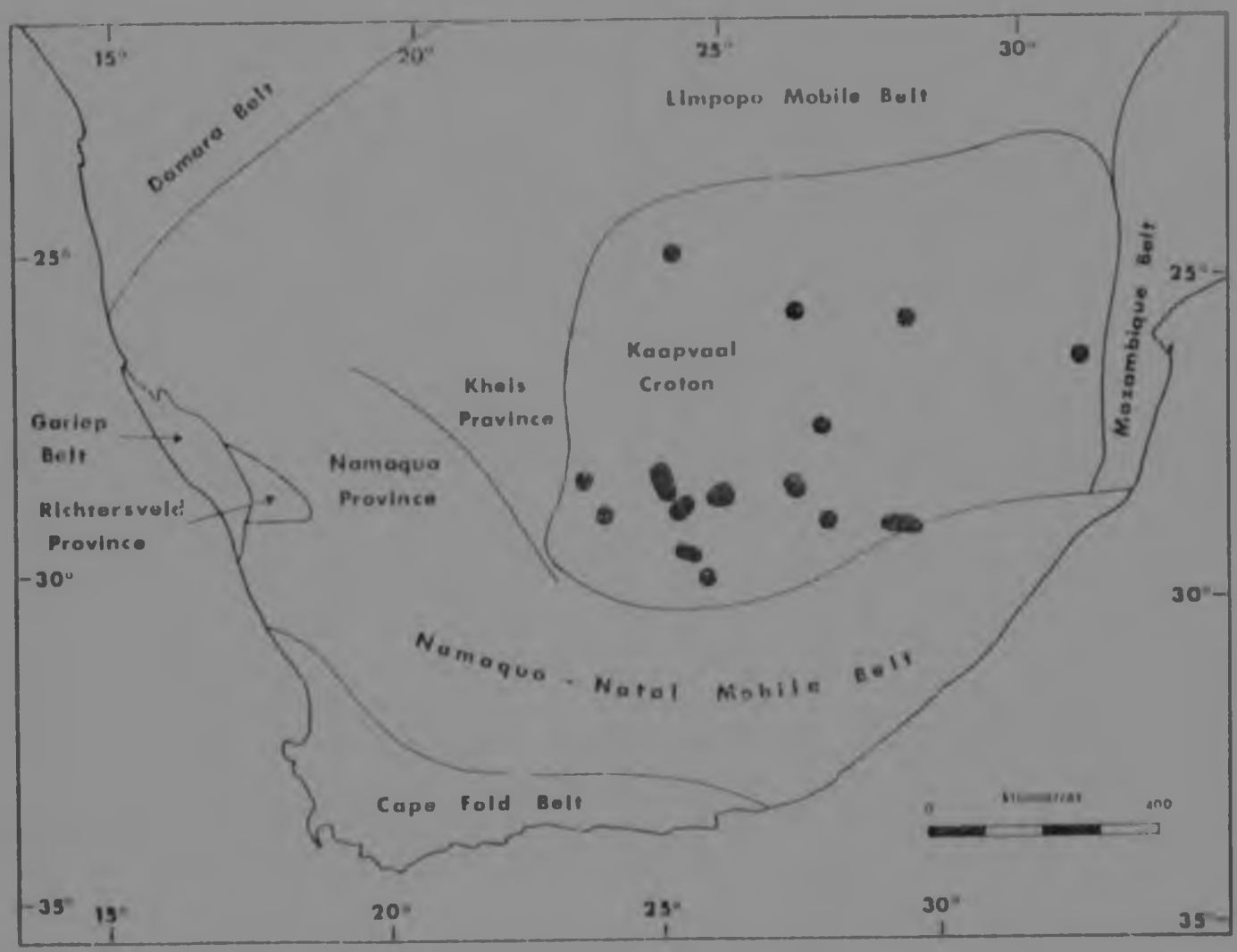

FIGURE 10.1 The distribution of major occurrences of diamondiferous kimberlites in South Africa (largely after Dawson, 1970 and Gurney and Harte, 1980).

...explain ... in the ...rden region ... of the latter.

... the temperature ... distribution in the upper mantle below the Namaqua Mobile Belt. A ...otherm was calculated in the same way as the Kaapvaal geotherms ... (see Table 9.3). This model was ... leads to a smaller contrast in lithospheric temperatures ... the Kaapvaal models. The temperature profile is shown in ... (curve N)*. Although an improved knowledge of the thermal ... of the Namaqua crust will probably alter the position ... lithosphere below the Namaqua Mobile Belt is evidently ... that below the craton (curves KI and KII, Figure 10.2).

... these geotherms are based on present-day measurements there is ... considerable justification for applying them to the period 130-90 m.y. ... when most of the kimberlites were erupted. A fairly recent, major ... event would be required if the geothermal gradients below ... Namaqua Mobile Belt and the Kaapvaal Craton were significantly ... different 100 m.y. ago (see Figure 9.1). It was shown in Chapter 9 ... that Cretaceous magmatism itself could not have constituted an important thermal event. Karoo volcanism and the break-up of Gondwana-... are unlikely to have had more than peripheral effects on the Namaqua Mobile Belt and the Kaapvaal Craton. There are no other surface ... of recent thermal events in southern Africa and it is likely

---

* ... yields a value for q_m which exceeds q_r in Table 9.3. ... was therefore taken to be equal to q_r.

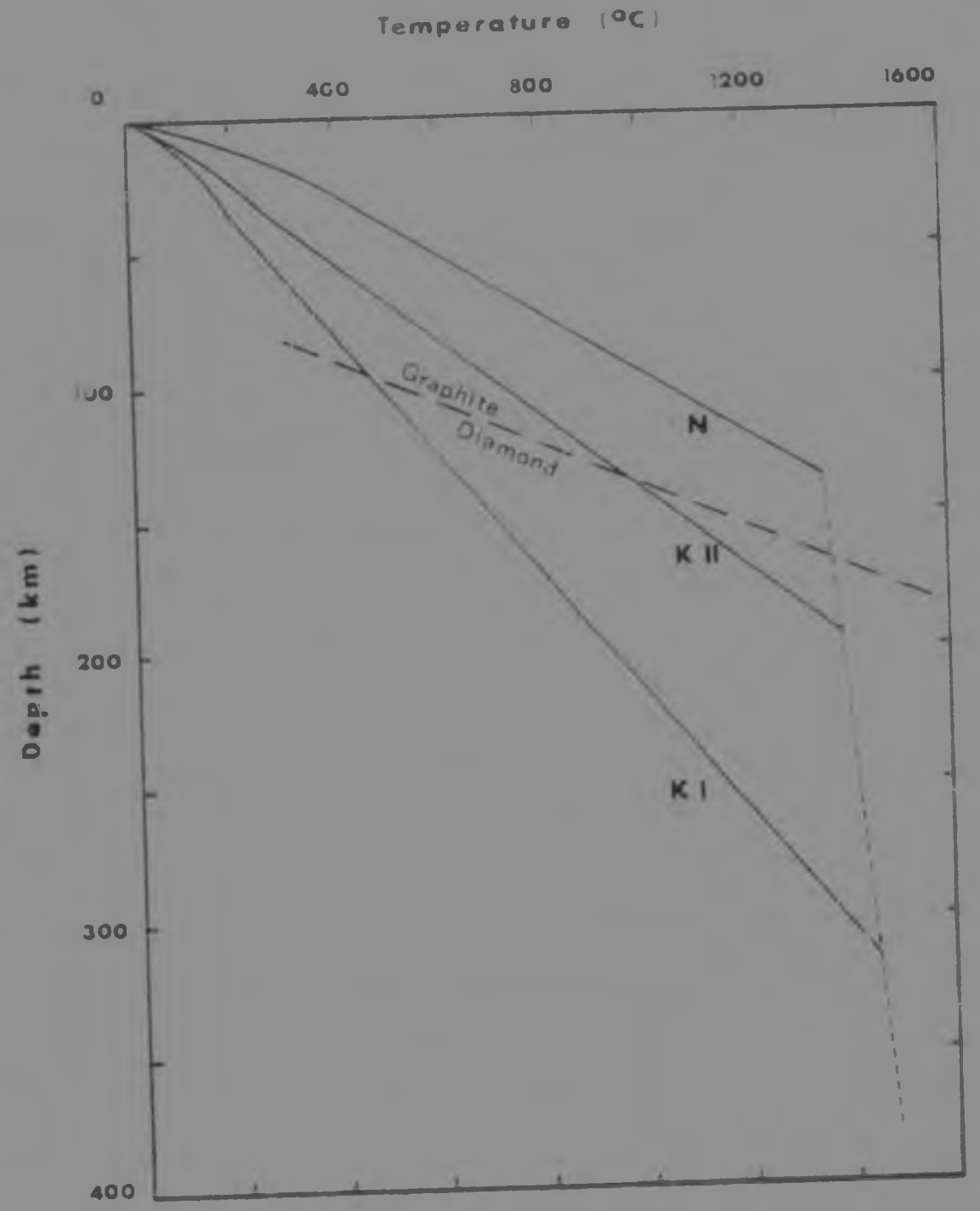

FIGURE 10.2 Kaapvaal model geotherms (KI and KII) and a tentative geotherm for the Namaqua Mobile Belt (N) in relation to the diamond-graphite equilibrium boundary (after Kennedy and Kennedy, 1976).

that the geothermal gradients have not changed significantly during the last 100 m.y.

Support for this conclusion comes from a Pb isotope study of sulphide inclusions in diamonds from the Kimberley and Finsch mines (Kramers, 1979). The data indicate that at least some of the diamonds are older than 2000 m.y. This implies that the temperature of the lower part of the lithosphere in this region has not been raised above the diamond-graphite equilibrium boundary (see Figure 10.2) during the past 2000 m.y. and that this area has been underlain by a cold thick lithosphere for at least this period of time.

Temperature-pressure data estimated from studies of phase equilibria in kimberlite inclusions are commonly used to make inferences about the thermal structure of the upper mantle below southern Africa during the Cretaceous (eg. Boyd, 1973; MacGregor and Basu, 1974; MacGregor, 1975; Boyd and Nixon, 1980). However, interpretation of these data in terms of geotherms is open to question. Large uncertainties arise out of both mineral equilibrium studies and their experimental calibrations and the application of these data, derived from simple chemical systems, to natural rock systems (Wilshire and Jackson, 1975; Mori and Green, 1978; Howells and O'Hara, 1978). In addition, Fraser and Lawless (1978) have questioned the assumption that nodules are in chemical equilibrium and Mitchell et al (1980) showed that T-P systems may be altered considerably by thermal interaction between the inclusions and the kimberlite melt. Although the data indicate that the Kaapvaal lithosphere was considerably colder and thicker than in the surrounding regions they do not provide an accurate check on the positions of geotherms calculated from heat flow data.

Figure 10.2 shows the positions of the model geotherms in relation to the graphite-diamond equilibrium boundary (dashed line) and also shows how the difference in thermal structure can explain the observed distribution of diamondiferous kimberlites. T-P estimates made on kimberlite inclusions, and their generally depleted composition, indicate that the maximum depth from which kimberlites are erupted is close to the base of the lithosphere; hotter, deeper and presumably undepleted material is apparently not sampled. The reason for this is not clear; the physical nature of sublithospheric mantle may inhibit crack propagation which is necessary for kimberlite eruption. Those kimberlites originating below the craton had ample space to sample potentially diamond-bearing lithosphere before reaching the graphite-diamond transition. Those in the Namaqua Mobile Belt originated within the graphite field and are barren.

This line of analysis indicates that there is a potential application of heat flow studies for understanding craton-mobile belt boundaries, and therefore, the distribution of diamondiferous kimberlites. A wider coverage of heat flow-heat production stations in southern Africa is likely to provide better detail regarding the relationship between diamondiferous kimberlite occurrences and low heat flow and also permit a more exact investigation of the thermal structure of the lithosphere. It may then be possible to extend the above explanation to unexplored regions. While T-P studies on kimberlite nodules may yield similar information, heat flow investigations are more economical and are not restricted to areas of known kimberlite occurrence.

11 CONCLUSIONS

The main conclusions that can be drawn from this investigation are summarized below:

1. Systematically increasing temperature gradients to depths of approximately 200 m in boreholes in the Namaqua Mobile Belt and Kaapvaal Craton reflect a rise in surface temperature of about 1 °C during the past century. Decreasung gradients to approximately 60 m in the Klerksdorp boreholes suggest that the surface temperature has started to decline there. These trends are consistent with variations of the mean annual air temperature during the period of the meteorological record at stations in South Africa, Europe and the U.S.A.; a climatic warming, starting up to 150 years ago, seems to be a world-wide phenomenon while declining temperatures are evident in some areas. Several heat flow measurements require small corrections for these effects.

2. Surface temperature variations during the past few hundred years may obscure the effects of palaeoclimatic variations, which are usually measured in thousands of years, in the upper few hundred metres of a borehole. Observations in shallow boreholes should not be used as supporting evidence for Quaternary climatic reconstructions.

3. None of the boreholes investigated was deep enough to show the effects of Quaternary climatic variations. Perturbations of thermal gradients have previously been observed in several deep boreholes in South Africa but the trends are not well defined and

their causes have not been established. Although climatic modelling for the northern continents suggests that the heat flow may be depressed by as much as 25% in some areas there is no supporting evidence for this in deep boreholes. Because of this and the lack of detailed climatic reconstructions for southern Africa there is no justification for applying palaeoclimatic corrections to the heat flow data.

4. The heat flow from the Namaqua Mobile Belt is variable, ranging between 39 and 81 mWm^{-2}. The average heat flow, 61 ± 11 mWm^{-2}, is 20-25 mWm^{-2} higher than the equilibrium value given by Polyak and Smirnov (1968) for continents; this represents a significant anomaly. The high average near-surface heat production, 2,3 ± 1,2 μWm^{-3}, and the absence of independent geophysical evidence for a high mantle heat flux suggest that the anomaly is due to enhanced upper crustal radioactivity. Although heat flow-heat production pairs do not yield a simple linear correlation the averaged data plot close to the relationship observed in the Superior Province; on this basis crustal radioactivity is estimated to contribute 50-60% to the surface heat flow.

5. Stations from the Springbok district yield a mean heat flow which is not significantly different from that of the Namaqua Mobile Belt as a whole. However, small variations in heat flow are correlated with locally extreme values of heat production. The anomalous heat production is associated with a sheet-like granitic intrusion 1-2 km thick. This is similar to the depth parameter relating heat flow and heat production and differential erosion of this layer may account for much of the heat flow variation. Data from such thin, enriched

bodies may lead to overestimates of the mean surface heat production, and therefore the contribution due to crustal radioactivity, in gneissic terranes such as the Namaqua Mobile Belt.

6. Although boreholes close to the Kheis boundary of the Namaqua Mobile Belt yield a lower mean heat flow than the remaining stations in the mobile belt, this difference can be attributed to a difference in the depth integrated average heat production.

7. The single station from the Richtersveld Province yields heat flow and heat production values which are close to the means for the Namaqua Mobile Belt. This suggests that these regions are characterized by similar thermal parameters.

8. The mean heat flow from the Klerksdorp district of the Kaapvaal Craton (33 ± 2 mWm^{-2}) is among the lowest in the world, while the heat production of the near-surface basement rock is relatively high ($2,2 \pm 0,8$ μWm^{-3}). Similar low heat flows are obtained by subtracting the radiogenic contribution of Proterozoic strata from previous heat flow determinations and the mean heat flux from the basement in the centre of the craton is 36 ± 5 mWm^{-2}. The heat flow increases towards the margins of the craton, reflecting a transition between different thermal regimes.

9. Although the heat flow in the centre of the Kaapvaal Craton is not much less than the equilibrium continental value of Polyak and Smirnov (1968), high and uniform values at widespread localities and a heat production-depth profile from the Vredefort dome indicate that a significant proportion of this heat flow is due to crustal radioactivity. The probable range of mantle heat flux below the craton,

estimated by making use of data from the Vredefort profile and by comparing the Kaapvaal data with those from the western Australian Shield, is 14-22 mWm^{-2}. This range requires a lithospheric thickness of 1,5-2,5 times that below an equilibrium ocean.

10. The high elevation of the Kaapvaal Craton relative to other Archaean terranes indicates that the lithosphere is bouyant. This bouyancy reflects a decrease in lithospheric density which offsets the increase in density due to thermal contraction. A substantial decrease in lithospheric density appears to have occurred during the Cretaceous when the crust was uplifted and invaded by numerous kimberlites.

11. The persistent nature of Cretaceous uplift and the low cratonic heat flow indicate that uplift cannot be due to expansion caused by thermal transients. The mechanism considered to achieve uplift involves the introduction of CO_2 and H_2O from deep-seated mantle sources. The influx of CO_2 and H_2O depresses the mantle solidus below the geotherm and kimberlitic partial melts are generated without a significant thermal perturbation. Reactions between CO_2 and H_2O and the mantle result in the formation of carbonate and/or hydrous phases and therefore a permanent lowering of the lithospheric density. The low cratonic heat flow does not permit widespread introduction of heat producing elements during this process.

12. There is a correlation between tectonic age, heat flow and distribution of diamondiferous kimberlites. The presence of diamondiferous kimberlites in the Kaapvaal Craton and their absence in the Namaqua Mobile Belt can be understood in terms of the thermal structure of the lithosphere as deduced from the heat flow data. The lower

part of the Kaapvaal lithosphere lies within the diamond stability field and kimberlites erupted from this region are diamond bearing; the Namaqua lithosphere is mostly, or entirely, within the graphite stability field and kimberlites are barren.

APPENDIX I OCEANIC HEAT FLOW

Heat flow patterns are now well established in most of the major oceans and can be accounted for by relatively simple models for the thermal evolution of oceanic lithosphere. In the plate tectonic model, oceanic crust is created by the intrusion of basaltic magma at the centre of a spreading ridge (Hess, 1962). New crust and lithospheric mantle move away from the spreading centre where younger material is intruded. Newly formed crust is magnetized with the polarity of the earth's magnetic field (Vine and Matthews, 1963) and polarity reversals recorded by the pattern of magnetic lineations on the ocean floor give an estimate for the age of the crust. Near zero free air gravity anomalies over ocean ridges (Talwani et al, 1965) suggest that the lithosphere is isostatically compensated and that thermal expansion of the lithosphere accounts for the ridge elevation. Even in these simple terms plate tectonic theory predicts two importart relationships. Conductive cooling and thermal contraction of the spreading lithosphere should result in a decrease in heat flow and elevation of the ocean floor with age.

A general decrease in heat flow with age has been noted by several authors (eg. Sclater and Francheteau, 1970; McKenzie and Sclater, 1971; Herman et al, 1977). In a recent analysis of oceanic heat flow data Sclater et al (1980) showed that the trends are the same for all major oceans. The heat flow is high and variable near ridge crests and decreases to low, relatively constant values of less than 50 mWm^{-2} in old ocean basins. This is illustrated in Figure I-1 which shows the mean heat flow and standard deviation for consecutive age groupings of all major oceans combined.

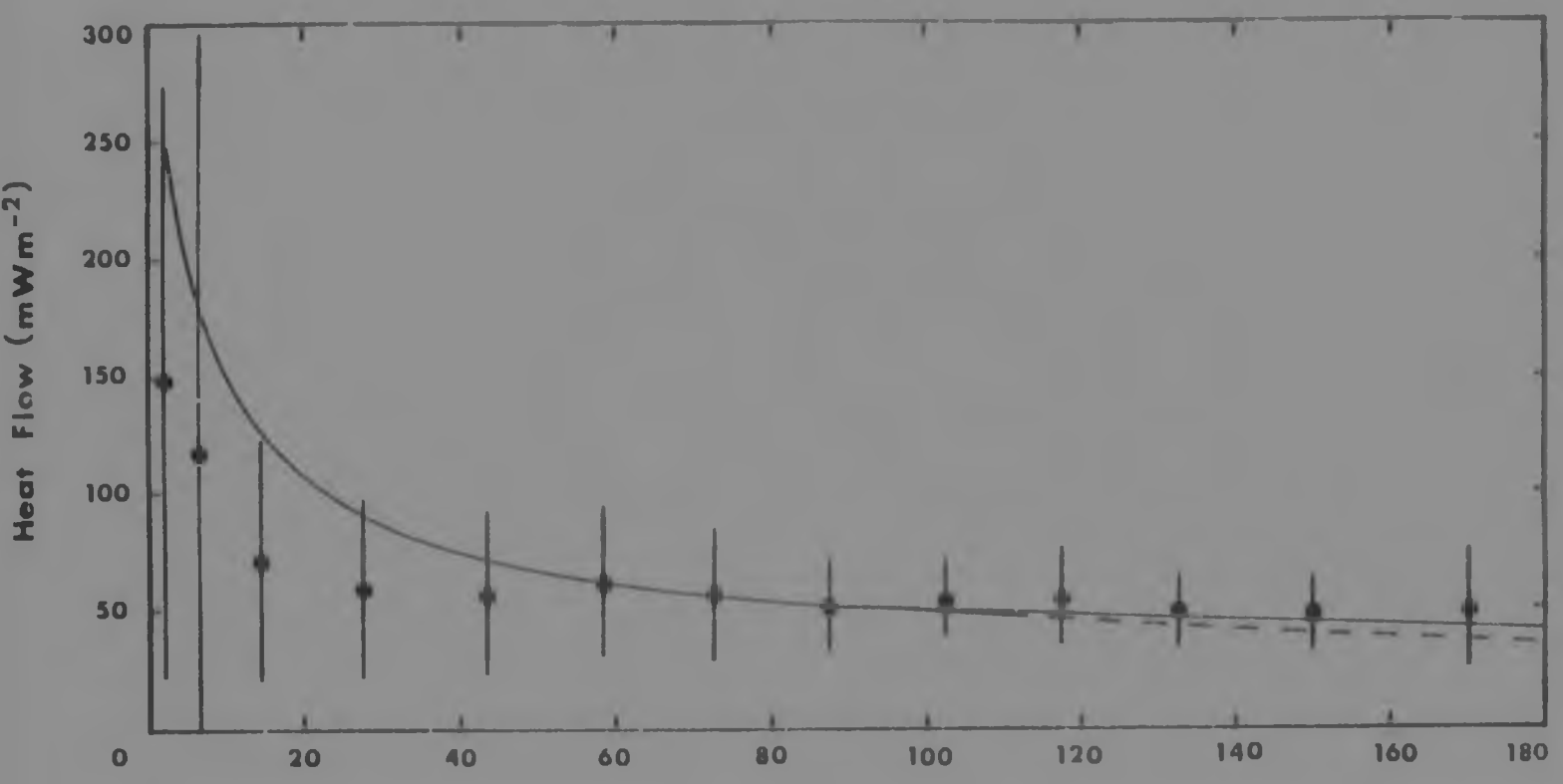

FIGURE I-1 Mean surface heat flow and standard deviation for all the major oceans as a function of age. Theoretical heat flows are for the plate model (solid curve) and boundary layer model (dashed curve). Data points are from Sclater et al (1980) and predicted values are relationships estimated by Parsons and Sclater (1977).

Although several thermal models for the evolution of oceanic lithosphere have been advanced to account for this relationship, most are variations of the original proposals made by Turcotte and Oxburgh (1967) and McKenzie (1967). Only the basic models will be discussed below.

(1) Boundary layer model (Figure I-2a). Turcotte and Oxburgh (1967) applied cellular convection theory to the earth's mantle and described lithospheric plates as cold thermal boundary layers which form on divergent mantle flows at ocean ridges. Motion of the rigid boundary layer is related to the large scale convective overturn of the mantle. The boundary layer cools by conduction to the surface and thickens with age, the thickness of the plate being limited only by the maximum age of the oceans (approximately 200 m.y.). The thermal evolution of the lithosphere is approximated by the one-dimensional cooling of a half-space (equations 1.9-1.12, Chapter 1). The predicted surface heat flow (equation 1.12) is a function of square root of ocean floor age ($\sqrt{t}$) and is compared with the observed trend in Figure I-1. The depth of the ocean floor relative to the ridge crest is given by

$$d(t) = (T_m - T_o)\frac{2\rho_o \alpha}{\rho_o - \rho_w}\left(\frac{\kappa t}{\pi}\right)^{\frac{1}{2}} \qquad (I\text{-}1)$$

where ρ_o and ρ_w are the densities of mantle rock and sea-water respectively and α is the co-efficient of volume expansion of the upper mantle. Other parameters are defined in Section 1.2.

(2) Plate model (Figure I-2b). In the model suggested by McKenzie (1967) a slab of constant thickness moves away from the ridge crest. The base of the slab and the vertical boundary at the ridge crest are maintained at a constant temperature. Although the first of these

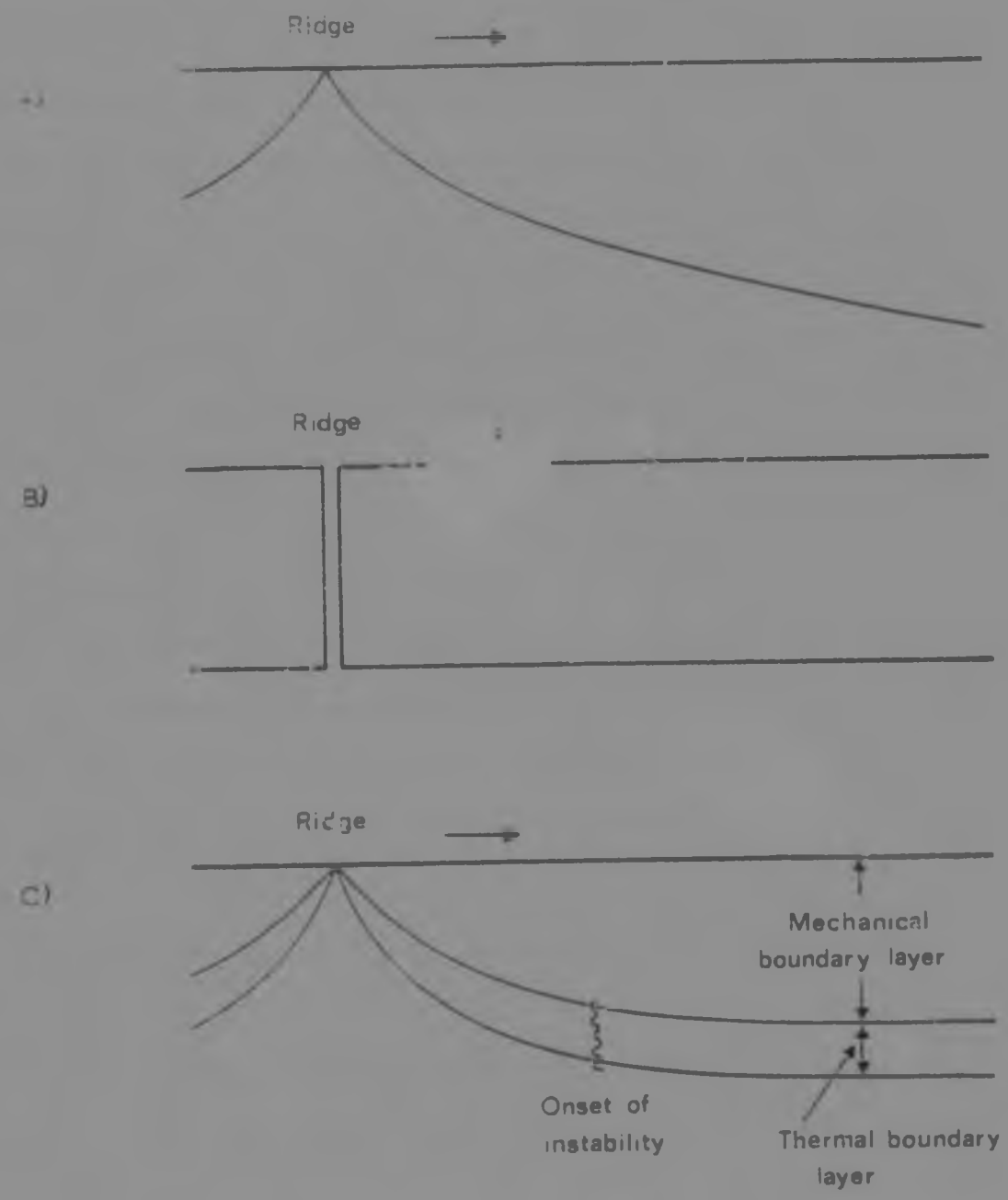

FIGURE I-2 Thermal models of the oceanic lithosphere in the vicinity of a spreading ridge. (a) Boundary layer model. (b) Plate model. (c) Two-layer model of Parsons and McKenzie (1978).

boundary conditions is physically unrealistic the model agrees well with heat flow and depth observations (Sclater and Francheteau, 1970; Sclater et al,1971). McKenzie's original formulation of the temperature distribution did not show an explicit $\sqrt{t}$ dependence but Parsons and Sclater (1977) demonstrated that for young crust the surface heat flow and elevation of the ridge do depend on $\sqrt{t}$. At greater ages these relationships break down and q_s and d decrease exponentially to constant values. The dependence of surface heat flow on age is shown in Figure I-1.

The heat flows predicted in these models are virtually identical in young ocean floor although they are well above the observed values. For ages greater than 50 m.y. the curves diverge but both are in good agreement with the measured heat flow; here the scatter in the data precludes their use as quantitative tests of different thermal models.

A much better constraint is provided by the relationship between depth and age of the sea floor (Sclater et al, 1971; Davis and Lister, 1974; Parsons and Sclater, 1977). Averaged depth data for the North Pacific and North Atlantic decrease from approximately 2500 m at the ridge crests to over 6000 m in old ocean basins (Figure I-3) and agree well with the linear $\sqrt{t}$ dependence for ages less than 80 m.y. Beyond 80 m.y. depths predicted by the plate model provide a better fit than the boundary layer model.

Armed with this information a closer inspection of the heat flow-age relationship is possible. The relatively low, variable heat flow through young ocean floor cannot be explained by purely conductive processes and a number of authors have suggested that circulation of sea water through fractured basaltic crust removes much of the heat

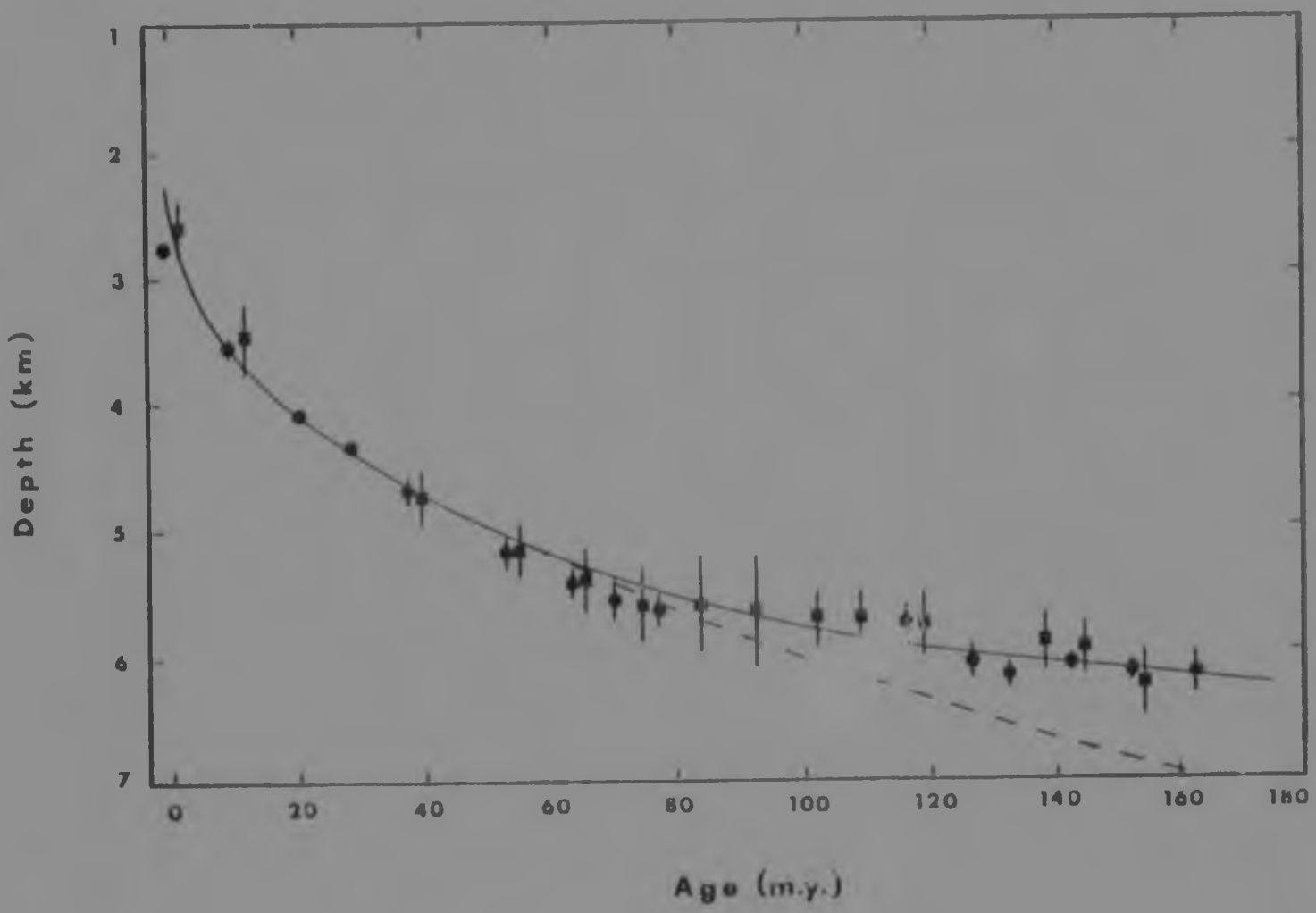

FIGURE I-3 Relationship between depth to the ocean floor and age. Mean depths and standard deviations are for the North Pacific (dots) and North Atlantic (squares). Data points are offset by -1 and +1 m.y. respectively from the mean age. Theoretical depths are for the plate model (solid curve) and boundary layer model (dashed curve), from Parsons and Sclater (1977).

(eg. Lister, 1972; Williams et al, 1974). It has been clearly shown (Sclater et al, 1974; Anderson and Hobart, 1976; Anderson et al, 1977; Davis and Lister, 1977) that there is a transition from predominantly convective heat transport in ridge crestal regions where permeable crust is in direct contact with sea water, to predominantly conductive transfer in older regions where water circulation is effectively halted by the thickening sedimentary blanket and sealing of fractures. In the latter regions the heat flow is less variable and approaches theoretical estimates while measurements in restricted sedimentary ponds in young ocean floor yield low and variable results.

Using selected means from young, well-sedimented crust in the Pacific Ocean, Sclater et al (1976) showed that the scatter in the data is greatly reduced and that the mean values are in excellent agreement with theoretical predictions (Figure I-4). Similar results were obtained in local studies by Davis and Lister (1977) for the Juan de Fuca Ridge and Sclater and Crowe (1979) for the Reykjanes Ridge. Both the plate and boundary layer models are consistent with this reassessment of the data but it is still not possible to distinguish between them on heat flow grounds.

Parsons and Sclater (1977) developed methods of inverting bathymetric and heat flow data to give physical properties of oceanic lithosphere. They showed that the plate model predicts a $\sqrt{t}$ dependence of heat flow and depth in young ocean floor and asymptotic decreases to constant values in old ocean floor. Only the bathymetric data provide accurate constraints on the model; best fits to the data show that the depth to the ocean floor departs from a $\sqrt{t}$ dependence at approximately 70 m.y. and may be represented by:

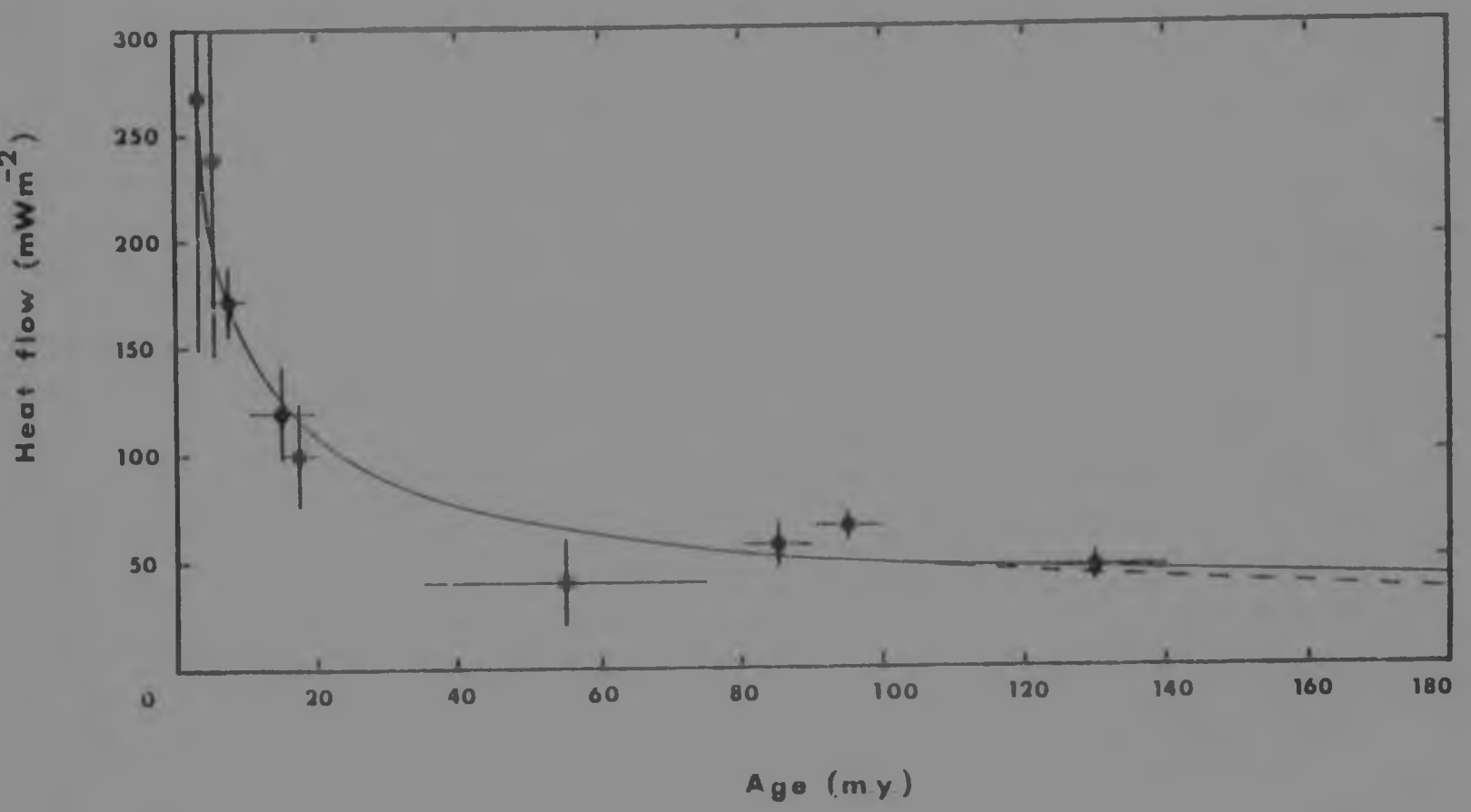

FIGURE I-4 Selective heat flow means and standard deviations of Sclater et al (1976) as a function of age of the ocean floor. Horizontal bars represent age ranges. Theoretical curves are as in Figure I-1.

$$d(t) = 2500 + 350\sqrt{t} \quad m \qquad (I-2)$$

for $0<t<70$ m.y. and

$$d(t) = 6400 - 3200\exp(-t/62,8) \quad m \qquad (I-3)$$

for $t>20$ m.y. Parsons and Sclater used values of $1,00 \times 10^{3}$ kgm^{-3} for the density of sea water, and $3,33 \times 10^{}$ kgm^{-3} for the density, $1,17 \times 10^{3}$ $Jkg^{-1}K^{-1}$ for the specific heat and 3,14 $Wm^{-1}K^{-1}$ for the thermal conductivity of mantle material to derive the following lithospheric parameters from the constants in expressions I-2 and I-3:

L	(plate thickness)	=	125 km
T_L	(bottom boundary temperature)	=	1 350 ^{o}C
α	(thermal expansion co-efficient)	=	$3,2 \times 10^{-5}$ $^{o}C^{-1}$

Even reliable heat flow data are too scattered to accurately estimate model lithospheric parameters but they apparently depart from a $\sqrt{t}$ dependence at a much older age (approximately 120 m.y., Figure I-4) than the elevation. The reason is that thermal contraction of the lithosphere responds to a bottom boundary condition almost instantaneously when compared with the characteristic time for heat conduction through the lithosphere. The surface heat flow may be represented by

$$q_0 = 473/\sqrt{t} \quad mWm^{-2} \qquad (I-4)$$

for $0<t<120$ m.y. The best estimate for the asymptotic mantle heat flux is obtained from results of the elevation - age relationship which gives

$$q_m = K\frac{T_L}{L} = 33,5 \text{ mWm}^{-2} \qquad (I-5)$$

The crustal radiogenic heat input is approximately 4,2 mWm^{-2} and the asymptotic surface heat flow is 37,7 mWm^{-2}. This is 9,6 mWm^{-2} lower

than the lowest of the reliable heat flow means which suggests that the heat flow has not reached equilibrium in the oldest ocean floor generated by the present cycle of plate movements.

Parsons and McKenzie (1978) later rationalized the plate model by suggesting that the lithosphere thickens with age in the same way as the boundary layer model until a new basal boundary condition is felt; after this the thickness remains constant (Figure I-2c). They advanced the suggestions of Richter (1973), Richter and Parsons (1975) and McKenzie and Weiss (1975) that in this region small scale convection in the upper mantle supplies additional heat which holds the isotherm at the base of the lithosphere at a constant depth. The lithosphere is divided into a cold rigid 'mechanical' boundary layer and a hotter viscous 'thermal' boundary layer both of which thicken with time. At an age corresponding to the break-down of the $\sqrt{t}$ dependence of topography ($\sim$70 m.y.) the thermal boundary layer attains a thickness such that it becomes unstable to small scale convection. This involves the break-away of cold dense material from the bottom of the lithosphere and its replacement by hotter material from below. Alternative suggestions for the additional source of heat necessary to support the basal isotherm include shear stress heating (Schubert et al, 1976), radiogenic heating (Forsyth, 1977) and heat released via the earth's hot spot network (Crough, 1979); from theoretical considerations and experimental analogues Parsons and McKenzie (1978) concluded that heat transfer in the lower, viscous part of the lithosphere cannot be solely conductive.

A third source of information about the thermal structure of the oceanic lithosphere comes from seismic evidence. Shear wave studies show that there is a zone of low seismic velocity near the base of the lithosphere

which is interpreted to reflect the onset of partial melting. Although the depth to the top of the low velocity zone does not necessarily coincide with the base of the lithosphere defined using thermal parameters, studies of its variation with age provide a potential constraint on the thermal evolution of oceanic lithosphere. Leeds et al (1974) and Forsyth (1977) showed that the depth to this boundary increases with age but the resolution is limited and it is not clear whether or not it approaches constant values in old ocean basins.

APPENDIX II COMPUTER PROGRAMMES

Appendix II gives listings of the computer programmes used in this investigation and quoted in Chapter 3.

Appendix II A is programme DEPTH which calculates the vertical depths of equally spaced points along inclined boreholes from the borehole survey data. The survey data may be entered as:

1) Vertical and horizontal co-ordinates of points along the borehole
2) Depth along borehole and inclination in degrees from the horizontal
3) Depth along borehole and vertical depth.

A spline function is used to interpolate between the surveyed points and depths along-hole are converted to the vertical. The programme was compiled by the author with the assistance of Dr D M Barrett.

Appendix II B is programme BETTER which converts the thermistor probe resistance, R, to temperature, T, using a polynomial fit of ln(R) to (1/T) with R in ohms and T in K. The polynomial co-efficients were determined by calibration against a platinum-resistance thermometer. Temperatures and temperature gradients (between successive measurements) are given as functions of depth. The programme was compiled by Dr S W Richardson.

Appendix II C is programme TOPO which calculates a correction to subsurface temperatures and temperature gradients due to topographic irregularities. The topography, digitized on a rectangular grid, is entered through subroutine HEIGHT, and averaged along circumferences of circles centred on the point to be corrected in subroutine SURCLE. Topographic corrections are calculated using the method of Jeffreys (1937) which is summarized in Section 3.3. The programme was compiled by Dr P C England; for further details see England (1976).

APPENDIX II A.

DOCUMENT DEPTH

```
*FORTRAN,
      LIST
      PROGRAM DEPTH
      INPUT=CARD
      OUTPUT=LPT
      COMPRESS INTEGER AND LOGICAL
      TRACE 2
      END
CCCCCCCCCCCCCCCCCCCCCCCCCCCCCCCCCCCCCCCCCCCCCCCCCCCCCCCCCCCCCCCCCCCCCCC
C     PROGRAM USES SPLINE FUNCTION TO FIND TRUE DEPTH OF POINTS
C     DOWN AN INCLINED BOREHOLE
C
C     INPUT FORMAT
C          TITLE
C          LXY,LAINT
C          LSTEP
C          BOTTOM
C          MODE
C          X(I) Y(I)
C
C     LXY=NO. OF POINTS -1
C     LXINT=NO. OF POINTS IN SPLINE,LXINT=LARGEST INTEGER SMALLER
C           THAN X(LXY) - X(1)
C     LSTEP=INTERVAL OF TERM. (EASIEST TO SET 5,10 OR 20 METRES)
C     BOTTOM=LENGTH OF FINAL MEASUREMENT
C     MODE=-1,0 OR +1
C          -1 : X IS VERTICAL AND Y IS HORIZONTAL CO-ORDINATE
C               OF POINT DOWN BOREHOLE
C           0 : X IS LENGTH ALONG BOREHOLE,Y IS INCLINATION
C               TO VERTICAL
C          +1 : X IS LENGTH ALONG BOREHOLE,Y IS TRUE DEPTH
C
C     NOTE : PROGRAM WILL NOT EXTRAPOLATE BEYOND LAST SURVEY
C            POINT
CCCCCCCCCCCCCCCCCCCCCCCCCCCCCCCCCCCCCCCCCCCCCCCCCCCCCCCCCCCCCCCCCCCCCCC
      MASTER DEPTHCOM
C     COMMON /A1/ X(200),Y(200),A(3,200)
      DIMENSION XI(200)
      DIMENSION Z(200),XL(200)
      DIMENSION TT(10)
      READ(5,100)(TT(JJ),JJ=1,10)
100   FORMAT(10A8)
      WRITE(6,200)(TT(JJ),JJ=1,10)
200   FORMAT(1H1,///,1X,80('='),/,1X,10A8,/,1X,80('='))
      READ(5,101)LXY,LXINT
101   FORMAT(2I0)
      WRITE(6,201)
201   FORMAT(///,4X,'INPUT DATA')
      WRITE(6,202)LXY,LXINT
202   FORMAT(//,3X,'LXY    = ',I4,/,3X,'LXINT = ',I4)
      READ(5,103)LSTEP
103   FORMAT(I0)
      READ(5,102)BOTTOM
102   FORMAT(F0.0)
      WRITE(6,203)LSTEP,BOTTOM
203   FORMAT(3X,'LSTEP = ',I4,//,3X,'BOTTOM = ',F7.2)
      READ(5,104)(X(I),Y(I),I=1,LXY)
104   FORMAT(2F0.0)
      IF(MODE)300,301,302
300   WRITE(6,204)
204   FORMAT(////,11X,'VERT. CO-ORD.',7X,'HORIZ. CO-ORD.',/)
      GO TO 1000
301   WRITE(6,205)
205   FORMAT(////,14X,'LENGTH',6X,'INCLINATION',/)
      GO TO 1000
302   WRITE(6,206)
206   FORMAT(////,14X,'LENGTH',6X,'VERT. DEPTH',/)
1000  WRITE(6,207)(X(I),Y(I),I=1,LXY)
207   FORMAT(1X,2F20.2)
      XINT=0.
      XSTEP=1.
      CALL SPLINE(LXY)
      CALL SPLINT(X,Y,Z,XL,LXY,XINTF,XINTO,YINT)
      XFINC=XINTF*X(1)+X(1)*(XINTF-1)
      M=LXINT+1
      YOUT(M)=YINT(LXINT)+YFINC
      WRITE(6,210)(TT(JJ),JJ=1,10)
      WRITE(6,208)
208   FORMAT(///,17X,'OUTPUT DATA')
      WRITE(6,209)
```

```
300 FORMAT(//,15X,'LENGTH',15X,
    WRITE(H(I))
    N=N+2
    Z(1)=
    IF(
105 DO 306 I=1,
306 Z(I)=YI.T(I)
    GO TO 1002
    DO 307 I=1,
307 YI
    DO 308 I=2,
308 Z(I)=Z(I-1)+SI ((YI.T(I-1)+YINT(I))/2.)
    GO TO 1002
303 XL(1)=0.0
    N=N+1
    DO 309 I=2,
309 XL(I)=XL(I-1)+SQRT((YINT(I)-YI.T(I-1))**2+1.)
    DO 310 I=2,N.
    E=FLOAT(I-1)
    DO 311 J=2,
    H=XL(J-1)
    C=XL(J)
    D=FLOAT(J-2
    IF(E-C.LT.0.0)GO TO 312
311 CONTINUE
312 Y(I)=D+(E-H)*(C-D)
310 CONTINUE
1002 DO 1003 I=1,N,LSTEP
    ZI=FLOAT(I-1)
    ZT=Z(I)
    WRITE(6,207)ZI,ZT
1003 CONTINUE
    IF(I-NT.NE.2)GO TO 1005
1004 ZT=Z(N)+(Z(N)-Z(N-1))*(ZI-FLOAT(I))
    WRITE(6,207)ZI,ZT
1005 STOP
    END

CCCC
```

```
      (illegible)
      A(1,IA)=0.
      A(2,IA)=0.
      A(3,IA)=0.
      A(4,IA)=0.
      Y1=Y(IA+1)
      Dx1=X(IA+2)-X(IA+1)
      IF(Dx1.EQ.0.) GO TO 10
      Y1P=(Y(IA+2)-X(IA+1))/Dx1
      GO TO 10
    2 CONTINUE
      Y0=Y1
      Y0P=Y1P
      Y1=Y(IA+1)
      Y1P=(Y(IA+1)-Y(IA))/Dx
      IF(IA.EQ.LXY1) GO TO 4
      Dx1=X(IA+2)-X(IA+1)
      IF(Dx1.LE.0.) GO TO 4
      Y2P=(Y(IA+2)-Y(IA+1))/Dx1
      YPMAX=AMAX1(ABS(Y1P),ABS(Y2P),YEPS)*0.01
      YEPS=AMAX1(YEPS,YPMAX*1.E-3)
      WT1=1./AMAX1(YPMAX,ABS(Y1P))
      WT2=1./AMAX1(YPMAX,ABS(Y2P))
      Y1P=(Y1P*WT1+Y2P*WT2)/(WT1+WT2)
    4 CONTINUE
      A1=Y0
      A2=Y0P
      YA1=(Y1-A1-A2*Dx1)/(Dx1*Dx1)
      YA2=(Y1P-A2)/Dx1
      A4=(YA2-2.*YA1)/Dx
      A3=YA1-A4*Dx
      A(1,IA)=A2
      A(2,IA)=A3
      A(3,IA)=A4
   10 CONTINUE
      RETURN
      END
```

```
CCCC
```

APPENDIX II.

DOCUMENT BETTER

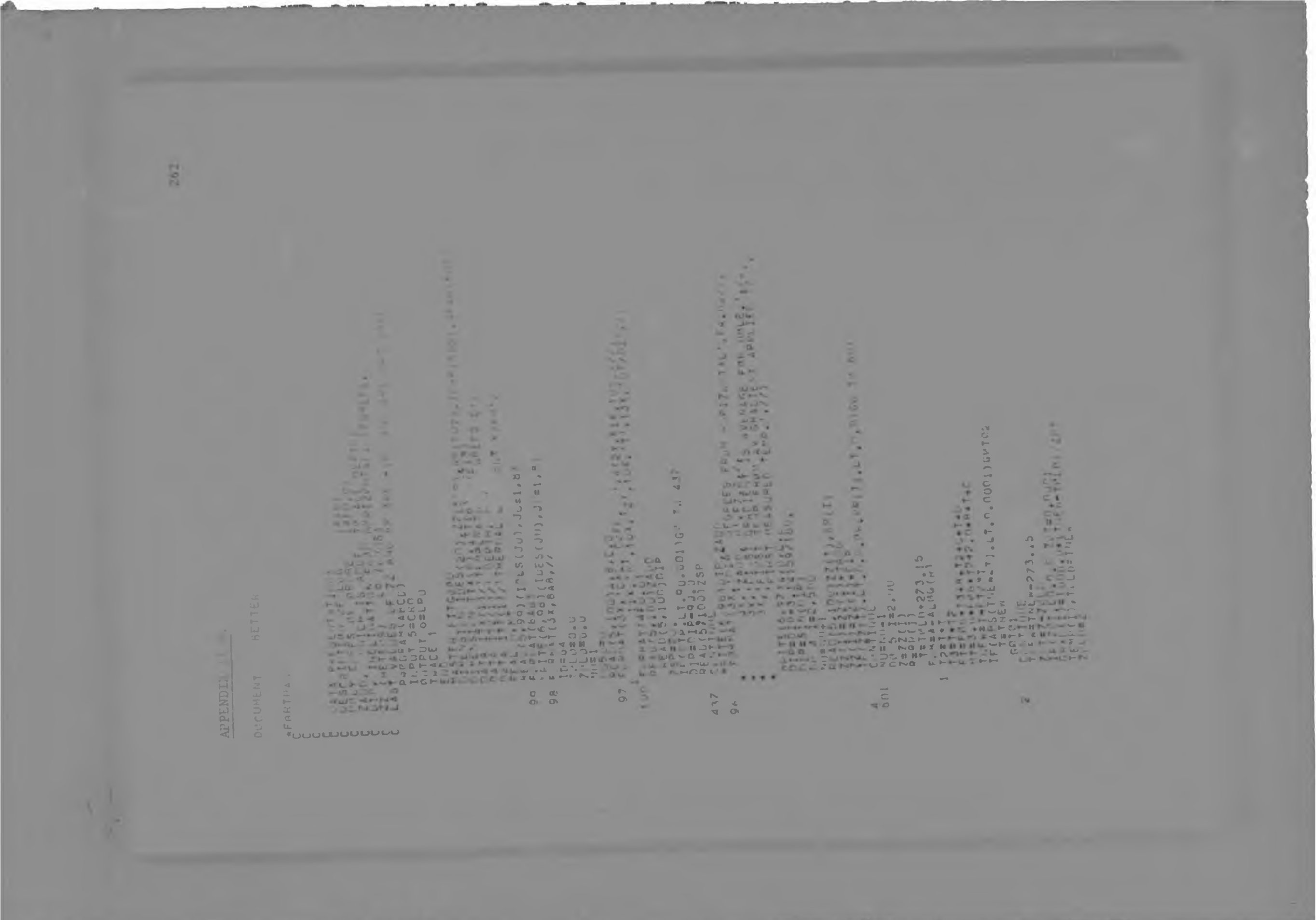

```
      IF(GRAD(I).GT.SL.)GRAD= GSL+1
     GRAD(I)=(TE-T(NU)-TEMP(2))*1.
     T=AMIN1((T+AMAX1(TT,TLES(I))
     IF(GRAD(1)=LT.0.)GRAD(I)=G
     ZSSC1=AINT((ZZ(NU)-Z(1)+2SP
     ZSSC1=ZSC+1.
     ZZ(1)=0.
     GRAD=AT(1,GSD)/FLOAT(I)
     DO 1 I=1,NU
     T=AMIN1((T+AMAX1(TT,TLES(I))
     IF(GRAD(I).LT.0.)GRAD(I)=0.
     ZSSC1=AINT((ZZ(NU)-Z(1))+2SP
     ZSSC1=ZSC+1.
     ZZ(1)=ZSP
     GGG1=0.
     IF(NU.EQ.1)GO TO 80
     TT1=(TMAX-TT)*GRAD(1)+TT
     TT2=1.
     IF(TMAX-TT1.GT.20.)GO TO 81
     TT2=2.
     CALL SCALE(TEMP(1),10.,NU,1)
     TT2=TEMP(NU+2)
     GRAD(NU+1)=GG1
     GRAD(NU+2)=GG2
     TEMP(NU+1)=TT1
     TEMP(NU+2)=TT2
     ZZ(NU+1)=ZZ1
     ZZ(NU+2)=ZZ2
     CALL SYMBOL(2.,0.,.15,TLES,0.,IU)
     CALL AXIS(2.,0.,TEMP,-21,10.,0.,TT,GG2
     GG1=(GRAD(1)-GG1)/GG2
     CALL PLOT(0.,0.,3)
     CALL PLOT(7SC,0.,2)
     Z2=FLOAT(I)
     Z1=Z2-0.5
     CALL PLOT(Z1,G1,2)
     CALL PLOT(Z2,G1,3)
     Z1=(ZZ(2)-ZZ)/GG2
     CALL PLOT(Z1,G1,3)
     CALL PLOT(7SC,0.,3)
     Z2=FLOAT(I)
     Z1=Z2-0.5
     CALL PLOT(Z1,G1,2)
     CALL PLOT(Z2,G1,3)
     Z1=(ZZ(2)-ZZ)/GG2
     CALL PLOT(Z1,G1,3)
     CALL PLOT(7SC1,0.,3)
     GRAD(I+1)=10.*GG2
     IF(GRAD(I+1).GT.10.*(W2)GRAD(I+1)=GRAD(I+1)-GG1)/GG2
     G1=(GRAD(I+1)-GG1)/GG2
     Z1=(Z1+Z2)*0.5
     Z2=Z1
     CALL PLOT(Z1,G1,2)
     CALL PLOT(Z2,G1,3)
     CALL PLOT(Z2,GM,PU,1)
     CALL PLOT(7SC1,0.,999)
77   CALL STOP
     END
     FINISH
     LINK LIB CALCOMP
     END
```

APPENDIX II C.

```
DOCUMENT    T,P,
*FORTRAN
C
C       INPUT FORMAT
C  GR G DA DB
C  DD RR FF
C  DIP TYPE DIFF          (X, F, I=)
C  STEM(1 TO 4) (8.5 4.5 FOR U.S.)
C  N M1 M2 N1 N2
C  FM (0.3048E096 OR 1.)
C  ----------------
C  INTEGER TOPOGRAPHY
C  ----------------
C  XP YP ZZ (0. FOR BOREHOLE)  SH (KM)
C  TITLE
C  TERMINATOR (2001. 0. 0. 0.)

      LIST
      PROGRAM(T,P2)
      INPUT 5=CI.0
      OUTPUT 6=LP0
      TRACE 1
      END
      MASTER TOPMEAN
      COMMON /BIG/ TIABLE(41,41),ANTIBAR(1
      DIMENSION STEM(8),T(100),A(2),I(
      DATA PI/3.14159/
      COMMON/D27/ AVAVH(200),DIST(200),HT(200),PHT(200)
      INTEGER XP,YP
      INTEGER DA,DB


C  PROGRAM OPERATES ON TOPOGRAPHY DIGITISED ON A GRID INPUT THROUGH HEIGHT.
C
C  GRID SPACING IS PE KILOMETERS
C  HEIGHTS AVERAGED ALONG THE CIRCUMFERENCE OF CIRCLES ABOUT THE POINT
C  TO BE CORRECTED. ARC LENGTH BETWEEN SUCCESSIVE SAMPLES
C  THE SPACING OF THE CIRCLES          IS 1/G GRID UNITS (LET G=A FOR 1KM GRID)
C  THERE ARE DP CIRCLES
C  RR = MAX HEIGHT SAMPLE SPACING ON CIRCLES (LET RR=FF/2)
C
C  FOR A BOREHOLE PUT ZZ=0 FOR CORRECTION IS MADE TO DEPTHS OF DA
C  METERS IN STEPS OF DB METERS.
C
C  DD = AVERAGE GRADIENT IN METERS (DIP/KM)
C  STEM GIVES SURFACE TEMP OF SOUTH AND NORTH SLOPES IN THE FORM
C  STEM(I) OF II = STEM(2) + (AV SURFACE HEIGHT)
C
C  FOR ANISOTROPIC STRATA DIP AND DIPD (AZIMUTH FROM GRID NORTH)
C  ARE IN DEGREES AND DIFF = (K PARALLEL)/(K PERP TO STRATA)
C
C  XP,YP IS THE M,N GRID REF OF THE POINT TO BE CORRECTED
C  SH = SURFACE HT OF POINT IN KILOMETERS
C  ZZ = DEPTH BELOW SURFACE (KM) BUT SEE ABOVE FOR A BOREHOLE
C
C  TI = TITLE
C  TERMINATOR IS XP > 1000.


      READ(5,100)GG,G,DA,DB
  100 FORMAT(6I0)
      READ(5,51)DD,RR,FF
   51 FORMAT(3F0.0)
      WRITE (6,103) XP,YP,ZZ,SH,DD,FF,RR
  103 FORMAT(////,5X,'GG =  G =  DA =  DB =  '
     1,//,12,A10,13),//,
     2,5X,'DD = ',F5.4,' DEG C/KM, FF = ',F6.3
     3,' RR = ',F6.3)
      READ(5,104) DIP,DIPD,DIFF
      IF(DIP.LT.1.)DIP=1.
      WRITE(6,102)DIP,DIPD,DIFF
  102 FORMAT(/,1X,'DIP = ',F5.2,' DEGREES AT ',F6.2,
     1,1X,'PARALLEL TO PERPENDICULAR CONDUCTIVITY RATIO IS ',
     2F6.2,'+1',//)
      READ(5,107)(STEM(I),I=1,4)
  107 FORMAT(4F0.0)
      STEM(5)=STEM(1)/2+STEM(3)/2
      STEM(6)=(STEM(2)+STEM(4))/2
      WRITE(6,108)(STEM(I),I=1,6)
  108 FORMAT(/1X,'SOUTH SLOPE TEMPERATURE = ',F6.4,' + ',F6.4,' DEG/KM',
     1/1X,'NORTH SLOPE TEMPERATURE = ',F6.4,' + ',F6.4,' DEG/KM',
     2/1X,'AVERAGE TEMPERATURE     = ',F6.4,' + ',F6.4,' DEG/KM')
      THE=DIP*PI/180.
      PSI=PI/2-DIPD*PI/180.
      PHI=ATAN(SQRT(DIFF)*TAN(THE))
```

```
      A1=COS(THE)*COS(PSI)/COS(PHI)
      A2=COS(THE)*SIN(PSI)/COS(PHI)
      A3=-SIN(PSI)
      A4=COS(PSI)
      A5=SIN(PHI)/SIN(THE)
      WRITE(6,1001)A1,A2,A3,A4,A5
 109  FORMAT(//,5X,'TRANSFORMATION MATRIX:',
     1       //,5X,F7.4,2X,F7.4,2X,'0.000',
     2       //,5X,F7.4,2X,F7.4,2X,'0.000',
     3       //,5X,'0.000','0.000',F7.4)
      AKH=(COS(THE)**2+(1FF+1)*SIN(THE)**2
      WRITE(6,1091)AKH
 1091 FORMAT(//1X,'VERTICAL CONDUCTIVITY ',F12.4///)
      STEM(6)=(10-STEM(6))
      STEM(4)=(10-STEM(4))
      STEM(2)=(10-STEM(2))
      CALL HEIGHT(M,N,A5)
  10  READ(5,1044) XP,YP,ZZ,SH
      XM=XP
 1044 FORMAT(4F).0)
      IF(XP.GT.1000) STOP
 104  FORMAT(3F0.0)
      READ(5,1004)(T1(JJ),JJ=1,10)
 1004 FORMAT(10A4)
      WRITE(6,1005)(T1(JJ),JJ=1,10)
 1005 FORMAT(1H1,1X,80('='),/,14,10A4,/,14,80('='))
      WRITE(6,105) XP,YP,ZZ,SH
 105  FORMAT(//,1X,' POSITION CORRECTED:X= ',F6.3,' Y= ',F6.3,
     1' DEPTH =',F8.4,' M',//,2X,'SURFACE HEIGHT =',F6.3,' M',////)
      IX=AINT(XP)
      IY =AINT(YP)
      IXX =IX+1
      IYY=IY+1
      A=Z(IX,IYY)
      B=Z(IXX,IYY)
      C=Z(IX,IY)
      D=Z(IXX,IY)
      NM=0
      XPM=XP
      YPM=YP
 107  E=XP-IX
      F=YP-IY
      Z1=(C+(D-C)*E)*(1-F)+(B+(D-B)*E)*F
      Z2=(C+(A-C)*E)*(1-E)+(D+(B-D)*E)*E
      ZC=(Z1+Z2)/2/A5
      DIFF=ZC-SH
      IF(ABS(DIFF).LE.0.01) GOTO 100
      G1=(D-C+B-A)/2
      G2=(A-C+B-D)/2
      GALL=SQRT(G1*G1+G2*G2)
      XP=XP-DIFF*G1/(GALL*GALL)
      YP=YP-DIFF*G2/(GALL*GALL)
      IF(ABS(XPM-XP).GT.1.OR.ABS(YPM-YP).GT.1)GOTO 195
      GOTO 107
 195  WRITE(6,1003)DIFF
 1003 FORMAT(1X,'HEIGHT IN ERROR BY  ',F12.6,' UNITS'//)
      XC=XP
      YC=YP
      ZC=SH
 100  WRITE(6,1006)XC,YC,ZC,ZF
      AVAVH(1)=STEM(6)+STEM(4)+STEM(2)+ZC+A5
      DO 109 I=2,NM+1
      W=FLOAT(I)-1.0
      DIST(I)=W*FF
      CALL SWOLF(M,N,XC,YC,A,Z,P,Q,PP,A1,A2,A3,A4,B,STEM,DIST)
      WHT(I)=IFIX(AVZ(3))
      AVAVH(I)=AVZ(1)
 109  HT(I)=AVZ(2)
      HT(1)=ZC
      CALL DEPCOR(ZZ,DETF,DW,AS,DA,DB,FF,G)
      GOTO 10
      STOP
      END
C
C
      SUBROUTINE DEPCOR(Z,DETF,DW,AS,DA,DB,FF,G)
      INTEGER DW,DA,DB,G
      COMMON/ZZ/ AVAVH(200),DIST(200),HT(200),WHT(200)
      DIMENSION DW(200),V(200)
      ZZ=Z
      NM=0
      IF(Z.LT.5)GOTO 2
      WRITE(6,902)
  902 FORMAT(///,1X,'SPECIFIED CORRECTION, DEPTH =200M.')
      Z=0.2
    2 CONTINUE
      WRITE(6,900)
  900 FORMAT(//1X,'DATA',6X,3X,'AV',4X,'AV + V',1X,3X,'CORRECTION'
     1,3X,'THICKNESS',5X,'AV',4X,'FACTOR',7X,'DEG C')
      AV=AVAVH(1)
      DO 910 I=1,NM+1
  910 AVAVH(I)=AVAVH(I)-AV
```

```
 905  CORR=.0
      Z=.5
      DO 1 I=1,NM1
      DD=SQRT(DIST(I)**2+Z*Z)
      IF(I.E
      IF(I.E
      V(I)=-AVAVM(I)*DIST(I)*Z/DD**3
C4    V(I)=-AVAVM(I)*(DIST(I)**3-Z**2*DIST(I))/DD**
C5    V(I)=-AVAVM(T)*DIST(I)/DD**3
 911  IF(I
      CORR=CORR+V(I)
      GOTO 112
 111  CORR=CORR+.5*V(I)
 112  RUN(I)=(CORR-V(I)-V(I))*FF/3./FLOAT(G)
   1  CONTINUE
      CORR=CORR-V(1)-V(NM1)
      CORR=CORR/3.*FF/G
      UK=0.
      DO 909 I=1,10
      III=NM1-I+2
 910  UK=UK+AVAVM(III)
      UK=UK/10
      CORC=-UK*Z/DD
      TOT=CORR+CORC
      IF(UK.E.1) GOTO 900
      DO 8 I=1,NM1
      WRITE(6,801) DIST(I),AV-VV(I),RUN(I),V(I),TOT(I)
  801 FORMAT(1X,F5.2,5A,F8.3,5X,F8.3,5X,F8.3,5X,F8.3,5X,F8.3,5X,F8.3)
      WRITE(6,910)CORR
  910 FORMAT('//1X,'CORRECTION FROM GRID   ',F6.4,' DEG C.')
      WRITE(6,911)CORC
  911 FORMAT(//1X,'INTEGRATED CORRECTION TO INFINITY   ',F6.4,' DEG C.')
      WRITE(6,903) TOT
  903 FORMAT(//,1X,'TOTAL CORRECTION = ',F6.4,' DEG C')
      IF (ZZ.LT.5) RETURN
      WRITE(6,904)
  904 FORMAT(//,6X,'LEFT',10X,'RIGHT',10X,'TEMPERATURE PERTURBATION',
     1  /,5X,'CORR CORR',5X,'TOT',10X,'GRAD',/)
      TOTAV=0.
      DO 3 J=1,DA+1,DR
        Z=FLOAT(J-1)/1000.
      GOTO 905
 906  CONTINUE
      GRAD=(TOT-TOTAV)/(DR*1.E-3)
      WRITE(6,907)Z,CORL,CORC,TOT,GRAD
      TOTAV=TOT
    3 CONTINUE
 907  FORMAT(10X,F8.4,4(1X,F7.4))
      RETURN
      END
```

```
C  RH = FACTOR WHICH CONVERTS HEIGHTS GIVEN IN METERS.
C  M1,M2,N1,N2 ARE SMALL (<10) UPPER INTEGERS MARKING COORDINATES
C  ON THE MAP AS FOLLOWS.
C  IN THIS EXAMPLE M=9  N=13  M1=3  M2=7  N1=5  N2=0
C
C                  NORTH
C     1  2 M1  4  5  6 M2  8  M
C  1  A     B     C     X     X
C  2
C  3  X     X     X     X     X
C  4
C N1  X     X  R  X  S  X     X
C  6          T  Z  Z  Z  Z
C  7  X     X  Z  X  Z  X     X
C  8          Z  Z  Z  Z  Z
C N2  X     X  Z  X  Z  X     X
C 10
C 11  Y     X     X     X     X
C 12
C  N  X     X     X     X     X
C                  SOUTH
C
C  THE INTEGER HEIGHTS ARE PRESENTED AS FOLLOWS:
C  A  M  C  X  X
C  X  X  X  X  X
C  X  X  X  X  X
C  X  X  X  X  X
C  X  X  X  X  X
C  X  X  X  X  X
C  X  X  X  X  X
C  S
C  Z  Z  Z  Z
C  Z  Z
C  Z  Z  Z  Z
C  Z  Z
C
C  IF M1=0 THE HEIGHT AT EVERY GRID INTERSECTION IS READ IN
C  A STRAIGHTFORWARD ORDER
C
C      SUBROUTINE HEIGHTIN(M,N,RH)
C      DIMENSION Z(M1:M2,N1:N2),RH(M,N)
```

```
      SUBROUTINE
      READ(5,20,END=20)M1,M2,N1,N2
      READ(5,1A,ERR=20)F
1A    FORMAT(W0F0.0)
20    FORMAT(80)
      WRITE(6,19)M1,M2,N1,N2
19    FORMAT(1X,'M1  M2  N1  N2',6X,'S',
     1 /1X,I4,I4,I4,I4,
     2 //,1X,'M1=',I3,2X,'M2=',I3,2X,'N1=',I3,2X,'N2=',I3)
      IF(M1.EQ.0)GO TO 3
      DO 23 IN=1,2
      DO 21 IM=1,M
      KK(IM,IN)=0
21    IF(IM.LE.(M/2))GO TO 22
      READ(5,20,END=20)(KK(IM,IN),IM=1,M,2)
      DO 22 IM=2,M-1,2
      KK(IM,IN)=INT(0.5*(KK(IM-1,IN)+KK(IM+1,IN)))
22    CONTINUE
23    CONTINUE
      DO 24 IM=2,M-1,2
      DO 24 IN=1,N
      KK(IM,IN)=NINT(0.5*(KK(IM,IN+1)+KK(IM,IN-1)))
24    CONTINUE
      DO 25 IN=1,N2
      NL=(M-M/2)
      IF(NL.EQ.0)READ(5,20,ERR=20)(KK(IM,IN),IM=1,M,2)
      IF(NL.EQ.1)READ(5,20,ERR=20)(KK(IM,IN),IM=1,M-1,2)
25    CONTINUE
      GO TO 27
26    WRITE(6,28)
      STOP
27    CONTINUE
28    FORMAT(1X,'FAILURE IN READING ROUTINE HEIGHT')
      DO 3 IN=1,N
      DO 3 IM=1,M
      HT(IM,IN)=KK(IM,IN)*FM
29    FORMAT(1X,24I5)
      SUMZ=SUMZ+HT(IM,IN)
      ZHT(IM,IN)=(HT(IM,IN)+15+1.E-03
3     CONTINUE
      KM=(M-1)/24 +1
      DO 34 K=1,KM
      ML=(K-1)*24+1
      MU=K*24
      IF(MU.GT.M)MU=M
      DO 35 IN=1,N
      WRITE(6,29)(KK(IM,IN),IM=ML,MU)
34    CONTINUE
      WRITE(6,37)
37    FORMAT(51X,'SOUTH',////)
35    CONTINUE
      AVZ=SUMZ/FLOAT(M*N)
      WRITE(6,222) AVZ
222   FORMAT(////,1X,'AVERAGE HEIGHT OF TERRAIN ABOVE =',F5.1,
     1' METERS',///)
      RETURN
30    DO 31 IN=1,N
31    READ(5,20,ERR=20)(KK(IM,IN),IM=1,M)
      GO TO 27
      END

C
C
      SUBROUTINE SUMCLE(W,XO,YO,A,Z,M,N,PH,A1,A2,A3,A4,G,STEM,O)
      COMMON /B1/ Z(81,81)
      DIMENSION STEM(O),AVZ(3)
      INTEGER P,G
      DATA PI/3.14159/
      SUMZ,ZHAM=0.
      IJCH=0
      T=A1+A3+A1
      U=2*A1*A2+A3*A4)
      V=A2*A2+A4*A4
      IG= NINT(2*PI*M/PH)
      IF(IG.LT.32) IG=32
      DO 1 I=1,IG
      P=I
      TH=2*PI*P/IG
      C=COS(TH)
      SI=SIN(TH)
      R=W/SQRT(T+C*U+C*C*V+S*S*V+S*T
      X=XO+R*C
      Y=YO+R*S
      IX=AINT(X)
      IY=AINT(Y)
      IF(IX.GT.(M-1).OR.IY.GT.(N-1).OR.IX.LT.1.
     1OR.IY.LT.1) GO TO 2
      IAX =IX+1
      IYY=IY+1
      A=Z(IX,IYY)
      B=Z(IAX,IYY)
      C=Z(IX,IY)
      D=Z(IAX,IY)
```

```
      E=X-IX
      F=Y-IY
      Z1=(C+(D-C)*F)*(1-F)+(A+(B-A)*F)*F
      Z2 = (C+(A-C)*F)*(1-F)+(D+(B-D)*F)*E
      ZIN=(Z1+Z2)*0.5
      IF((A-C).GT.0.AND.(B-D).GT.[illegible]) GOTO 600
      IF((C-A).GT.0.AND.(D-B).GT.[illegible]) GOTO 601
      ZINCR=STEM(6)*(Z1+Z2)/2+STEM(5)
      GOTO 602
600   ZINCR=STEM(4)*(Z1+Z2)/2+STEM(3)
      GOTO 602
601   ZINCR=STEM(2)*(Z1+Z2)/2+STEM(1)
602   SUMZ=SUMZ+ZINCR
      ZBAR=ZBAR+ZIN
      INCR=INCR+1
2     CONTINUE
1     CONTINUE
      IF(INCR)603,603,604
604   AVZ(1)=SUMZ/INCR
      AVZ(2)=ZBAR/INCR
      AVZ(3)=FLOAT(INCR)
      RETURN
603   AVZ(1)=0.
      AVZ(2)=0.
      AVZ(3)=0.
      RETURN
      END
      FINISH
*END
```

APPENDIX III ANALYTICAL TECHNIQUES FOR THE DETERMINATION OF U, Th AND K

Delayed neutron activation analysis

The DNAA method established at the South African Atomic Energy Board (AEB) provides an economical and rapid means of measuring U concentrations with relatively high sensitivity at abundance levels as low as 1 p.p.m. A detailed description of the technique and the principles it employs is given by Smit (1976) in an internal AEB publication.

Duplicate samples of about 200 mg of powdered rock were sealed in polythene capsules which were sent in batches to AEB for analysis. The capsules were inserted into larger polythene containers, irradiated in the SAFARI 1 reactor and counted for pre-selected times. A thorium correction was provided by irradiating the duplicate sample of each pair inside a cadmium shield thereby permitting the effects of U and Th to be isolated. Other interfering elements are not sufficiently abundant in most geological samples to affect the U count rate significantly. Background corrections were provided by running a number of blanks with each batch of samples. The method is relatively free from matrix effects and specially prepared U solutions were used as standard reference materials.

The precision and accuracy of the method was determined jointly by Smit (1976) and R J Hart (NPRU, University of the Witwatersrand) using samples analysed by independent techniques. The relative precision is within 15% at the 1 p.p.m. level of abundance, 5% at 10 p.p.m. and better at higher concentrations. The mean U concentrations rarely differed from

DNAA data obtained at the Atomic Energy Research Establishment (AERE), Harwell, England, and isotope dilution (ID) data obtained at BPI by more than the statistical uncertainties. Some of these data are given in columns 3, 4 and 5 in the first half of Table III-1.

The results of further comparative tests carried out during the course of this study are also summarized in Table III-1. Column 2 gives the mean and standard deviation of replicate analyses on several samples. DNAA and ID data in columns 3, 4 and the first half of column 5 were provided by R J Hart along with all samples prefixed VT and KK. Samples prefixed L and B and the accompanying ID data were provided by J M Barton (BPI Geophysics, University of the Witwatersrand). Agreement between the data is good in most cases.

Neutron activation analysis

U and Th determinations by NAA were made by R J Hart at the Nuclear Physics Research Unit (NPRU), University of the Witwatersrand. Details of the method are summarized by Hart et al (1980). Samples of powdered rock (approximately 300 mg) were sealed in quartz vials which were placed in cadmium cans and irradiated in the SAFARI I reactor at AEB. Homogeneous iron wire was wrapped around each vial to monitor the neutron flux received by each sample. Samples were counted at NPRU for 60 minutes after optimum decay times.

Standardization was against a local granite sample whose U and Th concentrations were obtained by comparison with accurately determined gravimetric preparations. Five repeat measurements on the standard yielded 2-σ reproducibility errors of 3,3% for U (U concentration =

Table III-1 Comparison of U determinations by DNAA at AEB and Harwell and by ID at BPI. Concentrations in p.p.m.

Sample	DNAA (AEB)[1]	DNAA (AEB)[2]	DNAA (AERE)[2]	ID (BPI)[3]
VT 40	27,0	28,5	27,50	27,52
VT 41	19,2	20,7	19,67	19,37
VT 42	2,6 ± 0,2 (5)	-	2,72	-
VT 127	5,2 ± 0,4 (8)	5,23	5,18	5,40
VT 462	~0,3 (3)	0,20	0,13	0,20
VT 505	1,0 ± 0,1 (5)	0,96	0,97	1,13
KK 4	~0,3 (4)	0,24	0,2[illegible]	0,24
KK 8	1,5 ± 0,5 (4)	1,32	1,38	1,42
KK 10	0,9 ± 0,1 (2)	0,63	0,65	0,72
KK 15	0,4 ± 0,1 (2)	0,22	0,34	0,38
KK 16	2,4 ± 0,2 (2)	2,65	2,80	3,05
L 19	~0,3 (2)	0,3	-	0,30
L 21	0,4 ± 0,2 (4)	0,8	-	0,53
L 68	0,7 ± 0,2 (5)	0,7	-	1,17
L 73	2,1	1,9	-	1,90
B-75-24	9,5 ± 0,5 (3)	10,2	-	-
B-75-61	9,8 ± 1,5 (2)	9,8	-	-
B-76-5	~0,3 (2)	0,1	-	-
B-76-13	3,8 ± 0,4 (2)	4,8	-	-
B-76-22	3,1 ± 0,5 (2)	4,7	-	-
B-72-24	0,9 ± 0,3 (3)	1,0	-	-
B-76-104	1,1	-	-	1,49
B-76-113	~0,2	-	-	0,66

1 This tudy: mean, standard deviation, number of analyses

2 Analyses by R J Hart

3 Analyses by R J Hart or J M Barton

18,4 p.p.m.) and 2,2% for Th (Th concentration = 43,3 p.p.m.). A comparison of U and Th determinations by AA and ID for six granite samples from Granite Mountains (Wyoming), the U.S.G.S. basalt standard BCR-1 and a mafic granulite from Vredefort, South Africa, reveals excellent agreement between the two methods over the concentration ranges: U = 0,4 - 56 p.p.m. and Th = 1 - 63 p.p.m. The data are summarized by Hart et al (1980).

X-ray fluorescence spectrometry

Thorium

Approximately sixty samples were analysed for Th by XRF in the Department of Geochemistry, University of Cape Town (UCT) by R J Hart. The operating conditions were the routine procedures that have been adopted at UCT and are described by Cherry et al (1970) and Reid (1977). Loose powders were used and standardization was against four U.S.G.S rock standards (G-1, G-2, GSP-1, AGV-1). In order to estimate the precision and accuracy of the analyses replicate measurements were made on the U.S.G.S. standard BCR-1 and seven samples from Vredefort; the results are compared with published data obtained using other techniques in Table III-2. Reproducibility errors were commonly better than 10% but some results, particularly those for low Th concentrations, differ considerably from data obtained by DNAA at AERE (Table III-2). Hart et al (1980) showed that XRF only yields results which are comparable with intrinsically more accurate techniques such as ID at relatively high concentration levels (> 10 p.p.m.).

A further fifteen samples were analysed by the author in the Department

[illegible]

[illegible]	Th (ppm)*	Published	Source
[illegible]	[illegible]	[illegible]	Abbey (1977)
[illegible]	[illegible]	[illegible]	
[illegible]	[illegible]	[illegible]	
[illegible]	[illegible]	[illegible]	
[illegible]	[illegible]	[illegible]	Watt et al (1981)
[illegible]	[illegible]	[illegible]	UMAA (ABIIE)
[illegible]	[illegible]	[illegible]	
[illegible]	[illegible]	[illegible]	
[illegible]	[illegible]	[illegible]	

* mean, standard deviation, number of analyses

[illegible] mineralogy, Oregon University (OU). Operating conditions [illegible] those used at UCT except that pressed pellets were used instead of loose powder. Th determination was achieved by comparison [illegible] international rock standards (W-1, BCR-1, AGV-1, G-A, G-2, [illegible], SDC-1 and SCP-1 using Th concentrations recommended by Abbey (1977). Th concentrations were determined for ten samples which were previously analysed by XRA in (PAU). The data are compared in Table III-3. In most cases agreement is within 2 r.s.d.s. Relatively large discrepancies for [illegible], TCP 1411 and BKE 9340 may partly be due to sample [illegible]

Table III-3 Comparison of Th Concentrations (in p.p.m.) obtained by XRF at [illegible] and NAA at NECSU

Sample	XRF (OU)	NAA (NECSU)
KC 131.7	[illegible]	[illegible]
KC 114.4	[illegible]	[illegible]
KC 143.6	[illegible]	[illegible]
KC 98.7	[illegible]	[illegible]
KC 116.8	[illegible]	[illegible]
KC 208.1	[illegible]	[illegible]
CCX 1370	[illegible]	[illegible]
CCX 1472	[illegible]	[illegible]
HKE 1250	[illegible]	[illegible]
HKE 850	93.3	101.5

Preparation

[illegible] concentrations were determined by XRF in the Department of [illegible] University of the Witwatersrand and the Department of Geology and Mineralogy, Oxford University, using pressed powder pellets. Analytical procedures followed at both establishments were those described by Bar[illegible] (1978). The samples were broadly divided into groups of granitic and mafic composition and calibrated against international rock standards of similar composition. A mass absorption correction was not applied. The concentrations of the standards were those recommended by Abbey (1977). Each pellet was analysed at least twice and, in most cases, the results

agreed to within 2% of the quoted K concentrations.

Gamma-ray spectrometry

U, Th and K concentrations were determined by GRS at the Atomic Energy Research Establishment (AERE), Harwell, England, by R Thoreau. Rock samples were crushed to a maximum grain size of 2 mm, and approximately 400 g were weighed into plastic cans and sent to AERE to be counted. Calibration was against two commercially available USAEC standards (No. 77A and No. 84A) and a rock sample accurately spiked at Oxford University (U = 117.5 p.p.m., Th = 191.4 p.p.m.).

The results of replicate measurements made over a period of two years on a monitor sample (DC 46) are summarized in Table III-4. The 1-σ reproducibility for all three elements is approximately 2%. Radioelement concentrations were determined in three aggregate samples and are compared with data obtained by NAA, DNAA or XRF in Table III-5. Each sample was composed of several smaller samples which had a small range in U, Th and K contents; the NAA, DNAA and XRF data are average concentrations of the component fractions. Agreement between the methods is good in all cases. The cost of GRS analysis prohibited more extensive tests.

Table III-4 Determination of U, Th and K in sample DC 46 by gamma-ray spectrometry

	U (p.p.m.)	Th (p.p.m.)	K (%)
	3,67	19,7	3,06
	3,64	20,1	3,19
	3,72	19,9	3,13
	3,71	19,4	3,09
	3,69	20,5	3,16
	3,66	20,2	3,22
	3,54	19,9	3,12
mean	3,67	20,0	3,14
std. dev.	0,05	0,4	0,06

Table III-5 Comparison of U, Th and K determinations by GRS with data obtained by DNAA, NAA or XRF

Sample	U (p.p.m.)		Th (p.p.m.)		K (%)	
	GRS	Other	GRS	Other	GRS	Other
KG	1,45	(1,31 (DNAA) (1,46 (NAA)	10,1	9,2 (NAA)	0,84	0,94 (XRF)
POG 2	1,65	1,72 (DNAA)	--		--	
POG 3	4,31	4,55 (DNAA)	--		--	

APPENDIX IV HEAT FLOW AND HEAT PRODUCTION DATA

The following tables list individual measurements used in the determination of heat flow and heat production. Each of the next twenty one pages is headed by the table number and borehole name and contains three subtables. All depth data in the following tables are true vertical.

z-T-β data

The first table under each heading gives depth (z in m), temperature (T in ^{o}C) and temperature gradient between successive temperature measurements (β in K/km). Superscripts + on T and β headings indicate that a topographic correction has been applied. Note that the first two tables under IV-11 JACOMYNS PAN are z-T-β data for PC2-27 and PC2-30.

z-K data

The second table lists depth (z in m) and/or sample number, measured thermal conductivity (K in $Wm^{-1}K^{-1}$) and rock type.

z-A data

The third table lists depth (z in m) and/or sample number plus depth range (in m), U concentration (U in p.p.m.), Th concentration (Th in p.p.m.), K concentration (K in %), density (ρ in 10^{3} kgm^{-3}), heat production (A in μWm^{-3}) and rock type. Superscripts 1-4 on U, Th and K headings indicate the analytical technique used to determine the element concentrations:

1 - delayed neutron activation analysis

2 - neutron activation analysis

3 - X-ray fluorescence

4 - gamma-ray spectrometry.

In the sample descriptions, most rock types are qualified by prefixing with the predominant minerals present; the following abbreviations have been used:

q – quartz (quartzose)

f – feldspar (feldspathic)

b – biotite

a – amphibole

g – garnet

c – chlorite

Tab. 1 Analysen der Gesteine der Serie

#											
166,0	34,217	-	178,9	,752	16,389	498,1	40,874	25,164	634,3	34,430	19,446
170,3	24,961	18,224	294,8	3,140	19,639	494,1	31,293	17,231	639,3	34,830	19,337
175,9	25,044	19,210	318,8	28,426	14,096	499,7	31,635	18,933	679,5	35,186	17,845
179,9	25,192	17,442	338,3	28,841	9,217	519,6	32,695	20,156	699,3	37,367	19,048
179,9	25,961	22,347	359,9	28,935	13,223	539,8	32,649	20,484	719,4	35,921	17,174
189,9	26,269	19,942	379,3	29,261	10,427	559,6	32,855	20,280	739,4	36,498	18,929
219,8	26,469	20,275	399,7	29,665	20,193	579,6	33,280	19,873	759,4	36,666	18,139
229,8	27,034	17,934	419,7	30,261	19,663	599,4	33,841	19,535	779,3	37,091	19,931
239,8	27,444	20,117	439,1	30,431	20,359	619,1	34,239	19,934	799,3	37,389	17,133

#		rock type			rock type			rock type
381,5	3,01	q-f gneiss	505,1	3,01	S augen gneiss	615,2	2,31	q-f gneiss
385,6	3,82	"	517,3	3,02	q-f gneiss	646,2	5,08	"
394,1	3,52	" gneiss	521,1	1,27	"	655,1	3,44	"
410,0	3,36	q-f gneiss	534,3	3,38	"	685,8	3,38	"
420,6	3,38	"	536,4	2,21	"	694,8	2,71	"
423,2	3,14	"	539,3	3,22	S augen gneiss	711,8	3,22	"
443,0	3,12	"	541,0	1,31	q-f gneiss	721,9	3,11	"
454,2	3,42	"	555,5	3,50	"	731,8	3,23	"
460,1	3,01	"	560,9	3,39	"	734,6	2,48	"
469,6	2,69	"	563,9	3,40	"	740,4	3,02	"
480,1	3,10	"	584,5	1,94	S gneiss	748,3	3,47	"
486,2	3,21	q-f-b gneiss	596,4	3,16	q-f gneiss	765,6	3,33	"
491,9	2,99	"	611,1	3,18	"	783,3	3,29	"
501,4	3,31	"	616,7	3,08	"			

#						rock type
381,5	13,8	62,0	3,38	2,39	8,80	q-f gneiss
385,6	8,5	35,0	3,42	2,61	4,44	"
410,0	8,9	60,0	4,37	2,41	6,17	"
420,6	15,5	231,0	3,27	2,39	18,84	"
423,2	29,0	64,0	3,61	2,46	11,61	"
443,0	29,0	73,0	3,03	2,81	11,56	"
454,2	36,0	33,0	3,38	2,82	12,02	"
460,2	23,4	85,3	3,41	2,65	11,81	"
480,1	29,0	84,0	4,01	2,42	17,35	"
486,2	1,2	32,0	3,27	2,66	3,41	q-f-b gneiss
491,9	9,2	39,9	3,34	2,67	9,29	"
501,4	19,4	96,0	3,70	2,82	11,03	"
511,2	-	45,3	3,74	2,73	-	q-f gneiss
524,1	4,0	8,0	3,18	2,56	1,38	"
539,3	18,9	17,0	4,68	2,18	4,38	S augen gneiss
594,4	8,4	12,0	3,76	2,64	3,21	q-f gneiss
618,7	3,9	2,0	4,85	2,63	1,35	"
695,1	9,2	15,0	3,03	2,64	2,47	"
685,8	12,8	114,0	3,68	2,39	11,23	"
694,8	4,0	116,0	7,97	2,63	8,16	"
734,6	7,9	60,0	4,81	2,66	3,60	"
740,4	20,4	32,0	3,30	2,63	7,72	"
765,6	17,5	37,0	4,88	2,65	7,31	"

[illegible]

z			z			z			z		
38,5	[illegible]	-	151,8	[illegible]	[illegible]	245,5	[illegible]	[illegible]	339,2	23,604	[illegible]
48,0	22,440	[illegible]	162,3	24,283	[illegible]	256,2	25,668	[illegible]	358,5	28,268	[illegible]
57,6	22,564	[illegible]	171,9	24,467	[illegible]	265,8	25,704	[illegible]	367,8	28,540	[illegible]
67,1	[illegible]	[illegible]	181,5	24,964	[illegible]	275,3	26,348	[illegible]	407,0	[illegible]	[illegible]
76,7	22,877	[illegible]	191,0	[illegible]	[illegible]	284,4	27,370	[illegible]	416,3	29,309	[illegible]
86,2	23,008	[illegible]	200,6	[illegible]	[illegible]	313,8	[illegible]	[illegible]	425,6	[illegible]	[illegible]
95,8	23,169	[illegible]	210,1	[illegible]	[illegible]	323,3	[illegible]	[illegible]	434,8	29,680	[illegible]
105,3	23,330	[illegible]	219,6	[illegible]	[illegible]	332,8	[illegible]	[illegible]	444,0	29,844	[illegible]
114,8	[illegible]	[illegible]	229,0	[illegible]	[illegible]	[illegible]	[illegible]	[illegible]	453,2	30,032	[illegible]
124,3	[illegible]	[illegible]	[illegible]	[illegible]	[illegible]	[illegible]	[illegible]	[illegible]	462,4	30,210	[illegible]
133,8	[illegible]	[illegible]	[illegible]	[illegible]	[illegible]	[illegible]	[illegible]	[illegible]	467,0	30,301	[illegible]
143,3	[illegible]	[illegible]	[illegible]	[illegible]	[illegible]	[illegible]	[illegible]	[illegible]			

z	K	rock type	z	K	rock type	z	K	rock type
69,8	4,26	q-f gneiss	[illegible]	3,63	q-f gneiss	[illegible]	[illegible]	b gneiss
[illegible]	[illegible]	"	[illegible]	[illegible]	augen gneiss	[illegible]	[illegible]	q-f gneiss
[illegible]	[illegible]	"	[illegible]	[illegible]	q-f gneiss	[illegible]	[illegible]	"
[illegible]	[illegible]	"	[illegible]	[illegible]	augen gneiss	[illegible]	[illegible]	"
105,0	[illegible]	"	[illegible]	[illegible]	q-f gneiss	[illegible]	[illegible]	"
[illegible]	[illegible]	"	[illegible]	[illegible]	"	[illegible]	[illegible]	"
[illegible]	[illegible]	"	[illegible]	[illegible]	augen gneiss	[illegible]	[illegible]	"
[illegible]	[illegible]	"	[illegible]	[illegible]	q-f gneiss	[illegible]	[illegible]	"
[illegible]	[illegible]	augen gneiss	[illegible]	[illegible]	"	[illegible]	[illegible]	b gneiss
[illegible]	[illegible]	q-f gneiss	[illegible]	[illegible]	b gneiss	[illegible]	[illegible]	"
[illegible]	[illegible]	"	[illegible]	[illegible]	q-f gneiss			

z					K	rock type
[illegible]	[illegible]	[illegible]	[illegible]	[illegible]	[illegible]	q-f gneiss
[illegible]	[illegible]	[illegible]	[illegible]	[illegible]	[illegible]	"
[illegible]	[illegible]	[illegible]	[illegible]	[illegible]	[illegible]	"
[illegible]	[illegible]	[illegible]	[illegible]	[illegible]	[illegible]	"
[illegible]	[illegible]	[illegible]	[illegible]	[illegible]	[illegible]	"
[illegible]	[illegible]	[illegible]	[illegible]	[illegible]	[illegible]	"
[illegible]	[illegible]	[illegible]	[illegible]	[illegible]	[illegible]	"
[illegible]	[illegible]	[illegible]	[illegible]	[illegible]	[illegible]	"
[illegible]	[illegible]	[illegible]	[illegible]	[illegible]	[illegible]	augen gneiss
[illegible]	[illegible]	[illegible]	[illegible]	[illegible]	[illegible]	"
[illegible]	[illegible]	[illegible]	[illegible]	[illegible]	[illegible]	augen gneiss
[illegible]	[illegible]	[illegible]	[illegible]	[illegible]	[illegible]	q-f gneiss
[illegible]	[illegible]	[illegible]	[illegible]	[illegible]	[illegible]	"
[illegible]	[illegible]	[illegible]	[illegible]	[illegible]	[illegible]	"
[illegible]	[illegible]	[illegible]	[illegible]	[illegible]	[illegible]	b gneiss
[illegible]	[illegible]	[illegible]	[illegible]	[illegible]	[illegible]	"
[illegible]	[illegible]	[illegible]	[illegible]	[illegible]	[illegible]	q-f gneiss
[illegible]	[illegible]	[illegible]	[illegible]	[illegible]	[illegible]	"
[illegible]	[illegible]	[illegible]	[illegible]	[illegible]	[illegible]	"
[illegible]	[illegible]	[illegible]	[illegible]	[illegible]	[illegible]	b gneiss

[illegible]

a	[illegible]	[illegible]	[illegible]	[illegible]	[illegible]	[illegible]	[illegible]	[illegible]	[illegible]	[illegible]	[illegible]
97,6	24,782	-	213,3	23,726	17,307	326,0	29,773	18,284	435,5	27,864	19,589
118,5	24,884	17,140	232,=	24,268	17,380	344,4	26,122	18,804	453,5	28,214	19,295
138,3	22,430	17,772	251,3	24,407	18,334	362,8	26,461	18,553	471,0	28,570	19,796
155,6	22,743	16,262	270,1	24,150	18,242	381,7	26,808	18,978			
174,9	23,052	16,946	288,8	25,089	18,144	399,2	27,161	19,418			
194,1	23,393	17,734	307,4	25,453	18,318	417,6	27,519	19,251			

a	[illegible]	rock type	a	[illegible]	rock type	a	[illegible]	rock type
124,8	3,24	q-f gneiss	236,9	3,34	q-f gneiss	345,3	3,00	q-f gneiss
128,0	3,33	"	243,2	3,82	"	356,3	4,61	"
151,0	4,19	"	258,2	3,49	"	392,4	4,49	"
164,4	3,48	"	280,3	3,42	"	398,3	3,44	"
177,2	3,93	"	284,8	3,84	"	418,3	3,95	"
186,4	3,82	"	287,2	3,08	"	422,0	2,45	"
198,2	3,15	"	294,1	3,13	"	449,3	3,16	"
199,8	3,83	"	300,2	3,84	"	460,3	3,90	b gneiss
229,9	3,29	"	318,7	3,29	"	481,1	3,47	q-f gneiss

a	[illegible]	[illegible]	[illegible]	[illegible]	[illegible]	rock type
124,8	15,8	57,1	5,17	2,98	25,25	q-f gneiss
151,0	23,0	48,8	4,11	3,51	8,19	"
195,2	5,7	49,=	4,39	3,57	4,76	"
205,9	7,0	59,0	5,27	3,84	3,45	"
230,9	5,3	40,3	3,81	3,81	4,43	"
243,3	4,4	41,2	4,71	2,61	4,57	"
258,=	22,3	103,6	1,=1	3,91	11,13	"
277,3	13,4	61,8	4,71	3,49	8,42	"
294,7	8,4	36,5	4,88	3,96	8,28	"
303,=	7,1	84,2	3,77	3,91	8,04	"
309,3	3,3	31,2	5,76	2,93	9,39	"
366,5	3,9	36,1	4,70	2,70	9,32	"
387,4	3,2	47,7	4,84	2,82	4,58	"
398,3	3,1	44,1	5,14	2,93	4,74	"
412,7	4,1	24,9	5,33	2,67	3,24	"
431,0	3,9	18,6	6,00	2,19	3,44	"
449,3	7,4	39,4	5,30	2,87	3,04	"
460,3	23,8	19,0	8,49	3,39	4,82	b gneiss
481,1	9,9	25,4	7,65	3,90	5,44	q-f gneiss

IV-4 CAROLUSBERG WEST CCX-0429

29,6	21,876	-	138,3	22,501	5,900	296,4	24,972	15,771	452,8	28,083	18,795
39,5	21,701	-17,655	158,1	22,700	10,047	316,0	25,354	19,475	472,4	28,444	18,359
49,3	21,658	-7,114	177,9	22,965	13,356	335,6	25,735	19,408	492,0	28,860	18,740
59,2	21,666	0,836	197,7	23,239	13,874	355,1	26,168	22,254	511,4	29,211	20,662
69,0	21,721	5,629	217,5	23,610	18,740	374,7	26,535	18,680	530,8	29,556	17,732
78,9	21,803	8,234	237,3	23,964	17,852	394,3	26,943	20,865	550,1	29,919	18,862
98,7	22,188	19,432	257,0	24,298	16,957	413,8	27,304	13,467	569,4	30,277	18,537
118,5	22,384	9,899	276,7	24,661	18,458	433,4	27,719	21,207	588,6	30,587	16,122

		rock type			rock type			rock type
201,9	3,16	b gneiss	325,0	2,76	b augen gneiss	477,0	2,98	b augen gneiss
214,9	4,25	q-f gneiss	345,9	2,96	"	491,8	3,26	
229,0	2,67	b gneiss	357,8	3,69	"	503,7	2,32	q-f gneiss
238,1	1,32	q-f gneiss	372,6	3,13	"	524,4	3,34	b augen gneiss
247,1	3,66	"	390,6	3,59	"	539,1	2,39	q-f gneiss
262,1	3,68	"	402,5	3,10	"	545,0	3,32	b augen gneiss
271,2	4,09	"	411,5	2,50	q-f gneiss	550,9	3,06	q-f gneiss
280,1	3,84	b augen gneiss	417,4	3,11	b augen gneiss	568,5	3,88	
289,1	2,86	"	435,3	3,73	"	586,1	3,08	b augen gneiss
296,6	1,95	amphibolite	441,2	3,25	q-f gneiss	597,9	3,64	
310,0	3,00	q-f gneiss	459,0	2,90	b augen gneiss			

z	U[1,2]	Th[2]	K[3]	ρ	A	rock type
201,9	3,1	9,9	5,16	2,62	1,91	gneiss
238,1	2,6	52,1	3,66	2,64	4,51	q- gneiss
247,1	4,8	60,4	4,85	2,66	5,78	"
262,1	8,3	29,1	5,21	2,65	4,55	"
271,2	4,0	34,0	4,64	2,64	3,73	"
280,1	3,9	31,0	4,60	2,64	3,51	b augen gneiss
289,1	0,5	2,1	2,60	2,81	0,54	"
310,0	0,4	2,7	7,62	2,61	0,99	q-f gneiss
325,0	1,4	29,1	3,72	2,73	2,74	b augen gneiss
357,8	1,0	27,6	3,36	2,69	2,47	"
372,7	1,4	18,8	4,67	2,67	2,07	"
411,5	2,3	28,4	5,11	2,62	2,99	q-f gneiss
417,4	1,6	29,0	5,82	2,68	2,94	b augen gneiss
441,2	2,7	36,8	4,71	2,66	3,63	q-f gneiss
459,0	3,5	38,0	5,83	2,62	3,95	b augen gneiss
477,0	2,2	35,8	4,82	2,68	3,47	"
524,4	2,7	40,7	4,94	2,66	3,91	"
545,0	2,8	35,4	4,85	2,68	3,60	"
550,9	2,8	46,6	5,13	2,70	4,44	q-f gneiss
568,5	8,0	59,8	6,59	2,60	6,36	"
586,1	7,0	52,2	3,97	2,83	5,76	b augen gneiss
597,9	4,4	63,0	5,50	2,70	5,99	"

IV-5 AGGENEYS AG 140

z	T⁺	B⁺	z	T⁺	B⁻	z	T⁻	B⁺	z	T⁻	B⁻
60,0	24,173	-	300,0	28,443	19,348	530,0	32,474	17,267	650,0	33,989	10,865
80,0	24,463	14,158	320,0	28,814	18,514	540,0	32,605	13,041	660,0	34,098	10,924
100,0	24,778	13,708	340,0	29,166	17,268	550,0	32,735	13,126	670,0	34,255	13,708
120,0	25,096	15,946	360,0	29,539	18,569	560,0	32,898	16,161	680,0	34,461	20,808
140,0	25,441	17,241	380,0	29,880	17,001	570,0	33,001	10,347	690,0	34,669	20,808
160,0	25,791	17,506	400,0	30,239	17,941	580,0	33,120	11,893	700,0	34,847	17,773
180,0	26,147	17,810	420,0	30,655	20,909	590,0	33,285	16,474	710,0	34,945	9,762
200,0	26,532	19,207	440,0	31,038	19,996	600,0	33,421	13,576	720,0	35,092	14,727
220,0	26,935	20,132	460,0	31,378	16,294	610,0	33,527	10,620	730,0	35,273	18,148
240.0	27,313	18,865	480,0	31,681	15,168	620,0	33,649	12,207	740,0	35,389	11,632
260,0	27,675	18,071	500,0	32,003	16,107	630,0	33,772	12,280	750,0	35,556	16,727
280,0	28,055	18,983	520,0	32,302	14,931	640,0	33,880	10,807	752,6	35,657	38,833

z	K	rock type	z	K	rock type	z	K	rock type
235,6	3,02	pegmatite	320,0	3,27	b gneiss	412,2	2,62	pelitic gneiss
244,3	3,65		339,1		"	627,8	6,42	metaquartzite
248,5	3,32	b gneiss	348,1	3,56	"	637,4	6,59	"
251,3	1,58		353,1	3,53	"	644,5	5,45	"
269,1	3,48		358,3	1,38	b fels	652,8	6,94	"
284,8	2,60	f gneiss	367,3	3,14	amphibolite	656,4	6,16	"
291,9	3,35	b gneiss	371,4	3,36	schist gneiss	658,3	5,03	"
299,5	3,29		389,3	2,40	pelitic gneiss	664,1	2,56	"
310,3	3,39	pegmatite	396,4	3,33		668,3	4,03	"

z	U¹	Th¹	K¹	ρ	A	rock type
235,6	2,9	6,7	7,00	2,64	1,92	pegmatite
248,5	5,3	-	4,80	2,68	-	b gneiss
251,3	1,8	14,0	4,80	2,88	2,01	"
269,1	5,0	24,0	5,10	2,66	3,37	"
284,8	1,8	27,0	3,90	2,72	2,72	f gneiss
291,9	5,6	23,0	3,10	2,66	3,27	b gneiss
299,5	5,6	27,0	4,40	2,66	3,66	"
320,0	4,7	21,0	3,60	2,69	2,99	"
339,1	5,6	30,0	5,40	2,62	3,90	"
343,1	6,8	25,0	3,20	2,64	3,69	"
353,1	7,2	22,0	6,10	2,61	3,81	"
358,3	6,1	14,0	3,50	2,86	3,03	b fels
367,3	2,5	7,0	0,30	3,08	1,32	amphibolite
371,4	1,9	16,0	4,80	2,74	2,08	schist'gneiss
389,3	3,0	11,0	5,40	2,75	2,08	pelitic gneiss
396,4	3,1	14,0	5,40	2,78	2,87	"
412,2	4,0	14,0	3,90	2,73	2,39	"
644,5	2,7	13,0	0,70	2,95	1,81	mecaquartzite

IV-6 PUTS-BERG POG 32

z	T		z	T	δ	z	T		z	T	δ
79,7	22,460		198,8	24,277	16,447	317,1	26,308	17,511	434,8	28,341	17,930
99,6	22,735	1 ,825	218,6	24,598	16,224	336,7	26,631	16,488	454,4	28,675	17,[illegible]
119,5	23,033	14,931	238,4	24,925	16,489	356,3	26,971	17,320	473,9	29,002	16,767
139,4	[illegible]	14,232	258,0	25,267	17,430	376,0	27,316	17,527	493,2	29,347	17,861
159,	23,631	15,927	277,7	25,615	17,665	395,6	27,656	17,339	512,3	29,672	17,035
179,0	23,[illegible]	16,183	297,4	25,969	17,974	415,2	27,990	17,043			

z	K	rock type	z	K	rock type	z	K	rock type
108,0	5,35	q gneiss	277,8	2,64	b gneiss	418,9	5,96	metaquartzite
119,1	6,18	b gneiss	287,2	2,98	"	424,7	6,28	"
122,0	10,94	"	290,2	3,81	"	433,7	6,66	"
126,3	5,13	"	295,4	4,07	"	439,5	6,62	"
130,5	5,60	"	307,8	6,56	metaquartzite	449,7	4,21	b gneiss
135,1	6,14	"	318,3	4,42	b gneiss	454,3	5,89	gneiss quartzite
175,1	4,06	"	327,8	6,02	gneiss quartzite	467,9	4,39	metaquartzite
188,3	3,96	"	351,2	5,25	"	474,9	6,08	"
190,1	8,54	"	358,4	9,11	metaquartzite	486,1	8,82	"
222,0	4,45	"	365,4	7,50	"	492,4	5,18	"
230,6	3,28	"	386,5	6,48	"	502,4	8,51	"
242,7	3,11	"	391,0	6,91	"	507,4	7,50	"
248,0	3,46	"	402,0	5,41	"	512,3	3,52	"
259,3	2,80	"	411,5	6,90	"			

sample number	depth range	U*	Th*	K*	ρ	A	rock type
POG 1	100-200	4,78	22,1	3,03	2,70	3,04	b gneiss
POG 2	180-280	4,01	18,5	2,29	2,70	2,52	"
POG 3	330-440	1,60	10,5	1,34	2,63	1,24	mw quartzite
POG 4	450-520	2,50	7,1	2,13	2,63	1,30	

IV-8 ROZYNEN BOSCH RB 56

z	T	β	z	T	β	z	T	β	z	T	β
10,0	24,500	"	129,4	27,305	23,919	246,2	30,093	24,010	359,9	32,639	27,732
20,0	24,577	17,656	139,3	27,599	29,702	255,8	30,300	21,571	369,2	32,859	23,630
30,0	24,955	27,776	149,1	27,816	22,205	265,3	30,522	23,404	378,5	33,037	19,088
40,0	25,196	24,120	158,9	28,048	23,636	274,9	30,733	22,030	387,8	33,231	20,864
50,0	25,430	23,390	168,7	28,271	22,706	284,4	30,987	26,738	397,1	33,442	22,691
60,0	25,698	26,773	178,5	28,472	20,528	294,0	31,204	22,538	406,3	33,639	21,507
70,0	25,917	21,889	188,	28,675	20,947	303,5	31,395	20,126	415,6	33,824	19,823
79,9	26,148	23,425	197,9	28,904	23,664	312,9	31,574	19,061	424,8	34,057	25,298
89,9	26,351	20,244	207,6	29,173	27,736	322,4	31,769	20,493	434,0	34,292	25,583
99,8	26,566	21,751	217,3	29,446	28,103	331,8	31,951	19,410	443,1	34,578	31,430
109,7	26,806	24,197	227,0	29,647	20,681	341,2	32,164	22,610	452,2	34,803	24,746
119,6	27,070	26,725	236,6	29,862	22,427	350,5	32 27?	23,092			

z	K	rock type	z	K	rock type	z	K	rock type
148	2,50	b gneiss	288	3,82	b-g gneiss	369	3,77	b-g gneiss
151	3,31	"	292	3,84	b gneiss	377	4,01	"
154	3,32	"	296	3,80	b-g gneiss	380	4,25	pegmatite
156	3,00	"	304	3,82	"	388	3,98	b-g gneiss
160	49	"	311	4,18	"	394	3,98	b gneiss
164	3,25	"	319	3,89	q-f-g gneiss	402	4,39	q-f-g gneiss
166	3,20	"	323	3,95	"	407	3,90	q-f gneiss
170	3,29	"	330	3,70	b gneiss	416	3,57	b fels
178	3,48	pegmatite	336	3,82	"	421	3,64	b gneiss
183	3,10	"	347	3,68	"	427	3,67	"

sample number	depth range	U*	Th*	K*	ρ	A	rock type
RB 1	148-170	4,11	16,8	3,74	2,75	2,62	b gneiss
RB 2	288-323	5,33	28,3	5,85	2,66	3,82	mostly b(±g) gneiss
RB 3	330-427	4,79	27,0	4,92	2,66	3,51	"
RB 4	451-453	3,69	14,1	4,87	2,67	2,35	'basement' gneiss
RB 5	454-456	19,82	14,5	6,52	2.66	6,61	"

IV-9 AREACHAP AP 11

z	T	β	z	T	β	z	T		z	T	β
39,8	24,855	-	178,7	27,148	18,856	313,9	29,900	20,168	433,0	32,249	18,689
59,7	25,105	12,565	198,4	27,553	20,564	332,5	30,274	20,072	447,8	32,509	17,503
79,5	25,389	14,334	218,0	27,967	21,091	351,0	30,614	18,411	462,3	32,800	20,117
99,4	25,698	15,308	237,5	28,341	19,213	368,8	30,974	20,213	465,4	32,889	28,488
119,2	26,032	16,894	256,9	28,723	19,675	385,8	31,313	19,933			
139,0	26,394	18,263	276,2	29,124	20,792	402,1	31,657	21,137			
158,8	26,773	19,149	295,1	29,521	20,996	417,8	31,965	19,620			

z	K	rock type	z	K	rock type	z	K	rock type
104	3,01	f gneiss	242	3,31	b gneiss	367	2,94	b-a gneiss
117	3,42	b gneiss	252	3,00	augen gneiss	377	2,42	amphibolite
123	2,52	amphibolite	261	2,79	b gneiss	383	2,96	augen gneiss
136	2,00	"	273	4,09	augen gneiss	392	2,93	b-a gneiss
146	3,03	q gneiss	281	2,57	b gneiss	403	2,22	amphibolite
157	1,86	schistose gneiss	294	2,92	augen gneiss	411	2,42	"
169	3,06	q-f gneiss	304	2,75	b gneiss	419	3,45	"
178	3,14	"	311	2,54	"	429	3,00	b gneiss
189	2,18	amphibolite	319	2,89	"	434	2,74	f gneiss
197	2,47	"	330	2,77	"	443	1,85	b gneiss
212	3,06	q gneiss	342	3,11	b augen gneiss	450	3,21	"
225	2,33	amphibolite	349	2,06	amphibolite	457	2,06	amphibolite
23i	2,95	"	361	2,57	"	465	1,90	"

z	[illegible]	Th^3	[illegible]	ρ	A	rock type
104	24,8	23,2	1,90	2,65	8,01	f gneiss
123	0,4	0,9	0,90	3,01	0,28	amphibolite
136	1,1	1,6	1,10	2,94	0,54	"
146	7,3	66,4	0,20	2,63	6,32	q gneiss
178	5,1	58,3	2,60	2,60	5,38	q-f gneiss
189	0,8	4,6	1,50	2,99	0,74	amphibolite
212	3,3	28,7	5,00	2,60	3,18	q gneiss
225	1,0	4,5	0,40	2,95	0,66	amphibolite
242	1,2	11,0	0,60	2,70	1,13	b gneiss
252	2,8	17,5	2,90	2,62	2,14	augen gneiss
261	3,1	29,9	2,60	2,52	3,02	b gneiss
273	13,6	16,9	4,70	2,59	4,90	augen gneiss
281	2,0	31,0	2,30	2,65	2,82	b gneiss
294	31,5	41,9	4,80	2,60	11,02	augen gneiss
304	7,7	34,0	2,90	2,65	4,52	b gneiss
311	7,1	27,1	4,20	2,69	4,08	"
319	5,0	31,6	3,70	2,62	3,70	"
330	2,2	33,6	2,30	2,65	3,07	"
342	3,0	34,2	1,50	2,66	3,23	b augen gneiss
349	0,3	2,9	1,10	2,97	0,42	amphibolite
361	1,2	6,6	1,50	2,85	0,96	"
377	0,9	4,1	1,10	2,86	0,66	"
383	8,2	26,1	5,80	2,61	4,31	augen gneiss
392	0,5	7,2	1,50	2,72	0,77	b-a gneiss
403	0,4	3,4	1,00	3,00	0,48	amphibolite
419	0,3	6,3	0,90	2,70	0,60	"
429	-	12,8	0,30	2,62	-	b gneiss

IV-10 BOKS PUTS KC 12

z	T	S	z	T	S
58,0	24,142	-	154,1	25,095	13,154
77,3	24,258	5,981	172,9	25,348	13,462
96,6	24,413	8,029	191,6	25,594	13,155
115,8	24,579	8,644	210,0	25,854	14,103
135,1	24,845	13,806	214,3	26,001	34,139

z	K	rock type	z	K	rock type	z	K	rock type
115,5	2,71	b-c-a schist	147,4	2,96	b-c-a schist	177,0	2,64	b-c-a schist
121,4	3,02	"	150,3	2,94	"	180,4	2,69	"
124,2	4,35	"	153,1	[illegible]	"	185,9	3,17	"
127,1	2,50	"	158,4	2,94	"	189,2	2,83	"
130,1	2,61	"	161,2	2,94	"	191,7	2,67	"
135,7	3,00	"	163,9	2,96	"	194,9	3,40	"
138,5	2,79	"	166,6	[illegible]	"	199,1	2,92	"
141,6	2,88	"	169,3	2,79	"	203,1	2,65	"
144,5	2,98	"	172,2	3,07	"			

z	$U^{1,2}$	Th^2	K^3	ρ	A	rock type
94,7	1,4	11,2	0,91	2,84	1,28	b-c-a schist
101,1	1,7	6,1	0,26	3,18	1,03	"
109,8	1,0	5,8	0,81	2,74	0,73	"
112,5	1,2	14,5	0,29	2,81	1,38	"
121,4	1,1	8,8	1,07	2,69	0,99	"
127,1	0,7	4,3	1,08	2,91	0,61	"
132,9	1,3	9,1	0,47	2,76	1,02	"
138,5	1,8	10,3	1,82	2,79	1,38	"
144,5	1,6	9,3	2,09	2,87	1,33	"
161,2	1,8	10,6	2,27	2,86	1,49	"
163,9	1,6	11,6	1,65	2,81	1,41	"
169,3	1,8	10,2	0,32	2,81	1,23	"
172,2	1,4	9,1	0,77	2,75	1,08	"
180,4	1,4	6,0	0,53	2,76	0,83	"
185,9	1,0	3,5	0,33	2,76	0,54	"
191,7	2,2	16,9	1,05	2,88	1,94	"
199,1	1,7	17,2	0,23	2,87	1,75	"
200,7	1,4	8,3	1,59	2,84	1,13	"
203,1	0,8	2,9	0,37	2,69	0,43	"

PC2-27

z	T	β	z	T	β	z	T	β	z	T	β
96,0	23,650	-	225,0	25,440	15,807	340,1	27,294	15,830	433,3	28,941	15,886
114,7	23,876	12,078	242,6	25,718	15,810	354,8	27,542	16,897	445,4	29,137	16,171
133,4	24,095	11,704	260,0	25,990	15,611	368,7	27,782	17,264	457,0	29,322	15,962
151,9	24,355	14,056	277,1	26,255	15,479	382,5	28,036	18,441	468,3	29,509	16,536
170,5	24,608	13,637	293,6	26,523	16,256	396,0	28,271	17,345	479,4	29,722	19,267
188,9	24,875	14,503	309,7	26,784	16,205	408,9	28,519	19,288	489,8	29,951	22,010
207,0	25,156	15,500	325,3	27,059	17,654	421,1	28,747	18,670	495,5	30,105	27,023

PC2-30

z	T	β	z	T	β
60,0	23,160	-	160,0	24,491	[illegible]
80,0	23,371	10,555	161,6	24,608	73,418
100,0	23,631	13,003			
120,0	23,913	14,123			
140,0	24,190	13,845			

[illegible]	[illegible]	rock type	[illegible]	[illegible]	rock type	[illegible]	[illegible]	rock type
66* / 208	3,57	b-g gneiss	174* / 262	3,85	b-g gneiss	355	3,67	b-g gneiss
						360	2,89	"
85* / 218	3,50	"	272,6	3,44	"	365	3,32	"
			275	3,32	"	376	3,27	"
81* / 223	4,69	b gneiss	275,8	3,25	"	390,8	2,89	"
			277	3,33	"	422	3,13	"
107* / 229	5,28	[illegible]	292	3,76	"	436	3,51	"
			294	3,02	"	438,2	3,78	"
119* / 235	3,14	b-g gneiss	299,1	3,65	"	440,7	4,29	"
			311,5	3,60	"	441,2	3,51	"
147* / 248	3,54	"	314	3,17	"			
			325	4,51	"			
156* / 253	[illegible]	[illegible]	335	3,29	"			
			339	4,79	"			

*Depth in PC2-30. Equivalent depth in PC2-27.

borehole	depth or sample name	[illegible]	Th²	[illegible]	[illegible]	[illegible]	rock type
PC2-31	a	3,5	25,5	3,82	2,75	3,29	b-g gneiss
"	b	3,4	2,9	3,16	2,73	1,39	"
"	c	3,4	14,6	3,79	2,68	2,21	"
"	d	3,8	16,3	2,66	2,76	2,39	"
"	e	6,3	13,4	3,24	2,75	2,90	"
PC2-30	12	1,7	10,6	2,58	2,72	1,42	b gneiss
"	20	3,2	14,9	2,73	2,75	2,15	"
"	38	2,0	27,9	0,76	3,02	2,80	amphibolite
"	66	3,5	12,4	3,82	2,74	2,15	b-g gneiss
"	78	0,9	1,2	1,42	2,65	0,44	f-g gneiss
"	107	2,8	11,1	1,29	2,69	1,60	b gneiss
"	147	3,4	31,9	5,49	2,64	3,50	b-g gneiss
"	156	4,0	12,5	3,18	2,70	2,19	"
PC2-27	272,6	2,6	15,7	3,07	2,74	2,06	b-g gneiss
"	275	3,4	16,3	3,41	2,66	2,27	"
"	277	4,3	15,3	3,02	2,73	2,46	"
"	294	3,3	15,9	3,13	2,71	2,24	"
"	311,5	3,8	13,5	2,99	2,71	2,20	"
"	360	3,1	18,5	3,71	2,71	2,43	"
"	365	3,7	16,3	3,57	2,69	2,40	"
"	376	3,2	15,0	3,39	2,68	2,17	"
"	390,8	3,8	15,0	4,29	2,64	2,36	"
"	436	4,6	0,9	3,47	2,63	1,52	"
"	438,2	4,5	18,7	3,34	2,69	2,74	"
"	440,7	5,3	3,5	4,88	2,67	2,03	"

IV-12 VOGELSTRUIS BULT V 41

z	T	β	z	T	β	z	T	β	z	T	β
39,5	22,059	-	237,6	23,990	9,591	430,3	26,675	12,697	604,7	29,546	20,549
49,4	22,111	5,240	247,4	24,085	9,738	439,8	26,795	12,637	612,5	29,685	17,739
59,3	22,172	6,131	257,2	24,190	10,762	449,1	26,927	14,173	620,2	29,824	16,097
69,2	22,241	7,033	267,0	24,316	12,796	458,5	27,070	15,293	627,7	29,964	18,703
79,1	22,329	8,824	276,7	24,461	15,015	467,8	27,215	15,569	635,1	30,105	19,088
89,0	22,407	7,975	286,5	24,598	13,973	477,0	27,350	14,628	642,3	30,209	14,352
98,9	22,513	10,683	296,3	24,736	14,066	486,2	27,497	15,959	649,5	30,339	18,045
109,0	22,628	11,408	306,0	24,855	12,259	495,9	27,667	17,601	656,5	30,456	16,804
119,2	22,726	9,609	315,7	25,015	16,462	504,3	27,782	13,646	663,5	30,575	16,902
129,3	22,834	10,643	325,4	25,146	13,473	513,1	27,920	15,730	670,3	30,707	19,449
139,3	22,960	12,613	335,1	25,297	15,654	521,9	28,060	15,836	677,1	30,827	17,617
149,2	23,078	11,903	344,7	25,440	14,871	530,5	28,188	14,953	683,8	30,961	19,981
158,9	23,206	13,302	354,3	25,553	11,762	539,1	28,365	20,545	690,4	31,082	18,173
168,5	23,316	11,351	363,9	25,739	19,386	547,5	28,519	18,381	696,9	31,190	16,677
178,2	23,491	18,104	373,4	25,864	13,163	555,9	28,651	15,659	703,2	31,327	21,633
188,1	23,612	12,227	383,0	26,011	15,298	564,2	28,807	18,866	709,5	31,422	15,232
198,0	23,759	4,723	392,5	26,138	13,343	572,6	28,953	17,337	715,6	31,519	15,804
207,9	23,725	6,631	402,2	26,276	14,251	580,8	29,112	19,381	721,5	31,630	18,765
217,8	23,800	7,603	411,5	26,426	16,120	588,9	29,247	16,722	730,5	31,797	18,582
227,7	23,895	9,545	420,9	26,555	13,767	596,8	29,384	17,262			

sample number	K	rock type	sample number	K	rock type	sample number	K	rock type
A231*	3,24	b schist q-f gneiss	D 2	2,26	amphibolite	F645*	2,16	a gneiss
A 2	2,76	b schist	D 3	2,28	"	F648*	3,09	b-a gneiss
A 3	4,14	q-b schist	D 4	2,58	-	F 1	2,21	amphibolite
A 4	3,21	"	E558*	3,36	a gneiss	F 2	2,45	a-gneiss
A 5	3,51	-	E565*	2,50	amphibolite	G658*	3,43	q-b schist
A 6	3,86	"	E575*	2,55	a gneiss	G675*	2,45	amphibolite
B. 8*	3,63	"	E580*	3,02	q-b-g schist	G683*	2,[illegible]	q-b-a schist
B313*	3,67	"	E 1	3,20	"	G691*	2,33	"
B325*	2,68	b schist	E 2	3,64	a gneiss	G 1	2,49	"
B 1	3,53	q-b schist	E 3	2,33	amphibolite	G 2	2,13	"
B 2	2,5n	b schist	E 4	2,31	-	G 3	2,98	"
B 3	2,85	q-b schist	E 5	2,63	-	G 4	2,36	amphibolite
C261*	3,53	-	E 6	2,39	q-b schist	H727*	2,17	a-b schist
C381*	2,28	q-f gneiss	F604*	2,16	amphibolite	H740*	2,27	-
C 1	3,72	q-b schist	F608*	3,63	b schist	H 1	2,45	b-a-q schist
C 2	3,36	"	F626*	2,81	b-a-g schist	H 2	2,17	amphibolite
C 3	3,7-	"	F630*	3,34	-	H 9	2,14	a gneiss
C 4	2,86	q-b gneiss	F619*	2,61	a gneiss	H 10	2,15	-
D419*	3,03	b-a schist	F640*	3,07	q-b-g schist	H 11	2,68	-
D 1	2,59	amphibolite	F642*	3,80	q-f gneiss			

*Figures indicate vertical depths in metres.

sample number	U*	Th*	K*	σ	A	rock type
V 1	3,10	8,30	1,89	2,69	1,54	q-b schist from groups A, B and C
V 2	0,82	5,31	1,42	2,78	0,73	b schist from groups A to E
V 3	1,20	10,80	1,65	2,79	1,25	q-b schist from groups F, G and H
V 4	0,37	1,21	0,42	3,05	0,25	amphibolite and a schist from groups D, E and F
V 5	0,23	0,53	0,54	3,06	0,17	amphibolite and a schist from groups G and H

ZY-11 BLACK BACK BUTTAIX, IN 1

A	T	P	S	E	R	I	T	S
20,0	24,210	*	130,0	24,885	12,901	245,0	28,415	13,916
30,0	23,943	-28,364	140,0	25,035	13,985	250,0	28,550	14,017
40,0	23,911	2,849	150,0	25,156	13,074	260,0	28,694	14,111
50,0	24,009	3,707	160,0	25,250	14,177	270,0	28,828	13,118
60,0	24,085	7,437	170,0	25,443	14,216	280,0	28,950	13,202
70,0	24,151	8,581	180,0	25,574	13,349	290,0	27,091	13,287
80,0	24,287	10,591	190,0	25,718	14,478	300,0	27,226	13,376
90,0	24,393	10,638	200,0	25,934	13,936	310,0	27,350	13,340
100,0	24,820	12,965	210,0	25,940	13,629	311,8	27,368	10,313
110,0	24,638	11,766	220,0	26,138	14,780			
120,0	24,758	11,832	230,0	26,279	13,823			

IV-14 HAIB HB 77

z	T⁻	β⁻	z	T⁺	β⁺	z	T⁻	β⁺	z	T⁺	β⁺
100,0	28,456	-	220,0	10,005	14,325	340,0	32,000	16.536	460,0	34,317	20,936
120,0	28.692	11,779	240,0	,283	13,875	360,0	32,365	18,267	80,0	34,713	19,765
140,0	28,965	13,700	260,0	30,603	16,054	380,0	32,738	18,616	500,0	35,100	19,340
160,0	29,169	10,151	280,0	30,956	17,666	400,0	33,113	18,976	520,0	35,527	21,405
180,0	29,411	12,093	300,0	31,289	16,619	420,0	33,534	20,880	540,0	35,931	20,151
200,0	29,719	15,383	320,0	31,569	19,000	440,0	33,899	18,212			

z	K	rock type	z	K	rock type	z	K	rock type
114	4,62	q-f porphyry	244	3,18	q-f porphyry	422	3,28	q-f porphyry
139	3,42	"	268	[illegible]	altered rock	429	3,29	"
161	3,51	"	288	3,83	"	454	3,32	"
180	3,82	"	315	3,35	q-f porphyry	479	3,35	"
204	3,73	altered rock	338	3,16	"	494	[illegible]	"
208	3,72	"	356	3,19	"	519	3,29	altered rock
216	3,48	basic dyke	376	3,09	"	538	3,42	"
226	3,43	q-f porphyry	398	3,16	q-f granite			

sample number	depth range	U*	Th*	K*	ρ	A	rock type
HB 1	114-226	3,40	13,[illegible]	3,32	2,69	2,12	q-f porphyry
HB 2	244-398	2,76	[illegible]	4,03	2,67	2,10	"
HB 3	422-494	3,00	12,5	3,03	2,70	1,92	"
HB 4	- - -	1,96	10,5	3,28	2,66	1,51	altered rock

IV-15 RHENOSTERHOEK DRH 18

z	T	β	z	T	β	z	T	β	z	T	β
20,0	21,065	-	149,2	22,061	6,881	276,8	23,163	12,401	403,2	24,401	10,412
29,9	21,218	15,299	159,1	22,131	7,087	286,5	23,249	8,886	412,9	24,504	10,658
39,a	21,349	13,160	169,0	22,212	8,159	296,2	23,330	8,345	422,5	24,609	10,836
49,9	21,444	9,560	178,9	22,294	8,289	305,9	23,412	8,466	432,2	24,702	9,547
59,8	21,514	6,982	188,7	22,377	8,421	315,6	23,502	9,248	441,9	24,798	9,867
69,8	21,576	6,252	198,6	22,460	8,474	325,3	23,592	9,280	451,7	24,887	9,188
70,7	21,629	5,344	208,4	22,542	9,249	335,1	23,687	9,784	461,4	24,993	10,886
89,7	21,687	5,784	218,3	22,622	8,201	344,8	23,783	9,831	471,1	25,072	8,167
99,6	21,743	5,636	228,1	22,700	7,888	354,6	23,878	9,782	480,8	25,170	10,093
109,b	21,804	6,172	237,9	2 ,7.0	8,217	364,3	23,996	12,074	490,4	25,253	8,598
119,5	21,866	6,290	247,7	22,8.3	8,460	374,0	24,09	9,701	500,1	25,344	9,468
129,4	21,927	6,143	257,4	22,954	9,358	383,8	24,192	10,449	509,7	25,454	11,419
139,3	21,993	6,590	267,1	23,042	9,140	393,5	24,300	11,121	510,4	25,459	6,025

z	A	rock type	z	T	rock type	z	T	rock type
97,2	3,15	felsite	243,4	3,92	felsite	388,7	2,47	felsite
104,1	4,22	"	252,b	4,04	"	399,1	2,45	-
114,5	4,03	"	262,1	4,80	"	409,0	3,04	"
124,5	3,92	"	271,9	2,71	"	418,5	2,66	"
134,6	4,03	"	281,9	3,25	"	427,3	2,56	"
144,-	3,99	"	291,3	4,25	"	437,1	3,10	"
154,5	4,03	"	301,0	3,70	"	446,6	4,42	"
164,0	3,65	"	310,4	3,57	"	456,3	5,09	"
175,0	3,53	"	320,a	3,93	"	466,2	3,35	"
183,-	3,28	"	330,7	3,14	"	476,4	2,91	"
193,5	3,59	"	340,4	3,68	"	485,9	4,03	"
203,5	3,81	"	350,5	-,29	"	495,1	4,11	"
213,9	3,91	"	359,3	2,85	"	504,7	4,33	"
223,8	4,01	"	369,1	3,57	"			
233,2	3,82	"	379,2	2,97	"			

sample number	depth	U[b]	Th[b]	K[b]	ρ	A	rock type
DRH 1	963	3,12	8,19	2,96	2,65	1,62	q-f gneiss
DRH 2	963	3,77	8,61	2,86	2,63	1,78	"
DRH 3	967	5,11	9,25	3,62	2,65	2,25	"

IV-16 RHENOSTERBERGHÖHE [illegible]

z	T	S	z	T	S	z	T	S	z	T	S
30,0	20,860	-	130,0	21,453	6,656	230,0	22,308	9,519	330,0	23,196	8,943
40,0	20,913	5,290	140,0	21,530	7,637	240,0	22,415	10,787	340,0	23,284	8,800
50,0	20,946	3,344	150,0	21,611	8,173	250,0	22,503	8,725	350,0	23,368	8,378
60,0	20,985	3,841	160,0	21,702	9,055	260,0	22,583	8,054	360,0	23,460	9,155
70,0	21,039	5,406	170,0	21,778	7,564	270,0	22,682	9,868	370,0	23,549	8,918
80,0	21,096	5,750	180,0	21,875	9,731	280,0	22,761	7,948	380,0	23,631	8,210
90,0	2 ,166	6,922	190,0	21,954	7,888	290,0	22,845	8,339	390,0	23,694	6,273
100,0	21,237	7,112	200,0	22,042	8,782	300,0	22,927	8,194	400,0	23,798	10,437
110,0	21,310	7,304	210,0	22,123	8,128	310,0	23,014	8,772			
120,0	21,385	7,498	220,0	22,212	8,945	320,0	23,107	9,266			

z	K	rock type	z	K	rock type	z	K	rock type
84,1	[illegible]	felsite	198,5	3,79	felsite	311,4	3,39	felsite
95,4	4,23	"	209,4	3,68	"	321,4	3,35	"
104,5	2,99	"	219,3	3,70	"	333,0	3,61	"
116,5	2,62	"	229,7	3,26	"	342,6	3,34	"
126,7	3,44	"	241,9	3,77	"	352,4	3,39	"
137,0	3,66	"	249,9	3,65	"	363,0	3,20	"
147,0	3,45	"	260,0	3,41	"	372,8	3,64	"
157,9	3,53	"	269,3	3,82	"	383,9	3,07	"
167,5	3,70	"	279,9	3,20	"	393,5	3,43	"
178,5	3,94	"	290,5	3,74	"	401,8	3,58	"
188,3	3,59	"	300,8	4,40	"			

sample number	depth	U*	Th*	K*	ρ	A	rock type
DRB 1	1278	4,01	10,36	4,01	2,74	2,15	b gneiss
DRB 2	1279	3,59	9,44	3,86	2,75	1,97	"
DRB 3	1280	4,74	9,76	3,98	2,73	2,29	"

IV-17 RIETKUIL DRL 17

z	T	β	z	T	β	z	T	β	z	T	β
20,0	20,027	-	90,0	20,825	9,066	160,0	21,500	9,464	230,0	22,215	10,852
30,0	20,225	19,810	100,0	20,919	9,353	170,0	21,599	9,932	240,0	22,317	10,211
40,0	20,363	13,741	110,0	21,015	9,643	180,0	21,694	9,558	250,0	22,401	8,418
50,0	20,468	10,569	120,0	21,113	9,773	190,0	21,800	10,542	260,0	22,488	8,719
60,0	20,557	8,864	130,0	21,210	9,739	200,0	21,903	10,341	265,4	22,536	8,837
70,0	20,644	8,663	140,0	21,308	9,787	210,0	22,001	9,793			
80,0	20,735	9,105	150,0	21,405	9,669	220,0	22,107	10,534			

z	K	rock type	z	K	rock type	z	K	rock type
66,1	3,23	felsite	134,6	3,90	felsite	194,7	3,55	felsite
76,3	3,35	"	145,9	3,33	"	205,3	3,69	"
93,1	3,32	"	154,7	3,34	"	214,5	3,95	"
104,7	3,10	"	165,3	3,29	"	224,9	3,05	"
115,7	2,96	"	176,6	4,00	"			
125,3	3,04	"	185,3	3,29	"			

sample number	depth	U*	Th*	K*	ρ	A	rock type
DRL 1	282	1,98	9,61	1,97	2,67	1,34	b gneiss
DRL 2	283	1,57	8,17	2,02	2,66	1,14	"
DRL 3	285	1,80	13,12	1,79	2,68	1,53	"

									z	T	
30,0	20,352		219,8	22,335	9,989	408,7	24,378	10,917	596,2	26,523	11,528
40,0	20,683	13,086	229,8	22,438	10,39.	418,6	24,489	11,196	606,0	26,637	11,593
50,0	20,790	10,742	239,7	22,542	[illegible]	428,5	24,603	11,544	615,8	26,757	12,216
60,0	20,877	8,685	249,7	22,649	10,691	438,4	24,707	10,427	625,6	26,875	12,077
70,0	20,960	8,242	259,6	22,756	10,749	448,3	24,818	11,282	635,4	26,986	11,359
80,0	21,034	7,448	269,6	22,858	10,266	458,3	24,930	11,244	645,2	27,105	12,127
90,0	21,111	7,723	279,3	22,959	10,148	468,1	25,042	11,330	655,0	27,224	12,186
100,0	21,200	8,920	[illegible]	23,067	10,849	478,0	25,155	11,382	664,7	27,340	11,823
110,0	21,284	8,370	299,4	23,174	10,714	487,9	25,264	11,048	674,5	27,456	11,891
120,0	21,376	9,249	309,4	23,279	10,598	497,8	25,382	11,946	684,3	27,573	11,972
130,0	21,468	9,208	319,3	23,389	11,119	507,7	25,494	11,417	694,0	27,690	12,041
140,0	21,561	9,252	329,3	23,499	10,994	517,5	25,610	11,690	703,8	27,808	12,124
149,9	21,649	8,787	33 ,2	23,609	11,066	527,4	25,729	12,098	713,5	27,923	11,720
159,9	21,744	9,516	349,1	23,719	11,116	537,2	25,839	11,215	723,3	28,036	11,668
169,9	21,842	9,905	359,1	23,826	10,809	547,1	25,953	11,597	733,0	28,151	11,745
179,9	21,936	9,343	369,0	23,946	12,139	556,9	26,069	11,783	742,7	28,280	13,263
189,9	22,036	10,012	378,9	24,052	10,719	566,7	26,191	12,391	750,2	28,337	7,551
199,8	22,136	10,052	388,8	24,161	10,895	576,5	26,308	11,935			
209,8	22,235	9,939	398,8	24,269	10,966	586,4	26,410	10,364			

z	K	rock type	A	K	rock type	A	K	rock type
107,7	3,98	felsite	316,6	3,21	felsite	517,3	3,04	felsite
118,0	3,35	"	326,1	3,87	"	527,6	2,93	"
126,8	3,12	"	336,9	3,28	"	537,9	2,93	"
135,2	2,93	"	344,7	3,12	"	548,1	3,60	"
148,0	2,86	"	357,6	3,17	"	558,9	3,20	"
157,7	3,15	"	366,7	3,27	"	568,5	2,89	"
168,4	3,03	"	379,4	3,11	"	578,3	2,69	"
180,9	4,03	"	389,0	3,39	"	587,8	3,04	"
191,7	3,79	"	396,2	3,38	"	598,8	3,35	"
202,2	3,16	"	406,7	3,59	"	609,4	3,27	"
212,2	3,11	"	417,2	3,19	"	620,5	3,18	"
222,3	3,22	"	427,7	3,26	"	629,4	2,81	"
231,1	2,70	"	437,4	3,29	"	639,4	2,57	"
242,7	3,30	"	448,0	2,88	"	655,1	3,19	"
253,7	2,87	"	459,1	4,62	"	659,2	3,07	"
261,5	2,97	"	468,2	3,04	"	669,6	3,07	"
272,4	3,36	"	477,4	3,00	"	679,6	2,80	"
285,5	3,11	"	487,2	3,11	"	690,1	3,25	"
295,0	3,15	"	496,6	3,77	"	699,8	2,82	"
306,1	3,49	"	508,4	2,76	"	710,6	3,06	"

sample number	depth	U*	Th*	K*	ρ	A	rock type
BSF 1	770	3,52	28,27	4,26	2,66	3,21	b gneiss
BSF 2	773	7,33	21,03	4,52	2,65	3,69	"
BSF 3	775	5,57	22,10	4,18	2,65	3,29	"

0,1	1,361		40,1	21,611	1,188	110,0	14,36	3,573	130,0	22,497	10,342
10,1	1,361	0,00	50,0	20,815	1,817	120,0	17,663	0,182	140,0	22,573	10,84
20,1	20,704	3,643	60,0	20,998	0,584	140,0	19,764	0,184	170,0	22,618	10,179
40,1	20,284	1,831	70,1	21,080	1,930	200,0	21,973	0,821	280,0	22,724	10,723
50,0	20,393	1,369	80,1	21,167	2,712	210,0	21,976	0,122	190,0	21,815	10,298
60,1	20,497	0,181	140,0	21,272	0,430	220,0	22,083	10,773	300,0	22,849	12,048
70,1	20,588	0,871	150,0	21,368	7,941	230,0	22,183	10,056	301,2	22,966	13,534
80,1	20,679	1,339	160,0	21,467	1,898	240,0	22,301	12,030			

		rock type			rock type			rock type
49,1	1,86	talcite	149,1	1,64	talcite	220,9	3,99	talcite
59,1	1,41		154,1	1,61	"	238,1	3,17	"
69,1	1,91		164,1	1,81	"	245,1	3,40	"
79,1	1,11		175,0	1,49	"	263,1	3,78	q-f gneiss
85,1	1,77		185,1	1,03	"	274,6	3,91	b gneiss
115,1	1,80		195,1	1,85	"	285,1	3,36	q-f gneiss
125,1	1,28		205,1	2,25	"	297,1	3,40	b gneiss
135,1	1,27		215,1	2,17	"			

sample number	depth	C^{13}	O^{18}	S^{34}	δ	Δ	rock type
185	200-220	0,21	9,58	0,25	1,78	0,16	talcite
185	194 - 221	1,41	10,28	4,23	2,61	1,28	q-f gneiss to b gneiss
185	183 - 194	1,31	11,34	4,41	1,70	1,98	"

I' -20 MAHEMSVLEI BMV -

z	T	B	z	T	B	z	T	B	z	T	B
10,0	20,892		160,0	21,870	8,536	309,8	23,318	10,495	459,4	24,894	1,466
20,0	21,045	15,283	170,0	21,955	8,487	319,8	23,416	9,891	469,4	25,004	1,018
30,0	21,165	12,015	180,0	22,052	[illegible]	329,7	23,514	9,764	479,3	25,125	[illegible]
40,0	21,082	-3,237	190,0	22,163	11,082	339,7	23,616	10,270	489,3	25,233	10,853
50,0	21,102	1,974	200,0	22,258	[illegible]	349,7	23,726	10,982	499,3	25,334	10,094
60,0	21,129	2,552	210,0	22,357	9,980	359,7	23,828	10,296	509,2	25,450	11,674
70,0	21,188	6,024	220,0	22,471	11,343	369,6	23,931	10,244	519,2	25,561	11,134
80,0	21,245	5,711	229,8	22,550	7,960	379,6	24,050	11,922	529,2	25,67	10,988
90,0	21,323	7,806	239,9	22,648	9,773	389,6	24,153	10,369	539,1	25,778	10,745
100,0	21,381	5,839	249,9	22,718	7,056	399,6	24,257	10,412	549,1	25,884	10,687
110,0	21,466	8,447	259,9	22,794	7,530	409,6	24,359	10,272	559,0	25,996	11,295
120,0	21,536	6,969	269,9	22,897	10,345	419,5	24,461	10,238	569,0	26,106	11,028
130,0	21,628	9,274	279,9	23,000	10,329	429,5	24,563	10,192	578,9	26,204	9,806
140,0	21,704	7,535	289,8	23,108	10,828	439,5	24,672	10,925	588,9	26,304	10,068
150,0	21,784	8,083	299,8	23,213	10,521	449,4	24,780	10,797	595,2	26,365	9,560

z	K	rock type	z	K	rock type	z	K	rock type
106,2	3,03	felsite	274,9	3,63	felsite	446,5	3,06	felsite
117,7	3,76	"	284,9	3,01	"	457,1	3,39	"
124,6	2,90	"	296,7	3,17	"	465,9	2,78	"
135,5	2,86	"	304,8	3,93	"	476,7	3,14	"
146,3	3,92	"	313,9	2,72	"	485,5	3,00	"
155,6	3,96	"	324,1	3,02	"	494,8	3,46	"
165,1	2,82	"	334,1	3,37	"	503,8	2,78	"
175,3	2,98	"	344,4	2,93	"	512,5	3,22	"
185,1	3,16	"	354,4	3,11	"	523,4	2,83	"
194,8	2,90	"	364,8	2,70	"	548,3	2,89	"
205,0	2,89	"	374,6	2,86	"	538,6	3,32	"
215,4	3,24	"	385,4	2,83	"	546,8	3,1	"
225,5	3,19	"	395,6	3,01	"	553,8	3,96	"
234,3	3,80	"	406,7	3,47	"	564,0	3,89	"
244,8	3,10	"	416,8	3,06	"	570,4	3,10	"
256,8	3,20	"	427,3	3,11	"			
264,7	3,34	"	436,3	2,87	"			

sample number	depth	U*	Th*	K*	ρ	A	rock type
BMV 1	397	2,64	12,52	2,39	2,65	1,74	q-f gneiss
BMV 2	600	1,84	8,32	2,23	2,64	1,23	

IV-21 TWEELINGFONTEIN BTF 1

z	T	B		T	B		T	B		T	B
30,0	20,471		149,9	21,219	7,856	269,9	22,318	9,612	389,7	23,530	11,142
40,0	20,572	10,146	159,9	21,301	8,129	279,5	22,414	9,867	399,7	23,636	10,560
50,0	20,599	-,645	169,9	21,386	8,305	289,8	22,511	9,508	409,6	23,748	11,275
60,0	20,640	4,179	179,9	21,473	8,793	299,8	22,609	9,763	419,6	23,862	11,423
70,0	20,699	5,876	189,9	21,563	8,992	309,8	22,710	10,159	429,6	23,971	10,822
80,0	20,754	5,495	199,9	21,651	8,788	319,8	22,817	10,671	439,6	24,073	10,317
90,0	20,804	5,019	209,9	21,742	9,073	329,8	22,909	9,183	449,6	24,165	9,216
100,0	20,861	5,687	219,9	21,837	9,552	339,8	23,001	9,235	459,6	24,277	11,193
110,0	20,927	6,595	229,9	21,933	9,598	349,7	23,110	10,909	464,2	24,321	9,477
120,0	20,991	6,460	239,9	22,027	9,386	359,7	23,208	9,879			
130,0	21,066	7,467	249,9	22,126	9,843	369,7	23,314	10,563			
140,0	21,141	7,488	259,9	22,222	9,662	379,7	23,419	10,538			

		rock type			rock type			rock type
124,6	3,23	felsite	235,8	2,92	felsite	356,6	3,82	felsite
132,5	3,35	"	246,4	3,74	"	366,5	3,13	"
144,7	3,97	"	255,9	2,97	"	377,0	2,96	"
155,7	3,24	"	267,2	3,53	"	387,9	3,54	"
164,3	3,09	"	277,7	3,39	"	401,8	3,43	"
175,0	3,46	"	290,2	2,85	"	405,6	2,31	"
184,9	3,23	"	303,6	2,85	"	412,2	3,30	"
195,6	3,54	"	310,4	2,83	"	422,7	2,95	"
205,4	2,99	"	322,1	4,23	"	433,8	3,09	"
214,7	3,35	"	331,4	2,97	"	441,8	3,15	"
225,0	3,92	"	344,6	3,05	"			

sample number	depth	U°	Th°	K°	ρ	A	rock type
BTF 1	469	6,57	17,90	-,85	2,69	3,18	b gneiss
BTF 2	470	4,97	23,73	3,96	2,64	3,22	"
BTF 3	472	4,20	17,05	2,92	2,65	2,48	"

APPENDIX V-A DETAILED CIRCUIT DIAGRAM OF SIEMENS BRIDGE

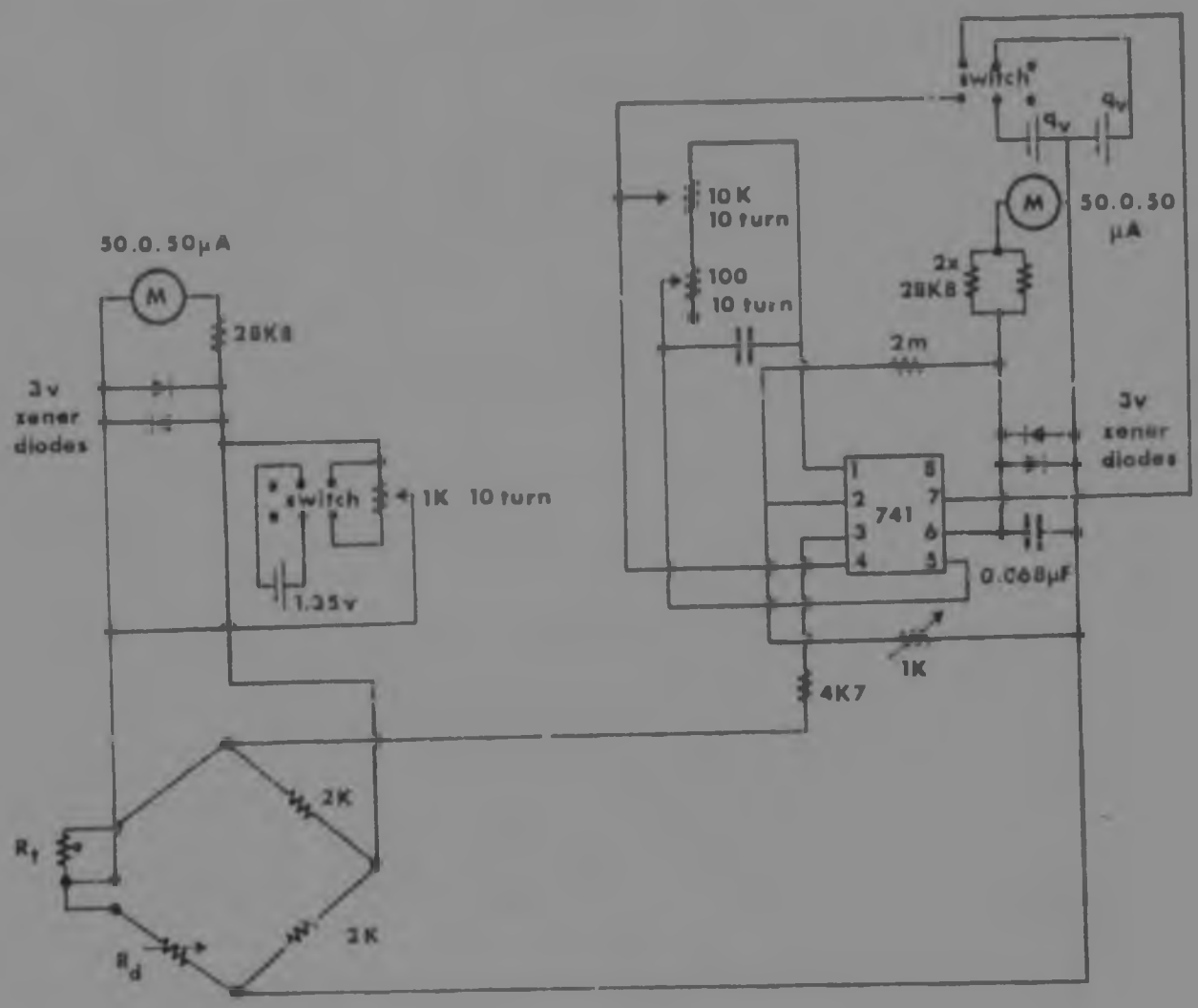

APPENDIX V-E HEATER CONTROL CIRCUIT

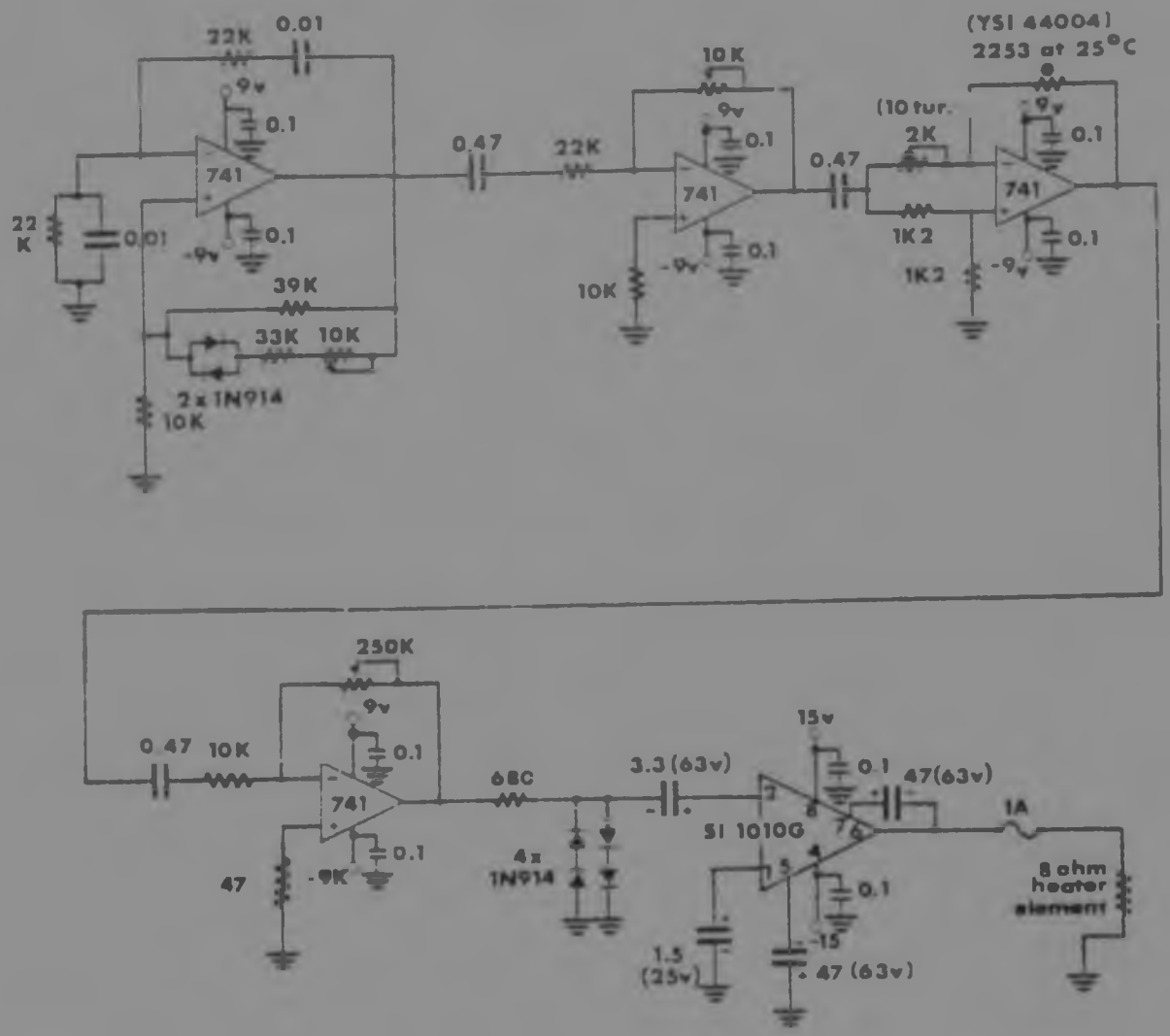

Capacitances in μF

REFERENCES

Abbey, S. (1977). Studies in "standard samples" for use in the general analysis of silicate rocks and minerals. Part 5: 1977 edition of "usable" values. Geological Survey of Canada, Paper 77-34, 31 pp.

Allis, R. G. (1979). A heat production model for stable continental crust. Tectonophys., 5[illegible], [illegible].

Anderson, R. N. and Hobart, M. A. (1976). The relation between heat flow, sediment thickness and age in the eastern Pacific. J. Geophys. Res., 81, 2968-2989.

Anderson, R. N., Langseth, M. G. and Schlater, J. [illegible] (1977). The mechanisms of heat transfer through the floor of the Indian Ocean. J. Geophys. Res., 82, 3391-3409.

Annhaeuser, C. R. (1973). The evolution of the early Precambrian crust of southern Africa. Phil. Trans. R. Soc. Lond., A 273, 359-388.

Annhaeuser, C. R., Mason, R., Viljoen, M. J. and Viljoen, R. J. (1969). A reappraisal of some aspects of Precambrian shield geology. Bull. Geol. Soc. Am., 80, 2175-2200.

Barton, E. S. and Burger, A. J. (1981). Reconnaissance isotopic investigation of the marginal zone of the Proterozoic Namaqua Mobile Belt, Upington Geotraverse. (in preparation).

Barton, E. S., Harmer, R. E. and Burger, A. J. (1981). Isotopic studies in the Namaqua-Natal Mobile Belt. Geol. Soc. S. Afr. Geodynamics Symp. Abstracts, 12-13.

Barton, J. M. Jr.(1981). The pattern of Archaean crustal evolution in southern Africa as deduced from the evolution of the Limpopo Mobile Belt and the Barberton Mountain Land. Geol. Soc. Australia Spec. Publ. 7, (in press).

Barton, J. M. Jr. and Key, R. M. (1981). The tectonic development of the Limpopo Mobile Belt and the evolution of the Archaean cratons of

southern Africa. In: Kröner, A. (ed.) Precambrian plate tectonics. Elsevier, Amsterdam, 185-212.

Beck, A. E. (1977). Climatically perturbed temperature gradients and their effect on regional and continental heat-flow means. Tectonophys., 41, 17-39.

Benedict, P. C., Wiid, D., Cornellisen, A. K. and Staff.(1964). Progress report on the geology of the O'okiep Copper District. In: Haughton, S. H. (ed.) The geology of some ore deposits of southern Africa, Vol 2. Geol. Soc. S. Afr., 238-314.

Benfield, A. E. (1939). Terrestrial heat flow in Great Britain. Proc. R. Soc. Lond., A 173, 438-449.

Birch, F. (1948). The effects of Pleistocene climatic variations upon geothermal gradients. Amer. J. Sci., 246, 729-760.

Birch, F. (1950). Flow of heat in the Front Range, Colorado. Bull. Geol. Soc. Am., 61, 567-630.

Birch, F. (1954). Heat from radioactivity. In: Faul, H. (ed.) Nuclear geology. Wiley, New York, 148-174.

Birch, F., Roy, R. F. and Decker, E. R. (1968). Heat flow and thermal history in New England and New York. In: Zen et al. (eds) Studies of Appalachian geology: northern and maritime. Interscience, New York, 437-451.

Blignault, H. J. (1974). Aspects of the Richtersveld Province. Bull. Precambrian Res. Unit, Univ. Cape Town, 15, 49-56.

Blignault, H. J. (1977). The tectonic evolution of the Richtersveld and Namaqua Provinces in the Ais-Ais and Haib River areas, South West Africa. Bull. Precambrian Res. Unit, Univ. Cape Town, 23, 197 pp.

Blignault, H. J. (1981). A review of the geology and regional setting of the Namaqualand Geotraverse. Geol. Soc. S. Afr. Geodynamics Symp. Abstracts, 24-25.

Blignault, H. J., Jackson, M. P. A., Beukes, G. J. and Toogood, D. J. (1974). The Namaqua Tectonic Province in South West Africa. Bull. Precambrian Res. Unit, Univ. Cape Town, 15, 29-47.

Botha, B. J. V. and Grobler, N. J. (1979). Models for the geotectonic evolution of the middle to late Precambrian Namaqua Mobile Belt in eastern Namaqualand, South Africa. Precambr. Res., 10, 21-41.

Botha, B. J. V., Grobler, N. J., Linstrom, W. and Smit, C. A. (1976). Stratigraphic correlation between the Kheis and Matsap Formations and their relation to the Namaqualand Metamorphic Complex. Trans. geol. Soc. S. Afr., 79, 304-311.

Botha, B. J. V., Grobler, N. J., Linstrom, W. and Smit, C. A. (1977). Major structural features of the area between the Langeberg Range and Kenhardt, northern Cape Province. Trans. geol. Soc. S. Afr., 80, 101-110.

Botha, B. J. V., Grobler, N. J. and Burger, A.J. (1979). New U-Pb age-measurements on the Koras Group, Cape Province and its significance as a time-reference horizon in eastern Namaqualand. Trans. geol. Soc. S. Afr., 82, 1-5.

Boyd, F. R. (1973). A pyroxene geotherm. Geochim. Cosmochim. Acta, 37, 2533-2546.

Boyd, F. R. and Nixon, P. H. (1980). Garnet lherzolite xenoliths from kimberlites in east Griqualand, South Africa. Yb. Carn. Inst. Wash., 79, 488-492.

Brown, P. R. (1963). Climatic fluctuations over the oceans and in the tropical Atlantic. Proc. UNESCO-W.M.O. Symp. Climatic Change, 109-123.

Bullard, E. C. (1938). The disturbance of the temperature gradient in the earth's crust by inequalities of height. Mon. Not. R. astr. Soc. geophys. Suppl., 4, 360-362.

Bullard, E. C. (1939). Heat flow in South Africa. Proc. R. Soc. Lond., A 173, 474-502.

Bullard, E. C. (1947). The time necessary for a borehole to attain temperature equilibrium. Mon. Not. R. astr. Soc. geophys. Suppl., 5, 127-130.

Burger, A. J. and Coertze, F. J. (1973). Radiometric age measurements on rocks from southern Africa to the end of 1971. Bull. Geol. Surv. S. Afr., 58, 46 pp.

Campion, P. J., Burns, J. E. and Williams, A. (1973). A code of practise for the detailed statement of accuracy. National Physics Laboratory, Dept. of Trade and Industry, Her Majesty's Stationary Office, London, 52 pp.

Carslaw, H. S. and Jaeger, J. C. (1959). Conduction of heat in solids (2nd ed.). Oxford University Press, London, 510 pp.

Carte, A. E. (1954). Heat flow in the Transvaal and Orange Free State. Proc. Phys. Soc., B 67, 664-672.

Carte, A. E. and van Rooyen, A. I. M. (1969). Further measurements of heat flow in South Africa. Geol. Soc. S. Afr. Spec. Publ. 2, 445-448.

Chapman, D. S. and Pollack, H. N. (1977). Heat flow and heat production in Zambia: evidence for lithospheric thinning in central Africa. Tectonophys., 41, 79-100.

Cherry, R. D., Hobbs, J. B. M., Erlank, A. J. and Willis, J. P. (1970). Thorium, uranium, potassium, lead, strontium and rubidium in silicate rocks by gamma-spectroscopy and/or x-ray fluorescence. Canadian Spectroscopy, 15, 1-8.

Clark, S. P. (1966). Thermal conductivity. In: Clark, S. P. (ed.) Handbook of physical constants. Geol. Soc. Am. Memoir 97, 459-482.

Clark, S.P., Peterman, Z. E. and Heier, K. S. (1966). Abundances of uranium, thorium and potassium. In: Clark, S.P.(ed.) Handbook of physical constants. Geol. Soc. Am. Memoir 97, 521-541.

Clifford, T. N. (1966). Tectono-metallogenic units and metallogenic provinces of Africa. Earth Planet. Sci. Lett., 1, 421-434.

Clifford, T. N. (1970). The structural framework of Africa. In: Clifford, T. N. and Gass, I. G. (eds) African magmatism and tectonics. Oliver and Boyd, Edinburgh, 1-26.

Clifford, T. N., Gronow, J., Rex, D. C. and Burger, A. J. (1975). Geochronological and petrogenetic studies of high-grade metamorphic rocks and intrusives in Namaqualand, South Africa. J. Petrology, 16, 154-188.

Cornell, D. H. (1975). Age and metamorphism of the Copperton Formation, Prieska district. Geol. Soc. S. Afr. Spec. Publ. 4, 223-234.

Cox, K. G. (1978). Flood basalts, subduction and the break-up of Goudwanaland. Nature, 274, 47-49.

Crampton, D. (1974). A note on the age of the Matsap Formation of the northern Cape Province. Trans. geol. Soc. S. Afr., 77, 71-72.

Crough, S. T. (1979). Hotspot epeirogeny. Tectonophys., 61, 321-333.

Crough, S. T. and Thompson, G. A. (1976). Thermal model of continental lithosphere. J. Geophys. Res., 81, 4857-4862.

Cull, J. P. (1980). Climatic corrections to Australian heat-flow data. BMR Journal of Australian Geology and Geophysics, 4, 303-307.

Davis, E. E. and Lister, C. R. B. (1974). Fundamentals of ridge crest topography. Earth Planet. Sci. Lett., 21, 405-413.

Davis, E. E. and Lister, C. R. B. (1977). Heat flow measured over the Juan de Fuca Ridge: evidence for widespread hydrothermal circulation in a highly heat transportive crust. J. Geophys. Res., 82, 4845-4860.

Dawson, J. B. (1970). The structural setting of African kimberlite magmatism. In: Clifford, T. N. and Gass, I. G. (eds) African magmatism and tectonics. Oliver and Boyd, Edinburgh, 321-335.

du Toit, A. L. (1954). The geology of South Africa (3rd ed.). Oliver and Boyd, Edinburgh, 611 pp.

England, P. C. (1976). Thermal modelling from heat flow and velocity modelling from seismological data, with special reference to the eastern Alps. D. Phil. thesis (unpubl.), Univ. of Oxford.

England, P. C. (1978). The effect of erosion on palaeoclimatic and topographic corrections to heat flow. Earth Planet. Sci. Lett., 39, 427-434.

England, P. C. and Richardson, S. W. (1980). Erosion and the age dependence of continental heat flow. Geophys. J. R. astr. Soc., 62, 421-437.

Forsyth, D. W. (1977). The evolution of the upper mantle beneath mid-ocean ridges. Tectonophys., 38, 89-118.

Fraser, D. G. and Lawless, P. J. (1978). Palaeogeotherms: implications of disequilibrium in garnet lherzolite xenoliths. Nature, 273, 220-223.

Gane, P. G., Atkins, A. R., Sellschop, J. P. F. and Seligman, P. (1956). Crustal structure in the Transvaal. Bull. Seismol. Soc. Am., 46, 293-316.

Geringer, G. J. and Botha, B. J. V. (1976). The quartz porphyry-granite relation in rocks of the Koras Formation west of Upington in the Gordonia district. Trans. geol. Soc. S. Afr., 79, 58-60.

Geringer, G. J. and Botha, B. J. V. (1977). The gneisses and regional structural pattern of the Namaqualand Mobile Belt in part of the Gordonia district, north-western Cape. Trans. geol. Soc. S. Afr., 80, 93-95.

Gough, D. I. (1963). Heat flow in the southern Karoo. Proc. R. Soc., A 272, 207-230.

Gray, C. M. (1977). The geochemistry of central Australian granulites in relation to the chemical and isotopic effects of granulite facies

metamorphism. Contr. Miner. Petrol., 33, 10-19.

Gray, C. M. and Oversby, V. M. (1972). The behaviour of lead isotopes during granulite facies metamorphism. Geochim. Cosmochim. Acta, 36, 939-952.

Gurney, J. J. and Harte, B. (1980). Chemical variations in upper mantle nodules from southern African kimberlites. Phil. Trans. R. Soc. Lond., A 297, 273-293.

Hart, R. J. (1978). A study of the isotopic and geochemical gradients in the old granite of the Vredefort structure, with implications for continental heat flow. Ph.D. thesis (unpubl.). Univ. of the Witwatersrand.

Hart, R. J., Reid. D. L., Stuckless, J. S. and Welke, H. J. (1980). Comparison of three techniques for the determination of uranium and thorium in rocks. Chemical Geology, 29, 345-350.

Hart, R. J., Welke, H. J. and Nicolaysen, L. O. (1981a). Geochronology of the deep profile through Archaean basement at Vredefort, with implications for early crustal evolution. J. Geophys. Res., (in press).

Hart, R. J., Nicolaysen, L. O. and Gale, N. H. (1981b). Radioelement concentrations in the deep profile through Precambrian basement of the Vredefort structure. J. Geophys. Res., (in press).

Haughton, S. H. (1969). Geological history of southern Africa. Geol. Soc. S. Afr., Cape Town, 535 pp.

Hawkesworth, C. J. (1974). Vertical distribution of heat production in the basement of the eastern Alps. Nature, 249, 435-436.

Heier, K. S. and Adams, J. A. S. (1965). Concentration of radioactive elements in deep crustal material. Geochim. Cosmochim. Acta, 29, 53-61.

Herman, B. M., Langseth, M. G. and Hobart, M. A. (1977). Heat flow in

...tonophys., ...

...rogency, and epeirogeny. In:
...rust ... the Earth - a symposium. Geol.
... Pap. No. 62, 391-408.

... History ... an basins. In: Engel et al. (eds)
...: ... volume in honor of A. F. Buddington. Geol.
..., ... ork, 590-620

..., ... (1963). Temperature and rainfall
... during the period of the meteorological
... symp. Climatic Change, 81-85.

..., ... J. (1978). Low solubility of alumina in
... Trans. R.
... Lond., A 288, 431-486.

..., ... evelopment in the Kaapvaal Craton, I.
... Precambr. Res., 1, 259-294.

..., ... (1974b). ...istal development in the Kaapvaal Craton, II.
... Precambr. Res., 1, 295-326.

..., ... (1), ...eat flow and radioactivity in Australia. Earth
...ane ... Lett., 2, 285-292.

... (1967). Disturbances of the temperature gradient in the
... by inequalities of height. Mon. Not. R. astr. Soc.
...phys. Suppl., 9, 309-312.

..., ... (1970). The effect of environment on divided bar
... ...nophys., 10, 39-49.

..., ..., ... Lewis, ... (1978). Heat flow and heat generation in
... ...nadian Shield, ...tonophys., 50,

..., ..., ... R. (1970). Two-dimensional thermal

conductivity anomalies and vertical heat-flow measurements. In: Cermak, V. and Rybach, L. (eds) Terrestrial heat flow in Europe. Springer, Berlin, 98-106.

Jordan, T. H. (1975). Lateral heterogeneity and mantle dynamics. Nature, 257, 745-750.

Jordan, T. H. (1978). Composition and development of the continental tectosphere. Nature, 274, 544-548.

Joubert, P. (1971). The regional tectonism of the gneisses of part of Namaqualand. Bull. Precambrian Res. Unit, Univ. Cape Town, 10, 220 pp.

Kennedy, C. S. and Kennedy, G. C. (1976). The equilibrium boundary between graphite and diamond. J. Geophys. Res., 81, 2467-2470.

King, L. C. (1963). South African Scenery (3rd ed.). Oliver and Boyd, Edinburgh, 308 pp.

Köppel, V. (1980). Lead-isotope studies of stratiform ore deposits of Namaqualand, N. W. Cape Province, South Africa, and their implications on the age of the Bushmanland sequence. Proc. 5th Quadr. IAGOD. Symp., Stuttgart, 195-207.

Kramers, J. D. (1979). Lead, uranium, strontium, potassium and rubidium in inclusion bearing diamonds and mantle derived xenoliths from southern Africa. Earth Planet. Sci. Lett., 42, 58-70.

Krige, L. J. (1939). Borehole temperatures in the Transvaal and Orange Free State. Proc. R. Soc. Lond., A 173, 450-474.

Kröner, A. (1977a). Precambrian mobile belts of southern and eastern Africa - ancient sutures or sites of ensialic mobility: A case for crustal evolution towards plate tectonics. Tectonophys., 40, 101-135.

Kröner, A. (1977b). The Precambrian geotectonic evolution of Africa: plate accretion versus plate destruction. Precambr. Res., 4, 6[illegible]

Krüner, A. and Blignault, H. J. (1976). Towards a definition of some tectonic and igneous provinces in western South Africa and southern South West Africa. Trans. geol. Soc. S. Afr., 79, 232-238.

Kutas, R. I. (1977). Investigation of heat flow in the territory of the Ukraine. Tectonophys., 41, 139-145.

Lachenbruch, A. H. (1968). Preliminary geothermal model of the Sierra Nevada. J. Geophys. Res., 73, 6977-6989.

Lachenbruch, A. H. (1970). Crustal temperature and heat production: implications of the linear heat flow relation. J. Geophys. Res., 75, 3291-3300.

Lachenbruch, A. H. and Bunker, C. M. (1971). Vertical gradients of heat production in the continental crust, 2. Some estimates from borehole data. J. Geophys. Res., 76, 3852-3860.

Lachenbruch, A. H. and Sass, J. H. (1977). Heat flow in the United States and the thermal regime of the crust. In: Heacock, J. G. (ed.) The Earth's crust. Geophys. Monogr., 20, AGU, Washington, D.C., 626-675.

Lambert, I. B. and Heier, K. S. (1967). The vertical distribution of uranium, thorium and potassium in the continental crust. Geochim. Cosmochim. Acta, 31, 377-390.

Lancaster, I. N. (1979). Quaternary environments in the arid zone of Southern Africa. Occasional Paper 22, Dept. of Geography and Environmental Studies, Univ. of the Witwatersrand, Johannesburg, 77 pp.

Leeds, A. R., Knopoff, L. and Kausel, E. G. (1974). Variations of upper mantle structure under the Pacific Ocean. Science, 186, 141-143.

Lewis, T. J. and Beck. A. E. (1977). Analysis of heat flow data - Detailed observations in many holes in a small area. Tectonophys., 41, 41-59.

Lister, C. R. B. (1972). On the thermal balance of a mid-ocean ridge. Geophys. J. R. astr. Soc., 26, 515-535.

Lloyd, F. E. and Bailey, D. K. (1975). Light element metasomatism of the continental mantle: the evidence and the consequences. In: Ahrens et al. (eds) Physics and chemistry of the Earth, vol. 9. Pergamon Press, Oxford, 389-416.

MacGregor, I. D. (1975). Petrologic and thermal structure of the upper mantle beneath South Africa in the Cretaceous. In Ahrens et al. (eds) Physics and chemistry of the Earth, vol. 9. Pergamon Press, Oxford, 455-466.

MacGregor, I. D. and Basu, A. R. (1974). Thermal structure of the lithosphere: a petrologic model. Science, 185, 1007-1011.

Mason, R. (1973). The Limpopo Mobile Belt - southern Africa. Phil. Trans. R. Soc. Lond., A 273, 463-485.

McCarthy, T. S. (1976). Chemical interrelationships in a low-pressure granulite terrain in Namaqualand, South Africa, and their bearing on granite gneisses and the composition of the lower crust. Geochim. Cosmochim. Acta, 40, 1057-1068.

McGetchin, T. R. and Silver, L. T. (1972). A crustal - upper-mantle model for the Colorado Plateau based on observations of crystalline rock fragments in the Moses Rock Dike. J. Geophys. Res., 77, 7022-7037.

McGetchin, T. R., Burke, K. C., Thompson, G. A. and Young, R. A. (1980). Mode and mechanisms of plateau uplifts. In: Bally et al. (eds) Dynamics of Plate Interiors, Geodynamics Series, vol. 1. AGU, Washington, D.C., 99-110.

McKenzie, D. P. (1967). Some remarks on heat flow and gravity anomalies. J. Geophys. Res., 72, 6261-6271.

McKenzie, D. P. (1978). Some remarks on the development of sedimentary basins. Earth Planet. Sci. Lett., 40, 25-32.

McKenzie, D. P. and Sclater, J. G. (1971). The evolution of the Indian Ocean since the late Cretaceous. Geophys. J. R. astr. Soc., 24, 437-528.

McKenzie, D. P. and Weiss, N. (1975). Speculations on the thermal and tectonic history of the earth. Geophys. J. Roy. astr. Soc., 42, 131-174.

Mitchell, R. H., Carswell, D. A. and Clarke, D. B. (1980). Geological implications and validity of calculated equilibrium conditions for ultramafic xenoliths from the Pipe 200 kimberlite, northern Lesotho. Contr. Miner. Petrol., 72, 205-217.

Moore, J. H. (1977). The geology of Namiesberg, northern Cape. Bull. Precambrian Res. Unit, Univ. Cape Town, 20, [illegible] pp.

Mori, T. and Green, D. H. (1978). Laboratory duplication of phase equilibria observed in natural garnet lherzolite. J. Geol., 86, 83-97.

Mossop, S. C. and Gafner, G. (1951). The thermal constants of some rocks from the Orange Free State. J. Chem. Soc. S. Afr., 52, 61-73.

Newton, A. R. (1973). A gravity-folding model of the Cape Fold Belt. Trans. geol. Soc. S. Afr., 76, 145-152.

Nicolaysen, L. O. (1981). Core-coupled tectonics: a global framework for alkaline ultramafic eruptions, cryptoexplosions and their sulphide mineralization. Geol. Soc. S. Afr. Geodynamics Symp. Abstracts, 165-166.

Nicolaysen, L. O. and Burger, A. J. (1965). Note on an extensive zone of 1000 milion-year old metamorphic and igneous rocks in southern Africa. Science de la Terre, 10, 497-516.

Nicolaysen, L. O., Hart, R. J. and Gale, N. H. (1981). The Vredefort radioelement profile extended to supracrustal strata at Carletonville, with implications for continental heat flow. J. Geophys. Res., (in press).

Nixon, P. H., Boyd, F. R. and Boullier, A. M. (1973). The evidence of kimberlite and its inclusions on the constitution of the outer part

of the earth. In: Nixon, P. H. (ed.) Lesotho Kimberlites. Cape and Transvaal Printers, Cape Town, 312-318.

Oxburgh, E. R. and Parmentier, E. M. (1977). Compositional and density stratification in oceanic lithosphere - causes and consequences. J. geol. Soc. Lond., 133, 343-355.

Parsons, B. and McKenzie, D. P. (1978). Mantle convection and the thermal structure of the plates. J. Geophys. Res., 83, 4485-4496.

Parsons, B. and Sclater, J. G. (1977). An analysis of the variation of ocean floor bathymetry and heat flow with age. J. Geophys. Res., 82, 803-827.

Pollack, H. N. and Chapman. D. S. (1977a). On the regional variation of heat flow, geotherms and lithospheric thickness. Tectonophys., 38, 279-296.

Pollack, H. N. and Chapman, D. S. (1977b). Mantle heat flow. Earth Planet. Sci. Lett.. 34, 174-184.

Polyak, B. E. and Smirnov, Y. B. (1968). Relationship between terrestrial heat flow and the tectonics of continents. Geotectonics, 4, 205-213.

Rao, R. U. M. and Jessop, A. M. (1975). A comparison of the thermal characters of shields. Can. J. Earth Sci., 12, 347-360.

Rao, R. U. M., Rao, G. V. and Narain, H. (1976). Radioactive heat generation and heat flow in the Indian Shield. Earth Planet. Sci. Lett., 30, 57-64.

Ratcliffe, E. H. (1959). Thermal conductivities of fused and crystalline quartz. Brit. J. Appl. Phys., 10, 22-25.

Reeves, C. (1976). The delineation of crustal provinces in southern Africa from a compilation of gravity data. Ann. Rep. Res. Inst. Afr. Geol., Univ. Leeds, 20, 36-41.

Reid, D. L. (1977). Geochemistry of Precambrian igneous rocks in the lower Orange River region. Bull. Precambrian Res. Unit, Univ. Cape

Town, 22, 397 pp.

Reid, D. L. (1979a). Total rock Rb-Sr and U-Th-Pb isotopic study of Precambrian metavolcanic rocks in the lower Orange River region, southern Africa. Earth Planet. Sci. Lett., 42, 368-378.

Reid, D. L. (1979b). Age relationships within the mid-Proterozoic Vioolsdrif batholith, lower Orange River region. Trans. geol. Soc. S. Afr., 82, 305-311.

Reid, D. L. (1981). Sm-Nd ages from the Namaqua and Richtersveld Provinces. Geol. Soc. S. Afr. Geodynamics Symp. Abstracts, 173-174.

Richardson, S. W. (1975). Heat flow processes. In: Geodynamics Today. The Royal Society, London, 123-132.

Richardson, S. W. and Oxburgh, E. R. (1978). Heat flow, radiogenic heat production and crustal temperatures in England and Wales. J. geol. Soc. Lond., 135, 323-337.

Richardson, S. W. and Powell, R. (1976). Thermal causes of the Dalradian metamorphism in the central Highlands of Scotland. Scot. J. Geol., 12, 237-268.

Richter, F. M. (1973). Convection and the large scale circulation of the mantle. J. Geophys. Res., 78, 8735-8745.

Richter, F. M. and Parsons, B. (1975). On the interaction of two scales of convection in the mantle. J. Geophys. Res., 80, 2529-2541.

Rosholt, J. N., Zartman, R. E. and Nkomo, I. T. (1973). Lead isotope systematics and uranium depletion in the Granite Mountains, Wyoming. Geol. Soc. Am. Bull., 84, 989-1002.

Roy, R. F., Blackwell, D. D. and Birch, F. (1968a). Heat generation of plutonic rocks and continental heat flow provinces. Earth Planet. Sci. Lett., 5, 1-12.

Roy, R. F., Decker, E. R., Blackwell, D. D. and Birch, F. (1968b). Heat flow in the United States. J. Geophys. Res., 73, 5207-5221.

Roy, R. F., Blackwell, D. D. and Decker, E. R. (1972). Continental heat flow. In: Robertson, E. C. (ed.) The nature of the solid earth. McGraw Hill, New York, 506-543.

Rybach, L. (1976). Radioactive heat production; a physical property determined by the chemistry of rocks. In: Strens, R. G. J. (ed.) The physics and chemistry of minerals and rocks. Wiley-Interscience, London, 309-318.

Sass, J. H. and Lachenbruch, A. H. (1979). Thermal regime of the Australian continental crust. In: McElhinny, M. W. (ed.) The earth - its origin, structure and evolution. Academic Press, London, 301-351.

Sass, J. H., Lachenbruch, A. H. and Jessop, A. M. (1971). Uniform heat flow in a deep hole in the Canadian Shield and its palaeoclimatic implications. J. Geophys. Res., 76, 8586-8596.

Schatz, J. F. and Simmons, G. (1972). Thermal conductivity of earth materials at high temperatures. J. Geophys. Res., 77, 6966-6983.

Schloessin, H. H. and Jacobs, J. A. (1980). Dynamics of a fluid core with inward growing boundaries. Can. J. Earth Sci., 17, 72-89.

Schubert, G., Froidevaux, C. and Yuen, D. A. (1976). Oceanic lithosphere and asthenosphere: thermal and mechanical structure. J. Geophys. Res., 81, 3525-3540.

Schulze, B. R. (1965). Climate of South Africa. Part 8: General survey. Weather Bureau, Department of Transport, Republic of South Africa, Government Printer, Pretoria, 330 pp.

Sclater, J. G. and Crowe, J. (1979). A heat flow survey at anomaly 13 on the Reykjanes Ridge: a critical test of the relation between heat flow and age. J. Geophys. Res., 84, 1593-1602.

Sclater, J. G. and Francheteau, J. (1970). The implications of terrestrial heat flow observations on current tectonic and geochemical models of the crust and upper mantle of the earth. Geophys. J. R. astr. Soc., 20, 509-542.

Sclater, J. G., Anderson, R. N. and Bell, M. L. (1971). Elevation of ridges and evolution of the central eastern Pacific. J. Geophys. Res., 76, 7888-7915.

Sclater, J. G., von Herzen, R. P., Williams, D. L., Anderson, R. N. and Klitgord, K. (1974). The Galapagos spreading centre: heat flow on the north flank. Geophys. J. R. astr. Soc., 38, 609-626.

Sclater, J. G., Crowe, J. and Anderson, R. N. (1976). On the reliability of oceanic heat flow averages. J. Geophys. Res., 81, 2997-3006.

Sclater, J. G., Jaupart, L. and Galson, D. (1980). The heat flow through oceanic and continental crust and the heat loss of the earth. Rev. Geophys. Space Phys., 18, 269-311.

Shackleton, N. J. (1980). Deep drilling in African lakes. Nature, 288, 211-212.

Sleep, N. H. (1971). Thermal effects of the formation of Atlantic continental margins by continental breakup. Geophys. J. R. astr. Soc., 24, 325-350.

Smit, M. C. B. (1976). The determination of uranium in geological material by delayed neutron counting. Atomic Energy Board, Pretoria, 19 pp.

Smithson, S. B. and Decker, E. R. (1974). A continental crustal model and its geothermal implications. Earth Planet. Sci. Lett., 22, 215-225.

Stowe, C. W. (1981). The Upington Geotraverse and its implications for craton margin tectonics. (in preparation .

Stuckless, J. S. and Nkomo, I. T. (1978). Uranium-lead isotope systematics in uraniferous alkali-rich granites from the Granite Mountains, Wyoming: implications for uranium source rocks. Econ. Geol., 73, 427-441.

Swanberg, C. A. (1972). Vertical distribution of heat production in the Idaho Batholith. J. Geophys. Res., 77, 2508-2513.

Swanberg, C. A., Chessman, M. D., Simmons, G., Smithson, S. B., Grønlie, G. and Heier, K. S. (1974). Heat flow - heat generation studies in Norway. Tectonophys., 23, 31-48.

Talma, A. S., Vogel, J. C. and Partridge, T. C. (1974). Isotopic contents of some Transvaal speleotherms and their palaeoclimatic significance. S. Afr. J. Sci., 70, 139-140.

Talwani, M., Le Pichon, X. and Ewing, M. (1965). Crustal structure of the mid-ocean ridges: 2. Computed model from gravity and seismic refraction data. J. Geophys. Res., 70, 341-352.

Truswell, J. F. (1970). An introduction to the historical geology of South Africa. Purnell, Johannesburg, 167 pp.

Turcotte, D. L. (1980). Models for the evolution of sedimentary basins. In: Bally et al. (eds) Dynamics of Plate Interiors, Geodynamics Series, vol. 1. AGU, Washington, D.C., 21-26.

Turcotte, D. L. and McAdoo, D. C. (1979). Geoid anomalies and the thickness of the lithosphere. J. Geophys. Res., 84, 2381-2387.

Turcotte, D. L. and Oxburgh, E. R. (1967). Finite amplitude convective cells and continental drift. J. Fluid. Mech., 28, 29-42.

Turcotte, D. L. and Oxburgh, E. R. (1969). Convection in a mantle with variable physical properties. J. Geophys. Res., 74, 1458-1473.

Vajner, V. (1974). The tectonic development of the Namaqua Mobile Belt and its forelands in parts of the northern Cape. Bull. Precambrian Res. Unit, Univ. Cape Town, 14, 201 pp.

van Zinderen Bakker, E. M. (1976). The evolution of late Quaternary palaeoclimates of southern Africa. Palaeoecology of Africa, 9, 160-202.

Veryard, R. G. (1963). A review of studies on climatic fluctuations during the period of the meteorological record. Proc. UNESCO-W.M.O. Symp. Climatic Change, 3-35.

Viljoen, R. P., Viljoen, M. J., Grootenboer, J. and Longshaw, T. G. (1975). ERTS-1 imagery: applications in geology and mineral exploration. Minerals Sci. Engng., 7, 132-168.

Vine, F. J. and Matthews, D. H. (1963). Magnetic anomalies over oceanic ridges. Nature, 199, 947-949.

Vitorello, I. and Pollack, H. N. (1980). On the variation of continental heat flow with age and the thermal evolution of continents. J. Geophys. Res., 85, 983-995.

Walsh, J. B. and Decker, E. R. (1966). Effect of pressure and saturating fluid on the thermal conductivity of compact rock. J. Geophys. Res., 71, 3053-3061.

Watanabe, T., Langseth, M. G. and Anderson, R. N. (197). Heat flow in back-arc basins of the western Pacific. In: Talwani, M. and Pitman, W. C. (eds) Island arcs, deep sea trenches, and back-arc basins. AGU, Washington, D.C., 137-161.

Wilcocks, J. R. N. (1977). Desert encroachment in South Africa. M.A. Thesis (unpublished), Univ. of the Witwatersrand.

Williams, D. L., von Herzen, R. P., Sclater, J. G. and Anderson, R. N. (1974). The Galapagos spreading centre: lithospheric cooling and hydrothermal circulation. Geophys. J. R. astr. Soc., 38, 587-608.

Wilshire, H. G. and Jackson, E. D. (1975). Problems in determining mantle geotherms from pyroxene compositions of ultramafic rocks. J. Geol., 83, 313-329.

Wyllie, P. J. (1980). The origin of kimberlite. J. Geophys. Res., 85, 6902-6910.

Yuen, D. A. and Schubert, G. (1981). Plateau uplifts as a consequence of frictional heating. Tectonophys., 76, 47-58.

Author Jones M Q W
Name of thesis Heat flow and Heat production studies in the Namaqua Mobile Belt and Kaapvaal Craton 1981

PUBLISHER:
University of the Witwatersrand, Johannesburg
©2013

LEGAL NOTICES:

Copyright Notice: All materials on the University of the Witwatersrand, Johannesburg Library website are protected by South African copyright law and may not be distributed, transmitted, displayed, or otherwise published in any format, without the prior written permission of the copyright owner.

Disclaimer and Terms of Use: Provided that you maintain all copyright and other notices contained therein, you may download material (one machine readable copy and one print copy per page) for your personal and/or educational non-commercial use only.

The University of the Witwatersrand, Johannesburg, is not responsible for any errors or omissions and excludes any and all liability for any errors in or omissions from the information on the Library website.